Towards a Smart Power Grid through Optimum Location of Control Devices

Thesis Submitted By

Jayanti Sarker (Bhattacharjee)

Doctor of Philosophy (Engineering)

Department of Electrical Engineering

Faculty Council of Engineering and Technology
Jadavpur University
Kolkata-700032,India

2019

INDEX NO. 299/14/E

1. Title of the thesis:

Towards a Smart Power Grid through Optimum Location of Control Devices

2. Name, Designation & Institution of Supervisors:

Prof. Swapan Kumar Goswami

Electrical Engineering Department

Jadavpur University

Kolkata-700032, West Bengal, India

3. List of Research International Journal Publication:

(i) Jayanti Sarker, S.K.Goswami, "*Solution of multiple UPFC placement problems using gravitational search algorithm*", **International Journal of Electrical Power & Energy Systems, Vol. 55, 2014, Pages-531-541.**

(ii) J. Sarker and S.K. Goswami, "*Optimal Location of Unified Power Quality Conditioner in Distribution System for Power Quality Improvement*", **Int. J. Electical Power and Energy Systems, 83 (2016) 309-324.**

Communicated/To be communicated

Journals

(i) J. Sarker and S.K. Goswami, "*Location and DC Link Capacitor Sizing Solution of UPFC*", IET Generation, Transmission and Distribution.

(ii) J. Sarker and S.K. Goswami, "*Optimal Placement of Hybrid Dynamic Voltage Restorer in Distribution System*", CSEE Journal of Power and Energy Systems.

4. List of Patents: Nil

5. List of Presentation in National/International /Conferences/Workshops: Nil

CERTIFICATE FROM THE SUPERVISOR/S

This is to certify that the thesis entitled "**Towards a Smart Power Grid through Optimum Location of Control Devices**" submitted by Smt. **Jayanti Sarker (Bhattacharjee)**, who got her name registered on 2nd May, 2014 for the award of Ph.D. (**Engg.**) degree of **Jadavpur University** is absolutely based upon her own work under the supervision of **Prof. Swapan Kumar Goswami** and that neither her thesis nor any part of the thesis has been submitted for any degree/diploma or any other academic award anywhere before.

_____

Prof. Swapan Kumar Goswami
(Skgoswami_ju@yahoo.co.in)
Supervisor
Department of Electrical Engineering
Jadavpur University
Kolkata-700032, West Bengal, India

Declaration

I hereby declare that the work which is being presented in the thesis entitled "**Towards a Smart Power Grid through Optimum Location of Control Devices**" in partial fulfillment of the requirements for the award of the degree of ***DOCTOR OF PHILOSOPHY*** (PhD) submitted to the Department of Electrical Engineering of **Jadavpur University, Kolkata**, **India** is an authentic record of my own work under the supervision of **Prof. Swapan Kumar Goswami**, Department of Electrical Engineering. I have not submitted the matter embodied in this thesis for the award of any other degree or diploma of the university or any other institute.

_____

Date: **Jayanti Sarker (Bhattacharjee)**

Contents

List of Tables

List of Figures

Chapter 1:
Introduction

Summary: *This chapter presents a brief discussion about the present thesis. Brief descriptions on power grid along with its monitoring and control devices are presented here. In addition, the idea about smart grid is also presented. The transformation of power grid to smart grid by using different monitoring and control devices is also highlighted. Finally, the objective of the present work is presented along with outcome of the research work in the context of smart grid.*

1.1. Introduction

Since the establishment of the first ever electric supply system in 1882, power system has evolved through different stages of development leading to the formation of today's modern power grids that are huge in dimension and thus really challenging to operate. Though the development of large power grids had both technological and economic justifications, managing large systems became increasingly difficult as maintaining synchronous operation of large AC system is not an easy task in the event of the occurrences of unpredictable faults. As a result large power systems world wide had to face occasional blackouts. The largest blackout had been the blackout of Indian power grid in 2012. The US Northeast blackout of 2003 was reported to be the largest before that. Events records and analysis of some major blackouts have been uploaded in the net by various power systems. Slow measuring systems, not so efficient control devices, failure of expansion of transmission network to keep pace with the increase of load and generation, age old generating facilities, lack of communications etc. have been identified to be the main reasons behind the occurrences of the blackouts. Though technological developments in communication and computing abilities were already there and developments of efficient devices for power system operation and control had been reported for quite a long time, their application in real life power systems was found to be miserably very poor and therefore, power grids were found to be rather old and fragile. It has been felt that better maintenance of the system alone can not help to get out of the situation. The grid rather has to be modernized. Woolenburg for the first time in his paper in 2006 coined the term 'Smart grid' to help visualize the power grid of the future.

1.2. Motive behind transformation of power grid to smart grid

Since the year 2005 the interest on smart grid is growing up. The de-carbonisation of power system at a realistic cost was a great challenge to power engineers. Smart grid concept aims to achieve this through the incorporation of the renewables. Besides, the following reasons strengthen the interest on smart grid.

1.2.1. Ageing assets and lack of circuit capacity

With rapid growth of electrical demand, the existing power system is required to expand and new equipments are to be installed. Besides, depreciation cost of old equipments is very high. In addition, the increased demand forces power system to use renewable generation. But the existing transmission and distribution capacity limits the implementation of these non-conventional generations and thereby further extension of existing grid is also interrupted.

1.2.2. Thermal constraints

It is very much related with current flowing through transmission line. Power flow beyond its rated capacity causes the over-heating of the conductor and may damage the insulation and there by increases possibilities of fault. So, it is very essential to modernize existing power system.

1.2.3. Operational constraints

There are standard voltage and frequency limits for stable operation of any power system. The violation of these limits may cause malfunction of the customer equipment, sudden trip of the line, insulation failure etc.

In addition, the lack of conventional resources such as fossil fuel has lead the power system to go to the non-conventional generation. But the major problems of these non-conventional generations are unpredictable and variable output. So it is necessary to integrate energy storage in the power system to supply demand during low output period. Again, this storage reduces the use of reserve power plant dynamic frequency response due to load changes and stability of the system is also improved.

1.2.4. Security of supply

The latest industry having critical loads demands stricter power quality as well as reliability. In traditional power system it was usual practice to install additional redundant circuit. Besides, the faulty section was normally disconnected and its restoration was very time consuming. In smart grid, post-fault reconfiguration is adopted and it leads to overcome high expense of multiple redundant circuits.

1.3. Concept of smart grid

There are several definitions of smart grid, found in open literature. These definitions have set the functions of smart grid in different aspects of power system. The Smart Grid concept combines a number of technologies, end-user solutions and addresses a number of policy and regulatory drives. It does not have a single clear definition.

(i) The European Technology Platform [1] defines the Smart Grid as:

"A SmartGrid is an electricity network that can intelligently integrate the actions of all users connected to it – generators, consumers and those that do both – in order to efficiently deliver sustainable, economic and secure electricity supplies."

(ii) According to the US Department of Energy [2]:

"A smart grid uses digital technology to improve reliability, security, and efficiency (both economic and energy) of the electric system from large generation, through the delivery systems to electricity consumers and a growing number of distributed-generation and storage resources."

(iii) In Smarter Grids: The Opportunity [3], the Smart Grid is defined as:

"A smart grid uses sensing, embedded processing and digital communications to enable the electricity grid to be observable (able to be measured and visualised), controllable (able to manipulated and optimised), automated (able to adapt and self-heal), fully integrated (fully interoperable with existing systems and with the capacity to incorporate a diverse set of energy sources)."

(iv) The literature [3–5] suggests the following attributes of the Smart Grid:

- It enables demand response and demand side management through the integration of smart meters, smart appliances and consumer loads, micro-generation, and electricity storage (electric vehicles) and by providing customers with information related to energy use and prices. It is anticipated that customers will be provided with information and incentives to modify their consumption pattern to overcome some of the constraints in the power system.
- It accommodates and facilitates all renewable energy sources, distributed generation, residential micro-generation, and storage options, thus reducing the environmental impact.
- It provides improved reliability, improved economics, and improved efficiency along with improved environment by reducing operational cost and increasing employee safety.

1.4. Evolution of Indian Power Grid

Indian Power Grid is also going through evolution like many other in the world. Our country has plenty of natural resources such as coal and water from which electrical energy is generated. The first 1360 MW hydro power plant in India was installed in 1890's in Darjeeling. After the enactment of Electricity Act in 1948, the entire power sector was governed by State Electricity Boards (SEBs). In 1975, Central Government took the responsibilities through Central Public Sector Undertakings (NTPC, etc.) in Generation and Transmission. In 1989, a large company Power Grid Corporation of India was formed for further development of transmission network and grid. In 1990, first HVDC bi-polar line was made operative. To cater effective operation and planning the whole power grid is divided into five regions namely Northern (NR), Eastern(ER), Western (WR), North-Eastern (NER) and South (SR) regions. In 1991, a connection is made between NER and ER. After that WR and ER-NER are inter-connected in 2003 followed by interconnection between NR and ER in 2006. Thereby a central grid is formed by those 4 regions NR, ER, WR and NER operating at common frequency. At last, SR is interconnected synchronously with central grid in 2013. Thus 'One nation' - 'One Grid'- 'One Frequency' is formed. Now, this One Grid is consisting of 1,39,708 circuit kms of transmission lines operating at 800/765kV, 400kV, 220kV, 132kV EHVAC and more than 500kV HVDC levels. In addition, 220 sub-

stations are associated with the Grid. According to data as on 30th April, 2017, the grid has transmission capacity of 2, 92,543 MVA. Total power transfer capacity of latest Power Grid is 75,050 MW. The present generating capacity of India is about 200GW (as on 2012). 64.6% of these generations is coming from thermal plant, 22.6% from hydro plant, 12% through renewable resources such as wind and rest from biomass and solar. But wind/solar generation are present at remote areas from which it is not possible to integrate high capacity transmission system with this generation. Thereby Indian power system has to meet different obstacles like poor distribution network, high power demand, poor asset management, high AT&C losses etc. That's why 'Smart Grid' concept is very relevant in this context.

1.5. Smart Grid initiatives in India

India Smart Grid Forum (ISGF) has been formed by the ministry of power. According to ministry of Power Government of India, a Smart Grid can be defined as an interconnected system of information, communication technologies and control systems used to interact with automation and business processes across the entire power sector encompassing electricity generation, transmission, distribution and the consumer. The idea of a Smart Grid is to make the existing grid infrastructure as efficient and robust as possible, through the use of intelligence and automation, by encouraging active supply and demand-side participation and by promoting innovative business practices and regulatory environments that provide incentives for efficient production, transmission, distribution and consumption of electricity across the entire value chain [6].

- The function of ISGF is to advise government a policies and programs for promotion of Smart Grid in India. ISGF has formed 8 working groups(WG) on different aspects of Smart Grid. These are:
- WG1: Grid modernization and Smart cities
- WG2: IOT, Smart metering, AI and Analysis
- WG3: Digital Architecture and Cyber Security
- WG4: Policy, Regulations and Business models
- WG5: Renewable and Microgrids
- WG6: Flexibility and Electric mobility
- WG7: Smart Gas
- WG8: Smart water.

The term Smart grid implies [7] a total transformation of existing power grid to a clean and intelligent grid with the incorporation of digital and communication technology along with the non-polluting power generation technology. It even encompasses the intelligent use and management of Gas and Water supply system. In recent years, technical publishing houses have launched new journals on Smart grid technology. The subjects covered by these journals also reveal that Smart grid is being seen as a multidisciplinary area. The basic infrastructure of Smart grid is undoubtedly the electrical power grid, but it requires participation from other disciplines as well in order to achieve the envisaged transformation. Researches reported on Smart grid therefore can be founded to be subscribed by researches and professionals from various disciplines. However, in the context of Indian power system, a lot of works are yet to be done before the digital and communication technologies may be incorporated into the power grid. Though projects on Smart cities, Smart metering are being reported, the Indian power grid is being reported to have a T&D losses of as high as 24%.. This clearly indicates that, our grid needs to be transformed in terms of incorporation of transmission-distribution facilities and with the facilities for efficient control of the system.

Energy Efficiency Services Ltd (EESL), the energy services company under the Union Ministry of Power, has announced the completion of the project to replace 50,000 conventional electricity meters with smart meters in the New Delhi Municipal Council (NDMC) area. India is making rapid strides in providing universal access to affordable power. The Centre is accelerating the adoption of smart meters to ensure efficient management of electricity by checking data-entry errors, billing inefficiencies, and cutting the costs of manual meter reading through web-based monitoring system [8].

Besides this, for the last few decades, SCADA was used as measuring technique. But SCADA does not capture sub-seconds changes; samples measurement once in 5-10 seconds. In this context, Wide Area Monitoring System (WAMS) samples many times in one second. So, as phasor measurement Unit (PMU) has also incorporated as a measuring device. Introduction of WAMS technology in Western Region would help in ensuring grid security and safety. In view of this, a wide area measurement system (WAMS) project based on Phasor Measurement Units has been initiated by Power Grid Corporation. This project is aimed at developing algorithms for optimal placement of PMUs and installation of about 25-30 PMUs in western grid [9].

1.6. Motivation behind the present research

The term 'Smart Grid' has become very popular to the power system community. The idea was to make the power grid reliable, flexible, efficient, cost effective and communicative (and sustainable or, in other word, making the power grid smart). While making the power grid smart requires to make it IT enabled, it may be understood that incorporation of efficient control devices is the primary precondition of a power grid being transformed into a Smart grid. In this thesis, therefore, the problem of optimal placement of different control devices has been dealt with. Efficient control of power grid requires efficient measurement of system state. Thus, the problem of placement of measuring units has also been studied. The placement of the control and measurement devices has to be done in an optimal way so as to ensure cost effectiveness and reliability of operation.

1.7. Objective of the thesis

The main objective of this thesis is to find out optimal locations of different FACTS devices for improved power system performance. This strategy includes reduction in system loss, voltage profile improvement, transmission capacity increment, and operational cost savings of the network. As this optimization method provides voltage support to the system, it increases system stability during fault condition. In addition, various FACTS devices equipped at different optimal locations reduce the chances of occurrences of fault in the modern network having critical loads. In this context some soft computing techniques are used for optimal power flow (OPF) based single objective scheme. In this regards, different penalties are also employed for violation of different operating constraints.

1.8. Outline of the thesis

The route map of the present thesis is outlined as follows:

Chapter1 delivers the basic knowledge about Smart Grid. It also describes the effect of smart grid technologies in modern power system. In addition, this chapter describes briefly about different smart mechanisms along with smart devices in Indian Power Grid.

Chapter2 gives an overview on transmission loss reduction by optimal allocation of Unified Power Flow Controller (UPFC). In this context, the incremental effect of UPFC number in transmission lines is also analyzed. In addition the optimal size of DC link and optimal range of UPFC along with effective operational cost are also highlighted.

Chapter 3 describes the distribution line loss reduction by optimal placement of Unified Power Quality Conditioner (UPQC) in different test distribution systems. In addition, change in cost savings and reductions in load disturbance with increase in UPQC number are also discussed.

Chapter 4 gives an idea about proposed device called Hybrid Dynamic Voltage Restorer (H-DVR) and its effects on distribution system. This chapter also reviews the comparison between H-DVR and DVR by using different soft computing techniques in terms of cost and performance.

Chapter 5 identifies the necessity of Phasor Monitoring Unit (PMU) and Power Flow Meter (PFM) in transmission system. It proposes different alternative objectives leading to single objective optimization formulations. This proposed scheme is solved by Cuckoo Optimization Algorithm (COA) to get full observable power system network by using minimum number of PMU and PFM.

At last, in this thesis, chapter 6 concludes the thesis and reports the drawbacks of the proposed methods. In addition, the future scope of present research work is also highlighted.

The appendix and references are given at the end of thesis. The real time data of Indian NER Grid and different standard test system taken here, are presented at the appendix. Besides brief descriptions of GSA and COA are presented in Appendix along with sag computation strategy.

Chapter 2:

Optimal Placement of UPFC for Improved Active Power and Voltage Control

Summary: *This chapter presents a new method for transmission line loss reduction and the cost reduction by using Unified Power Flow Controller (UPFC). This chapter also furnishes the results for optimal allocation of multiple UPFC devices in the test network. In addition, this chapter also focuses on optimal sizing of DC link and operating range of respective UPFC devices along with the operational cost. Gravitational Search Algorithm (GSA) has been applied to solve optimal power flow problem in the presence of multiple UPFC devices. Besides, the performance of GSA is compared for accuracy and convergence characteristics with heuristic search techniques like Biogeography-Based Optimization (BBO), Stud Genetic Algorithm (StudGA) , Genetic Algorithm (GA), Ant Colony optimization (ACO), Probability-Based Incremental Learning (PBIL), on the different cases of standard test systems and real life power system.*

2.1. Introduction

Due to increase in power demand today's power system is going through rapid changes. That's why it is a great challenge to electrical power engineers to maintain a balance between generation and demand along with stability in the system [10] in deregulated power market. In the present competitive power market, it is becoming very essential to open the unexplored potential of transmission system. But the cost of erection is the main factor which limits the transmission line expansion. In this context, flexible ac transmission system (FACTS) may be the remedy as they can direct the power in the desired path and control active and reactive powers in the network. Besides, these FACTS devices can have the potential to maintain the bus voltage at required level and thereby controlling the system in secured and economic way [11].

The development of Flexible AC Transmission (FACTS) controllers has been initiated by Electric Power Research Institute (EPRI) in which power flow is dynamically controlled by various power electronic devices [12]. Among a variety of FACTS devices, Unified Power Flow Controller (UPFC) is the most versatile one. The concept of UPFC has been established by L. Gyugyi [13]. From operating principle, UPFC functions in multi-dimensions such as series compensation mode, shunt compensation mode and phase shifting [14]. UPFC has a capability to simultaneously control the active and reactive power or voltage [15-16]. Without violating the operating limits UPFC regulates all three key power system variables simultaneously or any combination of them.

Though various authors have investigated the benefits of UPFC placement on several systems [13-15], the high cost involved is the major hurdle in optimal allocation problem of UPFC in power system. Since the last few years a number of publications have appeared in the open literature to find suitable location of UPFC [15-17]. But very few could be found dealing with the multiple UPFC devices placed in their optimal locations. In addition, in the present chapter, the optimal sizing of dc link capacitors and optimal operating ranges of UPFCs are also included which are not found in open literature.

The present chapter uses a heuristic method based on Gravitational Search Algorithm (GSA) [18] to find optimal number and location of UPFC considering generation cost and power system losses. The rest of the present chapter is organized as follows. The impact of UPFC on the transmission line along with its model description is detailed in section 2.2. After that UPFC placement problem is formulated in section 2.3. Next, the optimal placement method of UPFC is briefed in section 2.4. The proposed UPFC placement algorithm has been tested on several test and real life power systems and some of the results are produced in section 2.5 to establish

the computational ability and robustness of the method. In section 2.6, the influence of optimal operating ranges and dc link of respective UPFC devices on operating cost of UPFCs have been tested on several test and real life networks. In section 2.6, both the cost of UPFC and generation cost have been incorporated, whereas in section 2.5 only generation-cost has been computed. Finally the last section 2.6 concludes the chapter.

2.2. Impact of UPFC on transmission line

The basic operating principles of UPFC are already established in open literature. A schematic representation of voltage source converter-based UPFC is shown in Fig.2.1.

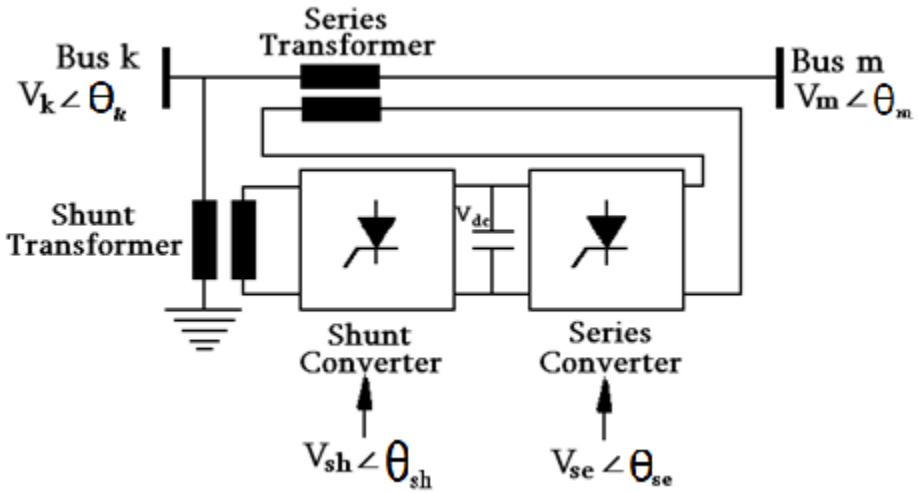

Fig.2.1. UPFC Model.

The UPFC has two self-commutating converters, DC storage capacitor. This DC capacitor functions as an energy storage element and is connected to both the converters. One converter is connected in shunt to the sending end node k through shunt coupling transformer and the second converter is associated with ac system through series coupling transformer between nodes k and m. Due to presence of lossless UPFC and coupling transformers [19], the active powers injected into PV bus k and extracted from PQ bus m are equal in magnitude. The shunt converter generates or absorbs the real power required by series converter at the dc terminals. The voltage stability can be maintained by shunt reactive compensation, which is independent.

From the equivalent circuit of UPFC as shown in Fig.2.2, the ideal shunt voltage source V_{sh} is represented as: $V_{sh} = V_{sh} \angle \theta_{sh}$ and the series voltage source V_{se} is represented as: $V_{se} = V_{se} \angle \theta_{se}$, where V_{sh}, V_{se} are controllable magnitudes in the ranges of $\left(V_{sh,\min} \le V_{sh} \angle V_{sh,\max}\right)$ and $\left(V_{se,\min} \le V_{se} \angle V_{se,\max}\right)$ and θ_{sh}, θ_{se} are controllable angles in the ranges of $\left(0 \le \theta_{sh} \angle 2\pi\right)$ and $\left(0 \le \theta_{se} \angle 2\pi\right)$ respectively.

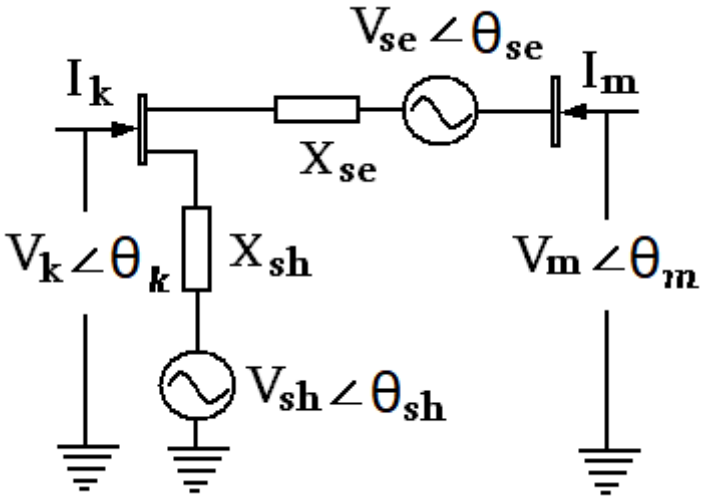

Fig.2.2. Equivalent Circuit of UPFC.

Based on the equivalent circuit shown in Fig.2.2, the active and reactive power equations are:

at node k:

$$\begin{aligned} P_k &= V_k^2 G_{kk} + V_k V_m \left(G_{km}\cos(\theta_k - \theta_m) + B_{km}\sin(\theta_k - \theta_m)\right) \\ &+ V_k V_{se} \left(G_{km}\cos(\theta_k - \theta_{se}) + B_{km}\sin(\theta_k - \theta_{se})\right) \\ &+ V_k V_{sh} \left(G_{sh}\cos(\theta_k - \theta_{sh}) + B_{sh}\sin(\theta_k - \theta_{sh})\right) \end{aligned} \quad (2.1)$$

$$\begin{aligned} Q_k &= -V_k^2 B_{kk} + V_k V_m \left(G_{km}\sin(\theta_k - \theta_m) - B_{km}\cos(\theta_k - \theta_m)\right) \\ &+ V_k V_{se} \left(G_{km}\sin(\theta_k - \theta_{se}) - B_{km}\cos(\theta_k - \theta_{se})\right) \\ &+ V_k V_{sh} \left(G_{sh}\sin(\theta_k - \theta_{sh}) - B_{sh}\cos(\theta_k - \theta_{sh})\right) \end{aligned} \quad (2.2)$$

At node m:

$$\begin{aligned} P_m &= V_m^2 G_{mm} + V_m V_k \left(G_{mk}\cos(\theta_m - \theta_k) + B_{mk}\sin(\theta_m - \theta_k)\right) \\ &+ V_m V_{se} \left(G_{mm}\cos(\theta_m - \theta_{se}) + B_{mm}\sin(\theta_m - \theta_{se})\right) \end{aligned} \quad (2.3)$$

$$\begin{aligned} Q_m &= -V_m^2 B_{mm} + V_m V_k \left(G_{mk}\sin(\theta_m - \theta_k) - B_{mk}\cos(\theta_m - \theta_k)\right) \\ &+ V_m V_{se} \left(G_{mm}\sin(\theta_m - \theta_{se}) - B_{mm}\cos(\theta_m - \theta_{se})\right) \end{aligned} \quad (2.4)$$

Series converter:

$$P_{se} = V_{se}^2 G_{mm} + V_{se}V_k \left(G_{km}\cos\left(\theta_{se} - \theta_k\right) + B_{km}\sin\left(\theta_{se} - \theta_k\right)\right) + V_{se}V_m \left(G_{mm}\cos\left(\theta_{se} - \theta_m\right) + B_{mm}\sin\left(\theta_{se} - \theta_m\right)\right) \quad (2.5)$$

$$Q_{se} = -V_{se}^2 B_{mm} + V_{se}V_k \left(G_{km}\sin\left(\theta_{se} - \theta_k\right) - B_{km}\cos\left(\theta_{se} - \theta_k\right)\right) + V_{se}V_m \left(G_{mm}\sin\left(\theta_{se} - \theta_m\right) - B_{mm}\cos\left(\theta_{se} - \theta_m\right)\right) \quad (2.6)$$

Shunt converter:

$$P_{sh} = -V_{sh}^2 G_{sh} + V_{sh}V_k \left(G_{sh}\cos\left(\theta_{sh} - \theta_k\right) + B_{sh}\sin\left(\theta_{sh} - \theta_k\right)\right) \quad (2.7)$$

$$Q_{sh} = V_{sh}^2 B_{sh} + V_{sh}V_k \left(G_{sh}\sin\left(\theta_{sh} - \theta_k\right) - B_{sh}\cos\left(\theta_{sh} - \theta_k\right)\right) \quad (2.8)$$

Where, $Y_{kk} = G_{kk} + jB_{kk} = Z_{se}^{-1} + Z_{sh}^{-1}$ (2.9)

$$Y_{mm} = G_{mm} + jB_{mm} = Z_{se}^{-1} \quad (2.10)$$

$$Y_{km} = Y_{mk} = G_{km} + jB_{km} = -Z_{se}^{-1} \quad (2.11)$$

$$Y_{sh} = G_{sh} + jB_{sh} = -Z_{sh}^{-1} \quad (2.12)$$

The active power supplied to the shunt converter, P_{sh}, must be equal to the active power demanded by the series converter, P_{se} [20], i.e,

$$P_{sh} + P_{se} = 0 \quad (2.13)$$

A number of research publications have dealt with the handling of UPFC equations in the power flow problem. Nabavi and Iravani proposed a way to handle UPFC with power flow algorithms by connecting the UPFC in the transmission line where sending end is represented as a PV bus and receiving end is represented as a PQ bus [21]. The active and reactive power loads in the PQ bus and the voltage magnitude at the PV bus are set at the values to be controlled by UPFC. The UPFC parameters are computed after the load flow converged [22].

2.3. Formulation of the UPFC placement problem

By optimal power flow [23-24] we mean an operating condition in which the power flow in an electrical system occurs to optimize one or more objectives while satisfying the specified operating limits of the system. In this chapter the objective functions to be optimized [25] are: (i) minimization of the operating cost,

(ii) minimization of transmission loss

Here the objective functions: (i) operating cost is expressed in term of fuel cost of the thermal generators as

$$\sum_{i=1}^{N_G} C_i\left(P_{G_i}\right) = \sum_{i=1}^{N_G}\left(a_i + b_i P_{G_i} + C_i P_{G_i}^2\right) \tag{2.14}$$

And (ii) the transmission loss is represented as:

$$\begin{aligned} P_L = & \sum_t \left(real\left(yline_t\right)\left(V_{k_t}^{\ 2} + V_{m_t}^{\ 2}\right)\right) \\ & - \left(V_{k_t} V_{m_t} abs\left(yline_t\right)\cos\left(\theta_{k_t} - \theta_{m_t} - \theta\left(yline_m\right)\right)\right) \\ & - \left(V_{m_t} V_{k_t} abs\left(yline_t\right)\cos\left(\theta_{m_t} - \theta_{k_t} - \theta\left(yline_m\right)\right)\right) \end{aligned} \tag{2.15}$$

Subject to the following constraints:

2.3.1. Equality constraints

The equality constraints consist of active and reactive power balance of load buses and active power balance of generator buses.

For each PQ bus, active and reactive power balance are represented by equations (2.16) and (2.17) respectively as

$$P_{G_i} - P_{D_i} - \sum_{m=1}^{n} |V_i||V_m||Y_{im}|\cos\left(\theta_{im} + \theta_m - \theta_i\right) = 0 \tag{2.16}$$

$$Q_{G_i} - Q_{D_i} + \sum_{m=1}^{n} |V_i||V_m||Y_{im}|\sin\left(\theta_{im} + \theta_m - \theta_i\right) = 0 \tag{2.17}$$

For each PV bus the active power balance is represented by equations (2.18) as

$$P_{G_i} - P_{D_i} - \sum_{m=1}^{n} |V_i||V_m||Y_{im}|\cos\left(\theta_{im} + \theta_m - \theta_i\right) = 0 \tag{2.18}$$

and for power system considered, the active power balance can be represented by equation (2.19) as

$$\sum_{i=1}^{N_G} P_{G_i} - P_D - P_L = 0 \tag{2.19}$$

Where N_G is the number of generator buses and n is the total number of buses, P_D is the system load-demand, P_L is system transmission loss. t is the transmission line number; V_{k_t}, V_{m_t} are voltage magnitudes of sending end and receiving end buses respectively connected with t^{th} transmission line; θ_{k_t}, θ_{m_t} are voltage

angles of sending end and receiving end buses respectively connected with t^{th} transmission line; $yline_t$ is the admittance of the t^{th} transmission line. a_i, b_i, c_i are cost-coefficients of the respective generators.

2.3.2. Inequality constraints

The inequality constraints of the OPF may be classified as,

- **Active and reactive power limit:**

. The maximum and minimum active power and reactive power of generators constitute the inequality constraints and these are given by

$$P_{G_i}^{\min} \le P_{G_i} \le P_{G_i}^{\max} \tag{2.20}$$

$$Q_{G_i}^{\min} \le Q_{G_i} \le Q_{G_i}^{\max} \tag{2.21}$$

- **Voltage limit :**

To maintain the quality of electrical service and system security, bus voltages usually have maximum and minimum magnitudes and this is expressed as follows

$$V_i^{\min} \le V_i \le V_i^{\max} \tag{2.22}$$

Voltage magnitudes of series and shunt converters limits are represented respectively as:

$$\left(V_{se,\min} \le V_{se} \le V_{se,\max}\right) \text{ and } \left(V_{sh,\min} \le V_{sh} \le V_{sh,\max}\right) \tag{2.23}$$

Voltage angles of series and shunt converters limits are represented respectively as:

$$\left(0 \le \theta_{se} \le 2\pi\right) \text{ and } \left(0 \le \theta_{sh} \le 2\pi\right) \tag{2.24}$$

The limit of active power flow through the transmission line connected with UPFC is given as:

$$\left(P_{mk} \le P_{mk,\max}\right) \tag{2.25}$$

2.4. Optimal placement of UPFC

Solution of the UPFC placement problem involves determination of optimal position of UPFC, which ultimately affects the reduction in real power loss and operating cost. The presence of five parameters for each UPFC along with the Generator active power outputs, Generator terminal voltages, tap positions of various reactive power controllers makes UPFC optimal placement problem very difficult to solve by conventional optimization techniques. Though different robust optimization techniques [26] can be used to solve the placement problem [27], only Gravitational Search technique [28] has been adopted in this chapter because of its fast convergence characteristics. Besides, different optimization techniques have been implemented to

compare with Gravitational Search technique. Gravitational Search algorithm is described in detail in Appendix A.1. GSA technique has been applied to several ongoing power system problems such as Post-Outage Bus Voltage Magnitude Calculations [29], combined economic and emission dispatch problems of power systems [30], Optimal power flow using gravitational search algorithm [31], Parameters identification of hydraulic turbine governing system [32], optimal static state estimation [33], multi –objective economic emission load dispatch solution [34], solution of unit commitment problem [35]. The procedural steps of UPFC placement problem by obeying GSA are given below:

(i) The gravitational constant and the population size N are selected randomly.

(ii) The active power generations, transmission lines to be connected with UPFC, active power flows through those transmission lines connected with UPFC, UPFC parameters settings are taken as dimensions in this chapter and it is denoted by n.

(iii) The upper limits and the lower limits of the optimization variables are provided by using equations (2.20), (2.21), (2.23), (2.24) and (2.25).

(iv)The cost of active power generations and loss of transmission lines by using equations (2.14) and (2.15) are taken as solution vectors.

(v) Check the voltage magnitudes by using equation (2.22).

(vi) If the voltage magnitude violates the limit discard the initial set of agents and go to step (iii) in the next iteration. This process continues until all the constraints are satisfied using equations (2.16) to (2.25).

(vii) Follow the steps (vii-xiii) given in section A.1.2.

2.5. Application of the proposed method

The proposed method is validated by applying it on a number of test and real life power systems. In this chapter, all the voltages and power quantities are in per unit. Bus voltage magnitude limits are 0.95 to 1.1 p.u. Tap setting limits are taken from 0.9 p.u. to 1.1 p.u. In all the test cases the GSA parameters are chosen as follows: gravitational constant, $G_0 = 100$;

User specified constant, $\alpha = 20$;

Number of agents, $N = 25$;

Maximum number of iteration=50 .

The UPFC parameters are taken as follows: [36]

Series reactance of UPFC, $x_{se} = 0.05 p.u$;

Shunt reactance of UPFC, $x_{sh} = 0.05 p.u$;

$$0 \le V_{se} \le 1.0 p.u ; 0 \le V_{sh} \le 1.1 p.u ; 0 \le \theta_{se} \le 2\pi ; 0 \le \theta_{sh} \le 2\pi$$

For each system there are three sections namely, impact of UPFC on voltage profile, influence of UPFC on real power loss and operating cost and the last one is comparative study on different optimization techniques adopted in this chapter. In fact, the optimization problems have been solved by applying BBO, StudGA, ACO and PBIL techniques and comparative results are furnished in respective sections accordingly.

2.5.1. Results for IEEE-14 bus system

The line data, bus data and generator cost data of IEEE-14 bus test transmission system are reported in Appendix A.4.1.

- **Effect of UPFC on voltage profile improvement**

The change in bus voltage magnitudes with the increase in UPFC number for both cost minimization and loss minimization are shown in Table 2.1.

Table 2.1. Generator terminal voltages (p.u.) of IEEE-14 bus system

Bus number	Bus voltage magnitude							
	Cost minimization				Loss minimization			
	Without UPFC	With 1 UPFC	With 2 UPFCs	With 3 UPFCs	Without UPFC	With 1 UPFC	With 2 UPFCs	With 3 UPFCs
1	1.06	1.06	1.06	1.06	1.06	1.06	1.06	1.06
2	1.045	1.045	1.045	1.045	1.045	1.045	1.045	1.045
3	1.01	1.01	1.01	1.01	1.01	1.01	1.01	1.01
4	0.9997	1	1.0015	1.0024	0.9997	1	1	1.0014
5	1.0052	1.0096	1.0101	1.0301	1.0052	1.0087	1.0112	1.0308
6	1.07	1.07	1.07	1.07	1.07	1.07	1.07	1.07
7	1	1.0094	1.0121	1.0466	1	1.0116	1.0118	1.0466
8	1.09	1.09	1.09	1.09	1.09	1.09	1.09	1.09
9	0.999	1.0036	1.009	1.0347	0.9998	1.0086	1.0091	1.0347
10	1	1	1.0084	1.0303	1	1.0087	1.0087	1.0303
11	1.0298	1.0298	1.045	1.0522	1.0243	1.0336	1.045	1.0522
12	1.0448	1.0453	1.0457	1.0478	1.045	1.0455	1.046	1.0478
13	1.0272	1.0354	1.0362	1.0399	1.0281	1.0357	1.0363	1.0399
14	0.9778	0.991	0.9945	1.0111	0.9796	0.9942	0.9943	1.0111

From Table 2.1 it is obvious that with the installation of single UPFC on optimal position in test system, the minimum and maximum load bus voltages increase from 0.9778 p.u to 0.991p.u and 1.0448p.u to 1.0453p.u

respectively under cost minimization and under loss minimization those vary from 0.9796 p.u. to 0.9942 p.u.and 1.045 p.u. to 1.0455 p.u. respectively. Table 2.1 also shows that with the installation of second UPFC on its optimal position in test network, those minimum and maximum load voltages change to 0.9945 p.u and 1.0457 p.u respectively under cost minimization and under loss minimization those became 0.9943 p.u. and 1.046 p.u. respectively. From Table 2.1 it is also shown that the third UPFC positioned optimally in IEEE 14 bus test system increases the minimum and maximum load bus voltages to 1.0024 p.u and 1.0522 p.u. respectively under cost minimization and under loss minimization those change to 1.0014 p.u. and 1.0522 p.u respectively. For a better visualization the system voltage profiles are shown in Fig 2.3 and Fig 2.4 for cost minimization and loss minimization respectively.

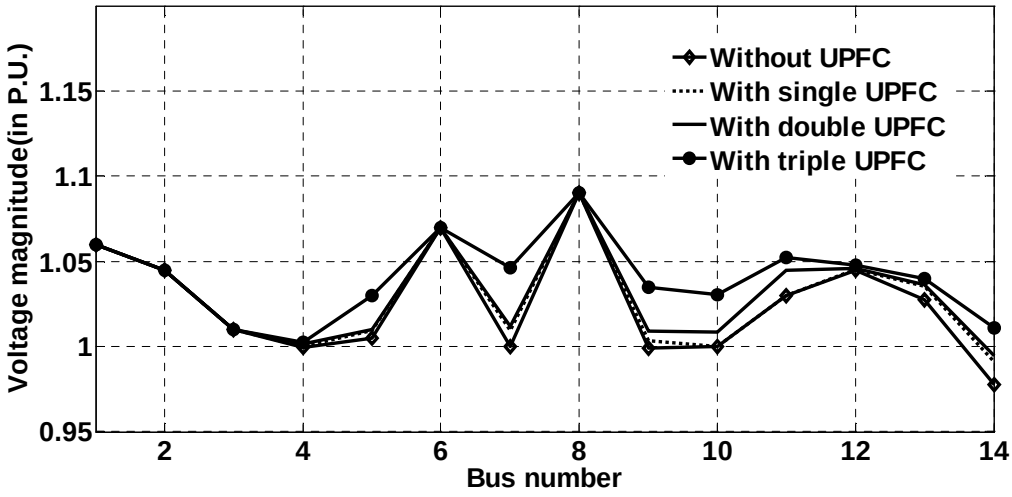

Fig.2.3. Voltage profile for cost minimization of IEEE-14 bus test system

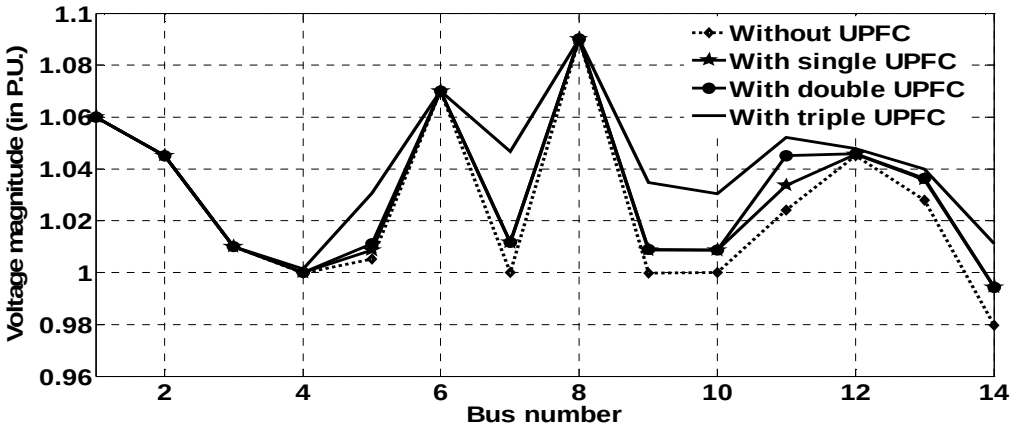

Fig.2.4. Voltage profile for loss minimization of IEEE-14 bus test system

- **Influence of UPFC on real power loss and operating cost**

The variation in real power loss along with operating cost for different optimal locations of UPFCs in IEEE-14 bus test system is furnished in Table 2.2.

Table 2.2. Optimal location of UPFC, real power flow, line loss and cost in IEEE-14 bus test system

Optimized parameter	Control Variables	Number of UPFCs			
		0	1	2	3
Cost minimization	Optimal locations of UPFC (k-m)		10-11	4-5,10-11	4-5,7-9,12-13
	Active power flow in line connected with UPFC (MW)		-20	-20, -20	62.89,24.67,7.58
	Real power loss (MW)	18.18	15.61	15.5	12.68
	Dispatch cost ($/hr)	5,629.50	2940.6	2937	2843.5
Loss minimization	Optimal locations of UPFC (k-m)		4-5	4-5,10-11	4-5,7-9,10-11
	Active power flow in line connected with UPFC (MW)		-23.77	-24.35,23.77	66.22,26.69,3.63
	Real power loss (MW)	18.07	14.47	13.74	12.15
	Dispatch cost ($/hr)	5,749.50	3533.50	3523.70	3482.8

From Table 2.2 it is shown that during cost minimization operational cost is decreased from 5,629.50 $/hr to 2940.6$/hr and transmission line loss is reduced from 18.18 MW to 15.61 MW by installing single UPFC in its optimal position. Table 2.2 also shows that the addition of another UPFC in IEEE14 bus test system reduces cost and loss further to 2937 $/hr and 15.5 MW respectively. From Table 2.2 it is also noticed that the further reduction in loss and cost are achieved by adding third UPFC in IEEE14 bus test system and they are 12.68 MW and 2843.5$/hr respectively.

Again Table 2.2 shows that during loss minimization operational cost is reduced from 5,749.50 $/hr to 3533.50 $/hr and transmission line loss is changed from 18.07 MW to 14.47 MW by placing single UPFC in its optimal position. Table 2.2 also depicts that the addition of second UPFC in IEEE14 bus test system reduces cost slightly to 3523.70 $/hr and loss further to 13.74 MW respectively. Besides, from Table 2.2 it is also noticed that the further reduction in loss and cost are achieved by adding optimally third UPFC in IEEE14 bus test system and they are 12.15 MW and 3482.8 $/hr respectively.

- **Comparison of performance of different optimization method in solving the UPFC placement**

The comparative results obtained by different soft computing techniques for IEEE 14 bus test system are reported in Table 2.3. The number of iterations needed by different methods is reported in Table 2.4. The convergence characteristics for four cases are shown in Fig 2.5, Fig 2.6, Fig 2.7 and Fig 2.8.

Table2.3. Comparison of the performance of different techniques in IEEE-14 bus test system

Parameter	Control Variables	With GSA	With BBO	With StudGA	With GA	With ACO	With PBIL
Cost minimization with single UPFC	Optimal locations of UPFC (k-m)	10-11	10-11	10-11	10-11	10-11	10-11
	Active power flow in line connected with UPFC (MW)	-20	-20	-20	-20	-20	-20
	Real power loss (MW)	15.61	15.6	15.61	15.61	15.61	15.61
	Dispatch cost ($/hr)	2940.6	2941	2940.6	2940.6	2940.6	2940.6
Loss minimization with single UPFC	Optimal locations of UPFC (k-m)	4-5	4-5	4-5	4-5	4-5	4-5
	Active power flow in line connected with UPFC (MW)	-23.77	-23.8	-23.77	-23.77	-23.77	-23.77
	Real power loss (MW)	14.47	14.5	14.47	14.47	14.47	14.47
	Dispatch cost ($/hr)	3533.5	3534	3533.5	3533.5	3533.5	3533.5

Parameter	Control Variables	With GSA	With BBO	With StudGA	With GA	With ACO	With PBIL
Cost minimization with three UPFC	Optimal locations of UPFC (k-m)	4-5,7-9,12-13	4-5,7-9,12-13	4-5,7-9,12-13	4-5,7-9,12-13	4-5,7-9,12-13	4-5,7-9,12-13
	Active power flow in line connected with UPFC (MW)	62.89,24.67,7.58	62.89,24.67, 7.58	62.89,24.67, 7.58	62.89,24.67, 7.58	62.89,24.67, 7.58	62.89,24.67, 7.58
	Real power loss (MW)	12.68	12.7	12.68	12.68	12.68	12.68
	Dispatch cost ($/hr)	2843.5	2844	2843.5	2843.5	2843.5	2843.5
Loss minimization with three UPFC	Optimal locations of UPFC (k-m)	4-5,7-9,10-11	4-5,7-9,10-11	4-5,7-9,10-11	4-5,7-9,10-11	4-5,7-9,10-11	4-5,7-9,10-11
	Active power flow in line connected with UPFC (MW)	66.22,26.69 ,3.63	66.22,26.69 ,3.63	66.22,26.69 ,3.63	66.22,26.69 ,3.63	66.22,26.69 ,3.63	66.22,26.69 ,3.63
	Real power loss (MW)	12.15	12.2	12.15	12.15	12.15	12.15
	Dispatch cost ($/hr)	3482.8	3483	3482.8	3482.8	3482.8	3482.8

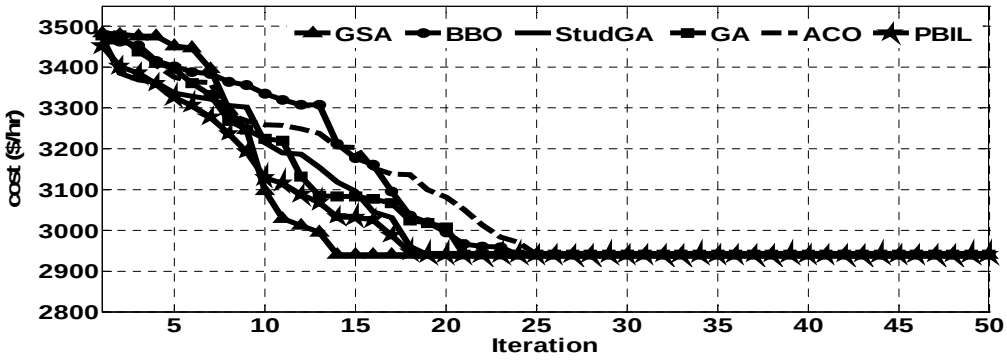

Fig.2.5. Cost minimization with single UPFC of IEEE-14 bus system.

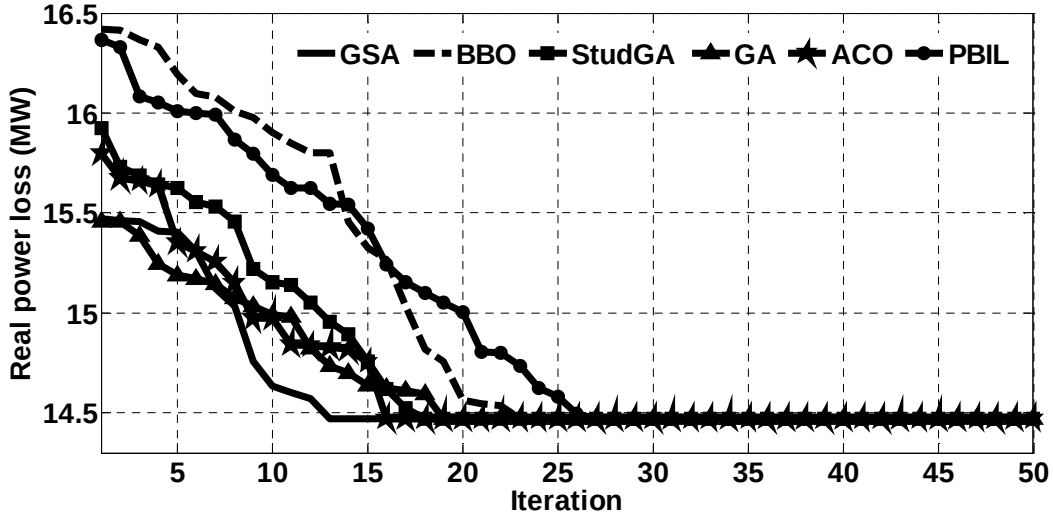

Fig.2.6. Loss minimization with single UPFC of IEEE-14 bus system.

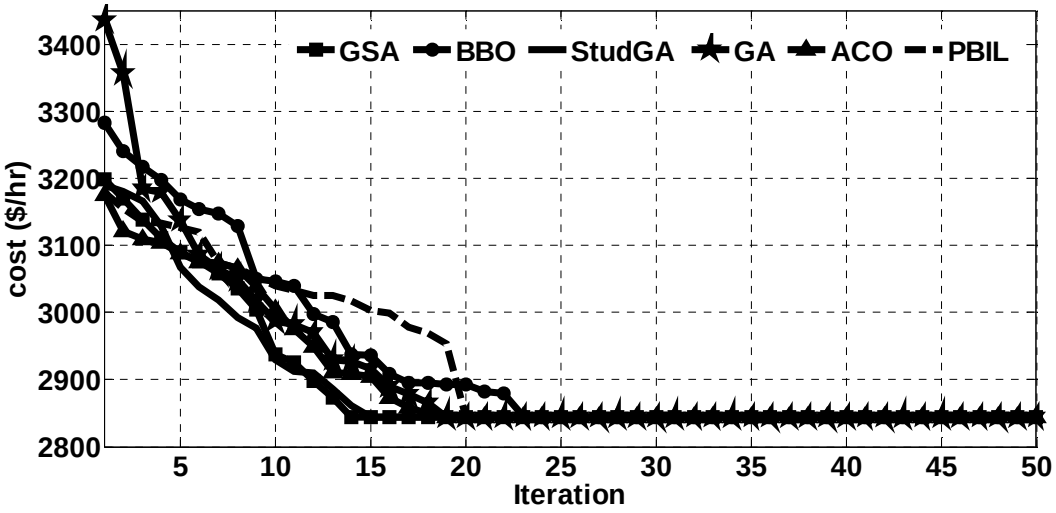

Fig. 2.7. Cost minimization with three UPFC of IEEE-14 bus system.

From Table 2.3 it is shown that the operational cost and transmission loss along with power flow through the line of optimal locations of UPFCs under cost minimization and loss minimization consideration are found to be same in different optimization techniques chosen in this chapter. But, Fig 2.5, Fig 2.6, Fig 2.7 and Fig 2.8 show difference between convergence characteristics of the adopted optimization techniques under cost minimization with single UPFC, loss minimization with single UPFC, cost minimization with three UPFC and loss minimization with three UPFC respectively. For better visualization the number of iterations required for convergence in different optimization techniques for IEEE14 bus system are summarized in Table 2.4.

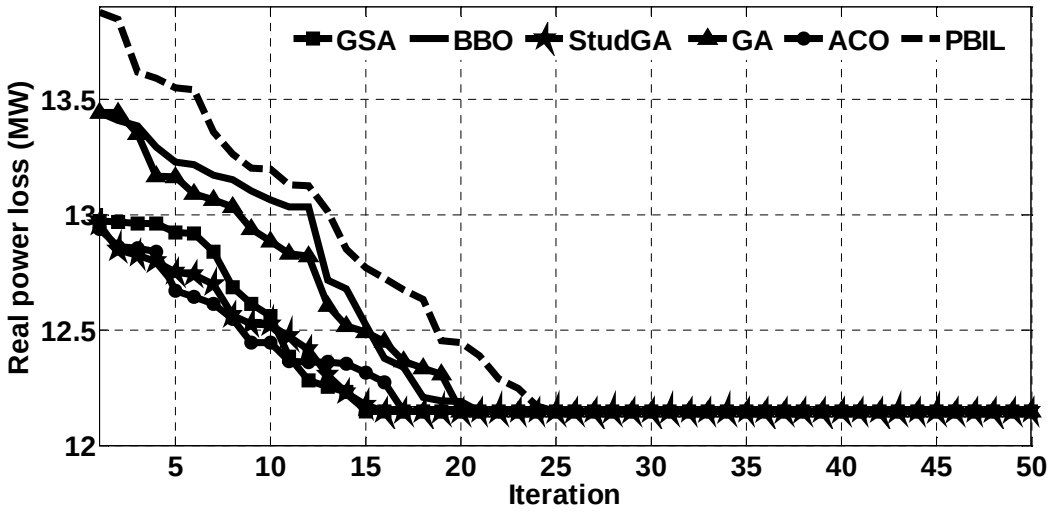

Fig.2.8. Loss minimization with three UPFC of IEEE-14 bus system.

Table 2.4. Number of iterations needed for optimum solution in IEEE-14 bus test system

Minimized parameter	Test system	With GSA	With BBO	With StudGA	With GA	With ACO	With PBIL
Cost minimization with single UPFC	IEEE-14 bus	13	23	18	20	24	18
Loss minimization with single UPFC		12	22	17	18	15	26
Cost minimization with three UPFC		14	24	15	18	18	19
Loss minimization with three UPFC		14	20	15	19	16	24

From Table 2.4, it is shown that number of iterations required in IEEE14 bus test system for cost and loss minimizations by single UPFC installation with GSA technique are found to be 13 and 12 respectively, while the number of iterations for cost and loss minimization by triple UPFCs installation is found to be same, i.e., 14. Table 2.4 also shows that these results found by GSA are minimum among all the different soft computing techniques adopted here in their respective cost/loss minimization by single/triple UPFC installation in IEEE14 bus test system.

2.5.2. Results for IEEE-30 bus system

The line data, bus data and generator cost data of IEEE-30 bus test transmission system are reported in Appendix A.4.2.

- **Effect of UPFC on voltage profile improvement**

The change in bus voltage magnitudes with the increase in UPFC number for both cost minimization and loss minimization are shown in Table 2.5.

Table 2.5. Generator terminal voltages (p.u.) of IEEE-30 bus test system

Bus number	Bus voltage magnitude							
	Cost minimization				Loss minimization			
	Without UPFC	With 1 UPFC	With 2 UPFCs	With 3 UPFCs	Without UPFC	With 1 UPFC	With 2 UPFCs	With 3 UPFCs
1	1.1	1.1	1.1	1.1	1.1	1.1	1.1	1.1
2	1.085	1.085	1.085	1.085	1.085	1.085	1.085	1.085
3	1	1.0724	1.0741	1.0758	1	1.0741	1.0778	1.078
4	1.0081	1.0657	1.0678	1.0696	1.008	1.0678	1.072	1.0723
5	1.052	1.052	1.052	1.052	1.052	1.052	1.052	1.052
6	1.0045	1.0551	1.0572	1.0574	1.0051	1.0572	1.0599	1.0601
7	0.9915	1.0465	1.0477	1.0478	0.9918	1.0477	1.0493	1.0494
8	1.054	1.054	1.054	1.054	1.054	1.054	1.054	1.054
9	1.0397	1.0555	1.0562	1.0655	1.0336	1.0655	1.068	1.0691
10	1.045	1.045	1.0478	1.0661	1.0326	1.0661	1.0695	1.0717
11	1.1	1.1	1.1	1.1	1.1	1.1	1.1	1.1
12	1.0162	1.0233	1.0253	1.0295	1	1.0295	1.0329	1.0337
13	1.063	1.063	1.063	1.063	1.063	1.063	1.063	1.063
14	1.0062	1.0127	1.015	1.0212	1.0047	1.0212	1.0251	1.0256
15	1.0066	1.0126	1.0153	1.0234	1.021	1.0234	1.0277	1.0277
16	1.0208	1.0263	1.0264	1.0377	1.0062	1.0377	1.041	1.045
17	1.0322	1.034	1.036	1.0522	1.0191	1.0522	1.0556	1.0599
18	1.0077	1.0127	1.0135	1.0263	1.0127	1.0263	1.0326	1.0311
19	1.0116	1.016	1.0156	1.0311	1.011	1.0311	1.0362	1.0366
20	1.0191	1.0221	1.0231	1.0391	1.0156	1.0391	1.0441	1.0443
21	1.033	1.0338	1.034	1.0536	1.0204	1.0536	1.057	1.0591
22	1.0203	1.0334	1.0349	1.054	1.021	1.054	1.0574	1.0594
23	1.0062	1.0109	1.0166	1.0274	1.0128	1.0274	1.0313	1.0319
24	1.0143	1.0173	1.0268	1.0412	1.0105	1.0412	1.0446	1.0459
25	1.0143	1.0428	1.0482	1.0581	1.0128	1.0581	1.0604	1.0613
26	0.9966	1.0256	1.0311	1.0411	0.995	1.0411	1.0435	1.0444
27	1.023	1.067	1.0699	1.0768	1.023	1.0768	1.0785	1.0792
28	1.0002	1.0505	1.0527	1.0533	1.0007	1.0533	1.0555	1.0557
29	1.0096	1.048	1.051	1.0581	0.9708	1.0581	1.0597	1.0604
30	1.005	1.0371	1.0401	1.0472	0.9241	1.0472	1.0489	1.0496

From Table 2.5 it is obvious that with the installation of single UPFC at optimal position in test system, the minimum and maximum load bus voltages increase from 0.9915p.u to 1.0109p.u and 1.0397p.u to 1.0724p.u respectively under cost minimization and under loss minimization those vary from 0.9241p.u. to 1.0212p.u.and

1.0336p.u. to 1.0768p.u. respectively. Table 2.5 also shows that with the installation of second UPFC at its optimal position in test network, those minimum and maximum load voltages change to 1.0135p.u and 1.0741p.u respectively under cost minimization and under loss minimization those become 1.0251p.u. and 1.0785p.u. respectively. From Table 2.5 it is also shown that the third UPFC positioned optimally in IEEE 30 bus test system increases the minimum and maximum load bus voltages to 1.0212 p.u and 1.0768 p.u. respectively under cost minimization and under loss minimization those change to 1.0256 p.u. and 1.0792p.u respectively. For a better visualization the system voltage profiles are shown in Fig 2.9 and Fig 2.10 for cost minimization and loss minimization respectively.

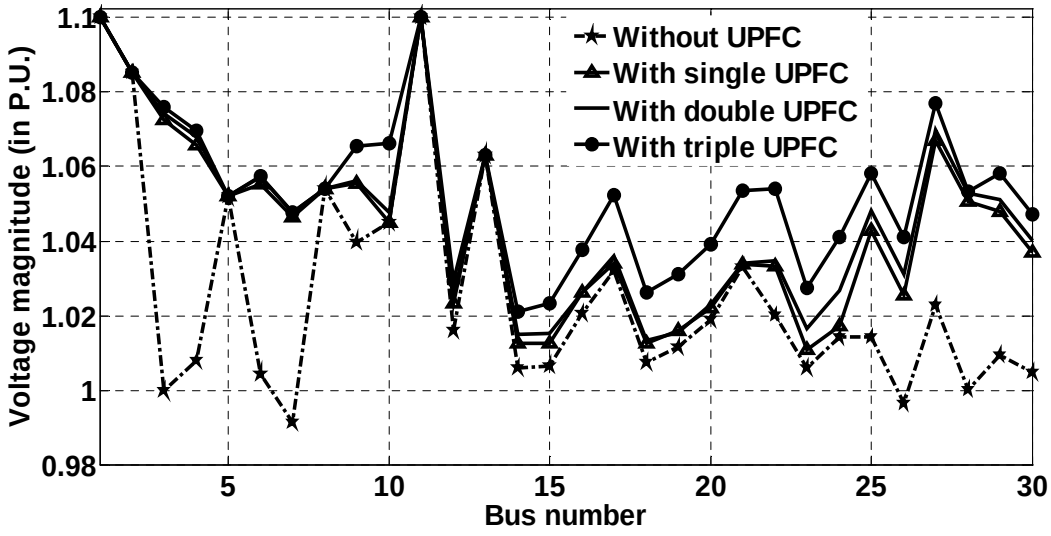

Fig.2.9. Voltage profile for cost minimization of IEEE-30 bus.

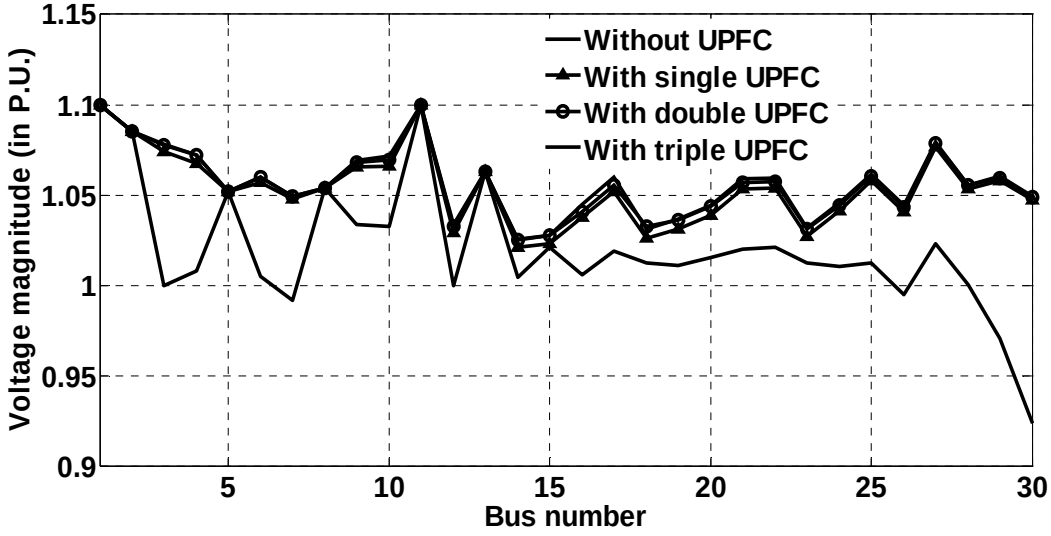

Fig.2.10. Voltage profile for loss minimization of IEEE-30 bus

- **Influence of UPFC on real power loss and operating cost**

The variation in real power loss along with operating cost for different optimal locations of UPFCs in IEEE-30 bus test system is furnished in Table 2.6.

Table 2.6. Optimal location of UPFC, real power flow, line loss and cost in IEEE-30 bus test system

Optimized parameter	Control Variables	Number of UPFCs			
		0	1	2	3
Cost minimization	Optimal locations of UPFC (k-m)		21-22	21-22,10-31	3-4,10-21,22-24
	Active power flow in line connected with UPFC (MW)		-20	-20,18.13	61.77,30,1
	Real power loss (MW)	16.53	10.13	10.01	8.95
	Dispatch cost ($/hr)	871.2043	804.0468	800.8884	786.2693
Loss minimization	Optimal locations of UPFC (k-m)		16-17	16-17,15-18	3-4,10-21,22-24
	Active power flow in line connected with UPFC (MW)		19.97	10.08,20	61.77,30,1
	Real power loss (MW)	15.24	10.08	8.89	6.22
	Dispatch cost ($/hr)	889.2033	804.769	801.12	792.9371

From Table 2.6 it is shown that during cost minimization operational cost is decreased from 871.2043 $/hr to 804.0468 $/hr and transmission line loss is reduced from 16.53 MW to 10.13 MW by installing single UPFC at its optimal position. Table 2.6 also shows that the addition of another UPFC in IEEE30 bus test system reduces cost and loss further to 800.8884 $/hr and 10.01 MW respectively. From Table 2.6 it is also noticed that the further reduction in loss and cost are achieved by adding optimally third UPFC in IEEE 30 bus test system and these reduced loss and cost are 8.95 MW and 786.2693 $/hr respectively.

Again Table 2.6 shows that during loss minimization operational cost is reduced from 889.2033 $/hr to 804.769 $/hr and transmission line loss is changed from 15.24 MW to 10.08 MW by placing single UPFC at its optimal position. Table 2.6 also depicts that the addition of second UPFC in IEEE30 bus test system reduces cost to 801.12 $/hr and loss further to 8.89 MW respectively. Besides, from Table 2.6 it is also noticed that the further reduction in loss and cost are achieved by adding optimally third UPFC in IEEE30 bus test system and they are 6.22 MW and 792.9371 $/hr respectively.

- **Comparison of performance of different optimization method in solving the UPFC placement**

The comparative results obtained by different soft computing techniques for IEEE 30 bus test system are reported in Table 2.7. The number of iterations needed by different methods is reported in Table 2.8. The convergence characteristics for four cases are shown in Fig 2.11, Fig 2.12, Fig 2.13 and Fig 2.14. From Table 2.7 it is shown that the operational cost and transmission loss along with power flow through the line of optimal

locations of UPFCs under cost minimization and loss minimization consideration are found to be same under different optimization techniques chosen in this chapter. But, Fig 2.11, Fig 2.12, Fig 2.13 and Fig 2.14 show difference between convergence characteristics of the adopted optimization techniques under cost minimization with single UPFC, loss minimization with single UPFC, cost minimization with three UPFC and loss minimization with three UPFC respectively. For better visualization the number of iterations required for convergence in different optimization techniques for IEEE30 bus system are summarized in Table 2.8.

Table2.7. Comparison of the performance of different techniques in IEEE-30 bus test system

Parameter	Control Variables	With GSA	With BBO	With StudGA	With GA	With ACO	With PBIL
Cost minimization with single UPFC	Optimal locations of UPFC (k-m)	21-22	21-22	21-22	21-22	21-22	21-22
	Active power flow in line connected with UPFC (MW)	-20	-20	-20	-20	-20	-20
	Real power loss (MW)	10.13	10.13	10.13	10.13	10.13	10.13
	Dispatch cost ($/hr)	804.0468	804.0468	804.0468	804.0468	804.0468	804.0468
Loss minimization with single UPFC	Optimal locations of UPFC (k-m)	16-17	16-17	16-17	16-17	16-17	16-17
	Active power flow in line connected with UPFC (MW)	19.97	19.97	19.97	19.97	19.97	19.97
	Real power loss (MW)	10.08	10.08	10.08	10.08	10.08	10.08
	Dispatch cost ($/hr)	804.769	804.769	804.769	804.769	804.769	804.769

Parameter	Control Variables	With GSA	With BBO	With StudGA	With GA	With ACO	With PBIL
Cost minimization with three UPFC	Optimal locations of UPFC (k-m)	3-4,10-21,22-24	3-4,10-21,22-24	3-4,10-21,22-24	3-4,10-21,22-24	3-4,10-21,22-24	3-4,10-21,22-24
	Active power flow in line connected with UPFC (MW)	61.77,30,1	61.77,30,1	61.77,30,1	61.77,30,1	61.77,30,1	61.77,30,1
	Real power loss (MW)	8.95	8.95	8.95	8.95	8.95	8.95
	Dispatch cost ($/hr)	786.2693	786.2693	786.2693	786.2693	786.2693	786.2693
Loss minimization with three UPFC	Optimal locations of UPFC (k-m)	3-4,10-21,22-24	3-4,10-21,22-24	3-4,10-21,22-24	3-4,10-21,22-24	3-4,10-21,22-24	3-4,10-21,22-24
	Active power flow in line connected with UPFC (MW)	61.77,30,1	61.77,30,1	61.77,30,1	61.77,30,1	61.77,30,1	61.77,30,1
	Real power loss (MW)	6.22	6.22	6.22	6.22	6.22	6.22
	Dispatch cost ($/hr)	792.9371	792.9371	792.9371	792.9371	792.9371	792.9371

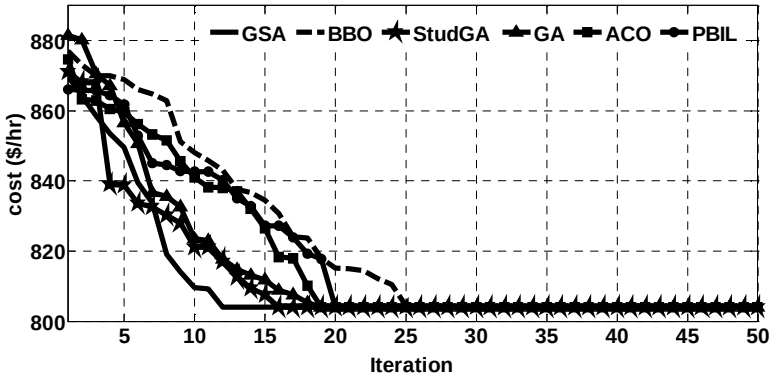

Fig.2.11. Cost minimization with single UPFC of IEEE-30 bus system.

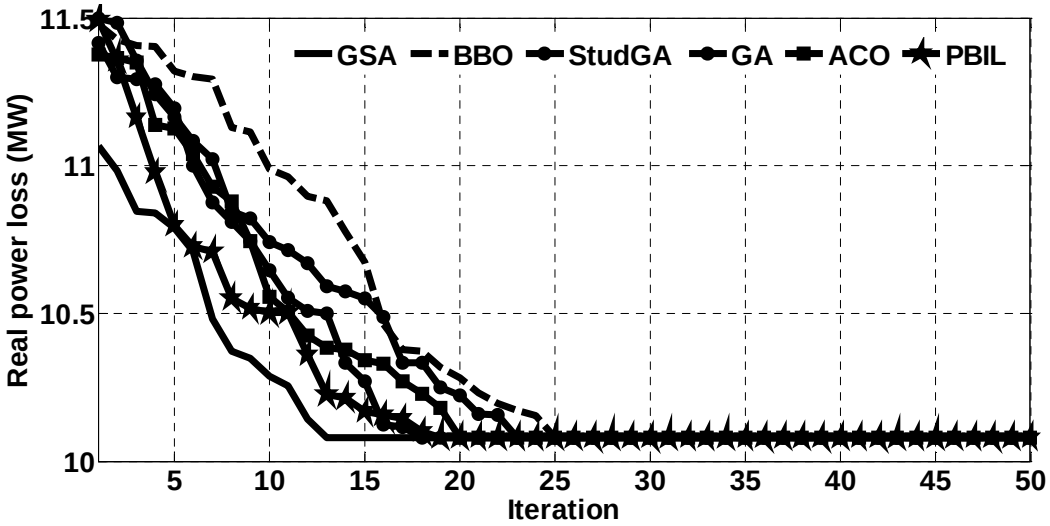

Fig.2.12. Loss minimization with single UPFC of IEEE-30 bus system.

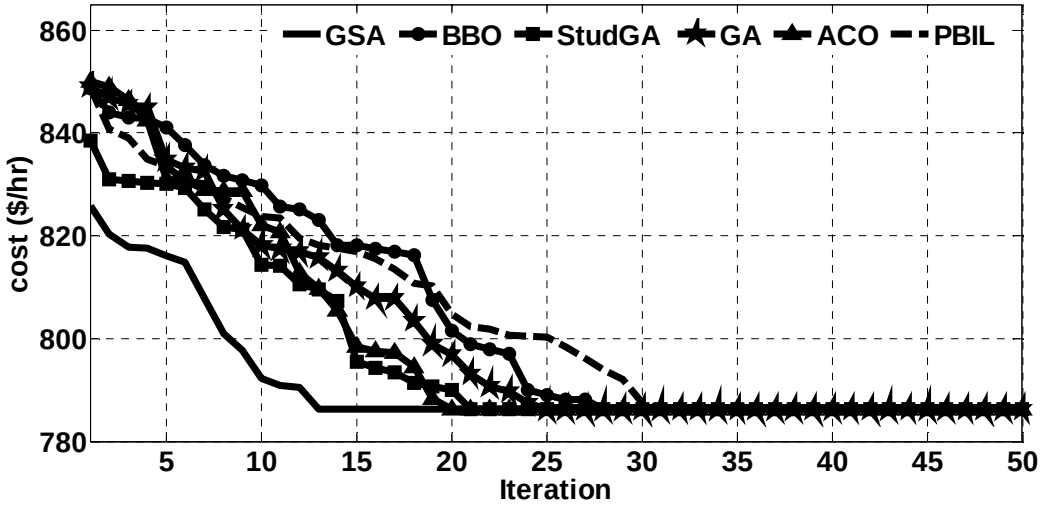

Fig. 2.13. Cost minimization with three UPFC of IEEE-30 bus system.

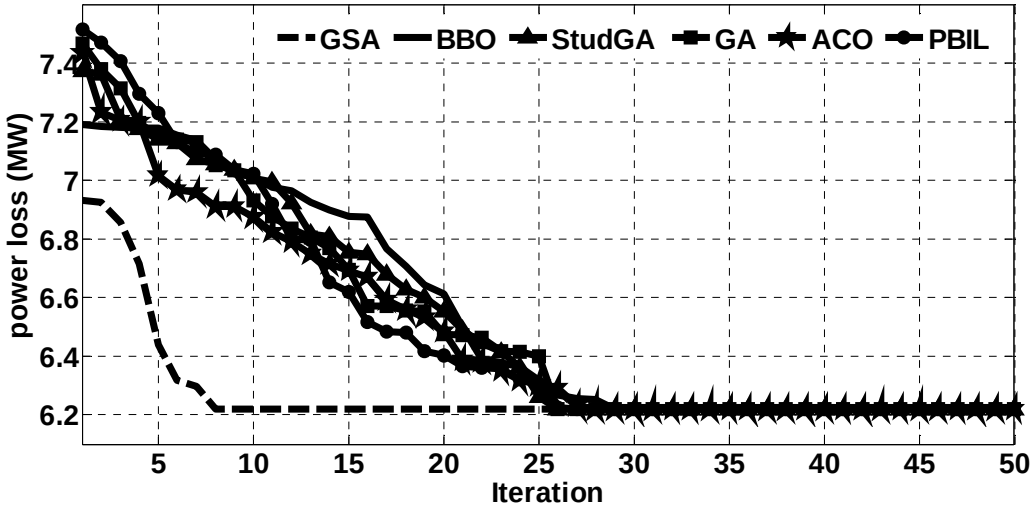

Fig.2.14. Loss minimization with three UPFC of IEEE-30 bus system.

Table 2.8. Number of iterations needed for optimum solution in IEEE-30 bus test system

Minimized parameter	Test system	With GSA	With BBO	With StudGA	With GA	With ACO	With PBIL
Cost minimization with single UPFC	IEEE-30 bus	11	25	15	18	18	19
Loss minimization with single UPFC		12	24	17	22	19	18
Cost minimization with three UPFC		12	27	20	24	19	31
Loss minimization with three UPFC		7	28	25	25	27	26

From Table 2.8, it is shown that iteration number required in IEEE30 bus test system for cost and loss minimizations by single UPFC installation with GSA technique are found to be 11 and 12 respectively, while those found for triple UPFCs installation are 12 and 7 respectively. Table 2.8 also shows that these results found by GSA are minimum among all the different soft computing techniques adopted here in their respective cost/loss minimization by single/triple UPFC installation in IEEE30 bus test system.

2.5.3. Results for IEEE-57 bus system

The line data, bus data and generator cost data of IEEE-57bus test transmission system are reported in Appendix A.4.3.

- **Effect of UPFC on voltage profile improvement**

The change in bus voltage magnitudes with the increase in UPFC number for both cost minimization and loss minimization are shown in Table 2.9.

Table 2.9. Generator terminal voltages (p.u.) of IEEE-57 bus test system

Bus number	Bus voltage magnitude							
	Cost minimization				Loss minimization			
	Without UPFC	With 1 UPFC	With 2 UPFCs	With 3 UPFCs	Without UPFC	With 1 UPFC	With 2 UPFCs	With 3 UPFCs
1	1.04	1.04	1.04	1.04	1.04	1.04	1.04	1.04
2	1.01	1.01	1.01	1.01	1.01	1.01	1.01	1.01
3	0.985	0.985	0.985	0.985	0.985	0.985	0.985	0.985
4	0.97	0.9798	0.9799	0.9799	0.9797	0.9798	0.9798	0.9799
5	0.9664	0.9761	0.9762	0.9762	0.9762	0.9762	0.9762	0.9762
6	0.98	0.98	0.98	0.98	0.98	0.98	0.98	0.98
7	0.9743	0.9833	0.9841	0.9865	0.9841	0.9843	0.9845	0.9858
8	1.005	1.005	1.005	1.005	1.005	1.005	1.005	1.005
9	0.98	0.98	0.98	0.98	0.98	0.98	0.98	0.98
10	0.9762	0.9861	0.9863	0.9877	0.9861	0.9865	0.9865	0.9888

Bus number	Bus voltage magnitude							
	Cost minimization				Loss minimization			
	Without UPFC	With 1 UPFC	With 2 UPFCs	With 3 UPFCs	Without UPFC	With 1 UPFC	With 2 UPFCs	With 3 UPFCs
11	0.964	0.9739	0.974	0.9848	0.9721	0.9737	0.9763	0.9843
12	1.015	1.015	1.015	1.015	1.015	1.015	1.015	1.015
13	0.9688	0.9787	0.9789	1	0.9785	0.9786	0.9797	1
14	0.96	0.9699	0.9702	0.985	0.9697	0.9699	0.971	0.9872
15	0.9778	0.9877	0.9879	0.9998	0.9877	0.9877	0.9885	1.0016
16	1.0033	1.0133	1.0134	1.0154	1.0134	1.0134	1.0163	1.0164
17	1.0072	1.0174	1.0174	1.0174	1.0174	1.0175	1.0208	1.0209
18	0.9777	0.9877	0.9885	0.9905	0.9876	0.9878	0.9881	0.9895
19	0.9246	0.9336	0.9443	0.9558	0.9333	0.9339	0.9455	0.9596
20	0.9289	0.9375	0.9489	0.9503	0.9373	0.9383	0.9406	0.9564
21	0.993	1.0039	1.0064	1.0174	1.003	1.0034	1.0065	1.0178
22	0.997	1.008	1.0104	1.0217	1.0071	1.0074	1.0108	1.0226
23	0.9956	1.0067	1.0095	1.0205	1.0057	1.0061	1.0094	1.0213
24	0.9873	0.9981	1.0083	1.0146	0.9973	0.9978	1.0004	1.0153
25	0.9706	0.9815	0.9909	0.9984	0.9804	0.9811	0.9849	1.0002
26	0.9475	0.9578	0.9688	0.9743	0.9571	0.9575	0.9598	0.9731
27	0.9709	0.981	1	1	0.9807	0.9808	0.982	1
28	0.9862	0.9911	0.9964	1.0046	0.9962	0.9962	0.997	1.0044
29	0.9998	1.0069	1.01	1.0153	1.0099	1.0099	1.0104	1.0163
30	0.9509	0.9617	0.9705	0.9783	0.9605	0.9615	0.9655	0.9799
31	0.9244	0.9352	0.9424	0.9505	0.9337	0.9352	0.9397	0.9518
32	0.9382	0.9495	0.9538	0.9621	0.9477	0.9499	0.9548	0.9626
33	0.9359	0.9472	0.9515	0.9599	0.9454	0.9476	0.9525	0.9603
34	0.9476	0.9592	0.9605	0.9691	0.9572	0.9595	0.9654	0.9714
35	0.9547	0.9662	0.9672	0.9757	0.9643	0.9666	0.9725	0.9779
36	0.9642	0.9759	0.9766	0.9851	0.9739	0.9763	0.9821	0.9871
37	0.9731	0.985	0.9856	0.9947	0.9829	0.9849	0.9904	0.9965
38	1.0007	1.0118	1.0133	1.0252	1.0108	1.0111	1.0147	1.0261
39	0.9711	0.9835	0.9835	0.9923	0.9809	0.983	0.989	0.9941
40	0.9612	0.9728	0.9736	0.9812	0.9709	0.9737	0.9801	0.9834
41	0.9855	0.9964	0.9965	1	0.9955	1	1	1.0139
42	0.9559	0.9666	0.967	0.9759	0.9656	0.9666	0.9751	0.9915
43	0.9991	1.0096	1.0097	1.0188	1.0022	1.0092	1.0162	1.0182
44	1.0049	1.0159	1.0171	1.0298	1.0151	1.0151	1.0184	1.0304
45	1.0247	1.0355	1.0357	1.0517	1.0337	1.0351	1.037	1.05
46	1.0482	1.0593	1.0598	1.0751	1.0586	1.0588	1.061	1.0615
47	1.0215	1.0325	1.0334	1.0471	1.0317	1.0318	1.0347	1.0482
48	1.0155	1.0265	1.0276	1.0404	1.0258	1.0259	1.0289	1.0417
49	1.0247	1.0357	1.0365	1.0473	1.0351	1.0356	1.0377	1.0502
50	1.0123	1.0229	1.0236	1.0315	1.0225	1.0233	1.0244	1.0345
51	1.0414	1.0521	1.0524	1.0551	1.0519	1.0527	1.0534	1.0583
52	0.9703	0.9781	0.9802	0.9845	0.9801	0.9805	0.9805	0.9849
53	0.961	0.9692	0.9708	0.9745	0.9707	0.9711	0.9712	0.9748
54	0.9862	0.9959	0.9962	0.9983	0.9962	0.9964	0.997	0.998
55	1.0205	1.0308	1.0308	1.0318	1.0308	1.0308	1.0308	1.0318
56	0.9576	0.9657	0.9682	0.983	0.9649	0.9673	0.9813	1
57	0.954	0.9641	0.9691	0.982	0.9597	0.9636	0.98	0.9925

From Table 2.9 it is obvious that with the installation of single UPFC at optimal position in test system, the minimum and maximum load bus voltages increase from 0.9244p.u to 0.9336 p.u and 1.0482p.u to 1.0593 p.u respectively under cost minimization and under loss minimization those vary from 0.9333 p.u. to 0.9339p.u.and 1.0586 p.u. to 1.0588p.u. respectively. Table 2.9 also shows that with the installation of second UPFC at its optimal position in test network, those minimum and maximum load voltages change to 0.9424p.u and 1.0598p.u respectively under cost minimization and under loss minimization those become 0.9397p.u. and 1.061p.u. respectively. From Table 2.9 it is also shown that the third UPFC positioned optimally in IEEE 57 bus test system increases the minimum and maximum load bus voltages to 0.9503p.u and 1.0751p.u. respectively under cost minimization and under loss minimization those change to 0.9518p.u. and 1.0615 p.u respectively. For a better visualization the system voltage profiles are shown in Fig 2.15 and Fig 2.16 for cost minimization and loss minimization respectively.

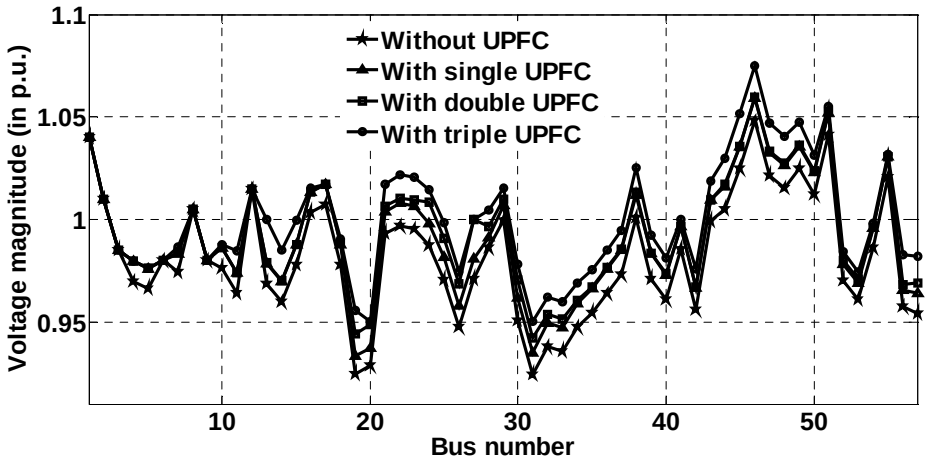

Fig.2.15. Voltage profile for cost minimization of IEEE-57 bus.

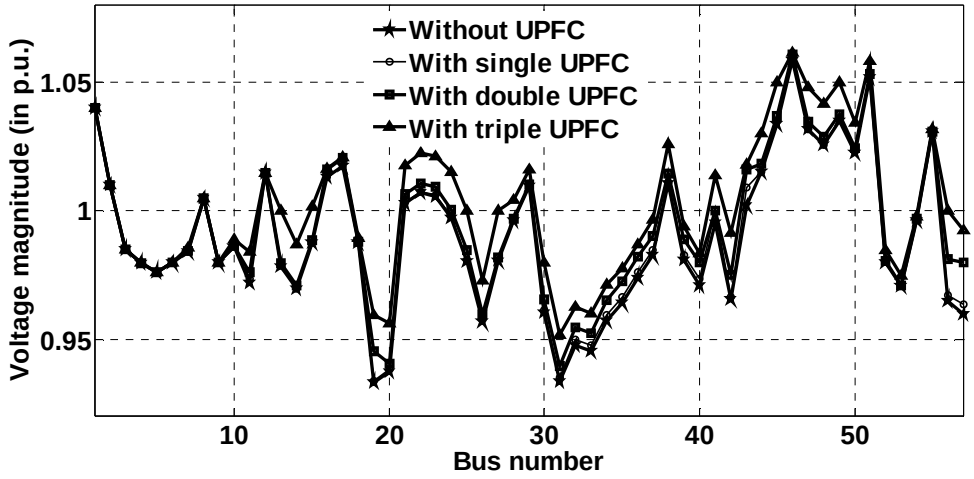

Fig.2.16. Voltage profile for loss minimization of IEEE-57 bus

- **Influence of UPFC on real power loss and operating cost**

The variation in real power loss along with operating cost for different optimal locations of UPFCs in IEEE-57 bus test system is furnished in Table 2.10.

Table 2.10. Optimal location of UPFC, real power flow, line loss and cost in IEEE-57 bus test system

Optimized parameter	Control Variables	Number of UPFCs			
		0	1	2	3
Cost minimization	Optimal locations of UPFC (k-m)		27-28	27-28,37-38	13-14,19-20,57-56
	Active power flow in line connected with UPFC (MW)		-21.39	25.22,-20	60.00,20.00,1.01
	Real power loss (MW)	28.07	18.17	18.03	14.23
	Dispatch cost ($/hr)	1,06,290	58,922.00	56260	52,045.00
Loss minimization	Optimal locations of UPFC (k-m)		41-43	41-43,	13-14,19-20,57-56
	Active power flow in line connected with UPFC (MW)		-26.17	33.99, -25	61.45,20.00,1.10
	Real power loss (MW)	27.98	14.46	14.32	14.08
	Dispatch cost ($/hr)	1,16,350	71,832.00	70250.00	69,380.00

From Table 2.10 it is shown that during cost minimization operational cost is decreased from 1,06,290 $/hr to 58,922 $/hr and transmission line loss is reduced from 28.07 MW to 18.17 MW by installing single UPFC in its optimal position. Table 2.10 also shows that the addition of another UPFC in IEEE57 bus test system reduces cost and loss further to 56260 $/hr and 18.03 MW respectively. From Table 2.10 it is also noticed that the further reduction in loss and cost are achieved by adding optimally third UPFC in IEEE 57 bus test system and they are 14.23 MW and 52,045 $/hr respectively.

Again Table 2.10 shows that during loss minimization operational cost is reduced from 1,16,350 $/hr to 71,832 $/hr and transmission line loss is changed from 27.98 MW to 14.46 MW by placing single UPFC in its optimal position. Table 2.10 also depicts that the addition of second one UPFC in IEEE57 bus test system reduces cost to 70250 $/hr and loss further to 14.32 MW respectively. Besides, from Table 2.10 it is also noticed that the further reduction in loss and cost are achieved by adding optimally third UPFC in IEEE57 bus test system and they are 14.08 MW and 69,380 $/hr respectively.

- **Comparison of performance of different optimization method in solving the UPFC placement**

The comparative results obtained by different soft computing techniques for IEEE 57 bus test system are reported in Table 2.11. The number of iterations needed by different methods is reported in Table 2.12. The convergence characteristics for four cases are shown in Fig 2.17, Fig 2.18, Fig 2.19 and Fig 2.20.

Table2.11. Comparison of the performance of different techniques in IEEE-57 bus test system

Parameter	Control Variables	With GSA	With BBO	With StudGA	With GA	With ACO	With PBIL
Cost minimization with single UPFC	Optimal locations of UPFC (k-m)	27-28	27-28	27-28	27-28	27-28	27-28
	Active power flow in line connected with UPFC (MW)	-21.39	-21.39	-21.39	-21.39	-21.39	-21.39
	Real power loss (MW)	18.17	18.17	18.17	18.17	18.17	18.17
	Dispatch cost ($/hr)	58,922.00	58,922.00	58,922.00	58,922.00	58,922.00	58,922.00
Loss minimization with single UPFC	Optimal locations of UPFC (k-m)	41-43	41-43	41-43	41-43	41-43	41-43
	Active power flow in line connected with UPFC (MW)	-26.17	-26.17	-26.17	-26.17	-26.17	-26.17
	Real power loss (MW)	14.46	14.46	14.46	14.46	14.46	14.46
	Dispatch cost ($/hr)	71,832.00	71,832.00	71,832.00	71,832.00	71,832.00	71,832.00

Parameter	Control Variables	With GSA	With BBO	With StudGA	With GA	With ACO	With PBIL
Cost minimization with three UPFC	Optimal locations of UPFC (k-m)	13-14,19-20,57-56	13-14,19-20,57-56	13-14,19-20,57-56	13-14,19-20,57-56	13-14,19-20,57-56	13-14,19-20,57-56
	Active power flow in line connected with UPFC (MW)	60.00,20.00, 1.01	60.00,20.00, 1.01	60.00,20.00, 1.01	60.00,20.00, 1.01	60.00,20.00, 1.01	60.00,20.00, 1.01
	Real power loss (MW)	14.23	14.23	14.23	14.23	14.23	14.23
	Dispatch cost ($/hr)	52,045.00	52,045.00	52,045.00	52,045.00	52,045.00	52,045.00
Loss minimization with three UPFC	Optimal locations of UPFC (k-m)	13-14,19-20,57-56	13-14,19-20,57-56	13-14,19-20,57-56	13-14,19-20,57-56	13-14,19-20,57-56	13-14,19-20,57-56
	Active power flow in line connected with UPFC (MW)	61.45,20.00, 1.10	61.45,20.00, 1.10	61.45,20.00, 1.10	61.45,20.00, 1.10	61.45,20.00, 1.10	61.45,20.00, 1.10
	Real power loss (MW)	14.08	14.08	14.08	14.08	14.08	14.08
	Dispatch cost ($/hr)	69,380.00	69,380.00	69,380.00	69,380.00	69,380.00	69,380.00

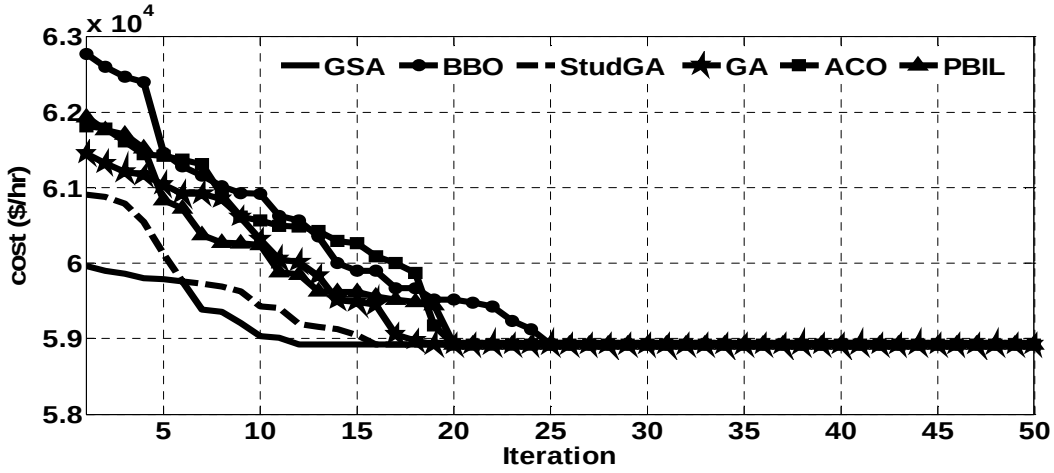

Fig.2.17. Cost minimization with single UPFC of IEEE-57 bus system

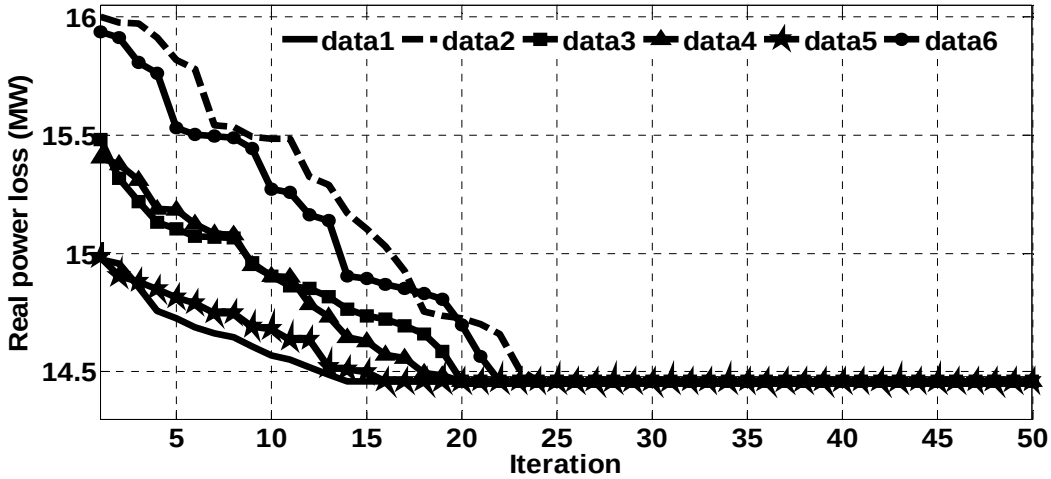

Fig.2.18. Loss minimization with single UPFC of IEEE-57 bus system

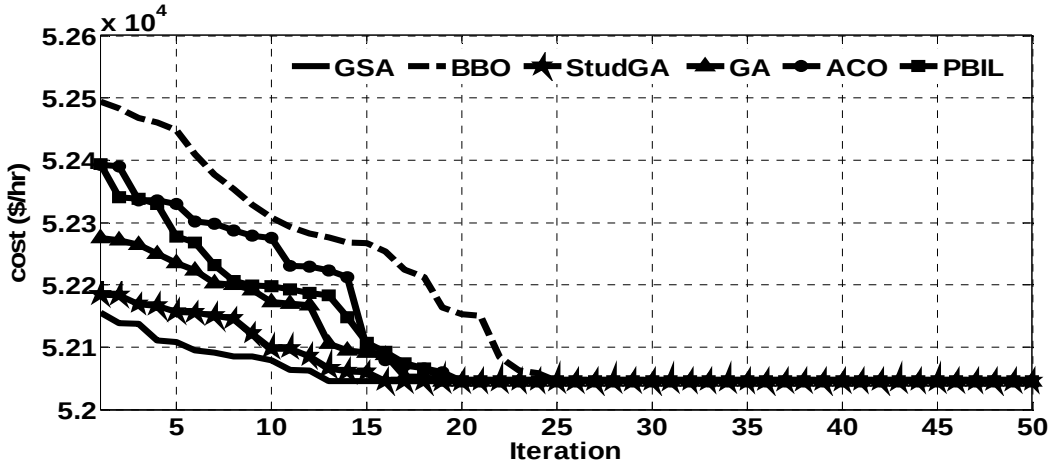

Fig. 2.19. Cost minimization with three UPFC of IEEE-57 bus system

From Table 2.11 it is shown that the operational cost and transmission loss along with power flow through the line of optimal locations of UPFCs under cost minimization and loss minimization consideration are found to be same under different optimization techniques chosen in this chapter. But, Fig 2.17, Fig 2.18, Fig 2.19 and Fig

2.20 show difference between convergence characteristics of the adopted optimization techniques under cost minimization with single UPFC, loss minimization with single UPFC, cost minimization with three UPFC and loss minimization with three UPFC respectively. For better visualization the number of iterations required for convergence in different optimization techniques for IEEE57 bus system are summarized in Table 2.12.

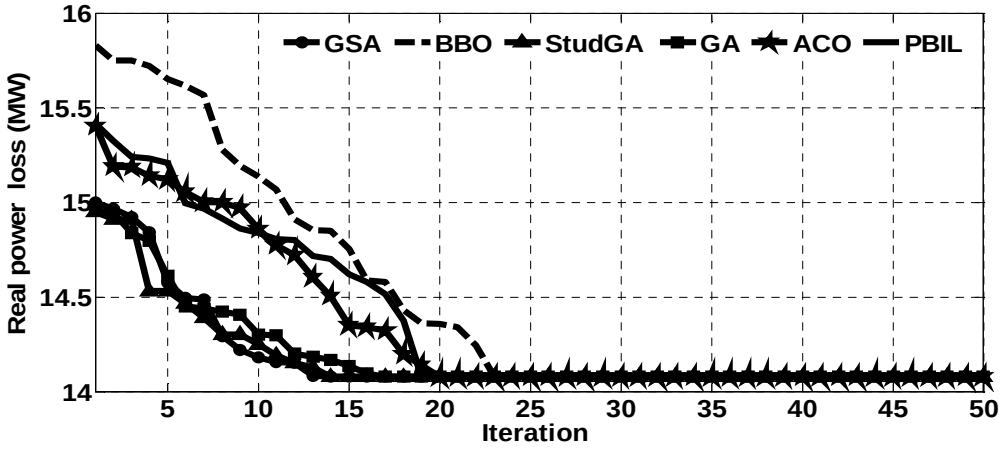

Fig.2.20. Loss minimization with three UPFC of IEEE-57 bus system.

Table 2.12. Number of iterations needed for optimum solution in IEEE-57 bus test system

Minimized parameter	Test system	With GSA	With BBO	With StudGA	With GA	With ACO	With PBIL
Cost minimization with single UPFC	IEEE-57 bus	11	21	17	20	20	19
Loss minimization with single UPFC		13	23	19	19	15	21
Cost minimization with three UPFC		12	24	15	18	19	19
Loss minimization with three UPFC		13	22	13	16	19	18

From Table 2.12, it is shown that iteration number required in IEEE57 bus test system for cost and loss minimizations by single UPFC installation with GSA technique are found to be 11 and 13 respectively, while those found for triple UPFCs installation are 12 and 13 respectively. Table 2.12 also shows that these results found by GSA are minimum among all the different soft computing techniques adopted here in their respective cost/loss minimization by single/triple UPFC installation in IEEE57 bus test system.

2.5.4. Results for NER system

To establish the capability of the proposed method further, the optimization problems have been solved for a real life Indian power system, namely the North-Eastern regional grid (NER) system. The system has a generating capacity of 3,079.89 MW and a connected load of 2974.0 MW. The system has been represented in the present work by 80 buses and 82 transmission lines.

The line data, bus data and generator cost data along with single-line diagram of NER transmission system are reported in Appendix A.4.4.

- **Effect of UPFC on voltage profile improvement**

The change in bus voltage magnitudes with the increase in UPFC number for both cost minimization and loss minimization are shown in Table 2.13.

Table 2.13. Generator terminal voltages (p.u.) of NER transmission system

Bus number	Loss minimization				Cost minimization			
	Bus voltage magnitude				Bus voltage magnitude			
	Without UPFC	With 1 UPFC	With 2 UPFCs	With 3 UPFCs	Without UPFC	With 1 UPFC	With 2 UPFCs	With 3 UPFCs
1	0.955	0.955	0.955	0.955	0.955	0.955	0.955	0.955
2	0.9721	0.9722	0.9722	0.9722	0.9721	0.9721	0.9722	0.9722
3	0.9675	0.9677	0.9684	0.9685	0.9675	0.968	0.9683	0.9684
4	0.998	0.998	0.998	0.998	0.998	0.998	0.998	0.998
5	0.9993	0.9994	1.0013	1.002	0.9993	0.9997	0.9997	1.0007
6	0.99	0.99	0.99	0.99	0.99	0.99	0.99	0.99
7	0.9893	0.9893	0.9894	0.9894	0.9893	0.9893	0.9894	0.9894
8	1.015	1.015	1.015	1.015	1.015	1.015	1.015	1.015
9	1.0636	1.0719	1.072	1.0722	1.0636	1.0719	1.0719	1.0722
10	1.05	1.05	1.05	1.05	1.05	1.05	1.05	1.05
11	0.9857	0.9857	0.9857	0.9857	0.9857	0.9857	0.9858	0.9858
12	0.99	0.99	0.99	0.99	0.99	0.99	0.99	0.99
13	0.971	0.971	0.9711	0.9711	0.971	0.9711	0.9711	0.9811
14	0.9853	0.9853	0.9853	0.9854	0.9853	0.9854	0.9854	0.9857
15	0.97	0.97	0.97	0.97	0.97	0.97	0.97	0.97
16	0.9857	0.986	0.9864	0.9867	0.9857	0.9863	0.9863	0.9873
17	0.9947	0.9957	0.9968	0.9978	0.9947	0.9955	0.9965	0.9965
18	0.973	0.973	0.973	0.973	0.973	0.973	0.973	0.973
19	0.963	0.963	0.963	0.963	0.963	0.963	0.963	0.963
20	0.9639	0.9663	0.9666	0.967	0.9639	0.9652	0.9662	0.9667
21	0.9669	0.9707	0.9711	0.9719	0.9669	0.9669	0.9705	0.9705
22	0.9784	0.9827	0.9832	0.9842	0.9784	0.9784	0.9825	0.9825
23	1.0042	1.006	1.0061	1.0065	1.0042	1.006	1.006	1.009
24	0.992	0.992	0.992	0.992	0.992	0.992	0.992	0.992
25	1.05	1.05	1.05	1.05	1.05	1.05	1.05	1.05
26	1.015	1.015	1.015	1.015	1.015	1.015	1.015	1.015
27	0.968	0.968	0.968	0.968	0.968	0.968	0.968	0.968
28	0.9628	0.9629	0.9629	0.9629	0.9628	0.9628	0.9628	0.9638
29	0.9637	0.9637	0.964	0.964	0.9637	0.9637	0.9637	0.9647
30	1.0294	1.0372	1.0377	1.0384	1.0294	1.0307	1.0376	1.0376
31	0.967	0.967	0.967	0.967	0.967	0.967	0.967	0.967
32	0.964	0.964	0.964	0.964	0.964	0.964	0.964	0.964
33	0.972	0.9743	0.9745	0.9755	0.972	0.972	0.9744	0.9765
34	0.986	0.986	0.986	0.986	0.986	0.986	0.986	0.986

Bus number	Loss minimization				Cost minimization			
	Bus voltage magnitude				Bus voltage magnitude			
	Without UPFC	With 1 UPFC	With 2 UPFCs	With 3 UPFCs	Without UPFC	With 1 UPFC	With 2 UPFCs	With 3 UPFCs
35	0.981	0.981	0.981	0.981	0.981	0.981	0.985	0.988
36	0.98	0.98	0.98	0.98	0.98	0.98	0.98	0.98
37	0.9933	0.9934	0.9937	0.9958	0.9933	0.9934	0.9937	0.9958
38	1.0254	1.0352	1.0361	1.0375	1.0254	1.0359	1.0359	1.0375
39	0.9715	0.9724	0.9724	0.9733	0.9715	0.9724	0.9724	0.9824
40	0.97	0.97	0.97	0.97	0.97	0.97	0.97	0.97
41	0.9677	0.9677	0.9677	0.9677	0.9677	0.9667	0.9677	0.9677
42	0.985	0.985	0.985	0.985	0.985	0.985	0.985	0.985
43	0.9818	0.9821	0.9822	0.9822	0.9818	0.9821	0.9821	0.9822
44	0.9799	0.9806	0.9811	0.9812	0.9799	0.9806	0.9807	0.9811
45	0.9831	0.9839	0.9844	0.9846	0.9831	0.984	0.9844	0.9846
46	1.005	1.005	1.005	1.005	1.005	1.005	1.005	1.005
47	1.0192	1.0212	1.0212	1.0212	1.0192	1.0212	1.0212	1.0212
48	1.021	1.021	1.021	1.021	1.021	1.021	1.021	1.021
49	1.025	1.025	1.025	1.025	1.025	1.025	1.025	1.025
50	1.0025	1.0043	1.0043	1.0043	1.0025	1.0034	1.0042	1.0042
51	0.9705	0.9739	0.9741	0.9741	0.9705	0.9706	0.9739	0.9742
52	0.9615	0.9654	0.9655	0.9656	0.9615	0.9634	0.9654	0.9654
53	0.9503	0.9522	0.9523	0.9523	0.9503	0.9512	0.9522	0.9526
54	0.955	0.955	0.955	0.955	0.955	0.955	0.955	0.955
55	0.952	0.952	0.952	0.952	0.952	0.952	0.952	0.952
56	0.954	0.954	0.954	0.954	0.954	0.954	0.954	0.954
57	0.9723	0.974	0.974	0.974	0.9723	0.973	0.974	0.9745
58	0.9618	0.9639	0.964	0.964	0.9618	0.9629	0.9639	0.9659
59	0.985	0.985	0.985	0.985	0.985	0.985	0.985	0.985
60	0.9935	0.9936	0.9936	0.9936	0.9935	0.9936	0.9938	0.9946
61	0.995	0.995	0.995	0.995	0.995	0.995	0.995	0.995
62	0.998	0.998	0.998	0.998	0.998	0.998	0.998	0.998
63	0.969	0.969	0.9966	1.0002	0.969	0.989	0.989	0.989
64	1.0025	1.0034	1.0044	1.01	1.0025	1.0102	1.0112	1.0125
65	1.005	1.005	1.005	1.005	1.005	1.005	1.005	1.005
66	1.05	1.05	1.05	1.05	1.05	1.05	1.05	1.05
67	1.0211	1.0218	1.0219	1.0219	1.0211	1.0214	1.0219	1.0229
68	1.0199	1.0201	1.0205	1.0208	1.0199	1.0208	1.0208	1.0208
69	1.035	1.035	1.035	1.035	1.035	1.035	1.035	1.035
70	0.984	0.984	0.984	0.984	0.984	0.984	0.984	0.984
71	0.9873	0.9874	0.9874	0.9877	0.9873	0.9874	0.9874	0.9876
72	0.98	0.98	0.98	0.98	0.98	0.98	0.98	0.98
73	0.991	0.991	0.991	0.991	0.991	0.991	0.991	0.991
74	0.958	0.958	0.958	0.958	0.958	0.958	0.958	0.958
75	0.9789	0.9802	0.9803	0.9803	0.9789	0.9803	0.9805	0.981
76	0.953	0.953	0.953	0.953	0.953	0.953	0.953	0.953
77	1.006	1.006	1.006	1.006	1.006	1.006	1.006	1.006
78	1.0018	1.0019	1.0019	1.002	1.0018	1.0018	1.0018	1.002
79	1.004	1.0047	1.0047	1.0047	1.004	1.0045	1.0047	1.0047
80	1.04	1.04	1.04	1.04	1.04	1.04	1.04	1.04

From Table 2.13 it is obvious that with the installation of single UPFC at optimal position in test system, the minimum and maximum load bus voltages increase from 0.9503p.u to 0.9522p.u and 1.0636p.u to 1.0719p.u

respectively under loss minimization and under cost minimization those vary from 0.9503p.u. to 0.9512p.u.and 1.0636p.u. to 1.0719p.u. respectively. Table 2.13 also shows that with the installation of second UPFC at its optimal position in test network, those minimum and maximum load voltages change to 0.9523p.u and 1.072 p.u respectively under loss minimization and under cost minimization those become 0.9522 p.u. and 1.0719 p.u. respectively. From Table 2.13 it is also shown that the third UPFC positioned optimally in NER transmission system increases the minimum and maximum load bus voltages to 0.9523p.u and 1.0722p.u. respectively under loss minimization and under cost minimization those change to 0.9526p.u. and 1.0722 p.u respectively. For a better visualization the system voltage profiles are shown in Fig 2.21and Fig 2.22for cost minimization and loss minimization respectively.

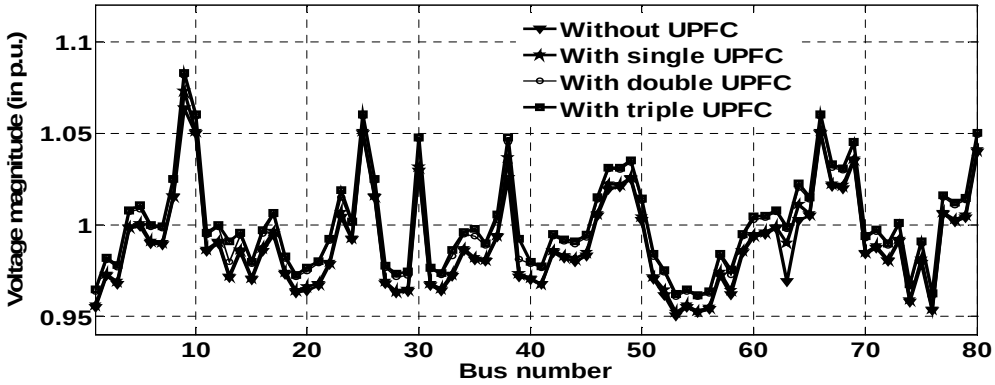

Fig.2.21. Voltage profile for cost minimization of NER transmission system.

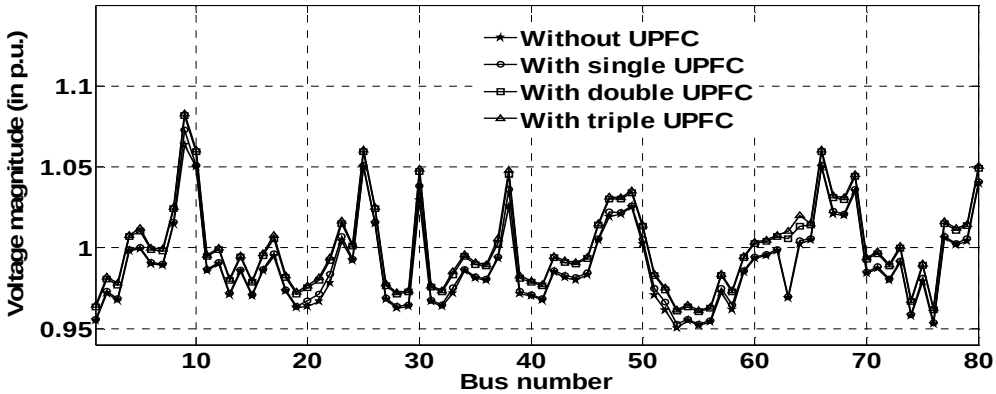

Fig.2.22. Voltage profile for loss minimization of NER transmission system

- **Influence of UPFC on real power loss and operating cost**

The variation in real power loss along with operating cost for different optimal locations of UPFCs in NER transmission system is furnished in Table 2.14.

Table 2.14. Optimal location of UPFC, real power flow, line loss and cost in NER transmission system

Optimized parameter	Control Variables	Number of UPFCs			
		0	1	2	3
Cost minimization	Optimal locations of UPFC (k-m)	-	33-37	33-37,63-64	3-4,10-21,22-24
	Active power flow in line connected with UPFC (MW)	-	-31.74	-31.74,-38.34	61.77,30,1
	Real power loss (MW)	105.89	38.95	28.56	26.36
	Dispatch cost ($/hr)	67983	1927.3	16172	786.2693
Loss minimization	Optimal locations of UPFC (k-m)	-	37-39	37-39,63-64	5-11,35-37,63-64
	Active power flow in line connected with UPFC (MW)	-	-33.79	-30.98,-33.79	-80.0;-80.0;-90.0
	Real power loss (MW)	104.74	24.95	24.33	23.44
	Dispatch cost ($/hr)	68175	21315	20603	11431

From Table 2.14 it is shown that during cost minimization operational cost is decreased from 67983 $/hr to 1927.3 $/hr and transmission line loss is reduced from 105.89 MW to 38.95 MW by installing single UPFC in its optimal position. Table 2.14 also shows that the addition of another one UPFC in NER transmission system reduces cost and loss further to 16172 $/hr and 28.56 MW respectively. From Table 2.14 it is also noticed that further reduction in loss and cost are achieved by adding optimally third UPFC in NER transmission system and they are 26.36 MW and 786.2693 $/hr respectively.

Again Table 2.14 shows that during loss minimization operational cost is reduced from 68175 $/hr to 21315 $/hr and transmission line loss is changed from 104.74 MW to 24.95 MW by placing single UPFC in its optimal position. Table 2.14 also depicts that addition of second UPFC in NER transmission system reduces cost to 20603 $/hr and loss further to 24.33 MW respectively. Besides, from Table 2.14 it is also noticed that the further reduction in loss and cost are achieved by adding optimally third UPFC in NER transmission system and they are 23.44 MW and 11431 $/hr respectively.

- **Comparison of performance of different optimization method in solving the UPFC placement**

The comparative results obtained by different soft computing techniques for NER transmission system are reported in Table 2.15. The number of iterations needed by different methods is reported in Table 2.16. The convergence characteristics for four cases are shown in Fig 2.23, Fig 2.24, Fig 2.25 and Fig 2.26.

Table2.15. Comparison of the performance of different techniques in NER transmission system

Parameter	Control Variables	With GSA	With BBO	With StudGA	With GA	With ACO	With PBIL
Cost minimization with single UPFC	Optimal locations of UPFC (k-m)	33-37	33-37	33-37	33-37	33-37	33-37
	Active power flow in line connected with UPFC (MW)	-31.74	-31.74	-31.74	-31.74	-31.74	-31.74
	Real power loss (MW)	38.95	38.95	38.95	38.95	38.95	38.95
	Dispatch cost ($/hr)	1927.3	1927.3	1927.3	1927.3	1927.3	1927.3
Loss minimization with single UPFC	Optimal locations of UPFC (k-m)	37-39	37-39	37-39	37-39	37-39	37-39
	Active power flow in line connected with UPFC (MW)	-33.79	-33.79	-33.79	-33.79	-33.79	-33.79
	Real power loss (MW)	24.95	24.95	24.95	24.95	24.95	24.95
	Dispatch cost ($/hr)	21315	21315	21315	21315	21315	21315

Parameter	Control Variables	With GSA	With BBO	With StudGA	With GA	With ACO	With PBIL
Cost minimization with three UPFC	Optimal locations of UPFC (k-m)	3-4,10-21,22-24	3-4,10-21,22-24	3-4,10-21,22-24	3-4,10-21,22-24	3-4,10-21,22-24	3-4,10-21,22-24
	Active power flow in line connected with UPFC (MW)	61.77,30,1	61.77,30,1	61.77,30,1	61.77,30,1	61.77,30,1	61.77,30,1
	Real power loss (MW)	26.36	26.36	26.36	26.36	26.36	26.36
	Dispatch cost ($/hr)	786.2693	786.2693	786.2693	786.2693	786.2693	786.2693
Loss minimization with three UPFC	Optimal locations of UPFC (k-m)	5-11,35-37,63-64	5-11,35-37,63-64	5-11,35-37,63-64	5-11,35-37,63-64	5-11,35-37,63-64	5-11,35-37,63-64
	Active power flow in line connected with UPFC (MW)	-80.0;-80.0;-90.0	-80.0;-80.0;-90.0	-80.0;-80.0;-90.0	-80.0;-80.0;-90.0	-80.0;-80.0;-90.0	-80.0;-80.0;-90.0
	Real power loss (MW)	23.44	23.44	23.44	23.44	23.44	23.44
	Dispatch cost ($/hr)	11431	11431	11431	11431	11431	11431

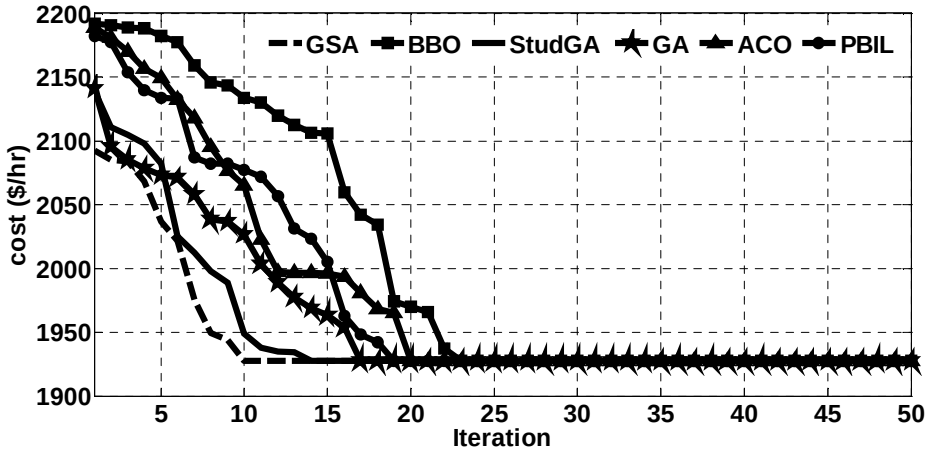

Fig.2.23. Cost minimization with single UPFC of NER transmission system

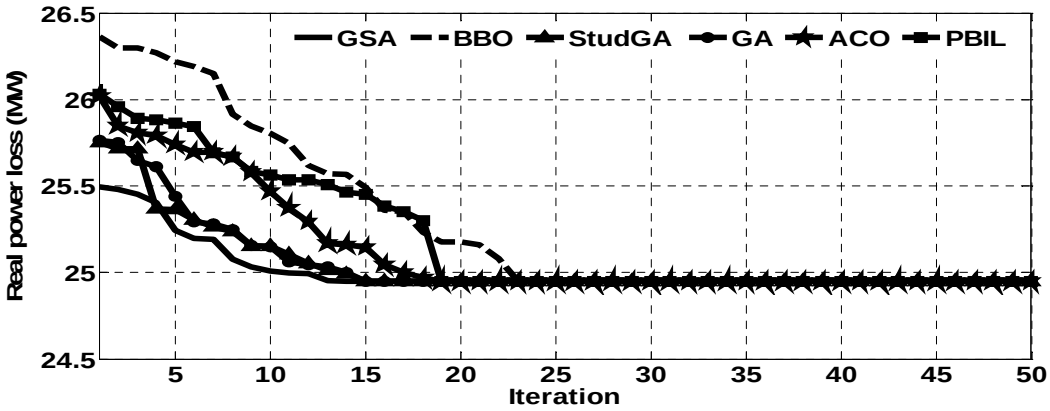

Fig.2.24. Loss minimization with single UPFC of NER transmission system.

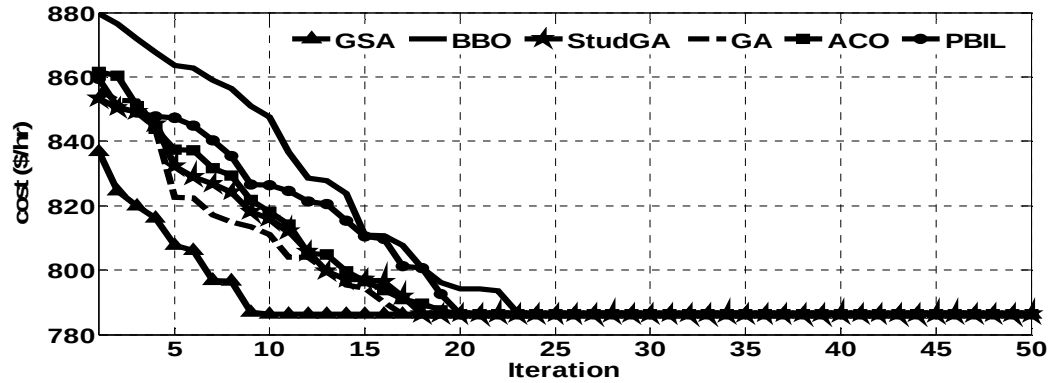

Fig. 2.25. Cost minimization with three UPFC of NER transmission system.

From Table 2.15 it is shown that the operational cost and transmission loss along with power flow through the line of optimal locations of UPFCs under cost minimization and loss minimization consideration are found to be same under different optimization techniques chosen in this chapter. But, Fig 2.23, Fig 2.24, Fig 2.25 and Fig 2.26 show difference between convergence characteristics of the adopted optimization techniques under cost minimization with single UPFC, loss minimization with single UPFC, cost minimization with three UPFC and loss minimization with three UPFC respectively. For better visualization the number of iterations required for convergence in different optimization techniques for NER transmission system are summarized in Table 2.16.

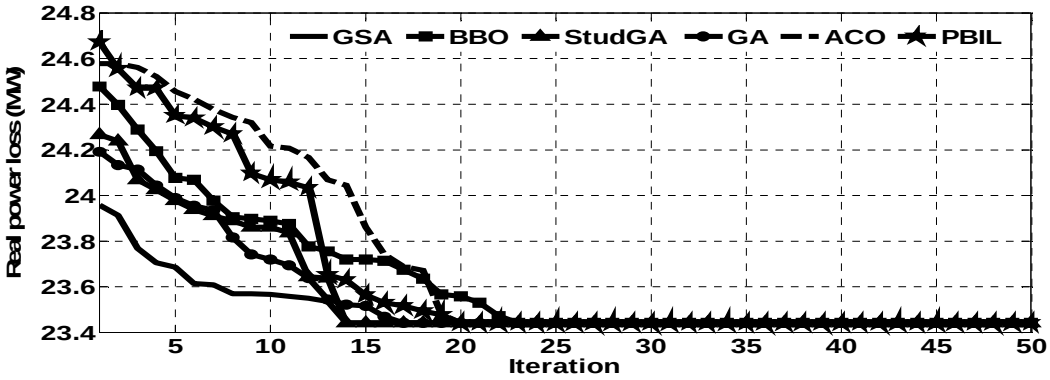

Fig.2.26. Loss minimization with three UPFC of NER transmission system.

Table 2.16. Number of iterations needed for optimum solution in NER transmission system

Minimized parameter	Test system	With GSA	With BBO	With StudGA	With GA	With ACO	With PBIL
Cost minimization with single UPFC	NER transmission system	11	21	17	20	20	19
Loss minimization with single UPFC		13	23	19	19	15	21
Cost minimization with three UPFC		12	24	15	18	19	19
Loss minimization with three UPFC		13	22	13	16	19	18

From Table 2.16, it is shown that iteration number required in NER transmission system for cost and loss minimizations by single UPFC installation with GSA technique are found to be 11 and 13 respectively, while those found for triple UPFCs installation are 12 and 13 respectively. Table 2.16 also shows that these results found by GSA are minimum among all the different soft computing techniques adopted here in their respective cost/loss minimization by single/triple UPFC installation in NER transmission system.

2.6. Influence of UPFC capacitor size and operating range of UPFC on operating cost of UPFC

In this section optimal sizing of dc link capacitor along with operating range of UPFCs are highlighted. Naturally, the operating costs of UPFCs are also affected. For this purpose, the voltage across DC link is to be accounted. This voltage across DC capacitor can be written as,

$$V_c = \left(2\sqrt{2}V_k / \Pi \right) \cos\alpha \tag{2.26}$$

Where α is firing angle of series converter.

The rating of capacitor can be written as,

$$C = Q_c / \omega V_c^2 \tag{2.27}$$

2.6.1. Formulation of the UPFC placement problem

The UPFC placement problem has already been formulated in section 2.3. In this section, the objective function operating cost is only modified, i.e., it is expressed as summation of fuel cost of the thermal generators and cost for UPFC devices. This modified operating cost can be expressed as

$$\text{Cos}t = \sum_{i=1}^{N_G} C_i\left(P_{G_i}\right) + \left(C_{UPFC}\right)_{Total} \tag{2.28}$$

The total cost for UPFC devices is expressed as,

$$\left(C_{UPFC}\right)_{Total} = \sum_{i=1}^{N}\left(C_{UPFC}\right)_i \tag{2.29}$$

where N is the total number of UPFCs installed in the test network. The cost [37] of each UPFC (in US$/kVA) can be expressed as,

$$C_{UPFC} = 0.0003S^2 - 0.2691S + 188.22 \tag{2.30}$$

where S is the operating range of UPFC in MVA and can be expressed as

$$S = \sqrt{P_c^{\,2} + Q_c^{\,2}} \tag{2.31}$$

Subject to the following constraints:

2.6.1.1. Equality constraints

The equality constraints have already been discussed in section 2.3.1.

2.6.1.2. Inequality constraints

Besides the inequality constraints of the OPF discussed in section 2.3.2, the additional inequality constraints considered for UPFC-cost calculation are as follows:

- **Active and reactive power compensation limit**

The maximum and minimum active and reactive powers controlled by UPFC in the connected transmission line can be expressed as,

$$P_{se} - V_k V_{se,\max} / X \le P_c \le P_{se} + V_k V_{se,\max} / X \tag{2.32}$$

$$Q_{se} - V_k V_{se,\max} / X \le Q_c \le Q_{se} + V_k V_{se,\max} / X \tag{2.33}$$

where, P_c and Q_c are controlled active and reactive power respectively. X is the reactance of the transmission line connected between buses k and m.

- **Firing angle limit**

The range of firing angle of each voltage source converter (VSC) plays an important role in power system. The upper and lower limit of firing angle of series VSC can be expressed as,

$$0 \le \alpha \le 90° \quad (2.34)$$

2.6.2. Results and Discussions

2.6.2.1. Impact of optimal capacitor sizing and optimal operating range of UPFC on operating cost

The variation in operating cost for different optimal locations of UPFCs in IEEE-14 bus, IEEE-30 bus, IEEE-57 bus and NER test systems are furnished in Table 2.17 to Table 2.20 respectively. The bus data and line data of different test systems have already been reported in section 2.5. The optimal locations of UPFC devices on different test systems along with transmission loss are already furnished in section 2.5. In this section only optimal capacitor sizes, optimal operating ranges of UPFC devices and thereby affected operational cost of UPFC devices have been introduced.

Table 2.17. Operating range of UPFC, capacitor sizing and cost in IEEE-14 bus test system

Optimized parameter	Control Variables	Number of UPFCs			
		0	1	2	3
Cost minimnization	Capacitor size (μF)	-	68	65, 98	64.5, 95, 1.04
	Operating range of UPFC (MVA)	-	1398.6	902.6, 943.36	300.9, 317.37 , 313.02
	Dispatch cost ($/hr)	5,629.50	3339.28	3328.07	3244.32
Loss minimization	Capacitor size (μF)	-	5.3	5.1, 2.21	4.9, 2.1, 1.43
	Operating range of UPFC (MVA)	-	1343.62	839.65, 911.37	433.42, 409.27, 448.98
	Dispatch cost ($/hr)	5,749.50	3901.74	3889.62	3866.95

From Table 2.17, it is shown that during cost minimization operational cost is decreased from 5,629.50 $/hr to 3339.28 $/hr by installing single UPFC in its optimal position. Table 2.17 also shows that the addition of another UPFC in IEEE14 bus test system reduces cost further to 3328.07 $/hr. From Table 2.17, it is also noticed that the further reduction in cost is achieved by adding third UPFC in IEEE14 bus test system and it is 3244.32 $/hr. In addition, the optimal sizing of capacitor of respective UPFC with UPFC operating range are found to be 68 µF and 1398.6 MVA for single UPFC, 65 and 98 µF with 902.6, 943.36 MVA for double UPFCs and 64.5, 95, 1.04 µF with 300.9, 317.37 and 313.02 MVA for triple UPFC installation in case of cost minimization.

Again Table 2.17 shows that during loss minimization operational cost is reduced from 5,749.50 $/hr to 3901.74$/hr by placing single UPFC in its optimal position. Table 2.17 also depicts that the addition of second UPFC in IEEE14 bus test system reduces cost slightly to 3889.62$/hr. Besides, from Table 2.17, it is also noticed that the further reduction in cost is achieved by adding optimally third UPFC in IEEE14 bus test system and it is 3866.95 $/hr. Table 2.17 also shows that for loss minimization the capacitor sizing and operating range of UPFC are found as 5.3 µF and 1343.62 MVA for single UPFC, 5.1 and 2.21 µF with 839.65, 911.37 MVA for double UPFCs and 4.9, 2.1 and 1.43 µF with 433.42, 409.27 and 448.98 MVA for triple UPFC installation respectively.

Table 2.18. Operating range of UPFC, capacitor sizing and cost in IEEE-30 bus test system

Optimized parameter	Control Variables	Number of UPFCs			
		0	1	2	3
Cost minimization	Capacitor size (μF)	-	4.56	4.5, 7.8	4.43, 0.72,0.95
	Operating range of UPFC (MVA)	-	1382.91	880.85, 950.04	419.19, 440.47, 380.47
	Dispatch cost ($/hr)	1271.2	1193.85	1182.17	1171.55
Loss minimization	Capacitor size (μF)	-	1.94	1.83, 0.79	0.79,1.70 ,0.71
	Operating range of UPFC (MVA)	-	1447.2	943.5, 865.45	458.22, 406.39, 461.94
	Dispatch cost ($/hr)	1289.2	1231.86	1188.53	1177.17

From Table 2.18, it is shown that during cost minimization operational cost is decreased from 1271.20 $/hr to 1193.85 $/hr by installing single UPFC at its optimal position. Table 2.18 also shows that the addition of another UPFC in IEEE30 bus test system reduces cost further to 1182.17 $/hr. From Table 2.18, it is also noticed that the further reduction in cost is achieved by adding optimally third UPFC in IEEE 30 bus test system and this reduced cost is 1171.55 $/hr. I addition, the optimal sizing of capacitor of respective UPFC with UPFC operating range are found to be 4.56 µF and 1382.91 MVA for single UPFC, 4.5 and 7.8 µF with 880.85, 950.04 MVA for double UPFCs and 4.43, 00.72 and 0.95 µF with 419.19, 440.47 and 380.47 MVA for triple UPFC installation in case of cost minimization.

Again Table 2.18 shows that during loss minimization operational cost is reduced from 1289.20 $/hr to 1231.86 $/hr by placing single UPFC at its optimal position. Table 2.18 also depicts that the addition of second UPFC in IEEE30 bus test system reduces cost to 1188.53 $/hr. Besides, from Table 2.18 it is also noticed that the further reduction in cost is achieved by adding optimally third UPFC in IEEE30 bus test system and it is 1177.17 $/hr. Table 2.18 also shows that for loss minimization the capacitor sizing along with operating range of UPFC are found as 1.94 µF and 1447.2 MVA for single UPFC, 1.83 and 0.79 µF with 943.5 and 865.45 MVA for double UPFCs and 0.79, 1.7 and 0.71 µF with 458.22, 406.39 and 461.94 MVA for triple UPFC installation respectively.

Table 2.19. Operating range of UPFC, capacitor sizing and cost in IEEE-57 bus test system

Optimized parameter	Control Variables	Number of UPFCs			
		0	1	2	3
Cost minimization	Capacitor size (μF)	-	1.56	1.34, 3.34	1.35,1.82 ,2.15
	Operating range of UPFC (MVA)	-	974.8	835.8, 769.52	699.22, 448.2, 509.65
	Dispatch cost ($/hr)	1,06,290	59,132.97	56591.66	52,448.60
Loss minimization	Capacitor size (μF)	-	2.17	2.05, 0.47	0.55, 1.39, 2.03
	Operating range of UPFC (MVA)	-	739.85	536.37, 592.91	480.15, 324.15, 407.35
	Dispatch cost ($/hr)	1,16,350	71,985.34	70514.32	69,769.07

From Table 2.19, it is shown that during cost minimization operational cost is decreased from 1,06,290 $/hr to 59,132.97 $/hr by installing single UPFC in its optimal position. Table 2.19 also shows that the addition of another UPFC in IEEE57 bus test system reduces cost to 56591.66 $/hr. From Table 2.19, it is also noticed that the further reduction in cost is achieved by adding optimally third UPFC in IEEE 57 bus test system and it is 52448.60 $/hr. In addition, the optimal sizing of capacitor of respective UPFC with operating range are found to be 1.56 µF and 974.8 MVA for single UPFC, 1.34 and 3.34 µF with 835.8 and 769.52 MVA for double UPFCs and 1.35, 1.82 and 2.15 µF with 699.22, 448.2 and 509.65 MVA for triple UPFC installation in case of cost minimization.

Again Table 2.19 shows that during loss minimization operational cost is reduced from 1,16,350$/hr to 71985.34 $/hr by placing single UPFC in its optimal position. Table 2.19 also depicts that the addition of second one UPFC in IEEE57 bus test system reduces cost to 70514.32 $/hr. Besides, from Table 2.19, it is also

noticed that the further reduction in cost is achieved by adding optimally third UPFC in IEEE57 bus test system and it is 69769.07 $/hr. Table 2.19 also shows that for loss minimization the capacitor sizing along with operating range of respective UPFC are found as 2.17 µF and 739.85 MVA for single UPFC, 2.05 and 0.47 µF with 536.37 and 592.91 MVA for double UPFCs and 0.55, 1.39 and 2.03 µF with 480.15, 324.15 and 407.35 MVA for triple UPFC installation respectively.

Table 2.20. Operating range of UPFC, capacitor sizing and cost in NER test system

Optimized parameter	Control Variables	Number of UPFCs			
		0	1	2	3
Cost minimization	Capacitor size (μF)	-	2.49	2.24, 1.38	1.02, 1.41, 1.1
	Operating range of UPFC (MVA)	-	557.91	453.45, 468.63	276.26, 227.68, 279.97
	Dispatch cost ($/hr)	67983	20587.6	16427.87	11844.4
Loss minimization	Capacitor size (μF)	-	2.35	1.97, 1.6	1,1.05, 1.3
	Operating range of UPFC (MVA)	-	545.85	442.15, 397.84	279.13, 284.57, 239.45
	Dispatch cost ($/hr)	68175	21445.71	20859.53	12019.4

From Table 2.20, it is shown that during cost minimization operational cost is decreased from 67983 $/hr to 20587.60 $/hr by installing single UPFC in its optimal position. Table 2.20 also shows that the addition of another one UPFC in NER transmission system reduces cost further to 16427.87 $/hr. From Table 2.20, it is also noticed that further reduction in cost is achieved by adding optimally third UPFC in NER transmission system and it is 11844.40 $/hr. In addition, the optimal sizing of capacitor of respective UPFC with operating range are found to be 2.49 µF and 557.91 MVA for single UPFC, 2.24 and 1.38 µF with 453.45 and 468.63 MVA for double UPFCs and 1.02, 1.41 and 1.1 µF with 276.26, 227.68 and 279.97 MVA for triple UPFC installation in case of cost minimization.

Again Table 2.20 shows that during loss minimization operational cost is reduced from 68175 $/hr to 21445.71 $/hr by placing single UPFC in its optimal position. Table 2.20 also depicts that addition of second UPFC in NER transmission system reduces cost to 20859.53$/hr. Besides, from Table 2.20, it is also noticed that the further reduction in cost is achieved by adding optimally third UPFC in NER transmission system and it is 12019.40 $/hr respectively. Table 2.20 also shows that for loss minimization that capacitor sizing along with operating range of UPFC are found as 2.35 µF and 545.85 MVA for single UPFC, 1.97 and 1.6 µF with 442.15

and 397.84 MVA for double UPFCs and 1, 1.05 and 1.3 μF with 279.13, 284.57 and 239.45 MVA for triple UPFC installation respectively.

2.6.2.2. Comparison of performance of different optimization method in solving the UPFC placement problem

The comparative results obtained by different soft computing techniques along with their respective iteration numbers for IEEE 14 bus, IEEE-30 bus, IEEE-57 bus and NER test systems are reported in Table 2.21 to Table 2.24 respectively. The convergence characteristics for four cases are shown in Fig 2.27 to Fig 2.42 respectively.

Table2.21. Comparison of the performance of different techniques in IEEE-14 bus test system

Parameter	Control Variables	With GSA	With BBO	With StudGA	With GA	With ACO	With PBIL
Cost minimization with single UPFC	Iteration number	13	23	18	20	24	18
	Dispatch cost ($/hr)	3339.28	3339.28	3339.28	3339.28	3339.28	3339.28
Loss minimization with single UPFC	Iteration number	12	22	17	18	15	26
	Dispatch cost ($/hr)	3901.74	3901.74	3901.74	3901.74	3901.74	3901.74
Cost minimization with three UPFC	Iteration number	14	24	15	18	18	19
	Dispatch cost ($/hr)	3244.32	3244.32	3244.32	3244.32	3244.32	3244.32
Loss minimization with three UPFC	Iteration number	14	20	15	19	16	24
	Dispatch cost ($/hr)	3866.95	3866.95	3866.95	3866.95	3866.95	3866.95

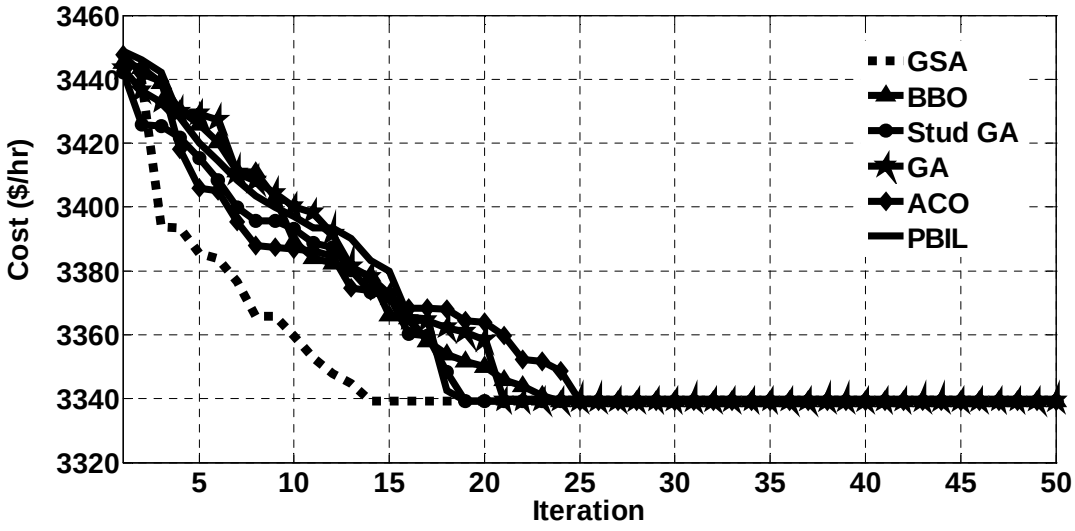

Fig.2.27. Cost minimization with single UPFC of IEEE-14 bus system.

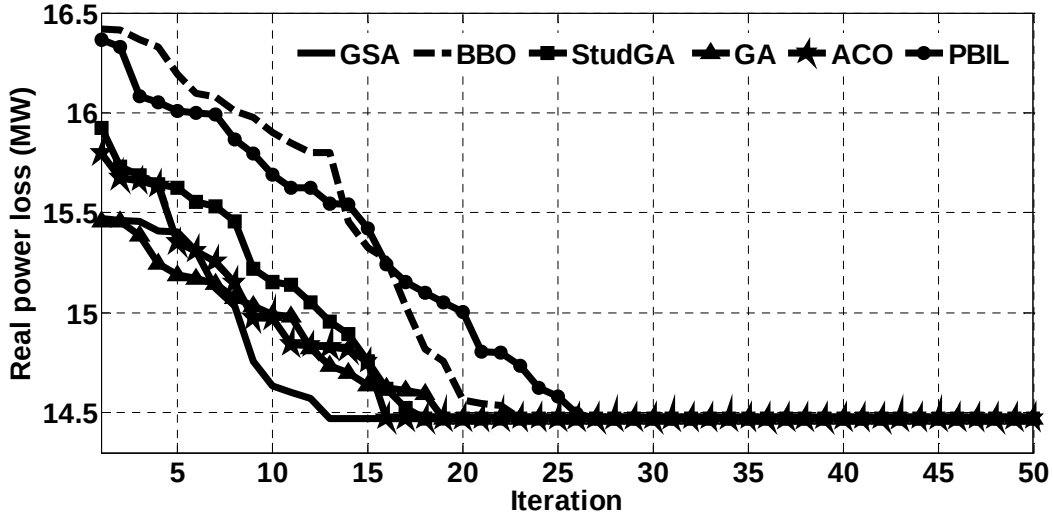

Fig.2.28. Loss minimization with single UPFC of IEEE-14 bus system.

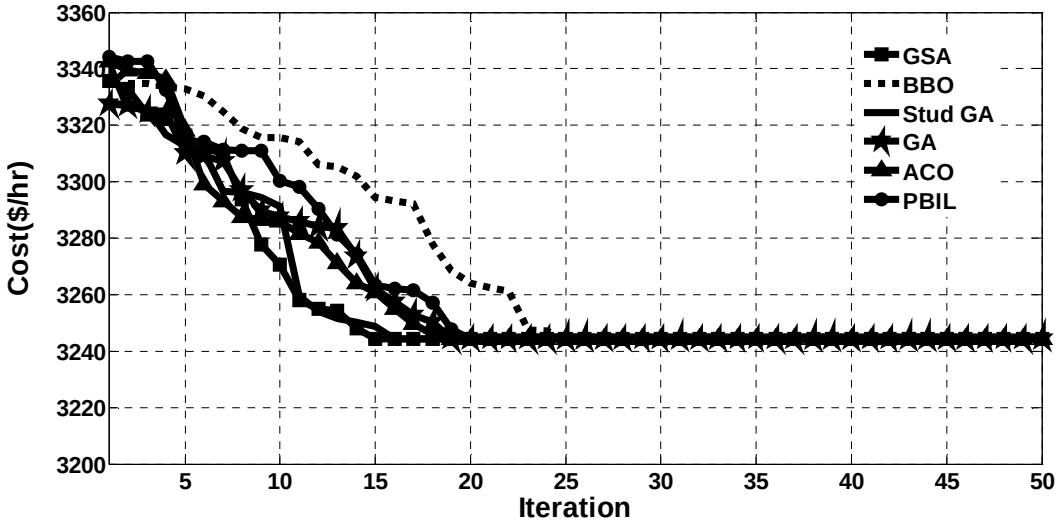

Fig. 2.29. Cost minimization with three UPFC of IEEE-14 bus system.

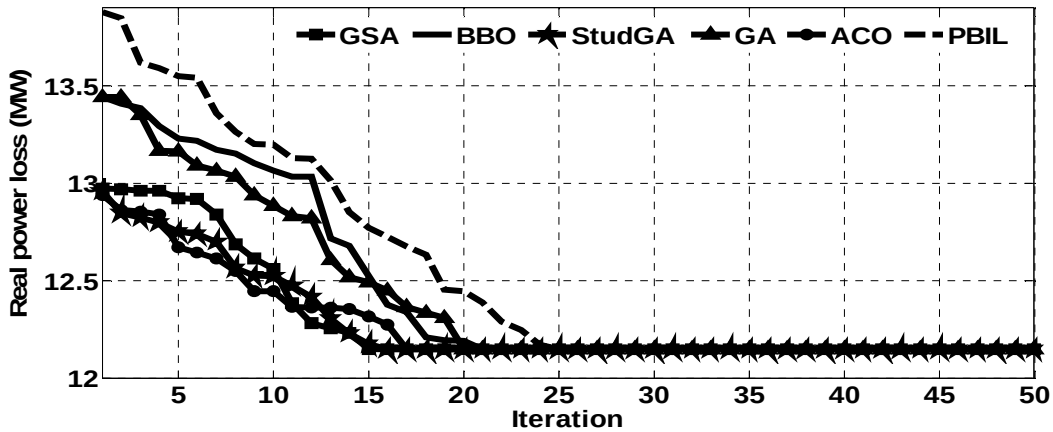

Fig.2.30. Loss minimization with three UPFC of IEEE-14 bus system.

From Table 2.21, it is shown that the operational cost under cost minimization and loss minimization consideration are found to be same in different optimization techniques chosen in this chapter. But, Fig 2.27 to Fig 2.30 show difference between convergence characteristics of the adopted optimization techniques under cost minimization with single UPFC, loss minimization with single UPFC, cost minimization with three UPFC and loss minimization with three UPFC respectively. For better visualization the number of iterations required for convergence in different optimization techniques for IEEE14 bus system is summarized in Table 2.21.

From Table 2.21, it is shown that iteration number required in IEEE14 bus test system for cost and loss minimizations by single UPFC installation with GSA technique are found to be 13 and 12 respectively, while the number of iterations for cost and loss minimization by triple UPFCs installation are found to be same, i.e., 14. Table 2.21 also shows that these results found by GSA are minimum among all the different soft computing techniques adopted here in their respective cost/loss minimization by single/triple UPFC installation in IEEE14 bus test system.

Table2.22. Comparison of the performance of different techniques in IEEE-30 bus test system

Parameter	Control Variables	With GSA	With BBO	With StudGA	With GA	With ACO	With PBIL
Cost minimization with single UPFC	Iteration number	11	25	15	18	18	19
	Dispatch cost ($/hr)	1193.85	1193.85	1193.85	1193.85	1193.85	1193.85
Loss minimization with single UPFC	Iteration number	12	24	17	22	19	18
	Dispatch cost ($/hr)	1231.86	1231.86	1231.86	1231.86	1231.86	1231.86
Cost minimization with three UPFC	Iteration number	12	27	20	24	19	31
	Dispatch cost ($/hr)	1171.55	1171.55	1171.55	1171.55	1171.55	1171.55
Loss minimization with three UPFC	Iteration number	7	28	25	25	27	26
	Dispatch cost ($/hr)	1177.17	1177.17	1177.17	1177.17	1177.17	1177.17

From Table 2.22, it is shown that the operational cost of UPFCs in IEEE-30 bus test system, under cost minimization and loss minimization consideration are found to be same under different optimization techniques chosen in this chapter. But, Fig 2.31 to Fig 2.34 show difference between convergence characteristics of the adopted optimization techniques under cost minimization with single UPFC, loss minimization with single UPFC, cost minimization with three UPFC and loss minimization with three UPFC respectively. For better visualization the number of iterations required for convergence in different optimization techniques for IEEE30 bus system are summarized in Table 2.22.

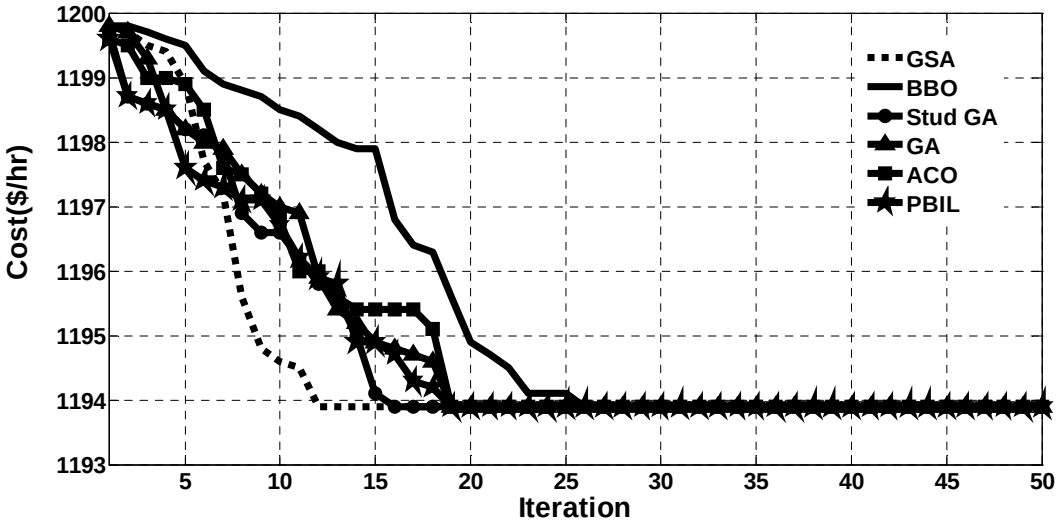

Fig.2.31. Cost minimization with single UPFC of IEEE-30 bus system.

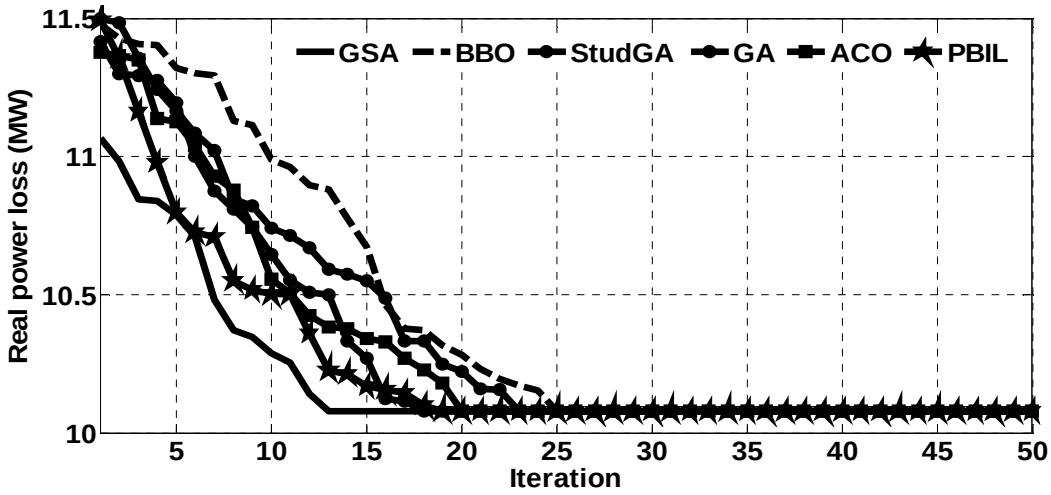

Fig.2.32. Loss minimization with single UPFC of IEEE-30 bus system.

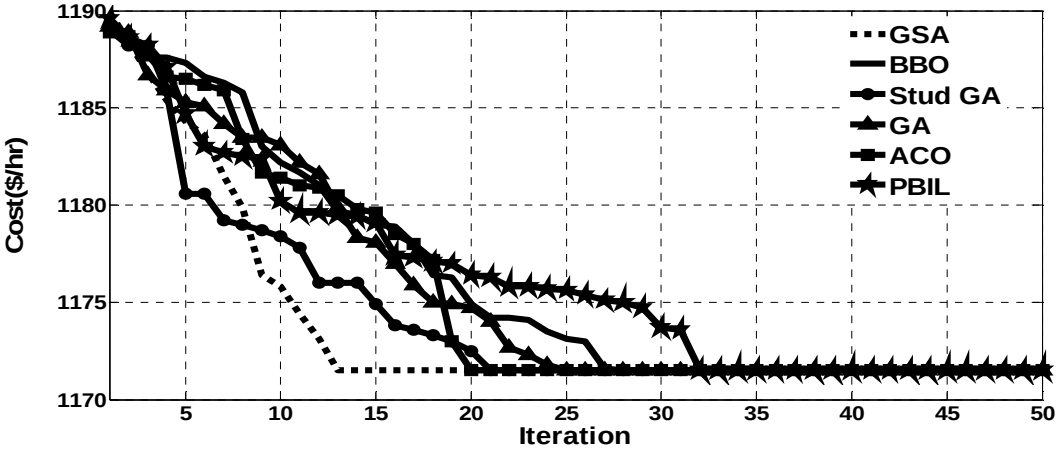

Fig. 2.33. Cost minimization with three UPFC of IEEE-30 bus system.

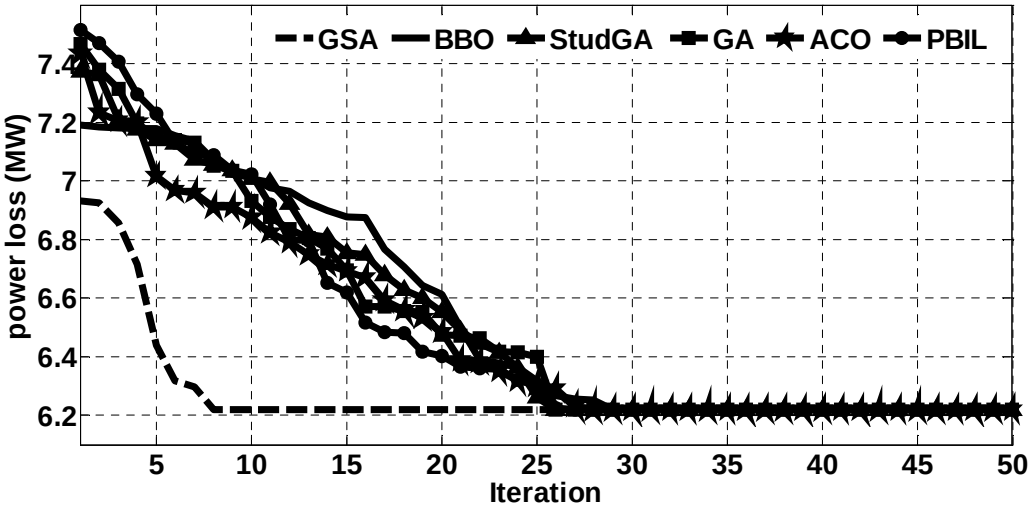

Fig.2.34. Loss minimization with three UPFC of IEEE-30 bus system.

From Table 2.22, it is shown that iteration number required in IEEE30 bus test system for cost and loss minimizations by single UPFC installation with GSA technique are found to be 11 and 12 respectively, while those found for triple UPFCs installation are 12 and 7 respectively. Table 2.22 also shows that these results found by GSA are minimum among all the different soft computing techniques adopted here in their respective cost/loss minimization by single/triple UPFC installation in IEEE30 bus test system.

Table 2.23. Comparison of the performance of different techniques in IEEE-57 bus test system

Parameter	Control Variables	With GSA	With BBO	With StudGA	With GA	With ACO	With PBIL
Cost minimization with single UPFC	Iteration number	11	21	17	20	20	19
	Dispatch cost ($/hr)	59132.97	59132.97	59132.97	59132.97	59132.97	59132.97
Loss minimization with single UPFC	Iteration number	13	23	19	19	15	21
	Dispatch cost ($/hr)	71985.34	71985.34	71985.34	71985.34	71985.34	71985.34
Cost minimization with three UPFC	Iteration number	12	24	15	18	19	19
	Dispatch cost ($/hr)	52448.6	52448.6	52448.6	52448.6	52448.6	52448.6
Loss minimization with three UPFC	Iteration number	13	22	13	16	19	18
	Dispatch cost ($/hr)	69769.07	69769.07	69769.07	69769.07	69769.07	69769.07

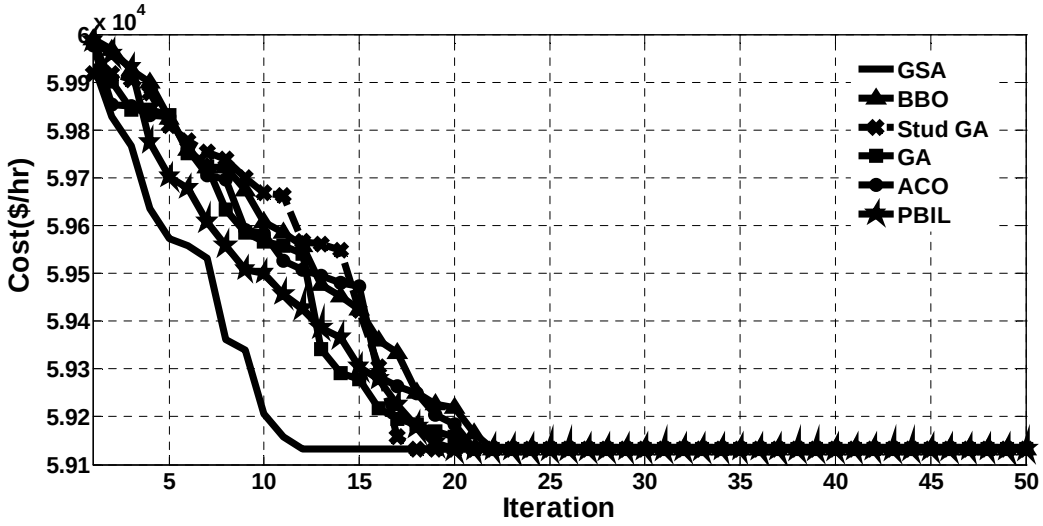

Fig.2.35. Cost minimization with single UPFC of IEEE-57 bus system.

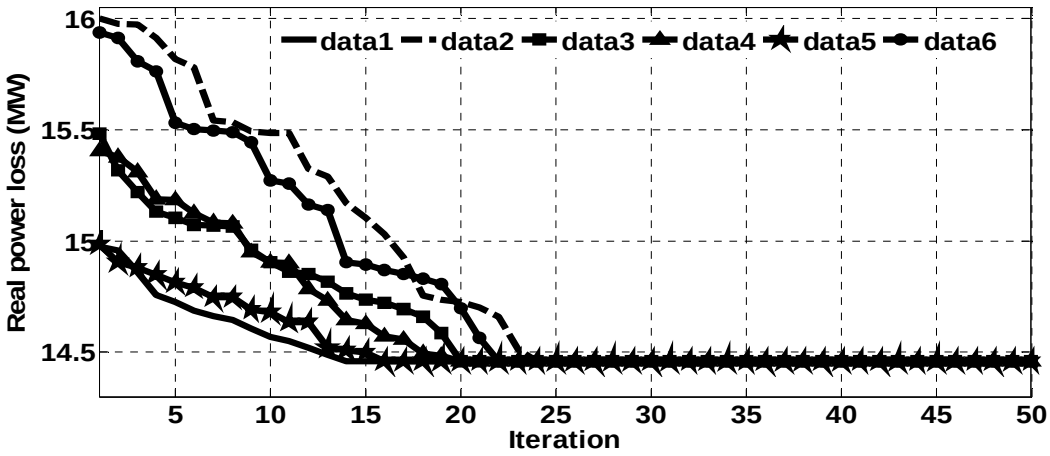

Fig.2.36. Loss minimization with single UPFC of IEEE-57 bus system.

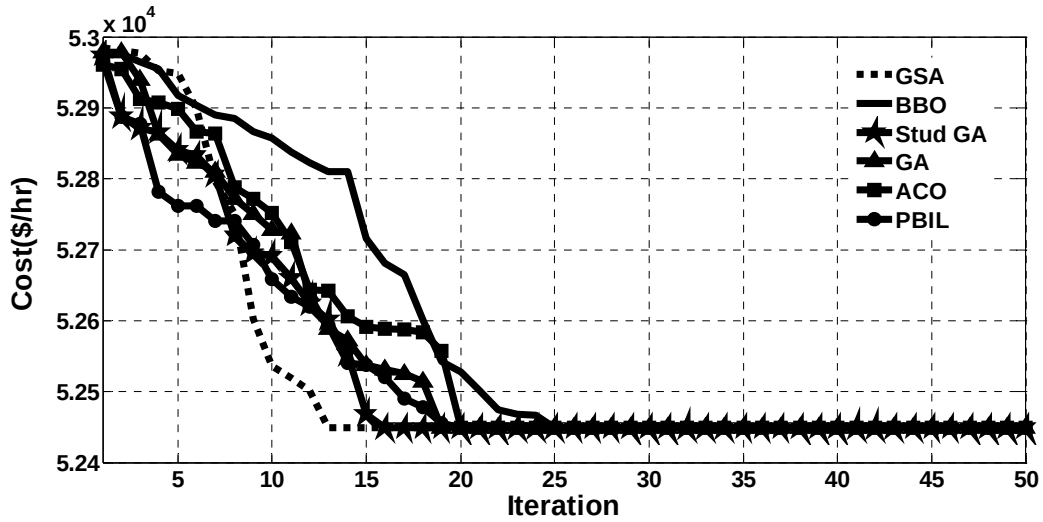

Fig. 2.37. Cost minimization with three UPFC of IEEE-57 bus system.

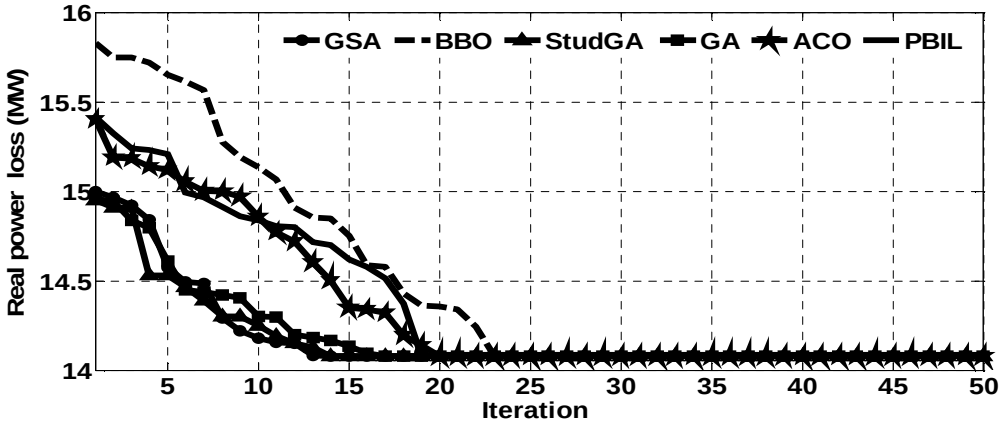

Fig.2.38. Loss minimization with three UPFC of IEEE-57 bus system.

From Table 2.23, it is shown that the operational cost of UPFCs in IEEE-57 bus test system, under cost minimization and loss minimization consideration are found to be same under different optimization techniques chosen in this chapter. But, Fig 2.35 to Fig 2.38 show difference between convergence characteristics of the adopted optimization techniques under cost minimization with single UPFC, loss minimization with single UPFC, cost minimization with three UPFC and loss minimization with three UPFC respectively. For better visualization the number of iterations required for convergence in different optimization techniques for IEEE57 bus system are summarized in Table 2.23.

From Table 2.23, it is shown that iteration number required in IEEE57 bus test system for cost and loss minimizations by single UPFC installation with GSA technique are found to be 11 and 13 respectively, while those found for triple UPFCs installation are 12 and 13 respectively. Table 2.23 also shows that these results found by GSA are minimum among all the different soft computing techniques adopted here in their respective cost/loss minimization by single/triple UPFC installation in IEEE57 bus test system.

Table 2.24. Comparison of the performance of different techniques in NER test system

Parameter	Control Variables	With GSA	With BBO	With StudGA	With GA	With ACO	With PBIL
Cost minimization with single UPFC	Iteration number	11	21	17	20	20	19
	Dispatch cost ($/hr)	20587.6	20587.6	20587.6	20587.6	20587.6	20587.6
Loss minimization with single UPFC	Iteration number	13	23	19	19	15	21
	Dispatch cost ($/hr)	21445.71	21445.71	21445.71	21445.71	21445.71	21445.71
Cost minimization with three UPFC	Iteration number	12	24	15	18	19	19
	Dispatch cost ($/hr)	11844.4	11844.4	11844.4	11844.4	11844.4	11844.4
Loss minimization with three UPFC	Iteration number	13	22	13	16	19	18
	Dispatch cost ($/hr)	12019.4	12019.4	12019.4	12019.4	12019.4	12019.4

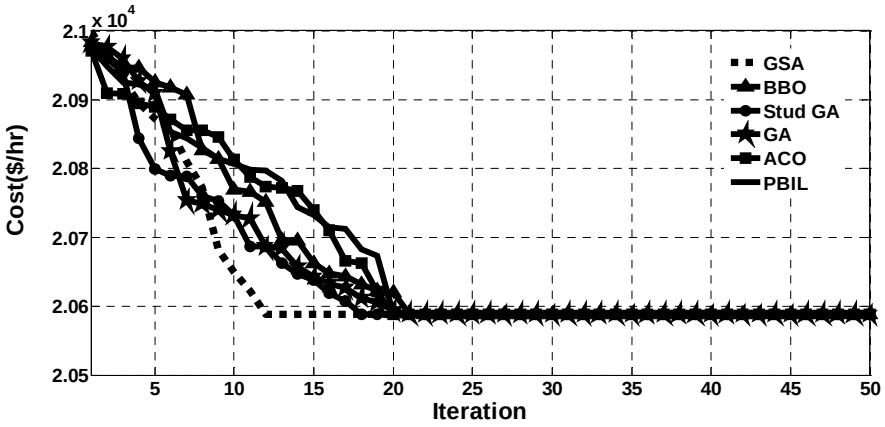

Fig. 2.39. Cost minimization with single UPFC of NER test system.

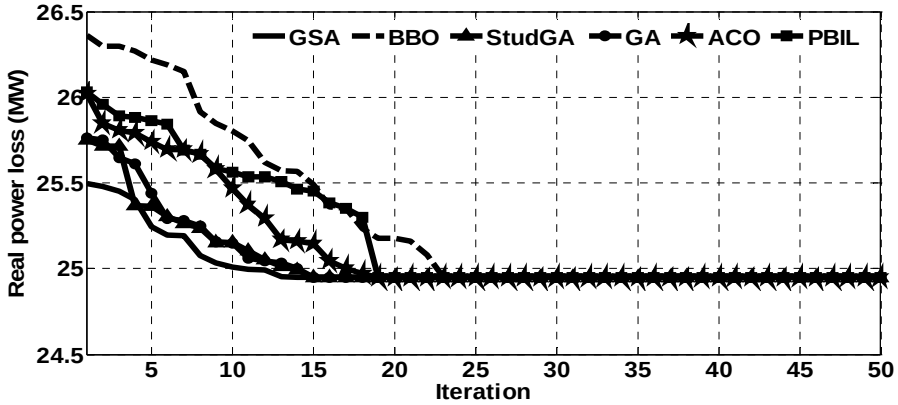

Fig.2.40. Loss minimization with single UPFC of NER test system.

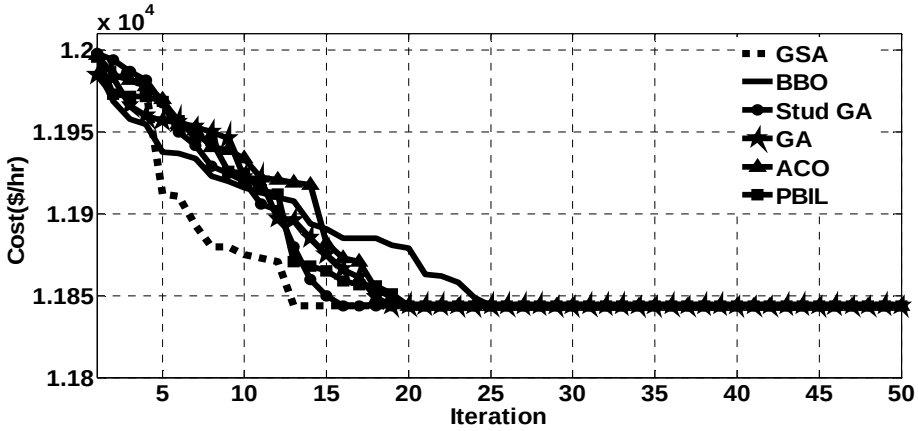

Fig. 2.41. Cost minimization with three UPFC of NER test system.

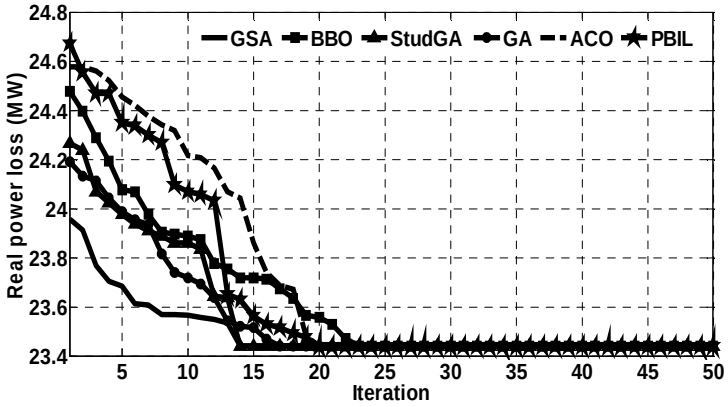

Fig. 2.42. Loss minimization with three UPFC of NER test system

From Table 2.24, it is shown that the operational cost of UPFCs under cost minimization and loss minimization consideration are found to be same under different optimization techniques chosen in this chapter. But, Fig 2.39 to Fig 2.42 show difference between convergence characteristics of the adopted optimization techniques under cost minimization with single UPFC, loss minimization with single UPFC, cost minimization with three UPFC and loss minimization with three UPFC respectively. For better visualization the number of iterations required for convergence in different optimization techniques for NER transmission system are summarized in Table 2.24.

From Table 2.24, it is shown that iteration number required in NER transmission system for cost and loss minimizations by single UPFC installation with GSA technique are found to be 11 and 13 respectively, while those found for triple UPFCs installation are 12 and 13 respectively. Table 2.24 also shows that these results found by GSA are minimum among all the different soft computing techniques adopted here in their respective cost/loss minimization by single/triple UPFC installation in NER transmission system.

The simulation program has been executed in MATLAB 7.8 and performed on an Intel I Core i5 CPU with 2.67 GHz and 4.00 GB memory.

2.7. Conclusion

In this chapter the problem of placement of UPFC in power system network has been solved through the solution of the optimal power flow problem using the GSA technique. To demonstrate the performance of GSA for optimal locations of single, double and three UPFC devices, different case studies of IEEE-14 bus test system, IEEE-30 bus test system, IEEE-57 bus test system and NER system have been analyzed. Results found in this chapter, have shown that

- the optimized systems have attained better voltage profile. From the graphs of voltage profile in different test network, it is obvious that voltage profile nearer to 1.0 p.u. have resulted in reduced system losses.
- from the optimized result it is found that with the increase in number of UPFC placed in optimal locations of test system, the operating range of UPFC is also minimized which results in optimization of dc link size of UPFCs. This operating range of UPFC also affects the UPFC cost minimization.
- the optimized solution has resulted in lower system costs and/or lower system loss as set by the respective objective functions thus shifting the system to better operating conditions. In addition to that, supported by the improved bus voltages, generator power share could reach to improved economic points such that the system operating cost also got reduced. The system in fact has attained a greater flexibility. The results reported in this chapter also show that the optimization technique GSA can effectively handle the power system optimization problem of placing the UPFCs.
- the optimized results appear to have increased benefits in terms of loss in comparison to other test systems presented, which is quite logical as the system is of much larger dimension compared to the standard test networks. It thus indicates that the application of UPFC is more justified for larger power systems.
- GSA tends to have steady and fast convergence characteristics as it approaches the optimal solution or near optimal within reasonable number of iterations. Besides, from the convergence characteristics graphs, it is obvious that GSA approach has good convergence characteristics compare to other optimization techniques. So as a whole, it can be said that GSA is efficient than other mentioned methods in solving the UPFC placement problem.
- The constrained optimization problems can be easily solved by GSA. The capability of GSA in handling large scale optimization problem such as the problem of placement of multiple UPFC has also been established. Such efforts of optimal placement of multiple UPFC devices cannot be commonly found in technical literature.

Chapter 3:

Optimal Placement of Unified Power Quality Conditioner in Distribution System for Power Quality Improvement

Summary: *The present chapter has adopted cuckoo optimization algorithm (COA) to find the optimal allocation of unified power quality conditioner (UPQC) in three phase unbalanced distribution network. The performance of UPQC is studied in terms of minimization of load disturbance during fault condition in the test systems, % reduction of total harmonic distortion and individual harmonics, minimization of real power loss, decrease in voltage unbalance and increase in cost savings during normal operating condition. The performance of COA is compared with other soft computing techniques to get the better results, i.e., better voltage profile, the optimal location and optimal number of UPQCs. The proposed method is implemented on IEEE-123 node test system and 25-bus radial distribution system to prove the computational ability and acceptability in the power system.*

3.1. Introduction

With the advancement of distribution system the usage of non-linear loads such as advanced power electronic and computer controlled devices are increasing day-by-day. It ultimately results in harmonics generation in load current and bus voltages. That's why the deterioration of secured level of power quality [38] has drawn a great attention of the power engineers specially, in the industry where stricter power quality is required [39]. Performances of the microprocessor based controllers are very much affected in these industries by line voltage distortion [40].

In such conditions, usual power quality improvement equipments are proving to be inadequate for these sophisticated applications and this fact has compelled the power engineers to develop dynamic and adjustable solutions to power quality problems. The compensating devices such as dynamic voltage restorer [41], uninterruptible power supplies [42] and active filters [43] are proposed to improve power quality. But, their capabilities are usually limited as they can only solve one or two power quality problems [44]. Recent research has shown that Unified Power Quality Conditioner (UPQC) can simultaneously fulfill different objectives, such as maintaining a sinusoidal voltage at the bus at which it is connected [45], maintaining voltage at desired level when there are voltage sags and swells in the system [46-48], filtering harmonics in the source currents [49], load balancing [50] and power quality improvement [50-52]. UPQC is a flexible device, that comprises of shunt and series Active Power Filters (APFs), sharing a common dc link [53].

A lot of researches have found UPQC as an eventual solution to improve the power quality in electrical distribution system [54]. But due to high cost involved, the location of UPQC in distribution system has to be decided with great care and should preferably be solved as an optimization problem. The optimization of UPQC placement problem in a competitive environment comprises of the minimization of power losses, total harmonic distortion (THD) minimization, voltage profile improvement and unbalance reduction under normal and voltage sag conditions [55].

This chapter presents a method based on Cuckoo Optimization Algorithm (COA) [56] to locate the optimal positions of UPQC device considering THD, voltage profile improvement and power system losses. The present chapter is arranged as follows. The model of UPQC along with its phasor diagram are shown in section 3.2. Then UPQC allocation strategy is discussed in section 3.3. After that optimal placement problem of UPQCs in distribution system is formulated in section 3.4. Next, optimal allocation methodology of UPFC is proposed in section 3.5. The procedural steps of Cuckoo Optimization algorithm and simulation procedure of UPQC controller are detailed in sections 3.5.1 and 3.5.2 respectively. The proposed method is tested on IEEE123 bus

distribution system and 25 bus distribution system and the results are furnished in section 3.6. Finally, the chapter is concluded in section 3.7.

3.2. Structure of UPQC

Generally, UPQC is made up of a series converter and shunt converter. A schematic representation of three-phase four wire voltage source converter-based UPQC is shown in Fig.3.1. The shunt APF is usually connected across the loads whereas the series APF is connected in series with a line through a three-phase series transformer [57]. The other ends of these two inverters are connected with a common dc storage capacitor.

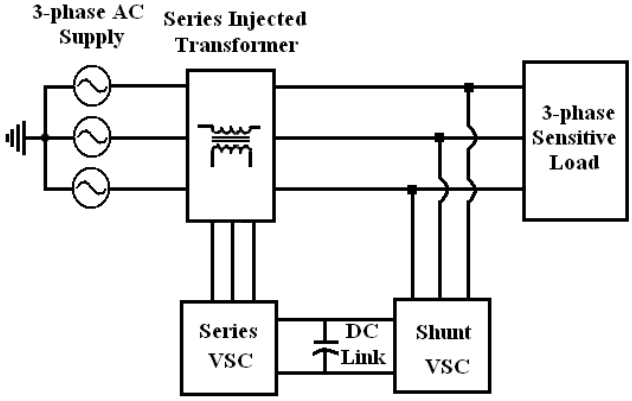

Fig.3.1. Schematic representation of UPQC

The phasor diagram of voltage and current injections by series and shunt inverter of UPQC is shown in Fig.3.2. The magnitude of injected voltage V_{se} by series inverter depends on maximum voltage sag to be mitigated [58].

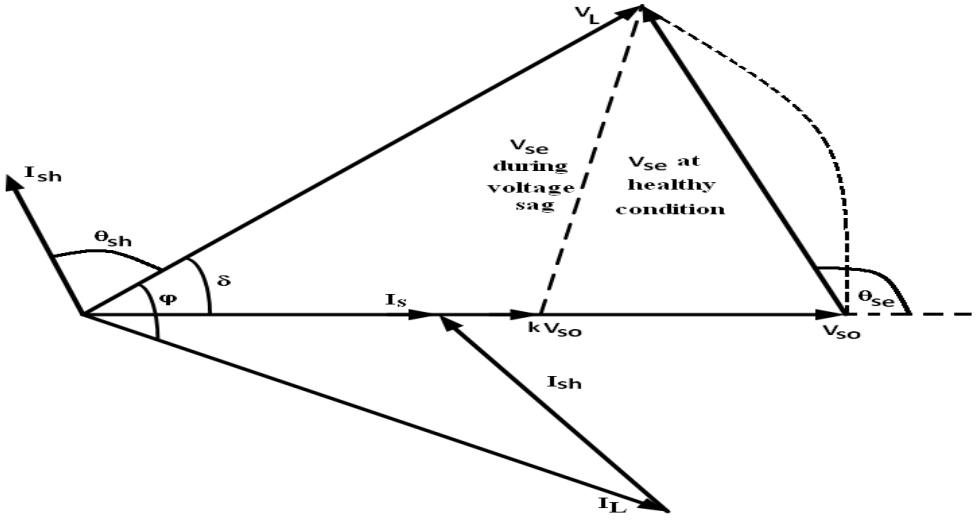

Fig.3.2. Phasor diagram of shunt and series compensation of UPQC during normal and voltage sag condition

Under normal condition, the source voltage magnitude is represented by $V_s = V_{S0}$ whereas during voltage sag conditions, the source voltage magnitude is denoted by $V_s = kV_{S0}$. In this chapter, $k_{sag} = (1-k)$, p.u. sag in source voltage.

At any condition load voltage, $V_L = V_{S0} = V_s$

To minimize k_{sag} p.u. amount of voltage sag the series converter injects the voltage by an amount of V_{se} and it can be written as

$$\begin{aligned} V_{se} &= \sqrt{V_L^2 + (kV_{S0})^2 - 2V_L(kV_{S0})\cos\delta} \\ &= V_s\sqrt{1+k^2-2k\cos\delta} \end{aligned} \tag{3.1}$$

By assuming a lossless UPQC, active power demanded by load can be expressed by active power drawn from source, i.e., $kV_sI_s = V_LI_L\cos\phi$, which yields the source current as,

$$I_s = I_L\cos\phi \Big/ k \tag{3.2}$$

Where, I_s and I_L are the compensated source-end current and load current respectively.

From equations (3.1) and (3.2) the VA rating of series inverter can be expressed as,

$$\begin{aligned} S_{se} &= V_{se}I_s \\ &= V_sI_L\cos\phi\sqrt{1+k^2-2k\cos\delta}\Big/k \end{aligned} \tag{3.3}$$

Active and reactive power delivered by series inverter can be expressed by equations (3.4) and (3.5) respectively, as given below:

$$P_{se} = S_{se}\cos\theta_{se} = V_{se}I_s\cos\theta_{se} \tag{3.4}$$

$$Q_{se} = S_{se}\sin\theta_{se} = V_{se}I_s\sin\theta_{se} \tag{3.5}$$

Where, $\theta_{se} = 180° - \tan^{-1}(\sin\delta/1-\cos\delta)$, given in [25]

Besides, the shunt converter compensates all current related problems by injecting current I_{sh}. From Fig.3.2, compensating current I_{sh} can be expressed as,

$$\begin{aligned} I_{sh} &= \sqrt{I_s^2 + I_L^2 - 2I_sI_L\cos(\phi-\delta)} \\ &= I_L\sqrt{1+\cos^2\phi\big/k^2 - 2\cos\phi\cos(\phi-\delta)\big/k} \end{aligned} \tag{3.6}$$

The harmonic present in load ends are compensated by shunt converter as equations (3.7) and (3.8), i.e.,

$$I_L^{dis} = I_{sh}^{dis} \tag{3.7}$$

$$THD_L I_L^f = THD_{sh} I_{sh}^f \tag{3.8}$$

Where, I_L^{dis}, I_L^f and THD_L are distortion component, fundamental component and total harmonic distortion of load current respectively. I_{sh}^{dis}, I_{sh}^f and THD_{sh} are distortion component, fundamental component and total harmonic distortion of shunt inverter current respectively.

So, by taking both the fundamental and harmonics into consideration, the total r.m.s value of shunt compensating current can be expressed as,

$$\begin{aligned} I_{sh} &= I_{sh}^f \sqrt{1+THD_{sh}^2} \\ &= I_L^f \sqrt{1+\cos^2\phi/k^2 - 2\cos\phi\cos(\phi-\delta)/k + THD_L^2} \end{aligned} \tag{3.9}$$

So, from equation (3.9), VA rating of the shunt inverter [25] can be expressed as,

$$\begin{aligned} S_{sh} &= V_s I_{sh} \\ &= V_s I_L^f \sqrt{1+\cos^2\phi/k^2 - 2\cos\phi\cos(\phi-\delta)/k + THD_L^2} \end{aligned} \tag{3.10}$$

Active and reactive powers delivered by shunt inverter are represented by equations (3.11) and (3.12) respectively, given below:

$$P_{sh} = S_{sh}\cos\theta_{sh} = V_s I_{sh}\cos\theta_{sh} \tag{3.11}$$

$$Q_{sh} = S_{sh}\sin\theta_{sh} = V_s I_{sh}\sin\theta_{sh} \tag{3.12}$$

Where, $\theta_{sh} = \tan^{-1}\{\cos(\phi-\delta) - \cos\phi/\sin(\phi-\delta)\} + 90° - \delta$, reported in [59].

By adding equations (3.5) and (3.12), total reactive power provided by UPQC is,

$$Q_{UPQC} = Q_{se} + Q_{sh} \tag{3.13}$$

3.3. UPQC allocation

Though many researchers have studied UPQC as an eventual solution to improve the power quality in electrical distribution system [60], but due to its high cost, the location of UPQC in distribution system has to be decided with great care and should preferably be solved as an optimization problem. The optimization of UPQC placement problem in a competitive environment comprises of the minimization of power losses, total harmonic distortion (THD) minimization, voltage profile improvement and unbalance reduction both under normal and voltage sag conditions [61]. The proposed methodology is described in sections 3.6 and 3.7.

3.4. Problem formulation

In this chapter, the objective function to be optimized consists of the following three parts:

- ***Part 1-*** To minimize the active power loss-cost in the system. This formulation reduces the distribution line losses by optimal allocation of UPQC in distribution system.

However, the total active power loss in the distribution system, to be minimized is represented as,

$$P_{Loss} = \sum_{k=1}^{N_L} Loss_k = \sum_{k=1}^{N_L} g_k \left\{ V_i^2 + V_j^2 - 2V_iV_j \cos\left(\delta_i - \delta_j\right) \right\} \tag{3.14}$$

Where, N_L is the total number of distribution lines. g_k is the conductance of the k^{th} line connected between buses i and j. V_i and V_j are the voltage magnitudes of buses i and j respectively. δ_i and δ_j are the voltage angles of buses i and j respectively.

- ***Part 2-*** To minimize load disturbance cost during fault. The main target of this formulation is to maintain continuity of the supply without disturbing voltage level and attenuating harmonics at different load ends during fault occurs on distribution line. This formulation, in turn, reduces the operating cost in great extent.

This total load disturbed due to voltage sag during fault condition, reported in [62], is expressed as,

$$S_{DIST} = \sum_{i=1}^{N_F} L_{DIST_i} \tag{3.15}$$

where, L_{DIST_i} is the load disturbed for the i^{th} fault and N_F is the total number of faults within the specified time duration considered.

- ***Part 3-*** To minimize the number of UPQC. This formulation involves optimal allocation of UPQC along with optimal number by satisfying equality and inequality constraints given below.

The above three formulation can be gathered together to get a single objective function and this cost function may be represented as,

$$Cost = K_{loss} \sum_{k=1}^{N_L} Loss_k + K_{MVA} \sum_{i=1}^{N_F} L_{DIST_i} + K_{size} \sum_{i=1}^{N_{UPQC}} S_{UPQC_i} \tag{3.16}$$

Where, K_{loss} denotes the cost of energy losses per unit, considered as 0.08 US$/kWh [62], K_{MVA} is the cost of unit load disturbed, taken as 4 US$/MVA [62]. K_{size} is the cost of each UPQC, following the details as

mentioned in [63]. N_{UPQC} is the total number of UPQCs used in the test systems. N_L and N_F are the total distribution lines and faults respectively in the respective distribution system.

The equality and inequality constraints satisfied by the single objective function given in equation (3.16) during cost minimization are mentioned in sections 3.6.1 and 3.6.2 respectively.

3.4.1. Equality constraints

Representing active and reactive power of the line in terms of bus voltage magnitude and phase angle, the power balance equations at the buses may be expressed as [62]:

The active power balance in the distribution system is represented as,

$$P_{G_i} - P_{D_i} - \sum_{k=1}^{N_L} g_{ik} \left\{ V_i^2 + V_j^2 - 2V_i V_j \cos\left(\delta_i - \delta_j\right) \right\} = 0 \tag{3.17}$$

and reactive power balance may be expressed as

$$Q_{G_i} - Q_{D_i} - \sum_{k=1}^{N_L} b_{ik} \left\{ V_i^2 + V_j^2 - 2V_i V_j \sin\left(\delta_i - \delta_j\right) \right\} = 0 \tag{3.18}$$

where, P_{G_i} , P_{D_i} and P_{Loss} are the active power injected at bus i, system active power demand and total active power loss respectively. Q_{G_i} , Q_{D_i} and Q_{Loss} are the reactive power injected at bus i, system reactive power demand and total reactive power loss respectively. N_L is the total number of distribution lines. g_{i-j} and b_{i-j} are the conductance and susceptance respectively of the line connected between buses i and j. V_i and V_j are the voltage magnitudes of buses i and j respectively. δ_i and δ_j are the voltage angles of buses i and j respectively.

3.4.2. Inequality constraints

Inequality constraints are included basically to express capacity and operational limits of the system. These inequality constraints may be grouped into three classes:

- **Line flow limit**

The line flow limit indicates the maximum capability of power transmission through a given transmission line under certain given conditions. The limit may depend either on thermal consideration for shorter lines or on the stability consideration. The power flow limit constraints of the line can be expressed as,

$$S_k \leq S_{k_{\max}} \tag{3.19}$$

Where, $S_{k_{\max}}$ is the maximum value of the power flow through k^{th} line.

- **Harmonic limits**

In this chapter, two type of harmonic constraints have been considered, namely, voltage total harmonic distortion limit and individual voltage harmonic limit.

The voltage total harmonic distortion constraint is expressed as,

$$THD_V \leq THD_{\max} \tag{3.20}$$

where, $THD_{\max}$ is the maximum value of THD, taken as 5% here, as per IEEE 519 standards.

Individual voltage harmonic limit constraint is expressed as,

$$V_h \leq V_{h_{\max}} \tag{3.21}$$

where, $V_{h_{\max}}$ is maximum individual harmonic voltage, taken as 3% which is standard limit.

- **Bus voltage limits**

Bus voltage limit has been considered in terms of node voltage magnitude limit and voltage unbalance limit respectively.

Three phase node voltage magnitude limit constraint is expressed as,

$$V_{\min} \leq V \leq V_{\max} \tag{3.22}$$

where, $V_{\min}$ and $V_{\max}$ are minimum and maximum values, taken as 0.85 p. u. and 1.05 p. u. respectively in this chapter.

The three phase voltage unbalance in distribution system is defined in [64] and the limit of this constraint is expressed as,

$$VU \leq VU_{\max} \tag{3.23}$$

where, $VU_{\max}$ is the permissible value of voltage unbalance, taken as 2% in this chapter.

For a better compatibility, the objective function of equation (3.16) and the constraints in equations (3.17-3.23) are combined together to form a single objective function without constraints as:

$$Cost = K_{loss}\sum_{k=1}^{N_L} Loss_k + K_{MVA}\sum_{i=1}^{N_F} L_{DIST_i} + K_{size}\sum_{i=1}^{N_{UPQC}} S_{UPQC_i}$$
$$+K_{flow}\sum_{k=1}^{N_i}\delta_{1k}\left|S_k - S_{k_{\max}}\right| + K_{volt}\sum_{k=1}^{N_b}\delta_{2k}\left|V_k - V_{k_{\min/\max}}\right|$$
$$+K_{harm}\sum_{k=1}^{N_b}\delta_{3k}\left|THD_{V_k} - THD_{\max_k}\right| + K_{harm-i}\sum_{k=1}^{N_b}\sum_{h=3,5,7}\delta_{4k}\left|V_{h_k} - V_{h_{\max}}\right|$$
$$+K_{vu}\sum_{k=1}^{N_b}\delta_{5k}\left|VU_k - VU_{\max}\right| \qquad (3.24)$$

Where, K_{flow}, K_{volt}, K_{harm}, K_{harm-i} and K_{vu} are the penalty multipliers for violation of power flow limit, voltage limit, voltage THD limit, individual voltage harmonics limit and voltage unbalance limit respectively. Each of the penalty multipliers are taken as 10^{12} [62]. δ_{1k}, δ_{2k}, δ_{3k}, δ_{4k} and δ_{5k} are the binary flags, reported in [62]. When the concerned variables are well within the limiting values, these flags are set to zero, thus imposing no penalty on the objective function. On the other hand, when the limits are violated, the solution represents an undesired operating condition. This is indicated by enforcing the binary flag to assume a value equal to 1, such that the cost function gets penalized accordingly. For example, $\delta_{1k} = 0$ when line flow of k^{th} line is within limit and $\delta_{1k} = 1$ when line flow of k^{th} line is outside its limit. N_b and N_L are total buses and distribution lines respectively in the respective distribution system.

3.5. Proposed methodology of optimal allocation of UPQC

Solution of the UPQC placement problem involves determination of the location and size of the UPQC. Placement of UPQC can have a beneficial effect on the degree of unbalances of the line power flows, distortion levels of the node voltages and also the sag voltages following disturbances. Determination of the impact of UPQC on the above mentioned factors requires an elaborate simulation of the UPQC both at normal operating condition as well as at those conditions which may generate a voltage sag event. The optimization technique to be used for the solution of the problem also has to be robust enough so as to be capable of handling large number of variables some of which may be of discrete nature. A good number of such robust optimization techniques are now available in open literature of which, in this chapter the Cuckoo search technique [56] has been employed considering the fact that this technique is comparatively a newer one and has not been greatly explored yet in solving power system problems of the type being dealt with in this chapter.

Evaluation of the objective function of equation (3.24) requires determination of the node voltages, voltage distortions, voltage unbalances, line flows, power losses and also the voltage sags during system disturbances.

Determination of the node voltage, voltage distortion, voltage unbalances and line flows requires solution of the power flow and harmonic flow problems. However, determination of the voltage sag requires to know the voltage conditions and its variation for a time scale of a few cycles. In this context, voltage sag estimation procedure is reported in Appendix A.3. Determination of voltage sag therefore, requires a detailed modeling of the UPQC such that complete simulation of the events are available in the form of node voltage waveforms. Determination of the amount of load disturbed can then be done from an analysis of the node voltage variations.

The problem formulated in this chapter consists of multi variables, multi dimensions and non-linear equations. These problems can be solved by many meta-heuristic/powerful optimization techniques reported in recent years. Among them Cuckoo Optimization Algorithm (COA) [56], is chosen in this chapter to achieve the optimal solution. The Cuckoo search optimization technique and Voltage sag calculation procedure are reported in Appendix A.1 and A.2 respectively. Thereafter, the UPQC simulation procedures [65] and brief description of UPQC simulation circuit are reported in the sections 3.5.1 and 3.5.2 respectively.

3.5.1. Cuckoo optimization algorithm

For the last few years, a number of evolutionary, multi-dimensional, powerful optimization techniques have been proposed to solve optimization problem, among which COA is a relatively recent technique. Till now, this method has been experimented on a limited number of power systems problems such as multi-objective short-term scheduling of thermoelectric power system [66], non-convex economic dispatch [67], capacitor allocation in radial distribution networks [68], comparative performance study of several FACTS devices in multi-area AGC [69], distribution network reconfiguration for power loss minimization and voltage profile improvement [70], load frequency controller design for non-linear interconnected power system [71], optimal power system stabilizers design [72] etc. A brief description of COA is given in Appendix A.2.

The procedural steps of COA are given below:

Step 1: Set control parameters, i.e., penalty constant, discovery rate of alien eggs/solution and maximum iteration number.

Step 2: Initiate randomly population of cuckoo habitats with egg laying capability.

Step 3: Set the variables of the habitat by using equations (3.19)-(3.23).

Step 4: Calculate fitness of each cuckoo according to equation (3.24).

Step 5: Define ‘ELR’ for each cuckoo by using equation (A.12) and let, cuckoos to lay eggs inside their corresponding ‘ELR’.

Step 6: Compute the fitness of the hatched eggs by using equation (3.24).

Step 7: Destroy the eggs of worst quality by equation (A.13) and find out the best.

Step 8: If best quality of current generation > best quality of previous generation, go to step 9. Otherwise go to next generation or iteration by equations (A.14)-(A.15) and repeat from step 5.

Step 9: If the difference between quality of current and previous consecutive iterations < small tolerance value, then display the optimal solution, otherwise go to next iteration by equations (A.14)-(A.15) and repeat from step 5.

3.5.2. Simulation of UPQC controller

Fig.3.3 illustrates the schematic diagram of simulation circuit of UPQC. It consists of series injected transformer, two voltage source converters (VSC), discrete PWM generator, low pass filter, and the necessary control system. Control system consists of current control loop, voltage control loop and discrete phase locked-loop (PLL).

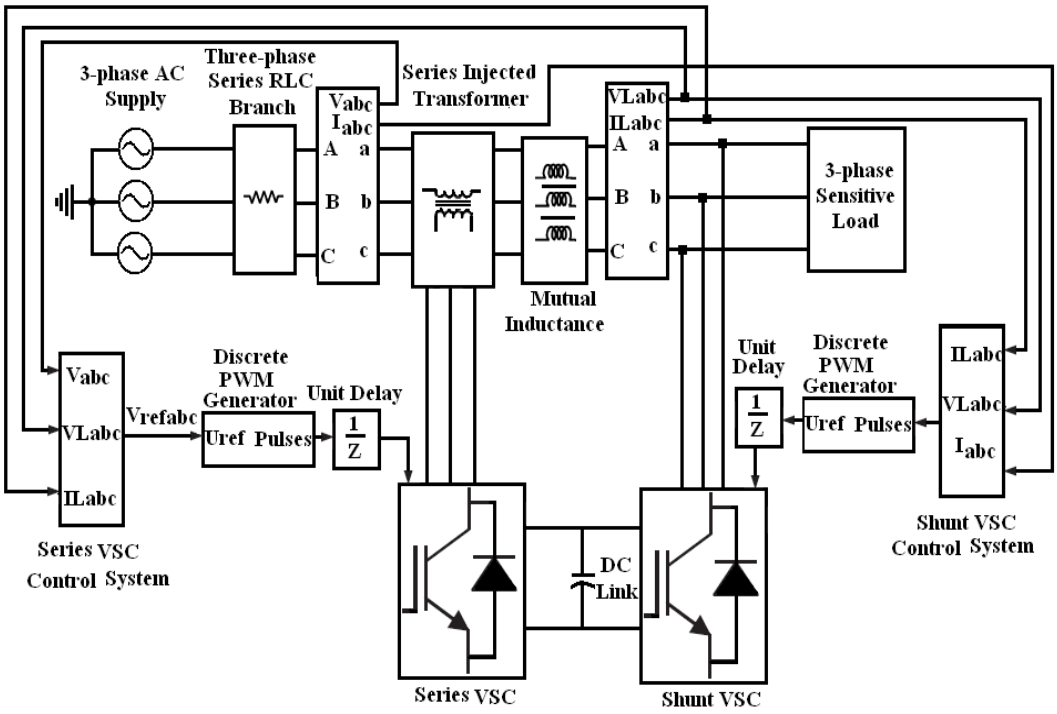

Fig.3.3. Schematic diagram of the simulation circuit of UPQC

The transient control algorithm for series APF is based on unit vector template generation scheme, whereas the control strategy for shunt APF is based on p-q theory [59]. According to this theory, a single phase system can be defined as a pseudo two-phase system by giving $\pi/2$ lead or $\pi/2$ lag, i.e., each phase voltage and current of the original three phase system can be considered as three independent two-phase systems. The resultant two-phase systems can be represented in $\alpha-\beta$ coordinates [73], and thus the p-q theory applied for balanced three-phase system can also be used for each phase of unbalanced system independently. The actual

load voltages and load currents are considered as α-axis quantities, whereas the $\pi/2$ lead or $\pi/2$ lag load voltages and $\pi/2$ lead or $\pi/2$ lag load currents are considered as β-axis quantities. In this chapter, $\pi/2$ lead is considered to achieve a two-phase system for each phase system. The reference load voltage signals extracted for series APF are used instead of actual load voltages.

By using the definition of three –phase $p-q$ theory for balanced three-phase system, the instantaneous active power can be represented by

$$p_{L,abc} = v_{L,abc\_\alpha} \cdot i_{L,abc\_\alpha} + v_{L,abc\_\beta} \cdot i_{L,abc\_\beta} \tag{3.25}$$

and the instantaneous reactive power as

$$q_{L,abc} = v_{L,abc\_\alpha} \cdot i_{L,abc\_\beta} - v_{L,abc\_\beta} \cdot i_{L,abc\_\alpha} \tag{3.26}$$

Considering phase-a, the instantaneous load active and reactive powers can be represented by

$$\begin{bmatrix} p_{La} \\ q_{La} \end{bmatrix} = \begin{bmatrix} v_{La\_\alpha} & v_{La\_\beta} \\ -v_{La\_\beta} & v_{La\_\alpha} \end{bmatrix} . \begin{bmatrix} i_{La\_\alpha} \\ i_{La\_\beta} \end{bmatrix} \tag{3.27}$$

Where

$$p_{La} = \overline{p}_{La} + \tilde{p}_{La} \tag{3.28}$$

$$q_{La} = \overline{q}_{La} + \tilde{q}_{La} \tag{3.29}$$

In equations (3.28) and (3.29), $\overline{p}_{La}$ and $\overline{q}_{La}$ represent the dc components that are responsible for fundamental load active and reactive powers, whereas, $\tilde{p}_{La}$ and $\tilde{q}_{La}$ represent the ac components that are responsible for harmonic powers. The phase-a fundamental instantaneous load active and reactive power components can be derived from p_{La} and q_{La}, respectively, by using a low pass filter.

Therefore, the instantaneous fundamental load active power for phase-a, b and c are given by

$$p_{La,1} = \overline{p}_{La}, p_{Lb,1} = \overline{p}_{Lb} \text{ and } p_{Lc,1} = \overline{p}_{Lc} \tag{3.30}$$

and the instantaneous fundamental load reactive power for phase- a, b and c are given by

$$q_{La,1} = \overline{q}_{La}, q_{Lb,1} = \overline{q}_{Lb} \text{ and } q_{Lc,1} = \overline{q}_{Lc} \tag{3.31}$$

Since the load current drawn by each phase may be different due to different loads that present inside the plant, the instantaneous fundamental load active power and instantaneous load reactive power demand for each phase may not be the same. In order to make this unbalance power demand as seen from the utility side, as a perfectly balanced fundamental three-phase active power, the unbalance load power should be properly redistributed

between utility, UPQC, and load, such that the total load seen by the utility would be linear and balanced load. The unbalanced or balanced reactive power demanded by the load should be handled by a shunt APF. The above mentioned task can be achieved by

$$p_{L,total} = p_{La,1} + p_{Lb,1} + p_{Lc,1} \tag{3.32}$$

$$p^*_{S/ph} = \frac{p_{L,total}}{3} \tag{3.33}$$

Equation (3.33) gives the redistributed per-phase fundamental active power demand that each phase of utility should supply in order to achieve perfectly balanced source currents. From equation (3.33), it is evident that under all the conditions, the total fundamental active power demanded by the loads would be equal to the total power drawn from the utility. Thus, the reference compensating currents representing a perfectly balanced three-phase system can be extracted by

$$\begin{bmatrix} i^*_{Sa\_\alpha} \\ i^*_{Sa\_\beta} \end{bmatrix} = \begin{bmatrix} v_{La\_\alpha} & v_{La\_\beta} \\ -v_{La\_\beta} & v_{La\_\alpha} \end{bmatrix}^{-1} \cdot \begin{bmatrix} p^*_{S/ph} + p_{dc/ph} \\ 0 \end{bmatrix} \tag{3.34}$$

In equation (3.34) $p_{dc/ph}$ is the precise amount of per-phase active power, taken from the source in order to maintain the dc-link voltage at a constant level and to overcome the losses associated with UPQC. The oscillating instantaneous active power $\tilde{p}_{La}$ should be exchanged between the load and shunt APF. The reactive power term q_{La} in equation (3.29) is considered as zero, since the utility should not supply load reactive power demand. In equation (3.34) the α-axis reference compensating current represents the instantaneous fundamental source current in original system and the β-axis reference compensating current represents the current that is at $\pi/2$ lead with respect to the original system.

Therefore,

$$i^*_{Sa}(t) = \frac{v_{La\_\alpha}(t)}{v^2_{La\_\alpha} + v^2_{La\_\beta}} \cdot \left[p^*_{S/ph}(t) + p_{dc/ph}(t) \right] \tag{3.35}$$

Similarly, the reference source current for phases b and c can be computed as

$$i^*_{Sb}(t) = \frac{v_{Lb\_\alpha}(t)}{v^2_{Lb\_\alpha} + v^2_{Lb\_\beta}} \cdot \left[p^*_{S/ph}(t) + p_{dc/ph}(t) \right] \tag{3.36}$$

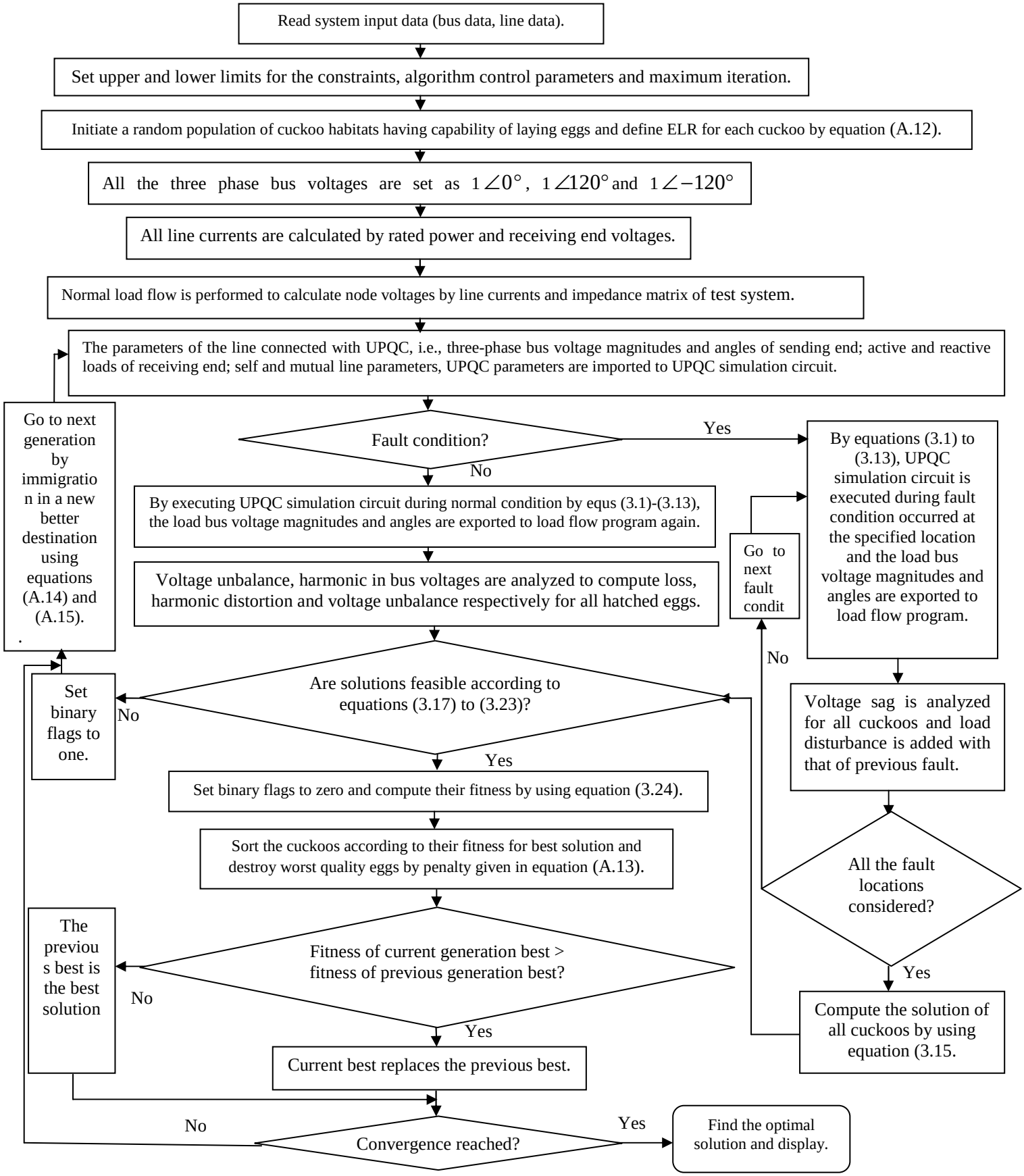

Fig.3.4. Flow chart of UPQC implementation by COA

$$i_{Sc}^{*}(t)=\frac{v_{Lc\_\alpha}(t)}{v_{Lc\_\alpha}^{2}+v_{Lc\_\beta}^{2}}\cdot\left[p_{S/ph}^{*}(t)+p_{dc/ph}(t)\right] \tag{3.37}$$

The reference neutral current signal can be extracted by simply adding all the sensed load currents, without actual neutral current sensing, as

$$i_{L\_n}(t)=i_{La}(t)+i_{Lb}(t)+i_{Lc}(t) \tag{3.38}$$

$$i_{Sh\_n}^{*}(t)=-i_{L\_n}(t) \tag{3.39}$$

The procedural steps for the simulation of UPQC are shown in flowchart of Fig.3.4.

From the flow-chart, shown in Fig.3.4, it is illustrated that, two conditions, namely with fault and without fault are analyzed on a given network. In both the conditions COA is applied to get the optimal location of UPQC. Firstly, normal load flow is executed to get node voltages. Then, from the analysis of fault condition, load disturbance due to voltage sag is obtained and from fault less condition loss, harmonic distortion and voltage unbalance are calculated.

Finally, the feasibility of the results obtained from both with fault and without fault conditions are checked by using equations (3.17)-(3.23). If feasible solutions are obtained, they are added together to get fitness function using equation (3.24). Otherwise, iteration number is increased by one and the procedure is repeated again from fault condition checking. This procedure is repeated until convergence criterion is reached.

3.6. Application of proposed method

In this section the optimal location of UPQC with the help of optimization technique is presented. The performance is studied on two test systems: (i) IEEE-123 node, unbalanced radial distribution test system and (ii) 25-node radial distribution test system. The respective results are reported below.

In this section, firstly the impacts of UPQCs on the test system during fault condition, occurred at the different locations are studied. Then the change in %THD with the installation of UPQCs in the test systems are shown. After that, the variations in bus voltage harmonics of different orders with the increase in UPQCs on test systems are depicted. Next, the change in % voltage unbalance with the change in UPQC numbers is studied. Then, the total load disturbance, cost savings and sag duration with implementation of UPQCs are evaluated and thereby the optimal number of UPQCs are found out. Finally, the results obtained by Cuckoo optimization technique are compared with some other powerful soft computing techniques.

In this chapter, the threshold voltage below which sensitive loads will experience disconnection resulting in load disturbance has been set as 0.85 p.u. The maximum permissible node voltage is 1.05 p.u.

3.6.1. Results for IEEE-123 node system

The single line diagram of IEEE-123 node test system shown in Appendix A.4.5, has 122 distribution lines, 123 buses, total active power demands of 28,400 kW, 18,300 kW and 23,100 kW for phases a, b and c respectively and total reactive power demands of 31,500 kVAR, 25,750 kVAR and 38,750 kVAR for phases a, b and c respectively. The total length of IEEE 123 node test feeder is 11.71194 km.

The self and mutual impedance data of IEEE 123 node test system is reported in [74]. The systems has only one substation with specified voltage of $1\angle 0°$ p.u. 50% of the total load has been taken as non-linear load in this systems. The procedures to obtain the UPQC parameters are found in [75].

- **Impact of UPQC on the area of load disturbance**

The influence of UPQCs on IEEE-123 node, 3-phase, unbalanced test network, during fault occurred at any one predictable location is shown in Fig.3.5.

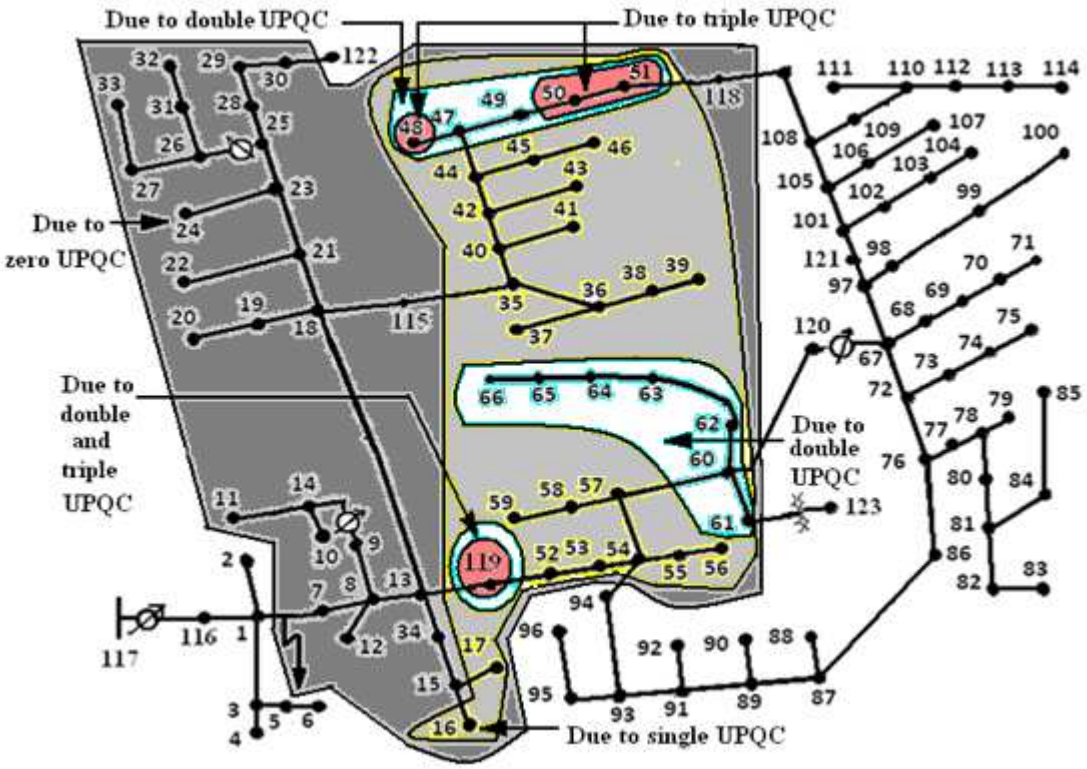

Fig.3.5. Impact of UPQCs on area of load disturbance of IEEE 123 node test feeder system

In Fig.3.5, the fault occurs on the line, connected between nodes 1 and 7, which in turn influence a large normal operating area to be a load disturbance area. With the installation of single UPQC on line (64-65), area 1(marked as "Due to zero UPQC") reduces to area 2 (marked as "Due to single UPQC"). The impact of one more UPQC placed on line (47-48), reduces the load disturbance area 2 to area 3(marked as "Due to double

UPQC"). Finally, three UPQCs are optimally located on distribution lines (64-65), (47-49) and (72-76) respectively and effectively influences load disturbed area 3 to be load disturbed area 4 (marked as "Due to triple UPQC"), having four weak buses 50, 51, 48 and 119 only. Hence, from Fig. 3.5, it is obvious that as the number of UPQC is increased the node voltages of affected area in IEEE-123 node test feeder system are also improved and hence load disturbance is also decreased.

- **Impact of UPQC on minimization of % THD**

In this chapter, the maximum value of % THD is allowed as 5%. From Fig. 3.6a-3.6c, it is found that the maximum % THD without UPQC allocation in IEEE 123 node test system is 12.3 % on bus 80 at phase a. From Fig. 3.6a-3.6c, it is also observed that with the use of single UPQC on the test system at optimal locations the maximum % THD falls within limit, which is a large change. However, there is no appreciable change in % THD with the increase in number of UPQCs.

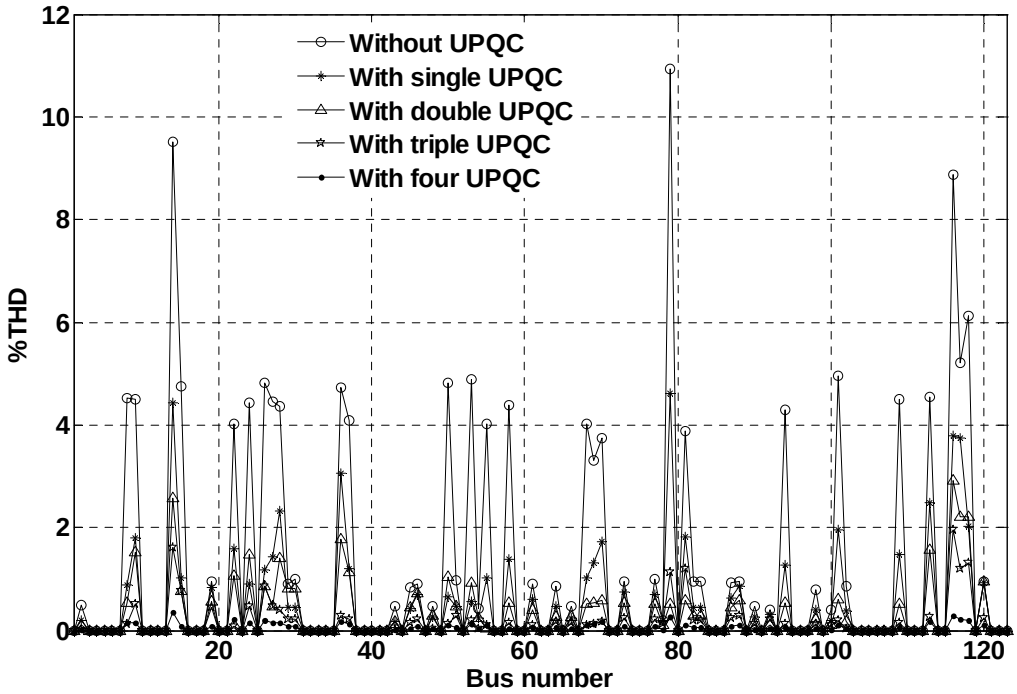

(a) Phase

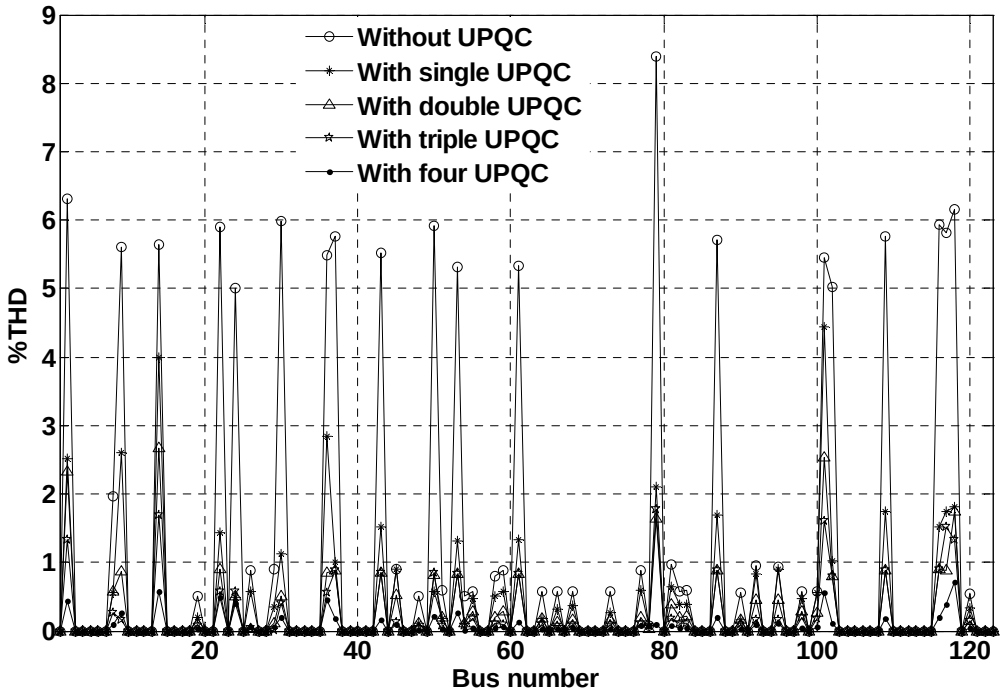

(b) Phase

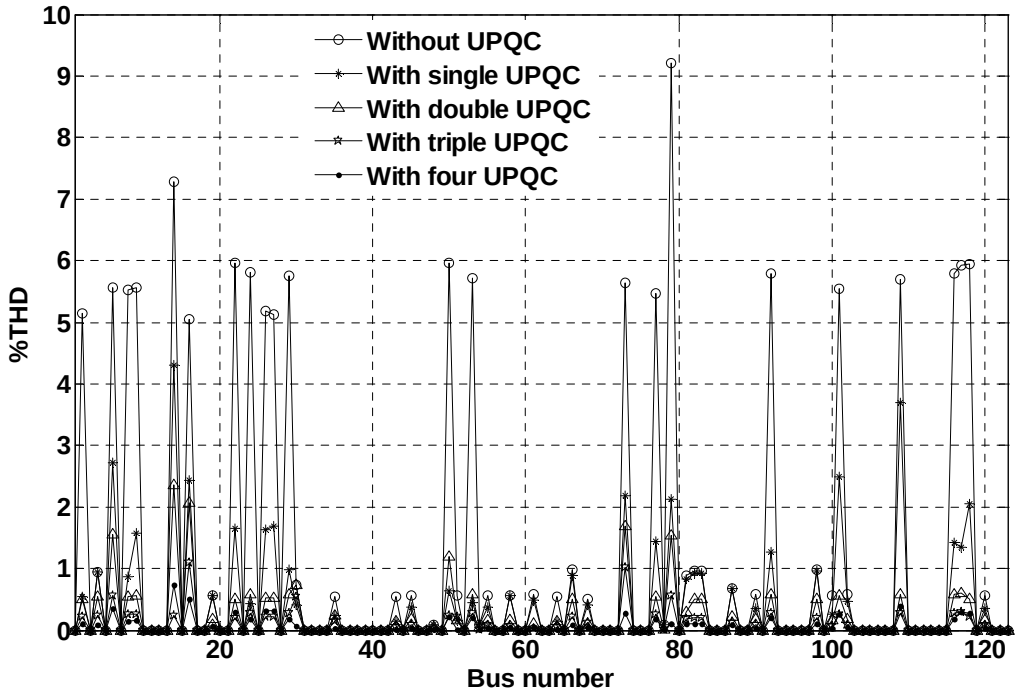

(c)- phase

Fig.3.6. Impact of UPQCs on change in %THD of IEEE 123 node test system, (a)a-phase, (b)b-phase, (c)c-phase

- **Impact of UPQC on individual harmonics**

The maximum tolerable limit of individual harmonic is taken as 3 % as per IEEE standard. Without UPQC in the test system, the maximum 5^{th}, 7^{th}, 11^{th}, 13^{th}, 17^{th} and 19^{th} voltage harmonic magnitudes are 4.29%, 4.28%, 4.27%, 3.89%, 3.59% and 3.3% respectively. From Figs. 3.7a-3.7c, it is observed that with the installation of three UPQCs on their optimal location, the maximum 5^{th} harmonic in IEEE 123 node test system is 2.9%, which is within limit and the 7^{th}, 11^{th}, 13^{th}, 17^{th} and 19^{th} voltage harmonic magnitudes are therefore reduced below 3%.

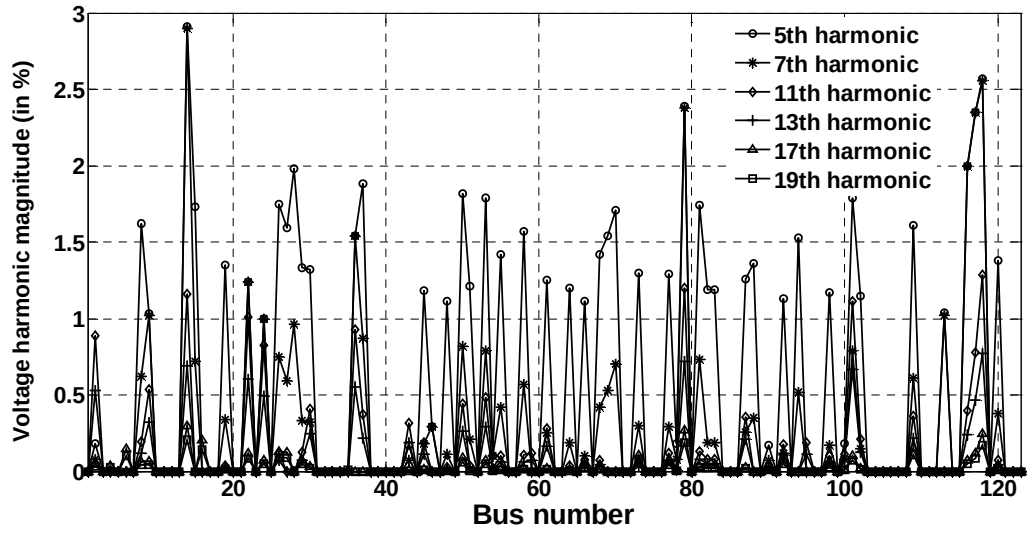

(a)-phase

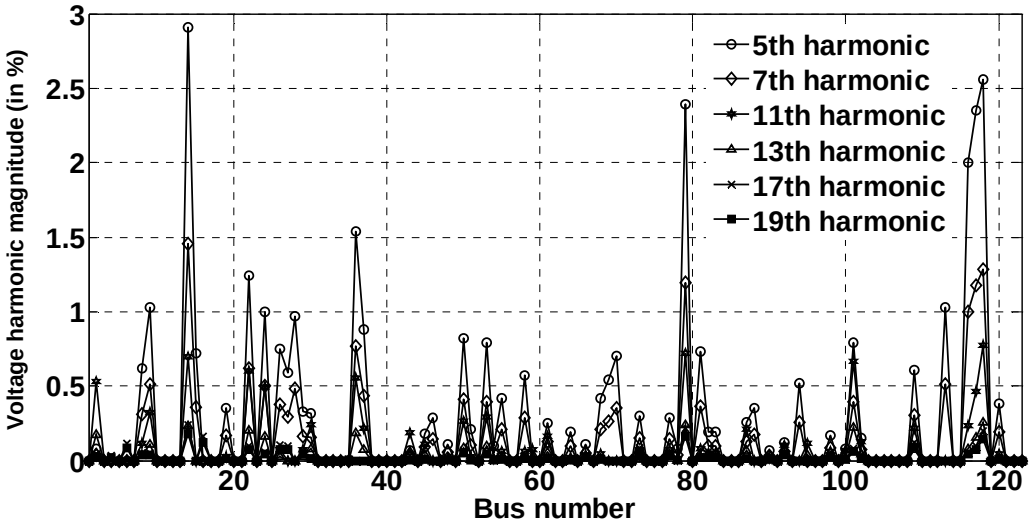

(b)-phase

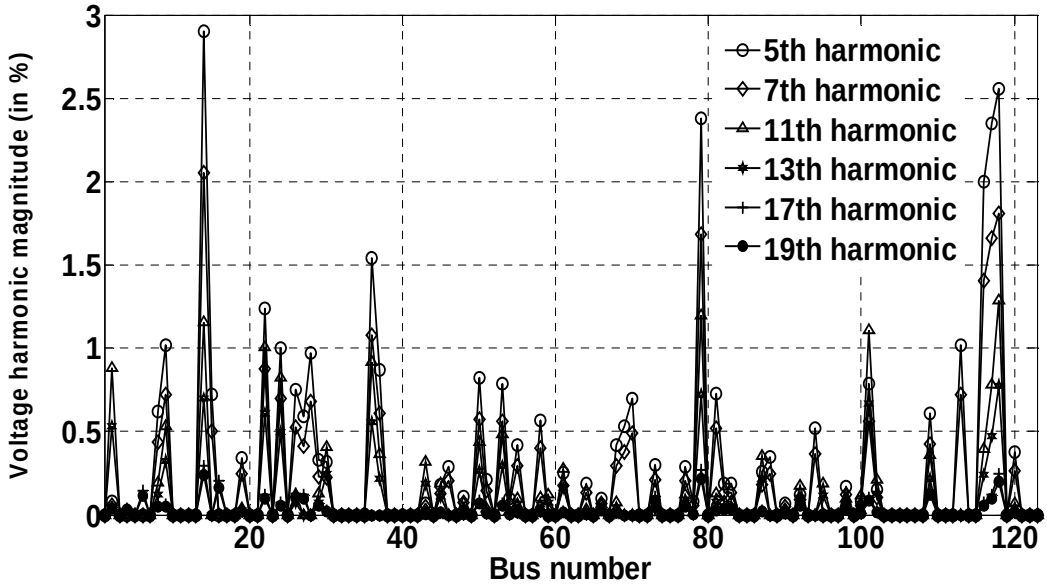

(c)-phase

Fig.3.7. Variation of individual harmonics of different buses with 3 UPQCs at their optimal locations of IEEE 123 node test system, (a) a-phase, (b) b-phase, (c) c-phase

- **Effect of UPQC on voltage unbalance**

From Fig.3.8, it is shown that without any UPQC installed in the IEEE123 node test system, the maximum voltage unbalance is 3.66%. With the installation of single UPQC on its optimal location, this maximum voltage unbalance decreases to 3.1%.With the installation of double and triple UPQCs at their optimal locations respectively, the maximum voltage unbalance reaches to 2.64% and 1.99 % respectively, which is within limit.

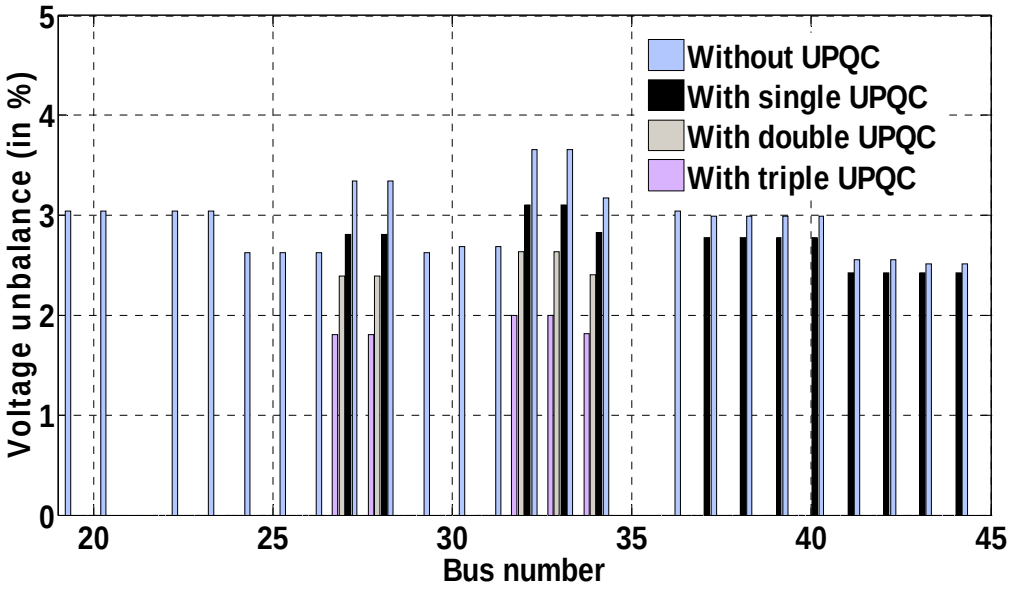

Fig.3.8. Effect of UPQCs on variation of three phase bus voltage unbalance of IEEE123 node test system

- **Influence of UPQC on real power loss, load disturbance and cost savings**

Table 3.1. Optimal location of UPQC, loss, cost, savings, sag, size and UPQC parameters with load disturbance of 0.85 p.u.

Control Variables		Without UPQC	With single UPQC	With double UPQC	With triple UPQC	With four UPQC
Optimal location of UPQC (line number)		-	64-65	64-65,47-48	64-65,47-48,72-76	64-65,47-48,72-76, 44-45
Cost (in million $)		8.6841	7.8708	7.0091	6.9731	7.0511
Cost savings (in %)		-	9.365	19.288	19.7	18.8
Loss(in kW)		1040	518.5	517	515.5	514.5
Load disturbance (in MVA)		245.9157	192.7574	173.6025	109.3608	107.40625
UPQC size (in kVAr)		-	700	500	200	50.4
UPQC parameters	Series resistance (in Ω)	-	1.5	0.2	0.1	0.1
	Series inductance (in mH)	-	5	3.5	3	1.5
	Shunt resistance (in Ω)	-	1	0.4	0.1	0.1
	Shunt inductance (in mH)	-	26	3	3	3

Tables 3.1 demonstrates the effectiveness of UPQC to ultimately compensate different types of voltage sag in terms of the optimal placement of UPQC devices, operational cost, cost savings, real power loss, total load disturbance, UPQC size and UPQC parameters for IEEE 123 node test system.

From Table 3.1, it is shown that in presence of single UPQC in IEEE 123 node test feeder system there is a rapid change in real power loss from 1040 kW to 518.5 kW. This reduction in real power loss ultimately results in cost savings of 9.365%.

Table 3.1 shows also that there is a small change in real power loss with the increase in number of UPQC. But the UPQC installation cost is increased with the increase in number of UPQC. That is why, though the load disturbance is decreased with the increase in UPQC, the cost savings is gradually decreased after achieving the maximum value for a certain number of UPQCs optimally placed in the test networks. These changes in cost savings and load disturbances are shown in Fig. 3.9a and 3.9b respectively for IEEE123 node test feeder system.

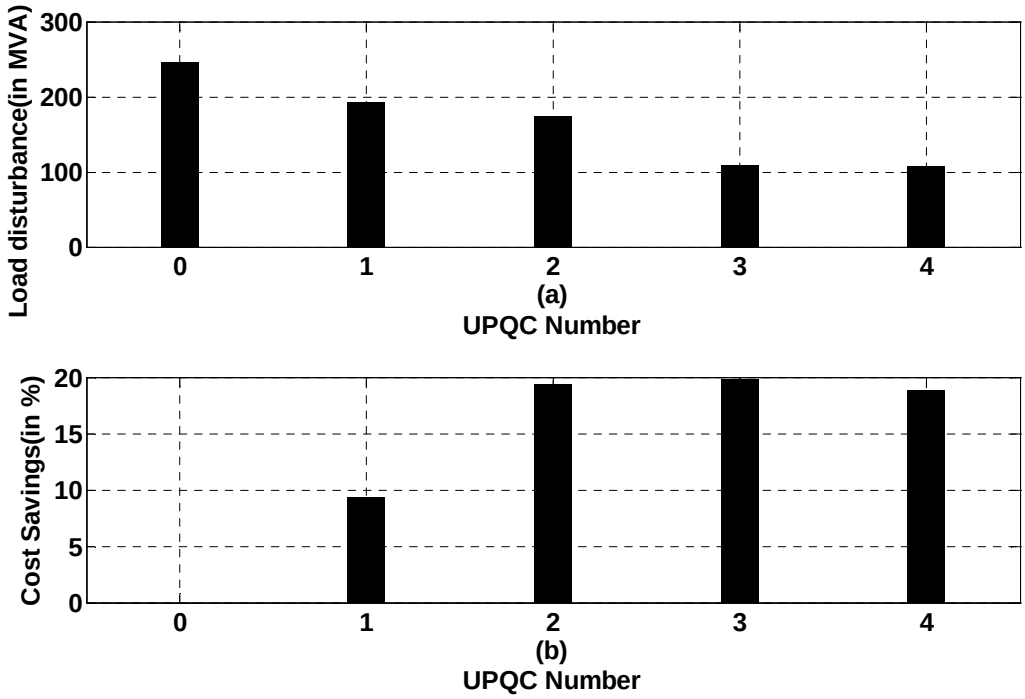

Fig.3.9. Variation of (a) load disturbance & (b) cost savings with the number of UPQC for IEEE 123 node test system

This optimal number of UPQCs is three for IEEE 123 node. At this instant, the operating cost is 6.9731 million $.

- **Effect of UPQC on voltage sag**

The worst case of voltage sag has been considered in this chapter. The voltage envelopes for IEEE123 node test system is shown in Fig.3.10. Fig.3.10 illustrate that during fault condition occurred on line (1-7), a-phase voltage magnitude at bus 34 without UPQC decreases from 0.9918 p.u. to 0.4523 p.u. at t=1.7 sec and it reaches again 0.9918 p.u. at t=1.8sec. But with the installation of single UPQC on its optimal location of IEEE123 node test system the bus voltage magnitude reaches to 0.7889 p.u. during this sag condition. However, with the installation of double and triple UPQCs on the test system the voltage magnitudes become 0.9681 p.u. and 0.9714 p.u. respectively. Thus with the installation of double UPQCs, the sag voltage magnitude recovers to normal operating voltage.

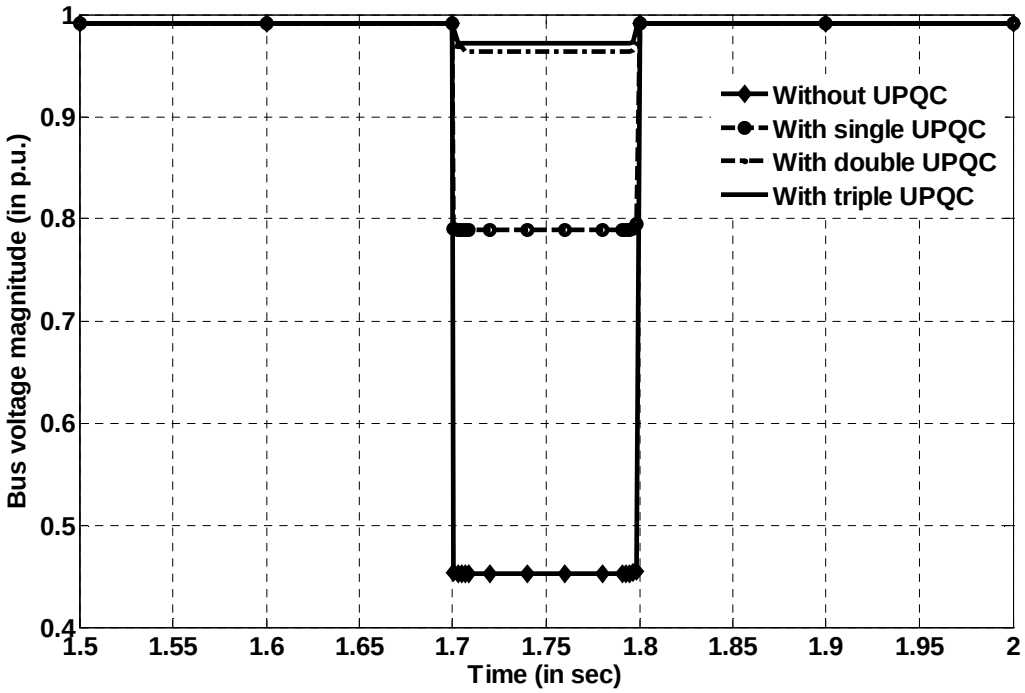

Fig.3.10. Variation of sag voltage magnitude at bus 34 with the number of UPQC for IEEE123 node test system

- **Comparative results analysis from different optimization techniques**

The optimization technique Cuckoo optimization algorithm (COA)s is used to solve the optimization problem. The optimization techniques selected in this chapter to compare the results obtained by COA are Genetic Search algorithm (GSA) [18], Differential Evolution Algorithm (DE) [76] and artificial bee colony (ABC) [77] techniques.

The parameters taken in this chapter for different soft computing techniques are reported in Table 3.2.

Table3.2. Parameters used in the different optimization techniques

Maximum number of iteration =100			
Population size=25			
COA	GSA	ABC	DE
Discovery rate of alien eggs/solutions, Pa=0.25	Gravitational constant, G0=100	Colony size=16	Weighting factor=0.5
Penalty constant=10^15	User specified constant, α=20	Number of food source=8	Cross over constant=0.5
		limit=5	

The implementation of all these selected optimization methods effect in quite similar results as reported in Table 3.3. However, from a closer inspection of the results, it can be said that in many situations more than one optimization technique give the best solution.

Table3.3. Analysis of the various methods for UPQC optimal placement problem of IEEE123 node test system

Number of UPQC	Control Variables	COA	GSA	ABC	DE
1	Optimal location of UPQC (line number)	64-65	64-65	64-65	64-65
	Cost (in million $)	7.8708	7.8708	7.8708	7.8708
	Savings (in %)	9.365	9.365	9.365	9.365
	Loss(in kW)	518.5	518.5	518.5	518.5
	Load disturbance, MVA	192.7574	192.7574	192.7574	192.7574
2	Optimal location of UPQC (line number)	64-65,47-48	64-65,47-48	64-65,47-49	64-65,47-48
	Cost (in million $)	7.0091	7.0091	7.0511	7.0091
	Savings (in %)	19.288	19.288	18.804	19.288
	Loss(in kW)	517	517	517.5	517
	Load disturbance, MVA	173.6025	173.6025	186.8581	173.6025
3	Optimal location of UPQC (line number)	64-65,47-48,72-76	64-65,47-48,72-76	64-65,47-48,72-76	64-65,47-48,72-76
	Cost (in million $)	6.9731	6.9731	6.9731	6.9731
	Savings (in %)	19.7	19.7	19.7	19.7
	Loss(in kW)	515.5	515.5	515.5	515.5
	Load disturbance, MVA	109.3608	109.3608	109.3608	109.3608

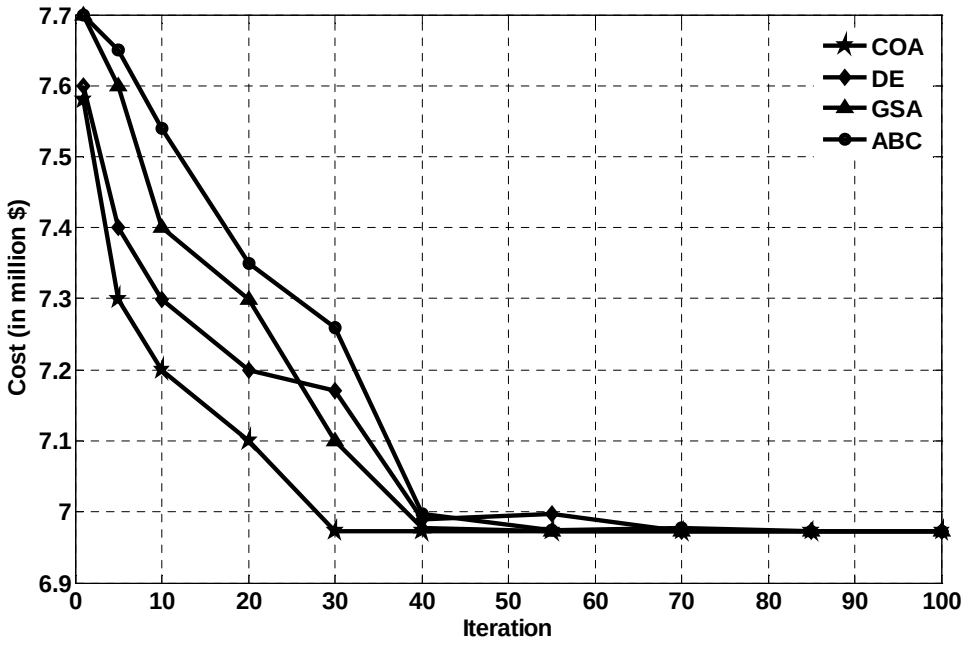

Fig.3.11. Cost optimization with three UPQC of IEEE 123 node test system

The convergence characteristics of different optimization techniques, chosen in this chapter, are shown in Fig.3.11, for three UPQCs placement problem in IEEE 123 radial test system. Hence from Table 3.3 and Fig.3.11, COA justifies the suitability of its application in solving the problem, considered in this chapter. Fig. 3.12 depicts that the optimal placement of UPQC in IEEE 123 node test system, clear the fault within 6 cycles. So it is obvious that the optimized system has a better voltage profile and it satisfies the CBEMA curve [78].

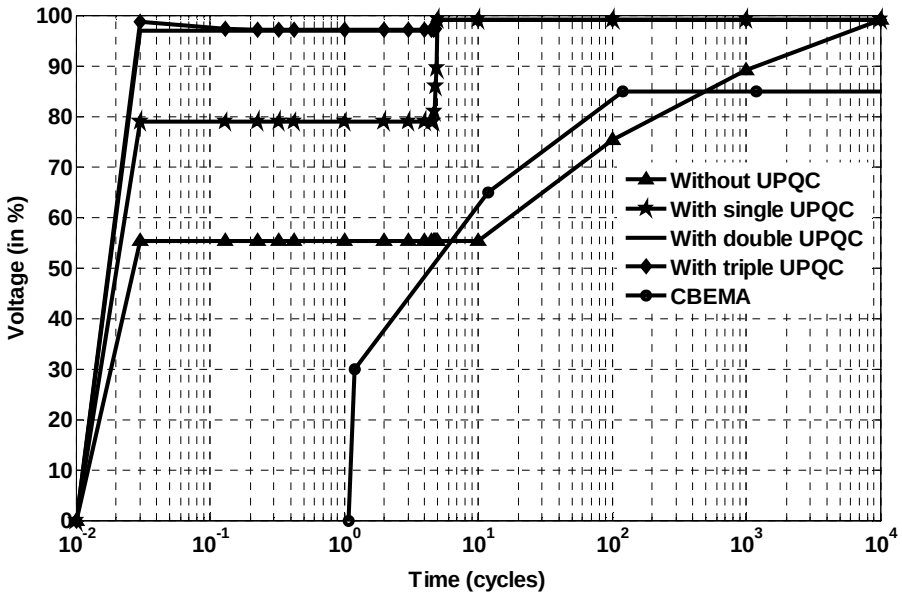

Fig.3.12. Range of equipment sensitivity to voltage sag in IEEE123 node test system at bus 34

3.6.2. Results for 25- node system

The network configuration of 25 node test system, illustrated in Appendix A.4, has total 24 distribution lines, 25 buses, total active power demands of 1020 kW, 980 kW and 1000 kW for phases a, b and c respectively and total reactive power demands of 765 kVAR, 735 kVAR and 750 kVAR for phases a, b and c respectively. The self and mutual impedance data of 25 node test system is reported in [79]. The system has one substation with specified voltage of $1\angle 0°$ p.u. 50% of the total load has been taken as non-linear load in the systems. The procedures to obtain the UPQC parameters are found in [75]. The total length of 25 node test system is 4.712 km.

- **Impact of UPQC on the area of load disturbance**

In Fig.3.13, the fault occurs on the line connected between nodes 7 and 9, which in turn influence a large normal operating area to be a load disturbed area. With the installation of single UPQC on line (5-4), area 1(marked as "Due to zero UPQC") reduces to area 2 (marked as "Due to single UPQC"). The impact of two UPQCs placed on lines (4-5) and (3-18), reduces the load disturbance area 2 to area 3(marked by "Due to double UPQC"). Finally, three UPQCs are optimally located on distribution lines (4-5), (3-18) and (6-8) respectively and effectively vanishes the load disturbing area. Hence, from Fig. 3.13, it is obvious that as the number of UPQC is increased the node voltages of affected area in 25- node test feeder system are also improved and hence load disturbance is also decreased.

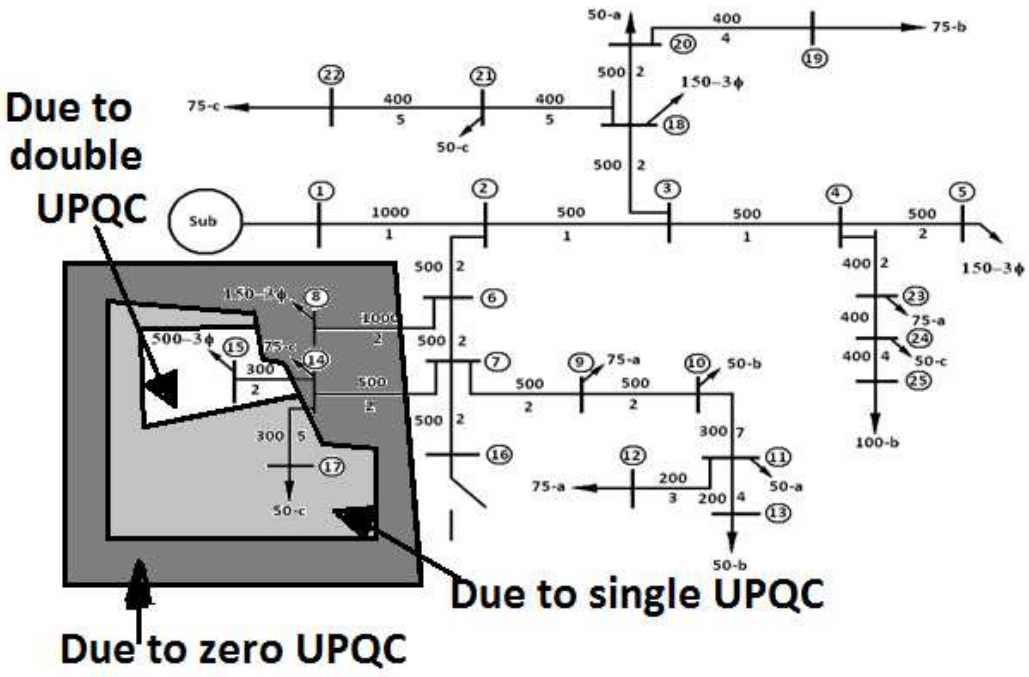

Fig.3.13. Impact of UPQCs on area of load disturbance of 25- node test feeder system

- **Impact of UPQC on minimization of % THD**

From Fig.3.14(a)-3.14(c), it is found that the maximum % THD without UPQC allocation in 25 node test system is 14.2 % on bus 14 at phase c. From Fig 3.14(a)-3.14(c), it is also observed that with the use of single UPQC on the system at optimal locations the maximum % THD falls within limit, which is a large change. However, there is no appreciable change in % THD with the increase in number of UPQCs.

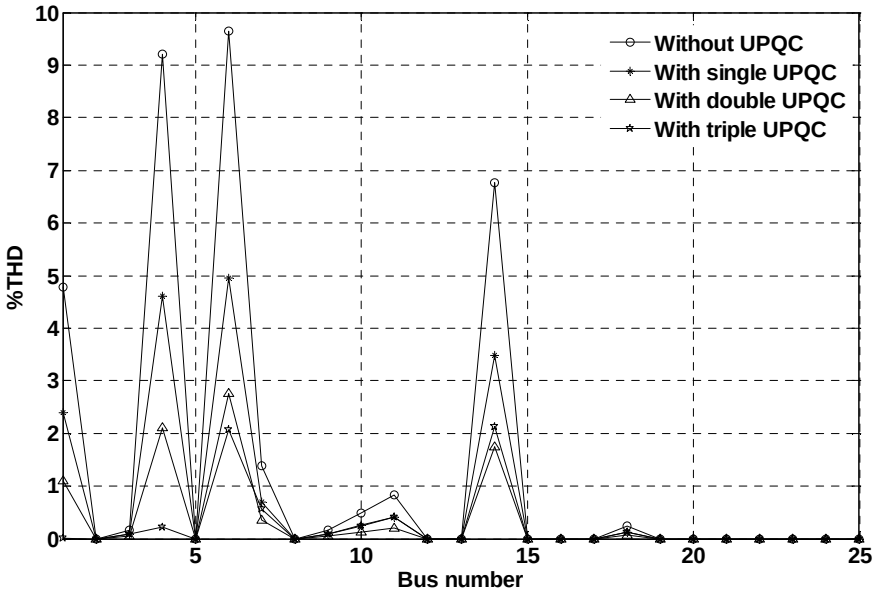

(a)-phase

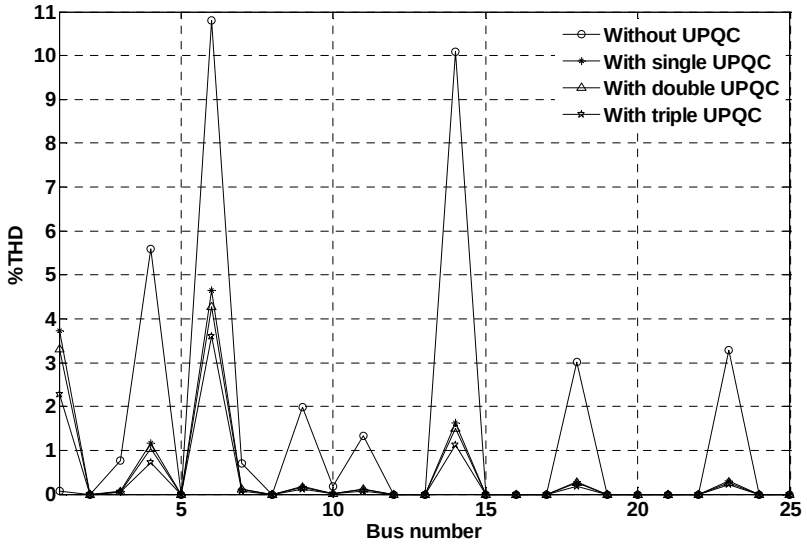

(b)-phase

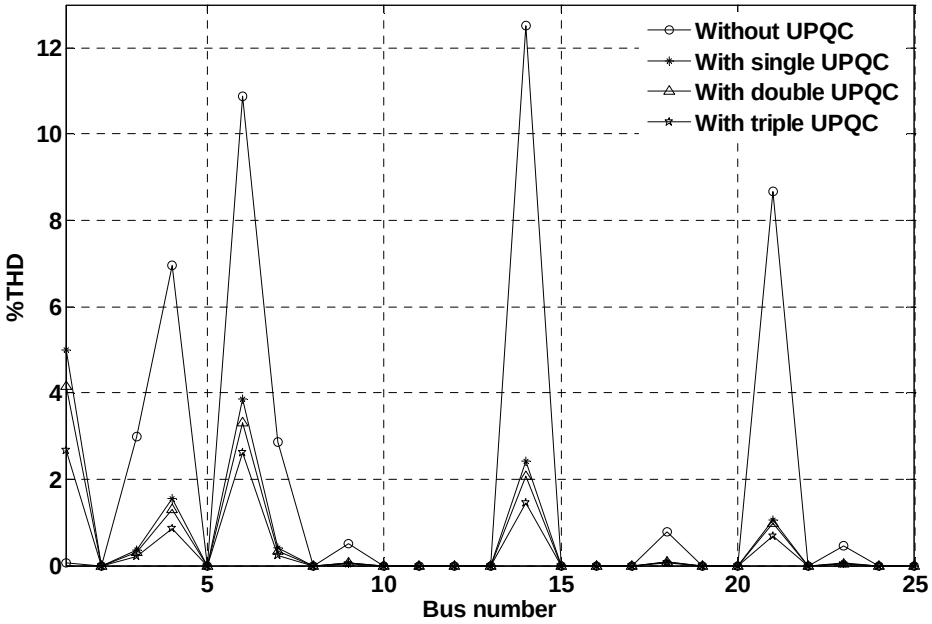

(c)-phase

Fig.3.14. Impact of UPQCs on change in %THD of 25 node test system, (a)a-phase, (b)b-phase, (c)c-phase

- **Impact of UPQC on individual harmonics**

Without installation of UPQC in 25 node test system, the maximum 5^{th}, 7^{th}, 11^{th}, 13^{th}, 17^{th} and 19^{th} voltage harmonic magnitudes are 5.08%, 5.03%, 5%, 4.43%, 4.21% and 3.34% respectively. In Figs. 3.15a, 3.15b and 3.15c, the maximum 5^{th} harmonic of phase a, b and c in different buses of 25 node test system are found as 1.2%, 2.4% and 1.8% respectively with two UPQCS on their optimal locations.

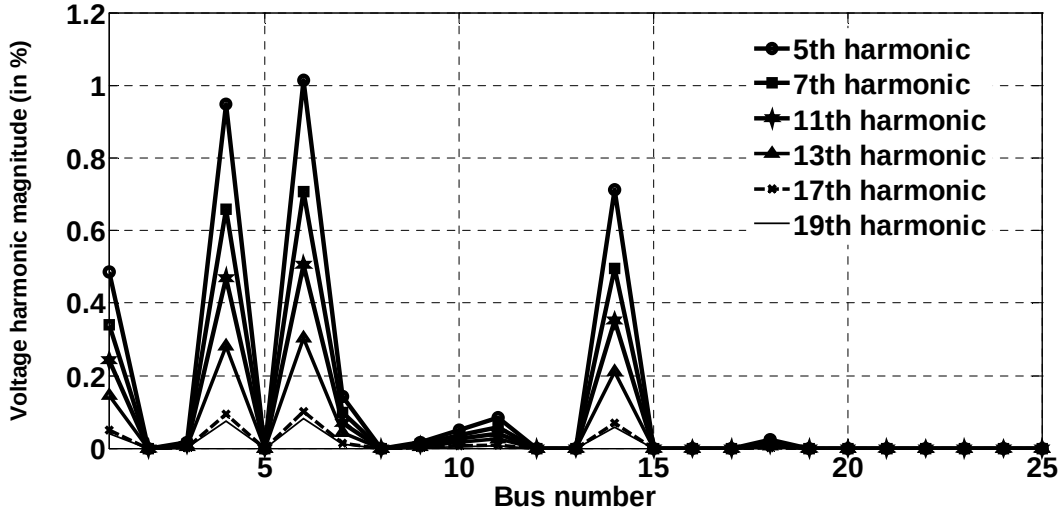

(a)-phase

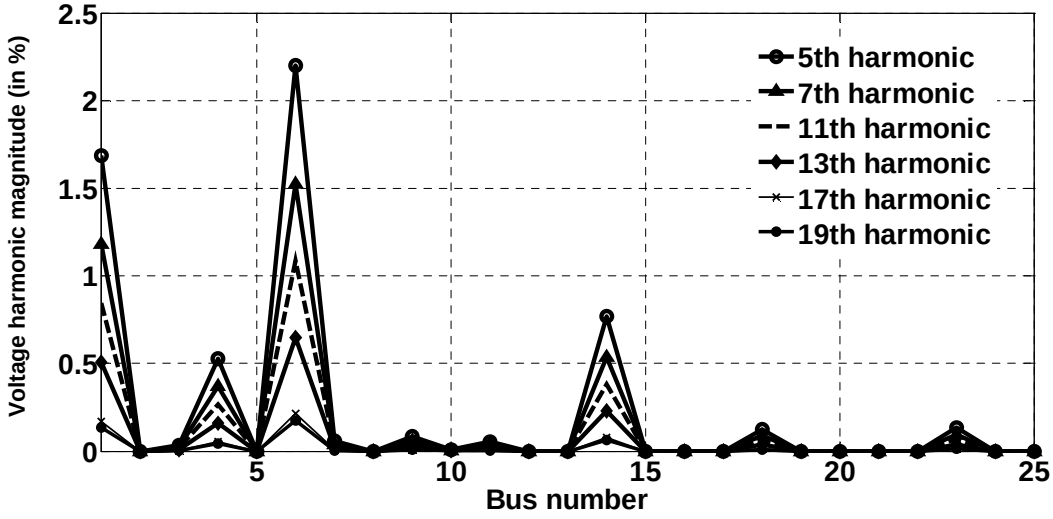

(b)-phase

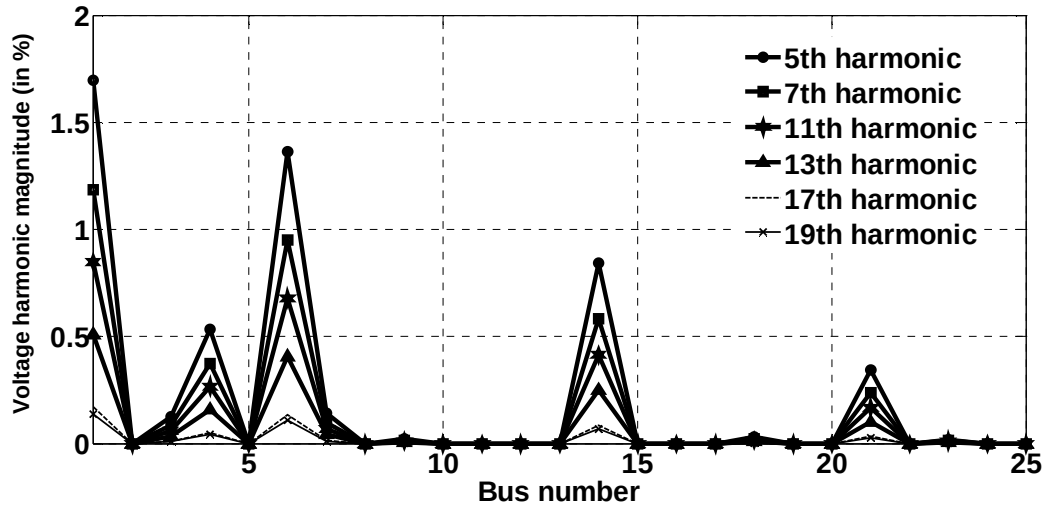

(c)-phase

Fig.3.15. Variation of individual harmonics of different buses with 3 UPQCs at their optimal locations of 25 node test system, (a) (a)a-phase, (b)b-phase, (c)c-phase

- **Effect of UPQC on voltage unbalance**

Fig. 3.16 depicts that without installation of UPQC in 25 node test system, the maximum voltage unbalance is 7.17%. But with the installation of single and double UPQCs on their optimal locations, maximum voltage unbalance changes to 4.93% and 1.69% respectively.

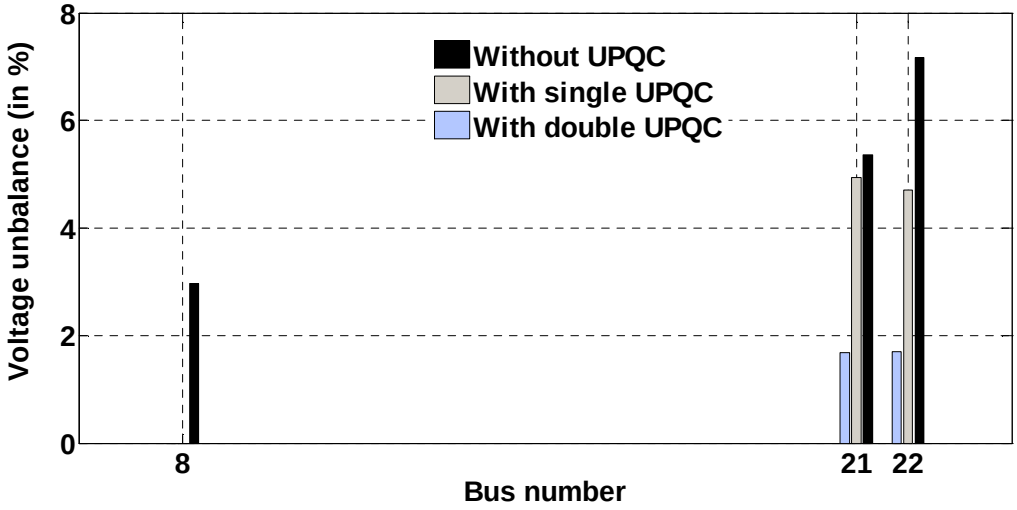

Fig.3.16. Effect of UPQCs on variation of three phase bus voltage unbalance of 25 node test system

- **Influence of UPQC on real power loss, load disturbance and cost savings**

Table 3.4 demonstrates the effectiveness of UPQC to ultimately compensate different types of voltage sag in terms of the optimal placement of UPQC devices, operational cost, cost savings, real power loss, total load disturbance, UPQC size and UPQC parameters for 25 node test system.

Table 3.4. Optimal location of UPQC, loss, cost, savings, sag, size and UPQC parameters with load disturbance of 0.85 p.u.

Control Variables		Without UPQC	With single UPQC	With double UPQC	With triple UPQC
Optimal location of UPQC (line number)		-	5-4	4-5, 3-18	4-5, 3-18, 6-8
Cost (in million $)		8.3287	1.1046	1.0676	1.0766
Cost savings (in %)		-	86.73	87.18	87.07
Loss(in kW)		1831	56	20	14
Load disturbance (in MVA)		239.7	229.075	187.425	170.15
UPQC size (in kVAr)		-	500	200	35
UPQC parameters	Series resistance (in Ω)	-	2	0.1	0.005
	Series inductance (in mH)	-	5	2	1
	Shunt resistance (in Ω)	-	0.6	0.01	0.0025
	Shunt inductance (in mH)	-	1.5	1	0.5

From Table 3.4, it is shown that in the presence of single UPQC in 25 node test feeder system, there is a rapid change in real power loss from 1831 kW to 56 kW. This reduction in real power loss ultimately results in cost savings of 86.73%.

Table 3.4 shows that there is a small change in real power loss with the increase in number of UPQC. But the UPQC installation cost is increased with the increase in number of UPQC. That is why, though the load disturbance is decreased with the increase in UPQC, but the cost savings is gradually decreased after achieving the maximum value for a certain number of UPQCs optimally placed in the test networks. These changes in cost savings and load disturbances are shown in Fig 3.17(a)-3.17(b) for 25 node test feeder system.

This optimal number of UPQCs is two for 25 node test system. At these instant, the operating cost is 1.0676 million $ respectively.

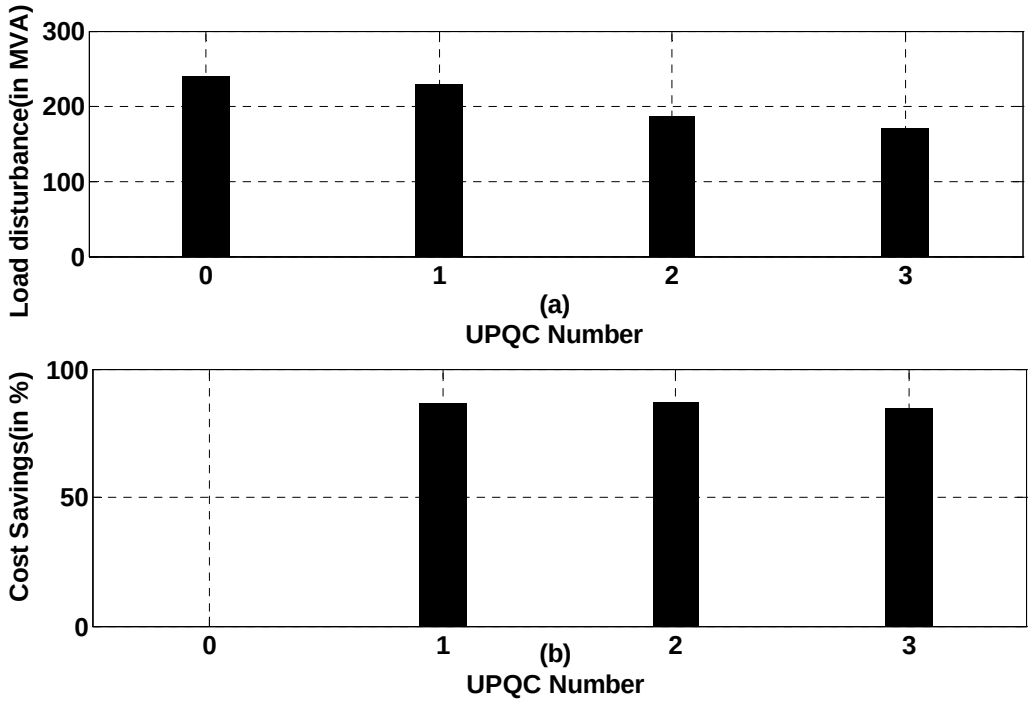

Fig.3.17. Variation of (a) load disturbance & (b) cost savings with the number of UPQC for 25 node test system

- **Effect of UPQC on voltage sag**

The worst case of voltage sag has been taken in this chapter. The voltage envelopes for 25 node test is shown in Fig. 3.18. From Fig.3.18, it is shown that during fault condition occurred on line (7-9) a-phase bus voltage magnitude of bus 5 decreases from 0.968 p.u. to 0.535 p.u. at t= 1.701 sec and this voltage again recovers to 0.968 p.u. at t=1.8 sec. The placement of single and double UPQCs decrease the duration of this abnormal voltage magnitudes and thereby remove the load disturbance problem from the system.

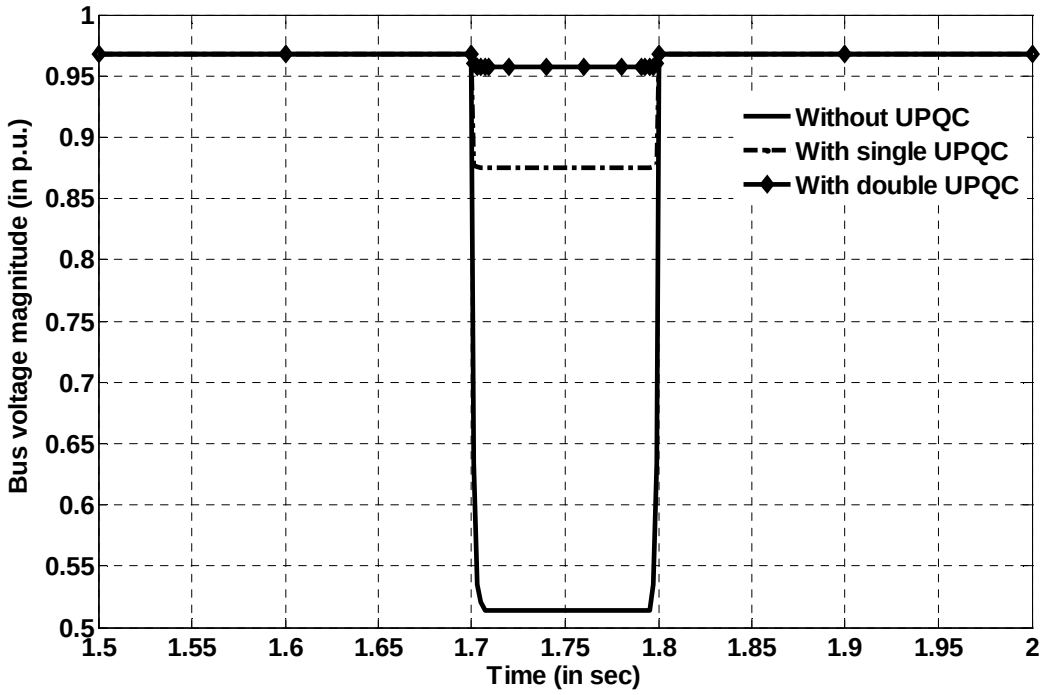

Fig.3.18. Variation of sag voltage magnitude at bus 5 with the number of UPQC for 25 node test system

- **Comparative results analysis from different optimization techniques**

  The parameters taken for different soft computing techniques are same as those of Table 3.2.

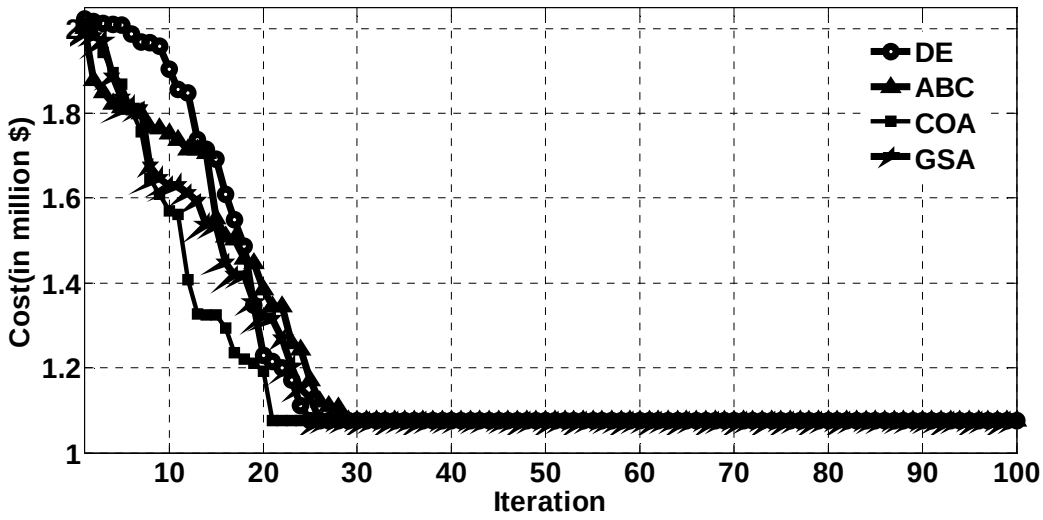

Fig.3.19. Cost optimization with three UPQC of 25 node test system

The convergence characteristics of different optimization techniques are shown in Fig.3.19, for three UPQCs placement problem in 25-node radial test system. Hence from Table 3.5 and Fig.3.19, COA justifies the suitability of its application in solving the problem, considered in this chapter.

Table3.5. Analysis of the various methods for UPQC optimal placement problem of 25 node test system

Number of UPQC	Control Variables	COA	GSA	ABC	DE
1	Optimal location of UPQC (line number)	4-5	4-5	4-5	4-5
	Cost (in million $)	1.1046	1.1046	1.1046	1.1046
	Savings (in %)	86.73	86.73	86.73	86.73
	Loss(in kW)	56	56	56	56
	Load disturbance, MVA	229.075	229.075	229.075	229.075
2	Optimal location of UPQC (line number)	4-5, 3-18	4-5, 3-18	4-5, 3-18	4-5, 3-18
	Cost (in million $)	1.0676	1.0676	1.0676	1.0676
	Savings (in %)	87.18	87.18	87.18	87.18
	Loss(in kW)	20	20	20	20
	Load disturbance, MVA	187.425	187.425	187.425	187.425
3	Optimal location of UPQC (line number)	4-5, 3-18, 6-8	4-5, 3-18, 6-8	4-5, 3-18, 6-8	4-5, 3-18, 6-8
	Cost (in million $)	1.0766	1.0766	1.0766	1.0766
	Savings (in %)	87.07	87.07	87.07	87.07
	Loss(in kW)	14	14	14	14
	Load disturbance, MVA	170.15	170.15	170.15	170.15

Fig. 3.20 depicts that the optimal placement of UPQC in 25 node test system, clear the fault within 6 cycles. So it is obvious that the optimized system has a better voltage profile and it satisfies the CBEMA curve [78].

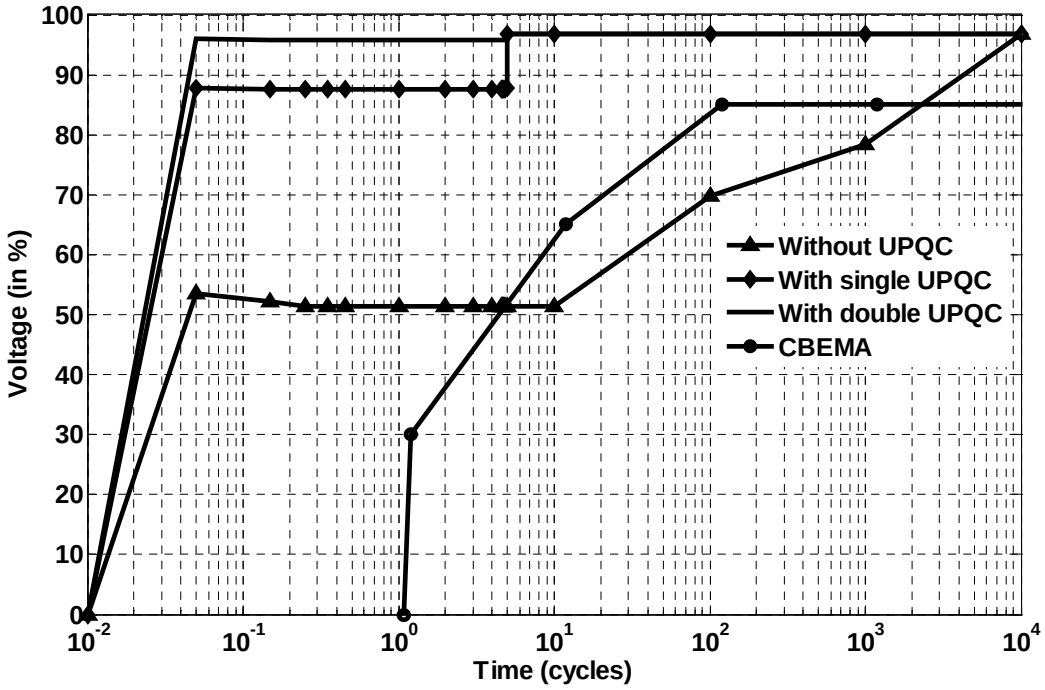

Fig.3.20. Range of equipment sensitivity to voltage sag in 25 node test system at bus 5

Both the simulation program and circuit simulation have been executed in MATLAB 7.8 and performed on an Intel I Core i5 CPU with 2.67 GHz and 4.00 GB memory.

3.7. Conclusion

In this chapter the UPQC placement problem in distribution system has been solved. UPQC placement is a very complex problem requiring transient simulation along with an optimization technique. To analyze the performance of UPQC, the different cases of UPQC placement have been studied on a 25 bus radial distribution network and IEEE123 node test feeder system. It is found that the installation of UPQCs in their optimal locations in the test systems result in

- increase in the bus voltage magnitudes during fault occurred in the test system and thereby reduction in the load disturbed area.
- reduction in %THD and individual bus voltage harmonics within standard limits.
- minimization of voltage unbalance leading to attain the standard tolerance given in this chapter.
- decrease in real power loss in the test system and thereby increase in cost savings.
- optimal number of UPQCs coming from variation of cost savings.

- removal of the fault from the test systems within limit cycles as shown by CBEMA curve in this chapter.

The effectiveness of UPQC in the test systems are investigated by COA, DE, GSA and ABC techniques, among which COA gives the better result and hence COA proves it's suitability in this application.

Chapter 4:

Improved Transient Performance of Distribution System through Optimal Placement of Hybrid Dynamic Voltage Restorer

---

Summary: *The present chapter proposes a model of hybrid-Dynamic Voltage Restorer (H-DVR) which is a compound FACTS device. This chapter also analyzes the capability of the device in minimization of voltage Total Harmonic Distortion (THD) and load harmonics, voltage profile improvement and loss minimization. The absence of transformer in H-DVR model improves the cost savings. Besides, the performance of H-DVR is compared with DVR to prove the effectiveness of H-DVR in the modern power system scenario. Both simulation results of H-DVR and DVR are provided to validate the correctness and effectiveness of the proposed H-DVR model.*

4.1. Introduction

With the abrupt change in secured level of power in modern distribution power system, the power quality problems, such as voltage sag, voltage swell, voltage unbalances, flicker, harmonics [80], short circuit faults are also increasing, which in-turn affects the power system stability and reliability. Voltage sag causes malfunction and damage of equipments leading to heavy financial losses [81]. As aftermath, end user financial losses are reflected in industrial and commercial operations also, which in turn damages the products, decreases equipment life and interrupts manufacturing processes [82].

There are various solutions to this problem, such as inverter drives for process equipment or installation of voltage correction devices [83]. It has been shown that to cope with the voltage sag problem, a series compensation device, commonly known as dynamic voltage restorer (DVR), may be identified as one of the best solutions [84]. This DVR consists of a voltage source converter (VSC), series injection transformer and a storage capacitor [85]. The main function of DVR is to maintain the amplitude and phase angle of load voltage and respond quickly to correct the problem after detecting a fault. But, DVR is capable to perform series compensation only. Shunt compensation is not possible by this custom device. This drawback of DVR can be overcome by a shunt compensating device, named as static synchronous compensator (STATCOM). STATCOM controls power flow and improves transient stability of power grid [86]. STATCOM regulates voltage at the point of common connection (PCC) by injecting or absorbing the required reactive power. STATCOM comprises of a voltage source converter (VSC) connected with secondary side of shunt coupling transformer and a storage capacitor.

Recent researches show that both these series and shunt compensation features are added in compound FACTS devices. Among these devices, unified power quality conditioner (UPQC) is very popular which has already been discussed in chapter 3. This UPQC consists of a shunt VSC, a series VSC, a sharing common dc link [87] and a series injection transformer.

The presence of this series injection transformer increases the cost of UPQC. Present chapter proposes to use a hybrid DVR (H-DVR), capable of both series and shunt compensation. By H-DVR the problems associated with current and voltage can be solved simultaneously. Besides, the uniqueness of this H-DVR is the absence of series-injection transformer, presence of single VSC, which ultimately reduces the cost of compensating device. This present chapter also finds the optimal location of H-DVR in distribution system. Minimization of power losses, total harmonic distortion (THD), system unbalance and improvement of node voltage profile and reduction of load curtailment due to voltage sag [88] are set as the objectives.

Cuckoo Optimization Algorithm (COA) [56] has been employed to solve the problem. The results obtained from H-DVR installation are compared with that of DVR. The proposed method has been tested on IEEE-123 bus test system and the results are produced. Finally, the results obtained by COA method are compared with some other soft computing techniques to find the robustness and suitability of COA technique in solving the problem. The rest of the present chapter is arranged as follows. The operating principle of H-DVR is briefed in section 4.2 by its structure along with phasor diagram. Section 4.3 formulates the optimal allocation problem of H-DVR by considering different constraints. The optimal allocation methodology of H-DVR is proposed in section 4.4 in terms of simulation procedural steps of H-DVR controller. The proposed method is tested on IEEE-123 node test system under different load conditions and some of the results are furnished in section 4.5 for better visualization of the method. Besides, a comparative result analysis of H-DVR and DVR is also illustrated in section 4.5. At last the present chapter is concluded in section 4.6.

4.2. Operation of H-DVR

Fig.4.1 shows a schematic representation of H-DVR based on single voltage source converter (VSC). It is

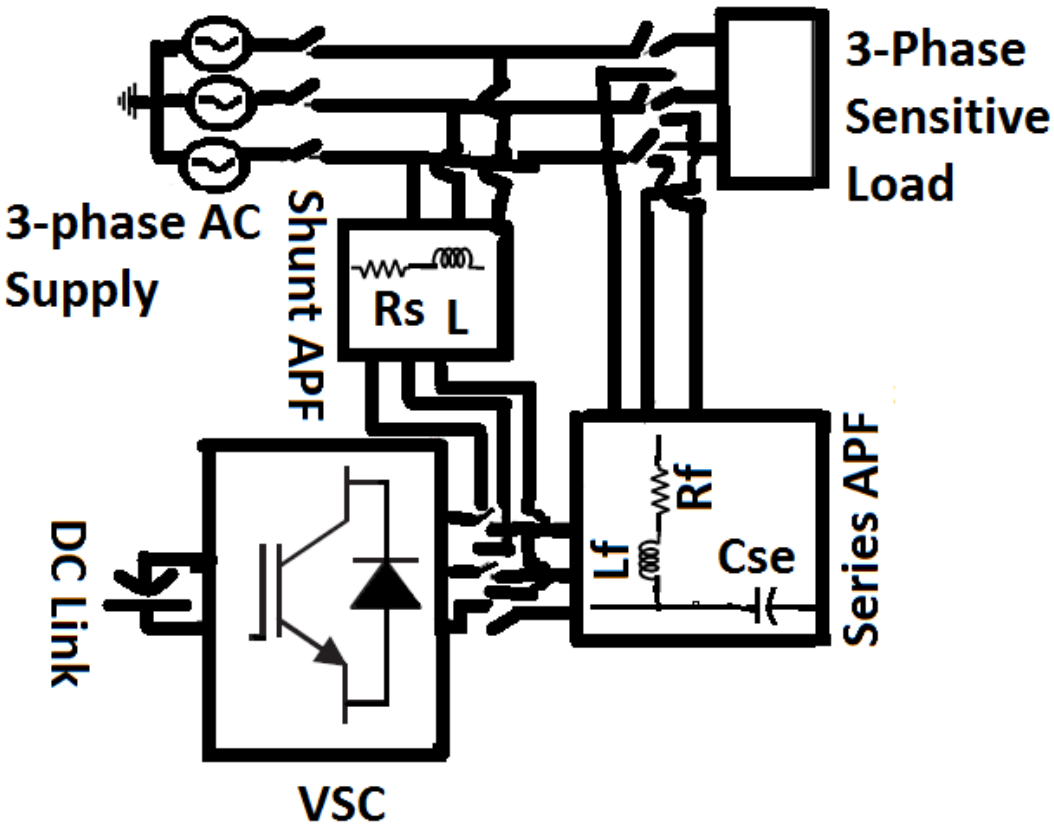

Fig. 4.1. Schematic diagram of H-DVR

made of a transformerless dynamic voltage restorer (DVR) and a transformerless STATCOM. The shunt compensator STATCOM is connected in parallel with the load and performs as a load compensator, thus provides reactive power supply, improves current harmonics problem and reduces load unbalances [86]. DVR operates in series with the line and performs as a voltage controller [89]. The STATCOM consists of multi-level cascaded bridge converter, shunt active power filter (shunt APF) having an inductor L, starting resistance R_S and dc capacitor C . L filters out ripples caused by PWM. The same converter along with dc capacitor C is shared by DVR also, which consists of output series active power filter (series APF) having inductor L_f and capacitor C_{se} . The voltage (V_{sr}) across the filter capacitor connected in series with the line is controlled to maintain desired voltage at the load point.

As the single converter is shared by both series and shunt compensator, a switch is connected with the bridge to connect either the series or the shunt filter depending upon the control requirement.

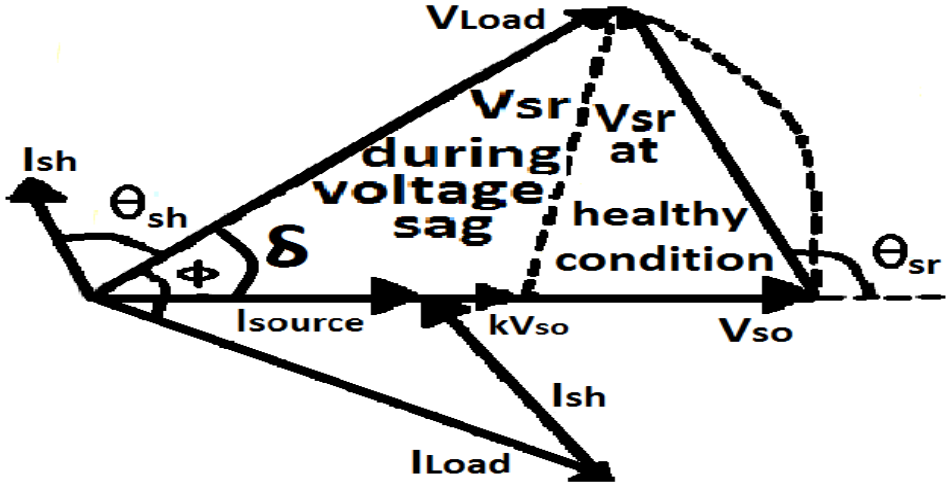

Fig. 4.2. Phasor diagram of H-DVR under healthy and voltage sag condition

The current and voltage injections by the converter in series and shunt mode respectively are illustrated in Fig.4.2. In Fig.4.2, V_{sr} and V_{sh} represent series and shunt injection voltages respectively produced by H-DVR. θ_{sr} and θ_{sh} represent series converter fed voltage angle and shunt converter fed current angle respectively. During normal and voltage sag condition, source voltage magnitudes are denoted by $V_{Source}=V_{S_0}$ and $V_{Source}=kV_{S_0}$, where $k<1$, $k_{sag}=(1-k)$, p.u. sag in source voltage. From Fig.4.2, ϕ is the angle between V_{Load} and I_{Load} while δ is the angle between V_{Load} and I_{Source}.

At any condition, $V_{Load}=V_{S_0}=V_{Source}$

- **Series compensation mode:**

When converter operates in series compensation mode, the series voltage injection required to mitigate k_{sag} p.u. voltage sag, can be calculated by,

$$\begin{aligned} V_{sr} &= \sqrt{V_{Load}^2 + \left(kV_{S_0}\right)^2 - 2V_{Load}\left(kV_{S_0}\right)\cos\delta} \\ &= V_{Source}\sqrt{1+k^2-2k\cos\delta} \end{aligned} \tag{4.1}$$

For a lossless H-DVR, the active power drawn by load is tantamount to active power supplied by source, i.e.,

$$kV_{Source}I_{Source} = V_{Load}I_{Load}\cos\phi, \text{ i.e., source current } I_{Source} = I_{Load}\cos\phi/k \tag{4.2}$$

Where, I_{Source} and I_{Load} are the source and load currents respectively after compensation.

The VA rating of converter in case of series inversion mode can be expressed using equations (4.1) and (4.2) as,

$$\begin{aligned} S_{sr} &= V_{sr}I_{Source} \\ &= V_{Source}I_{Load}\cos\phi\sqrt{1+k^2-2k\cos\delta}\Big/k \end{aligned} \tag{4.3}$$

The active and reactive power supplied by series compensation mode can be expressed as equations (4.4) and (4.5) respectively, given as follows:

$$P_{sr} = S_{sr}\cos\theta_{sr} \tag{4.4}$$

$$Q_{sr} = S_{sr}\sin\theta_{sr} \tag{4.5}$$

Where, $\theta_{sr} = 180° - \tan^{-1}\left(\sin\delta/1-\cos\delta\right)$

- **Shunt compensation mode:**

When converter operates in shunt compensation mode, the compensating current I_{sh} can be expressed as

$$\begin{aligned} I_{sh} &= \sqrt{I_{Source}^2 + I_{Load}^2 - 2I_{Source}I_{Load}\cos\left(\phi-\delta\right)} \\ &= I_{Load}\sqrt{1+\cos^2\phi/k^2 - 2\cos\phi\cos\left(\phi-\delta\right)/k} \end{aligned} \tag{4.6}$$

The distorted current due to the presence of non-linear loads is compensated by shunt compensation as

$$I_{Load}^{dis} = I_{sh}^{dis} \tag{4.7}$$

and $THD_{Load}I_{Load}^{f} = THD_{sh}I_{sh}^{f}$ (4.8)

where, I_{Load}^{dis} and I_{Load}^{f} are distortion and fundamental components respectively and THD_{Load} is the total harmonic distortion of load current. The distortion and fundamental current components of shunt inverter are represented by I_{sh}^{dis} and I_{sh}^{f} respectively while total harmonic distortion is represented by THD_{sh}.

So shunt compensating current can also be expressed as,

$$\begin{aligned} I_{sh} &= I_{sh}^{f}\sqrt{1+THD_{sh}^{2}} \\ &= I_{Load}^{f}\sqrt{1+\cos^{2}\phi/k^{2}-2\cos\phi\cos(\phi-\delta)/k+THD_{Load}^{2}} \end{aligned} \tag{4.9}$$

From equation (4.9), VA rating of H-DVR in case of shunt compensation mode, may be written as

$$\begin{aligned} S_{sh} &= V_{Source}I_{sh} \\ &= V_{Source}I_{Load}^{f}\sqrt{1+\cos^{2}\phi/k^{2}-2\cos\phi\cos(\phi-\delta)/k+THD_{Load}^{2}} \end{aligned} \tag{4.10}$$

Active and reactive power supplied by shunt inversion mode given in equations (4.11) and (4.12) respectively are as

$$P_{sh} = S_{sh}\cos\theta_{sh} \tag{4.11}$$

$$Q_{sh} = S_{sh}\sin\theta_{sh} \tag{4.12}$$

Where $\theta_{sh} = \tan^{-1}\left\{\cos(\phi-\delta)-\cos\phi/\sin(\phi-\delta)\right\}+90°-\delta$

From equations (4.5) and (4.12) total reactive power delivered by H-DVR is written as,

$$Q_{H-DVR} = Q_{sr} + Q_{sh} \tag{4.13}$$

From equations (4.3) and (4.10) total volt-ampere rating of H-DVR may be written as,

$$\begin{aligned} S_{H-DVR} &= S_{sr} + S_{sh} \\ &= \left(V_{sr}I_{Source} + V_{Source}I_{sh}\right) \end{aligned} \tag{4.14}$$

4.3. Problem formulation

In this section, the authors have minimized the objective function, i.e., operating cost consisting of the following three parts:

- ***Part 1-*** To minimize active power loss. This formulation reduces the operating cost of the system.

The active power loss in the system may be expressed as,

$$P_{Loss} = \sum_{k=1}^{N_L} g_k\left\{V_i^2 + V_j^2 - 2V_iV_j\cos\left(\delta_i-\delta_j\right)\right\} \tag{4.15}$$

Where, N_L indicates the total number of distribution lines in the test system. g_k represents the conductance of the k^{th} line connected between buses i and j. V_i and V_j are the voltage magnitudes of buses i and j respectively. δ_i and δ_j are the voltage angles of buses i and j respectively.

- ***Part 2-*** To minimize the load disconnection due to voltage sag

Another problem arising from voltage sag is the load curtailment which also affects the H-DVR installation. The total load disturbed due to voltage sag during fault condition, as reported in [62], can be expressed as,

$$S_{DIST} = \sum_{i=1}^{N_F} L_{DIST_i} \tag{4.16}$$

Where, L_{DIST_i} is the amount of load disturbed for the i^{th} fault and N_F is the total number of faults within this period.

- ***Part 3-*** To Minimize the total installation cost of H-DVR

This formulation reduces the operational cost for the expenditure due to the procurement of the sag compensating device, i.e., H-DVR. Total cost of H-DVRs will vary as the number of H-DVR changes and is obtained as the product of the total number of H-DVR (N_{H-DVR}) used and the cost of each H-DVR (k_{size}). This cost of H-DVR is taken same as that of UPFC, as the details mentioned in [37].

Thus, the objective of cost minimization of H-DVR can be formulated as,

$$\text{Minimise, } C_{H-DVR} = k_{size} \sum_{i=1}^{N_{H-DVR}} S_{H-DVR_i} \tag{4.17}$$

Where, C_{H-DVR} is the total cost associated with H-DVRs, S_{H-DVR_i} is the size of ith H-DVR, N_{H-DVR} is the total number of the H-DVR installed and k_{size} is the cost of H-DVR per kVA.

The objectives mentioned in equations (4.15-4.17), have to be minimized subject to the satisfaction of the equality and inequality constraints as mentioned below:

4.3.1. Equality constraint

In the distribution system, active power balance can be expressed as,

$$P_{G_i} - P_{D_i} - \sum_{k=1}^{N_L} g_{ik} \left\{ V_i^2 + V_j^2 - 2V_i V_j \cos\left(\delta_i - \delta_j\right) \right\} = 0 \tag{4.18}$$

and reactive power balance can be expressed as,

$$Q_{G_i} - Q_{D_i} - \sum_{k=1}^{N_L} b_{ik} \left\{ V_i^2 + V_j^2 - 2V_i V_j \sin\left(\delta_i - \delta_j\right) \right\} = 0 \tag{4.19}$$

Where, P_{G_i} , P_{D_i} , Q_{G_i} and Q_{D_i} are the active power injected at bus i, system active power demand, reactive power injected at bus i and system reactive power demand respectively. N_L is the number of lines, g_{i-j} and b_{i-j} represent conductance and susceptance respectively of the line connected between buses i and j. V_i and V_j are the voltage magnitudes of buses i and j respectively. δ_i and δ_j denote voltage angles of buses i and j respectively.

4.3.2. Inequality constraint

The inequality constraints consist of the following three classes:

- **Line flow limit:**

The maximum power flow capacity of distribution line can be expressed as,

$$S_k \le S_{k_{\max}} \tag{4.20}$$

Where, $S_{k_{\max}}$ is the maximum value of the power flow through k^{th} line.

- **Harmonic limits:**

The author has taken in this chapter two types of harmonic limits, namely voltage total harmonic distortion limit and individual voltage harmonic limit.

The voltage total harmonic distortion constraint can be expressed as

$$THD_v \le THD_{\max} \tag{4.21}$$

where, $THD_{\max}$ is maximum tolerance value, taken as 5% in this chapter, according to IEEE-519 standards.

Individual voltage harmonic constraint is expressed as,

$$V_h \le V_{h_{\max}} \tag{4.22}$$

where, $V_{h_{\max}}$ is maximum tolerance value, taken as standard limit 3%.

- **Bus voltage limit :**

Two types of voltage limit namely node voltage magnitude and voltage unbalance are considered.

The node voltage magnitude V limit may be expressed as,

$$V_{\min} \le V \le V_{\max} \tag{4.23}$$

where, $V_{\min}$ and $V_{\max}$ are treated as minimum and maximum node voltage magnitude respectively and taken as 0.85 p.u and 1.05 p.u. respectively in this chapter.

The three phase voltage unbalance (defined in [64]) limit in distribution system is given as,

$$VU \le VU_{\max} \tag{4.24}$$

where, $VU_{\max}$ is the permissible value of voltage unbalance, taken as 2% in this chapter.

For a better compatibility, all the objective functions mentioned in equations (4.15-4.17) may be converted into a single objective function in terms of cost by considering all the constraints specified in equations (4.18-4.24). Each objective function is multiplied by a penalty cost as they violate their respective limits. The single objective function in terms of costs is given as

$$\begin{aligned} Cost = {} & k_{loss}\sum_{k=1}^{N_L} Loss_k + k_{MVA}\sum_{i=1}^{N_F} L_{DIST_i} \\ & + k_{size}\sum_{i=1}^{N_{H-DVR}} S_{H-DVR_i} + k_{flow}\sum_{k=1}^{N_i}\left|S_k - S_{k_{\max}}\right| \\ & + k_{Volt}\sum_{k=1}^{N_b}\left|V_k - V_{k_{\min/\max}}\right| \\ & + k_{harm}\sum_{k=1}^{N_b}\left|THD_{v_k} - THD_{\max_k}\right| \\ & + k_{harm-i}\sum_{k=1}^{N_b}\sum_{h=3,5,7}\left|V_{h_k} - V_{h_{\max}}\right| \\ & + k_{VU}\sum_{\delta_{5k}}^{N_b}\left|VU_k - VU_{\max}\right| \end{aligned} \tag{4.25}$$

where k_{flow}, k_{Volt}, k_{harm}, k_{harm-i} and k_{VU} are the multipliers to penalize the violation of line power flow, node voltage, harmonic distortion and permissible voltage unbalance [62]. N_b and N_L represent total number of buses and distribution lines respectively in the test system. k_{loss}, k_{size} and k_{MVA} represent costs of energy losses, cost of each H-DVR and cost of load interruptions respectively. k_{loss} and k_{MVA} are taken as 0.08 US$/kWh and 4US$/MVA [62] respectively. k_{size} is taken by following the details, mentioned in [62]. In this chapter,

$$
\begin{aligned}
k_{flow} &= 10^{12}, \text{ if } S_k > S_{k_{\max}} \\
&= 0, \text{otherwise} \\
k_{Volt} &= 10^{12}, \text{ if } V_k > V_{k_{\min/\max}} \\
&= 0, \text{otherwise} \\
k_{harm} &= 10^{12}, \text{ if } THD_{v_k} > THD_{\max_k} \\
&= 0, \text{otherwise} \\
k_{harm-i} &= 10^{12}, \text{ if } V_{h_k} > V_{h_{\max}} \\
&= 0, \text{otherwise} \\
k_{VU} &= 10^{12}, \text{ if } VU_k > VU_{\max} \\
&= 0, \text{otherwise}
\end{aligned}
\tag{4.26}
$$

4.4. Proposed methodology of optimal allocation of H-DVR

Evaluation of single objective function, expressed in equation (4.25), requires to perform load flow, harmonic power flow and voltage sag analysis. This multi-dimensional single objective function, given in equation (4.25) is very difficult to solve by using conventional optimization technique due to the presence of non-linearity. To overcome this problem, several meta-heuristic methods have been increasingly used and among them Cuckoo Optimization Algorithm (COA) [56], Gravitational search algorithm (GSA) [18], Artificial bee colony (ABC) [77] and Differential evolution (DE) [76] have been adopted in this chapter. But for lack of space only the results obtained by COA have been furnished in details in this chapter.

Besides, the influences of H-DVR on power system during healthy and faulty conditions require elaborate simulation of H-DVR during both the conditions respectively. To obtain the simulation model of H-DVR, estimation procedure of voltage sag and a brief description of COA are given in Appendix A.3 and A.2 respectively. The implementation procedure of COA along with H-DVR simulation technique are described in the following section.

Fig. 4.3 illustrates the brief representation about simulation of H-DVR. From Fig. 4.3, it is obvious that the simulation procedure is classified as two conditions namely faulty and healthy. During fault condition, H-DVR simulation process is executed and the concerned load bus voltage magnitudes and angles are exported to load flow program.

During healthy conditions, only load flow program is executed and voltage unbalance, voltage harmonic, THD and system loss are determined. Next the solutions are checked whether they are optimized or not by COA, as given in Fig.4.3.

4.4.1. **Simulation of H-DVR controller**

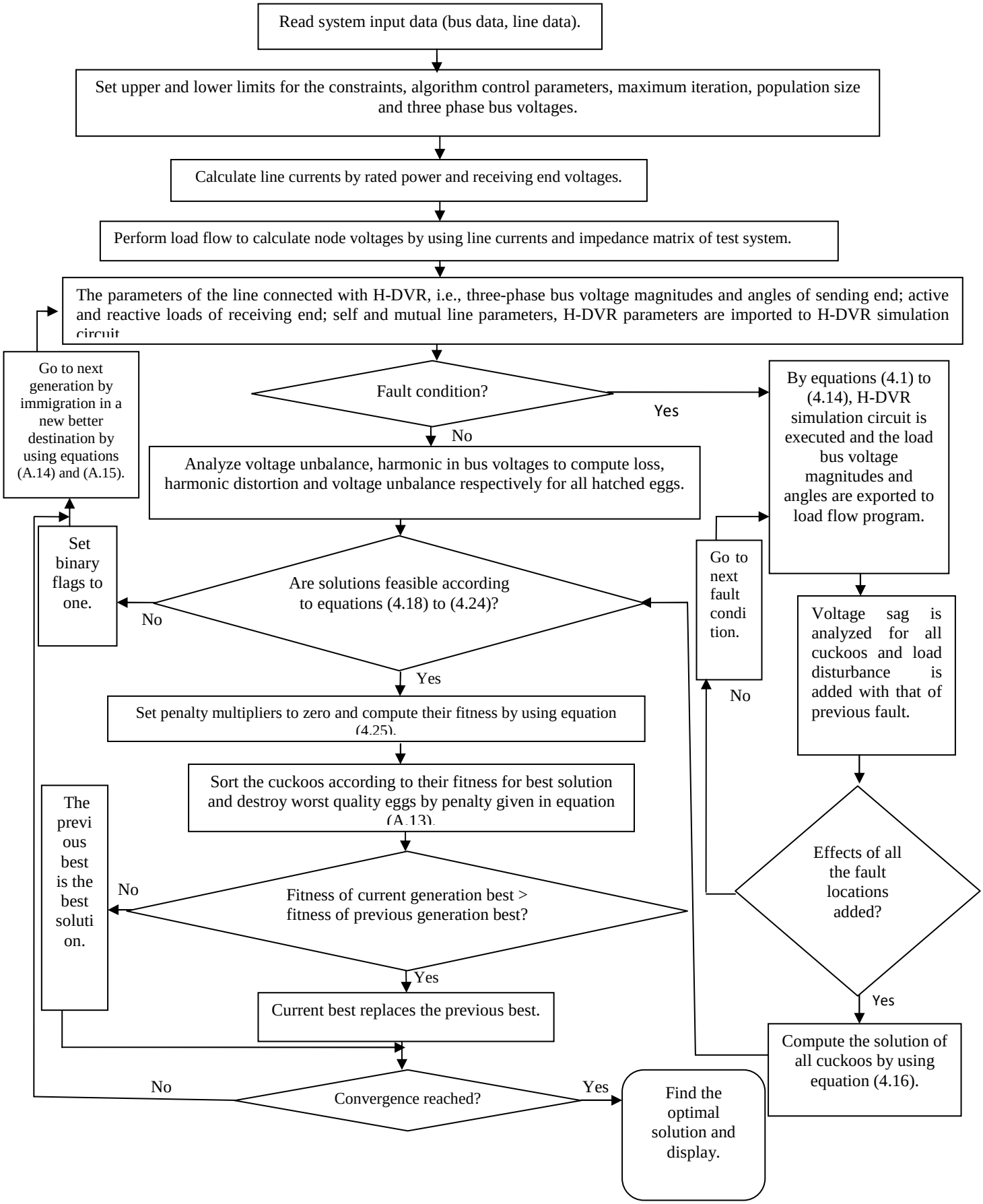

Fig.4.3. Flow chart of H-DVR implementation by COA

4.5. Application of proposed method

Results for IEEE-123 node system

In this section results of the optimal placement of H-DVR with the help of optimization technique is presented. The performance is studied on IEEE-123 node, unbalanced radial distribution test system. The data of IEEE 123 node test system is reported in [74]. The system has one substation with specified voltage of $1\angle 0°$ p.u. Two cases having 50% and 30% of the total load as non-linear load of the systems are studied. The results of the case with 50% nonlinear load and 30% nonlinear load are furnished in sections 4.5.1 and 4.5.2 respectively.

However, in this chapter, first section analyses the impact of H-DVR on the test network considering faults occurring at different location of the system. After that, second section discusses the variation in %THD in the system with the installation and increase in H-DVRs. Then, the changes in voltage harmonics of different orders with the increase in H-DVRs on test systems are reported. After that, the variation in % voltage unbalance against the change in H-DVR numbers is studied. The effect of H-DVRs in terms of total load disturbance, cost savings and sag are furnished and thereby the optimal number of H-DVRs are found out in the next two sections respectively. At last the comparative analysis of the results found by different soft computing techniques mentioned above are shown. The results obtained by H-DVR installation are compared with that of DVR installation for 50% non-linear load consideration only.

4.5.1. Results for 50% non-linear load

- **Impact of H-DVR on the area of load disturbance**

In this chapter, 0.85 p.u and 1.05 p.u are taken as lower and upper limits of node voltage to maintain the normal operation. The lower limit of voltage represents the threshold value below which sensitive loads will be disconnected from the supply.

The impact of H-DVR on IEEE-123 node, 3-phase, unbalanced test network is shown for worst case in Fig.4.4. In this case a single phase fault occurs on the distribution line connected between buses 1 and 7.

Fig.4.4 illustrates that with the occurrence of fault on the line connected between nodes 1 and 7, a large distribution area becomes a load shedding area and this load disturbed area is shown by ash colour in Fig. 4.4.

From Fig. 4.4, it is also shown that with single H-DVR installation on optimal location of test network, the previous disturbed area is reduced to the area having only two buses 65 and 66. But another area is affected by this fault (marked by light yellow colour) and the node voltage falls under threshold value in that area.

One more H-DVR located optimally, boosts up all the node voltages situated in the area marked by light yellow colour and thus the test network becomes a normal operating system.

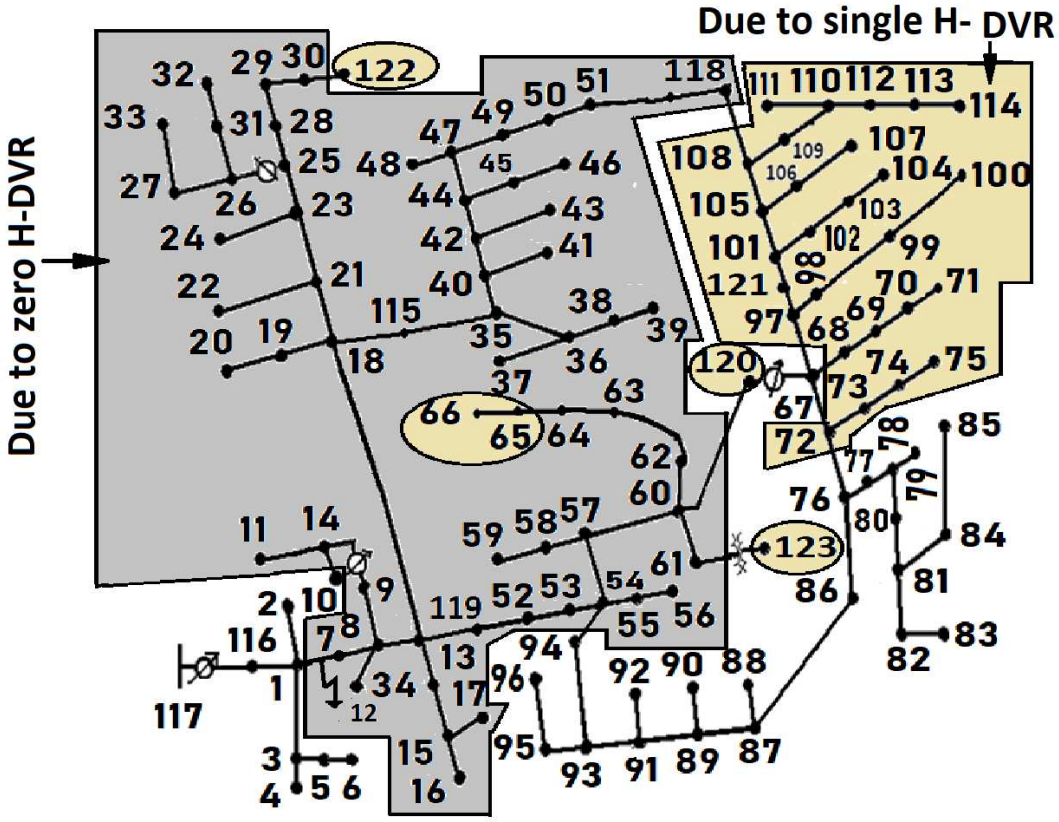

Fig.4.4. Effect of H-DVRs on load disturbed area in IEEE 123 bus test system

- **Impact of H-DVR on the THD**

From Fig.4.5, it is found that the maximum %THD without H-DVR is 16.132% at bus 78 at phase-a. With the installation of single H-DVR at its optimal position, this maximum % THD is slightly changed to 15.013% on bus 78 at phase-a. With the addition of another H-DVR in the system, the maximum %THD is further reduced to 4.52% on the same bus and phase and it is a large change compared to %THD found in optimal location of 2 H-DVR and falls below the maximum limit. However, there is no appreciable improvement in % THD with the addition of 3rd H-DVR on its optimal location of IEEE123 node test feeder.

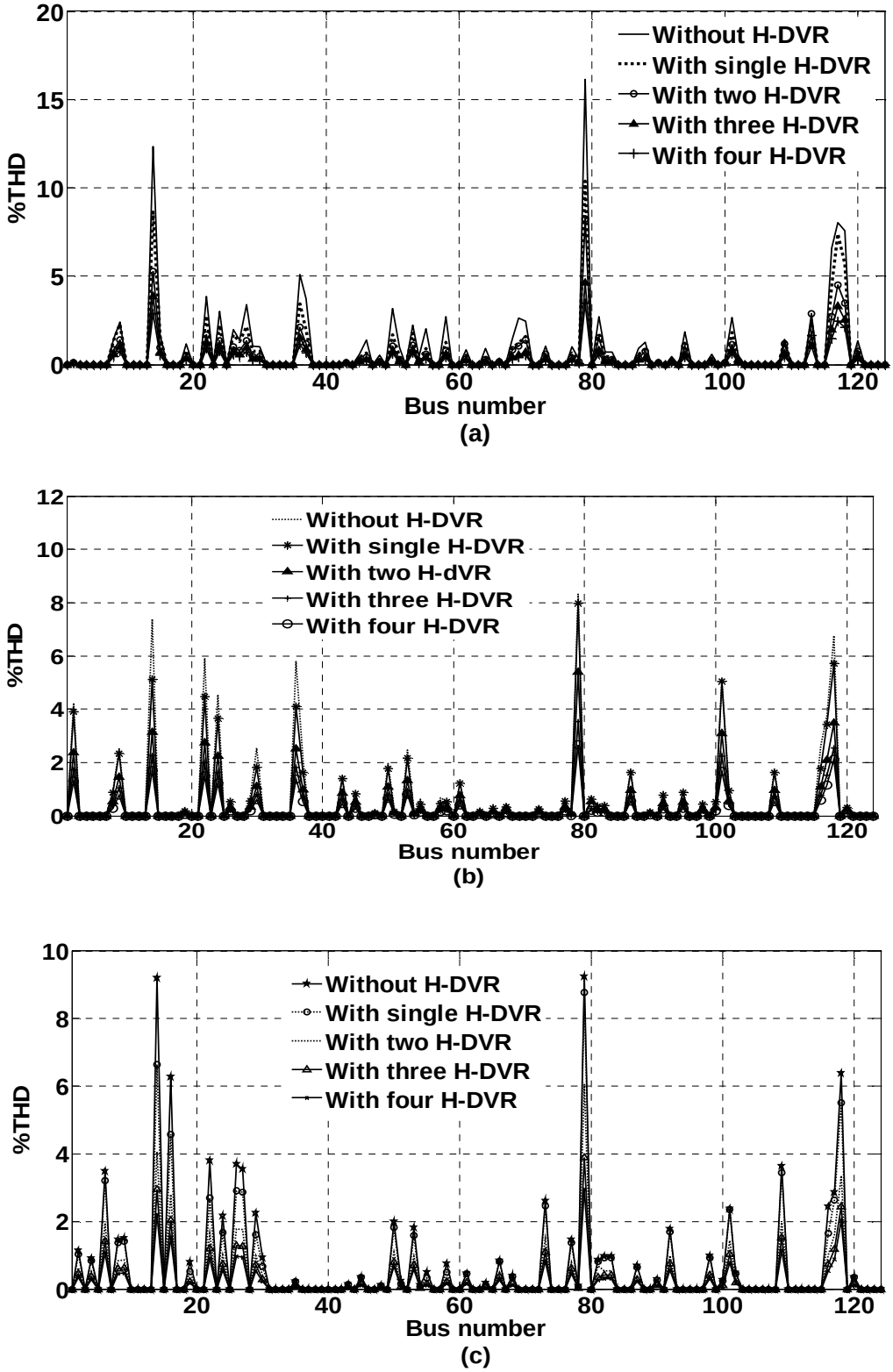

Fig.4.5. Impact of H-DVRs on %THD variation of IEEE 123 bus test system at (a)a-phase, (b)b-phase, (c)c-phase

- **Impact of H-DVR on individual harmonics**

Fig. 4.6 illustrates that without H-DVR, in the test system, the maximum 5^{th}, 7^{th}, 11^{th}, 13^{th}, 17^{th} and 19^{th} voltage harmonic magnitudes are found to be 5.038%, 5.02%, 5.019%, 5.016%, 5.011% and 5.01% respectively. From Fig.4.6 it is also shown that with the installation of two H-DVR on their optimal locations, the maximum 5^{th} harmonic in IEEE123 node test system is found to be 3.1%, which just violates the upper limit and the higher order voltage harmonic magnitudes fall below 3%.

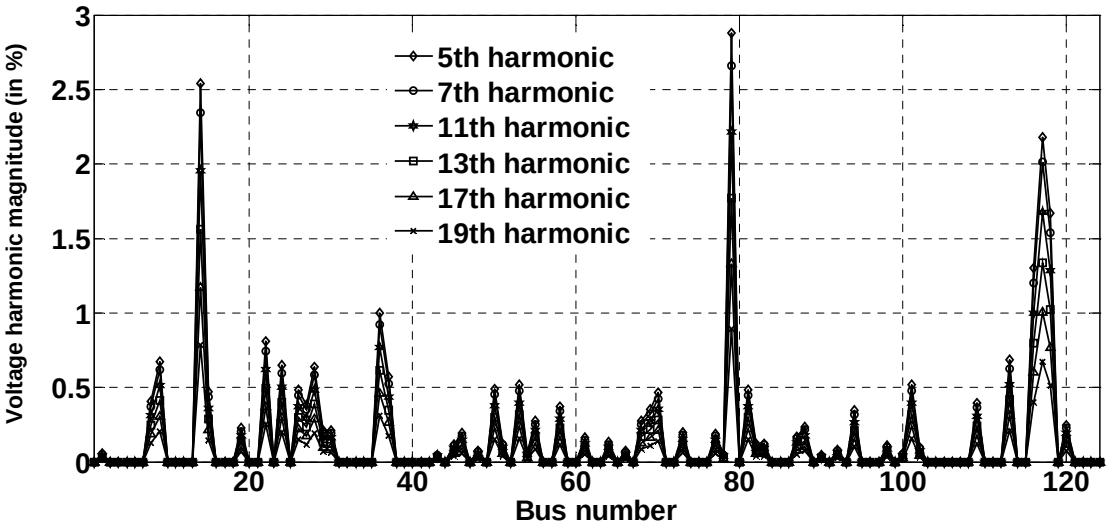

(a)

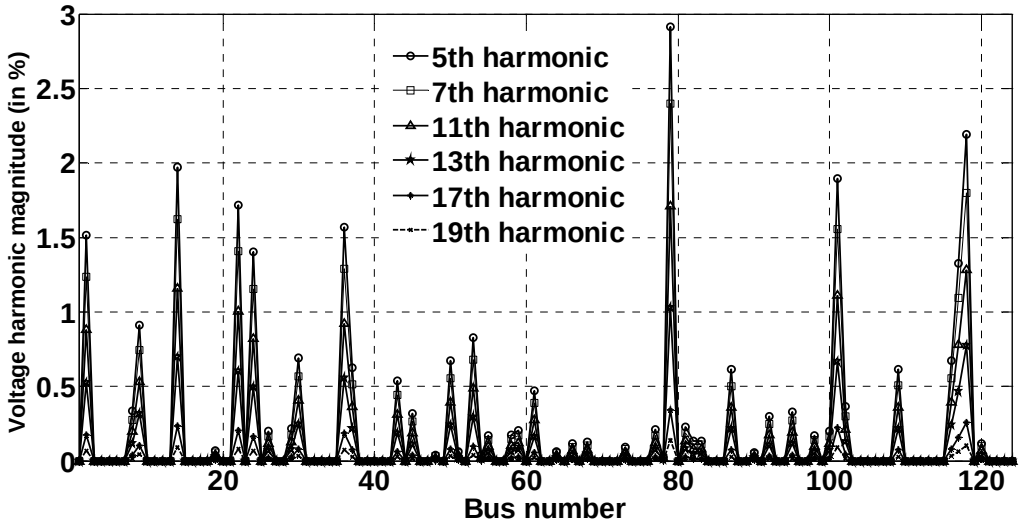

(b)

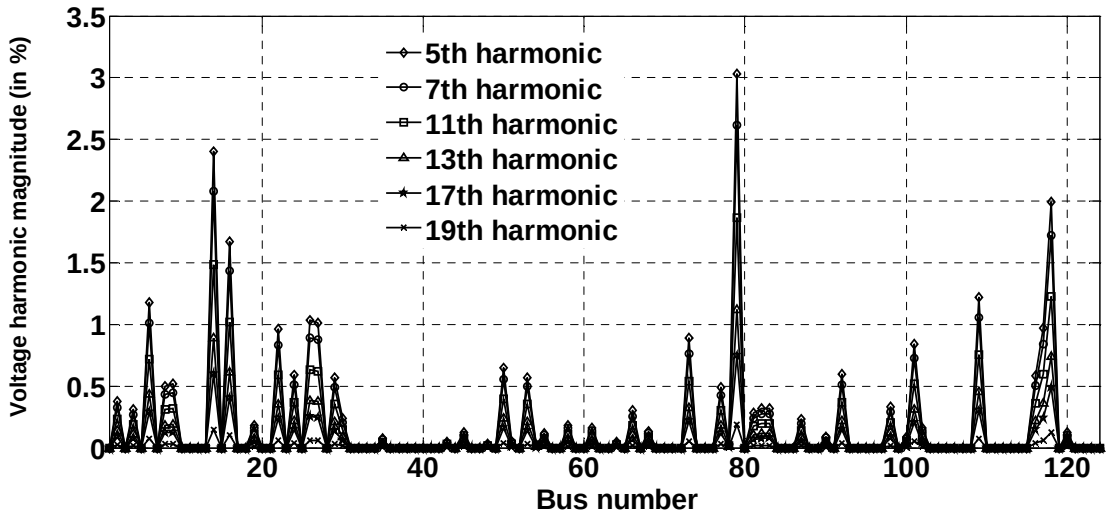

(c)

Fig.4.6. Change in individual harmonics at different buses with optimal installation of 2 H-DVRs in IEEE 123 bus test system, (a) a-phase, (b) b-phase, (c) c-phase

- **Effect of H-DVR on voltage unbalance**

The variation of bus voltage unbalances with respect to the number of H-DVR is shown in Fig.4.7. From Fig.4.7, it is obvious that without any H-DVR in the test system the maximum voltage unbalance is 5.2% and with the addition of single H-DVR on its optimal location it falls to 3.36%. With the installation of second H-DVR in the test system, the maximum voltage unbalance reduces to 2.65% and it is within limit. But the addition of third optimally situated H-DVR does not reduce the maximum %voltage unbalance to a great extent, it is 1.99% and falls within limit.

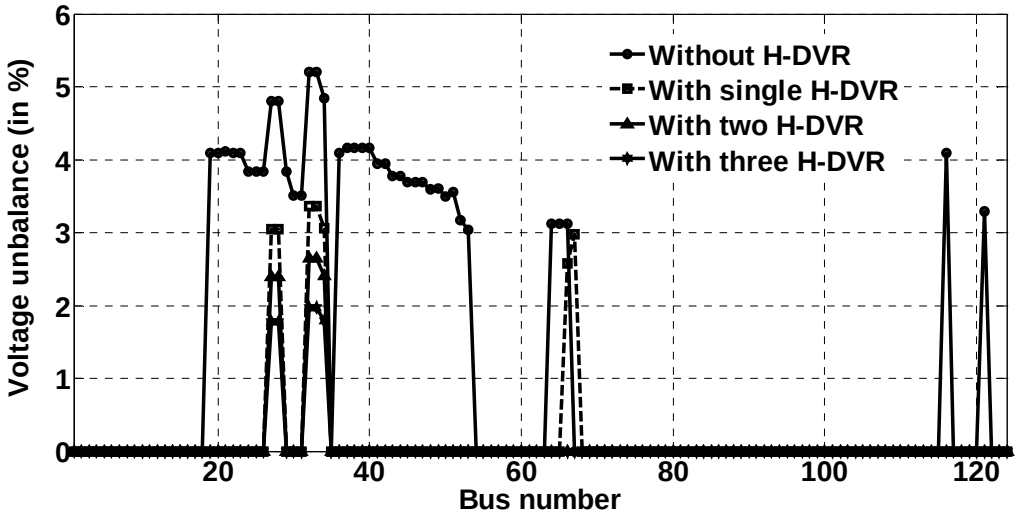

Fig.4.7. Effect of H-DVRs on variation of three phase bus voltage unbalance of IEEE123 bus test system

- **Influence of H-DVR on real power loss, load disturbance and cost savings for 50% non-linear load**

The effectiveness of H-DVR installation for sag compensation in IEEE-123 bus test system is reported in Table:4.1 in terms of optimal location of H-DVRs, cost, cost savings, real power loss and total load disturbances. From Table:4.1, it is shown that the addition of single H-DVR in the faulty system reduces the real power loss from 2,822 kW to 1131 kW and load disturbed from 18.7625 MVA to 11.007 MVA. Besides, with the installation of second H-DVR in its optimal location, the real power loss is reduced slightly from 1131 kW to 947 kW, but the load disturbed is reduced drastically from 11.007 MVA to 0 MVA. The addition of these real power loss and load disturbance reductions result in cost savings of 51.73% and 94.71% in the former and latter cases of H-DVR installation respectively.

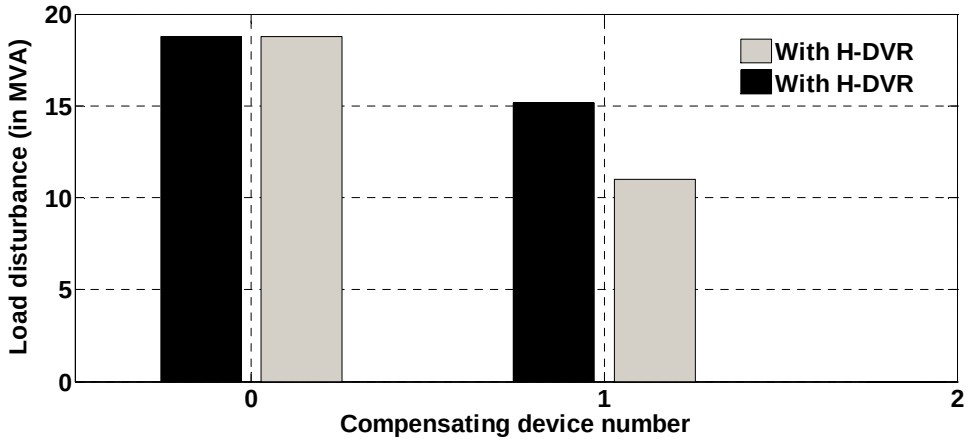

Fig.4.8. Effect of H-DVRs and DVRs on Change in load disturbance

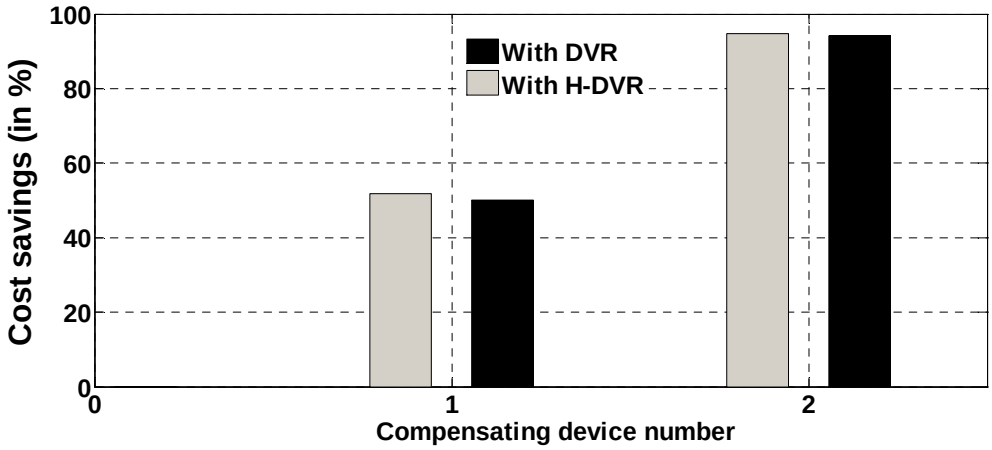

Fig.4.9. Change in cost savings with the change in H-DVR and DVR number in IEEE 123 bus test system

Table4.1. Optimal location of H-DVR, loss, cost, savings, sag and size with load disturbance of 0.85 p.u.

Control Variables	Without compensating device	With single H-DVR	With double H-DVR
Optimal location of compensating device (line number)	-	72-76	64-65,44-47
Total Cost (in billion $)	10150	4899.3	537
Savings (in %)	-	51.73	94.71
Loss(in kW)	2,822	1131	947
Load disturbance, MVA	18.7625	11.007	0
Compensating device size (in kVAr)	-	500	200

The variation of load disturbance and cost savings with the increase in H-DVR number are shown graphically in Fig.4.8 and Fig.4.9 respectively for IEEE123 node test system. The optimal number of H-DVR is found to be two and their optimal locations are the distribution lines connected between buses 64-65 and 47-48 respectively. The installation of single and double H-DVR results in operating costs of 4899.3 and 537 billion $ respectively.

- **Effect of H-DVR on voltage sag**

The result corresponding to voltage envelopes of IEEE123 node test system is shown in Fig.4.10, while considering the worst case of voltage sag. From Fig.4.10, it is found that a-phase voltage magnitude at bus 67 falls from 0.999 p.u. to 0.707 p.u at t=1.71 sec and it increases again to 0.999 p.u at t=1.8 sec while a-phase fault occurs on line (1-7). But during this sag condition, the single H-DVR installation on its optimal location of IEEE123 bus test system helps to improve the bus voltage magnitude to 0.9802 p.u., which is above the threshold voltage. In addition, there is a small improvement from 0.9802 p.u. to 0.9836 p.u, when another one H-DVR is installed on its optimal location in the test system.

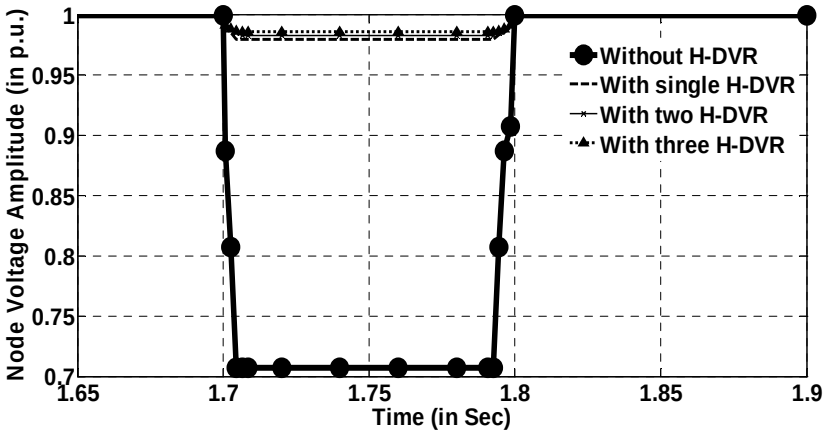

Fig.4.10. Change in sag voltage amplitude at bus 67 with the change in H-DVR number for IEEE123 bus test system

- **Comparative analysis of H-DVR and DVR performances**

Table4.2 shows that the optimal installation of single H-DVR in distribution network reduces the system loss from 2,822 kW to 1131kW, while the installation of DVR reduces the loss to 1187 kW, which is quite higher compared to that of 1 H-DVR. Besides, single DVR installation in the test network reduces the load disturbed from 18.7625 MVA to 15.1602 MVA, but the single H-DVR installation reduces the load disturbance to 11.007 MVA. These reductions in load disturbed and loss ultimately result in savings of 50.06% and 51.73% in the case of optimal installation of single DVR and H-DVR respectively. So, from Table 4.2, it is obvious that the results obtained by using H-DVR are better compared to that of DVR and it is shown graphically in Fig.4.8 and 4.9.

Table4.2. Comparison between DVR and H-DVR

Control Variables	Without compensating device	With single DVR	With single H-DVR	With double DVR	With double H-DVR
Optimal location of compensating device (line number)	-	72-76	72-76	64-65,44-47	64-65,44-47
Total Cost (in billion $)	10150	5068.6	4899.3	586	537
Savings (in %)	-	50.06	51.73	94.23	94.71
Loss(in kW)	2,822	1187	1131	972	947
Load disturbance, MVA	18.7625	15.1602	11.007	0	0
Compensating device size (in kVAr)	-	500	500	200	200

- **Comparative analysis on the performance of different optimization techniques in H-DVR placement problem**

Many robust, metaheuristic methods can be applied to solve the problem formulated in this chapter, but among them Gravitational search algorithm (GSA), Differential evolution (DE) algorithm and Artificial bee colony (ABC) algorithm have been used for the purpose of comparative analysis.

The parameters used for different soft computing techniques are reported in Table 4.3.

However, the application of different soft computing techniques mentioned in this chapter give almost similar results, as furnished in Table:4.4. But from Fig.4.11, it is obvious that the convergence characteristic of COA is the best among the four different soft computing techniques mentioned in this section.

Table4.3. Parameters used in the different optimization techniques

Maximum iteration number =90			
Size of population=25			
COA	GSA	ABC	DE
Discovery rate of alien eggs /solutions, Pa=0.25	Gravitational constant, G0=100	Colony size=16	Weighting factor =0.5
Penalty constant =10^15	User specified constant, α=20	Number of food source =8	Cross over constant =0.5
		limit=5	

Table4. 4. Comparative results of different methods for optimal installation of H-DVR problem in IEEE123 bus test system

Number of H-DVR	Control Variables	COA	GSA	ABC	DE
1	Optimal location of H-DVR (line number)	72-76	72-76	72-76	72-76
	Total Cost (in billion $)	4899.3	4899.3	4899.3	4899.3
	Savings (in %)	51.73	51.73	51.73	51.73
	Loss(in kW)	1131	1131	1131	1131
	Load disturbance, MVA	11.007	11.007	11.007	11.007
2	Optimal location of H-DVR (line number)	64-65,44-47	64-65,44-47	64-65,44-47	64-65,44-47
	Total Cost (in billion $)	537	537	537	537
	Savings (in %)	94.71	94.71	94.71	94.71
	Loss(in kW)	947	947	947	947
	Load disturbance, MVA	0	0	0	0

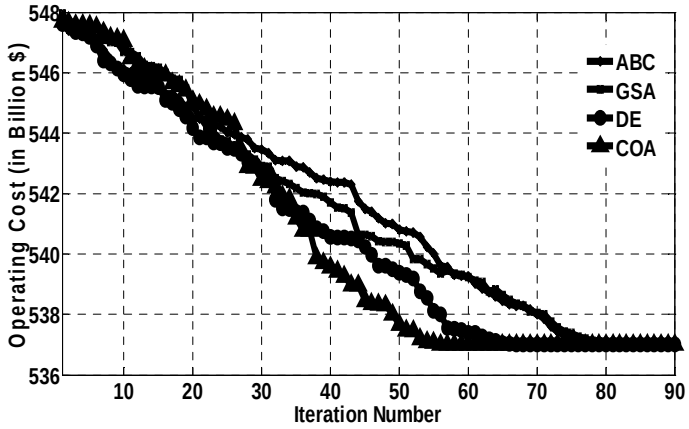

Fig.4.11. Cost optimization with installation of two H-DVR in IEEE 123 bus test system

Fig.4.12 illustrates that optimal placement of H-DVR in IEEE123 node radial test system removes the fault within 6 cycles. This phenomena ultimately results in better voltage profile and satisfies the CBEMA curve [78].

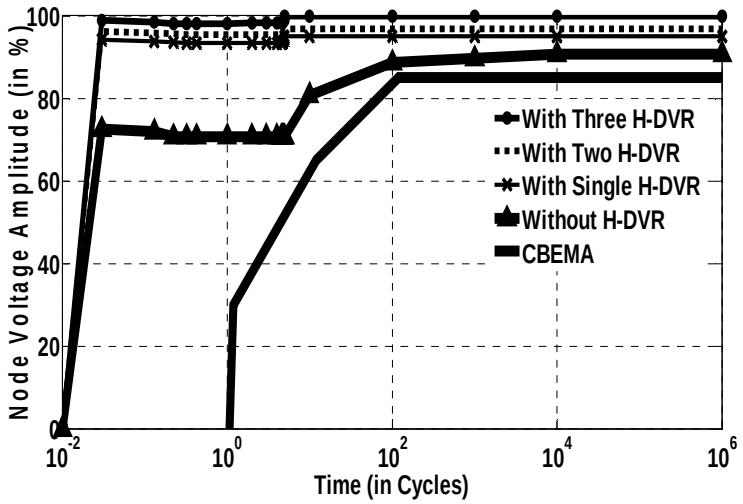

Fig.4.12. Sensitivity range of equipment with voltage sag in IEEE123 bus test system at bus 67

4.5.2. **Results for 30% non-linear load**

- **Impact of H-DVR on the area of load disturbance**

Fig.4.13 illustrates that with the occurrence of fault on the line connected between nodes 1 and 7, a large distribution area becomes a load shedding area and this load disturbed area is shown by ash colour in Fig. 4.13. From Fig. 4.13, it is also shown that with single H-DVR installation on optimal location of test network, the previous disturbed area is reduced to the area having only one bus 49. But another area is affected by this fault (marked by light yellow colour) and the node voltage falls under threshold value in that area. One more H-DVR

located optimally, boosts up all the node voltages situated in the area marked by light yellow colour and thus the test network becomes a normal operating system.

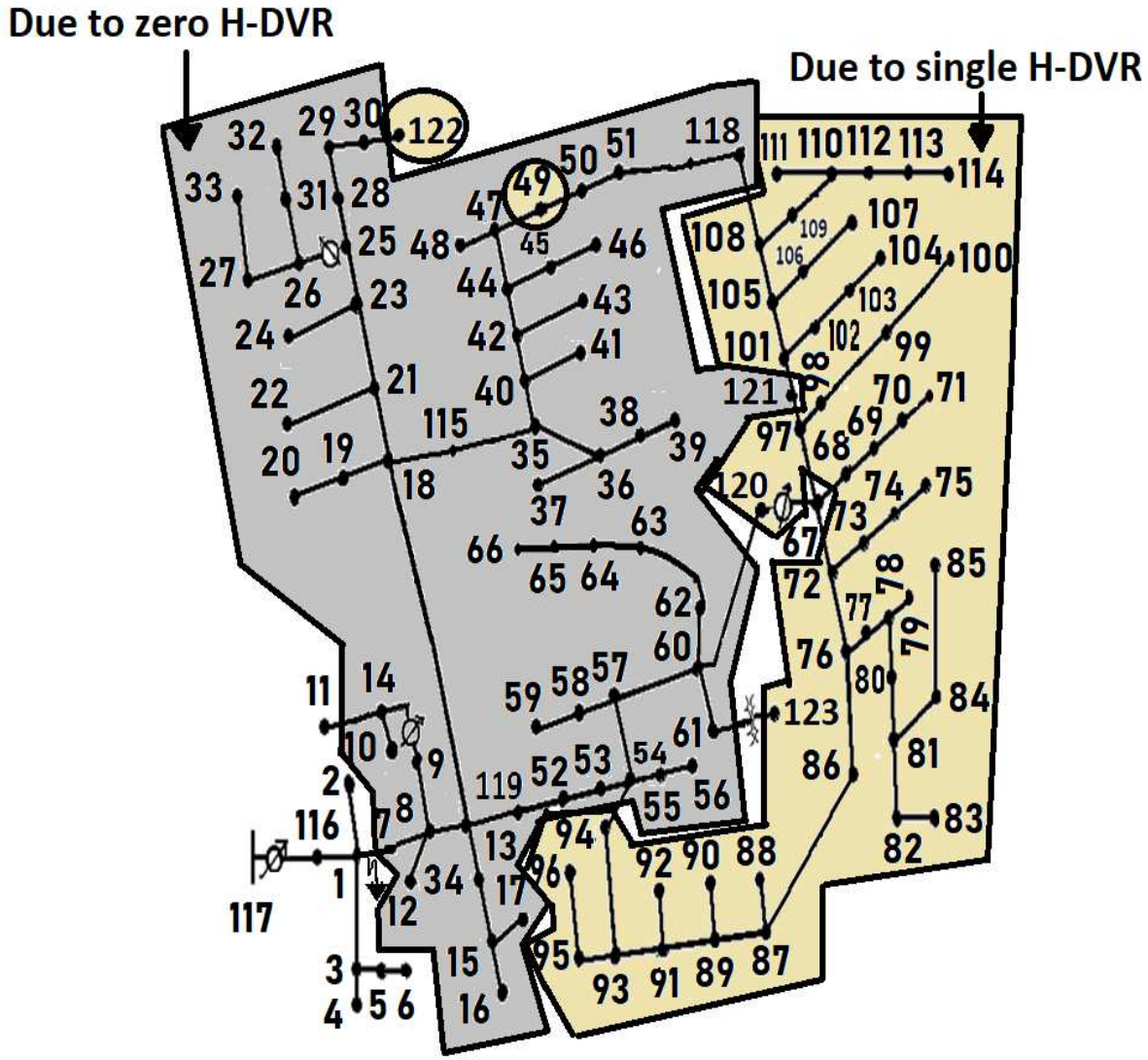

Fig.4.13. Effect of H-DVRs on load disturbed area in IEEE 123 bus test system

- **Impact of H-DVR on the THD**

From Fig.4.14, it is found that the maximum %THD without H-DVR is 15.2% at bus 78 at phase-a. With the installation of single H-DVR at its optimal position, this maximum % THD is changed to 10.2% on bus 79 at phase-a. With the addition of another H-DVR in the system, the maximum %THD is further reduced to 4.99% on the same bus and phase and it is a large change compared to %THD found in optimal location of 2 H-DVR and falls below the maximum limit.

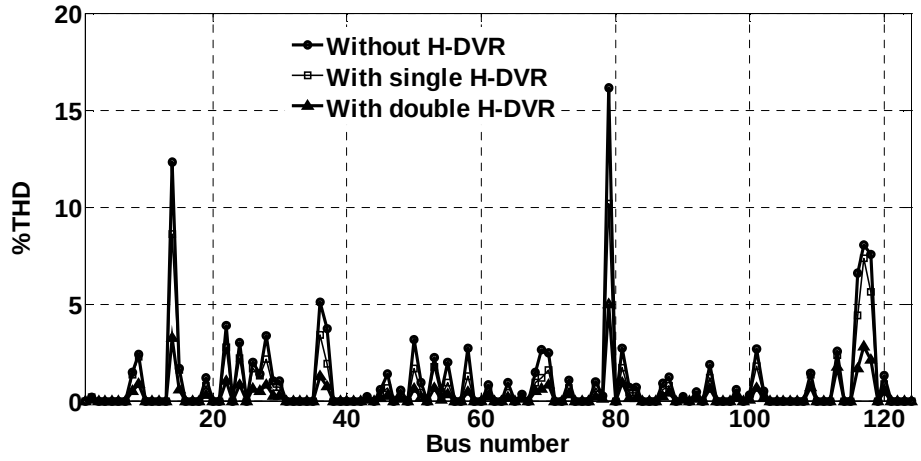

(a)

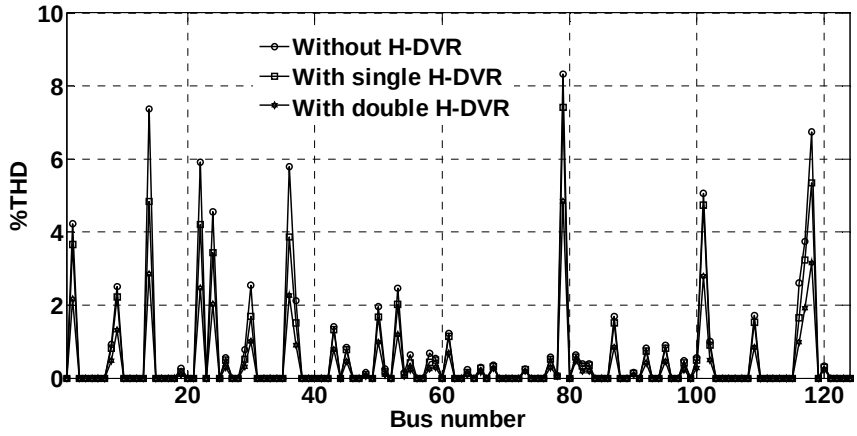

(b)

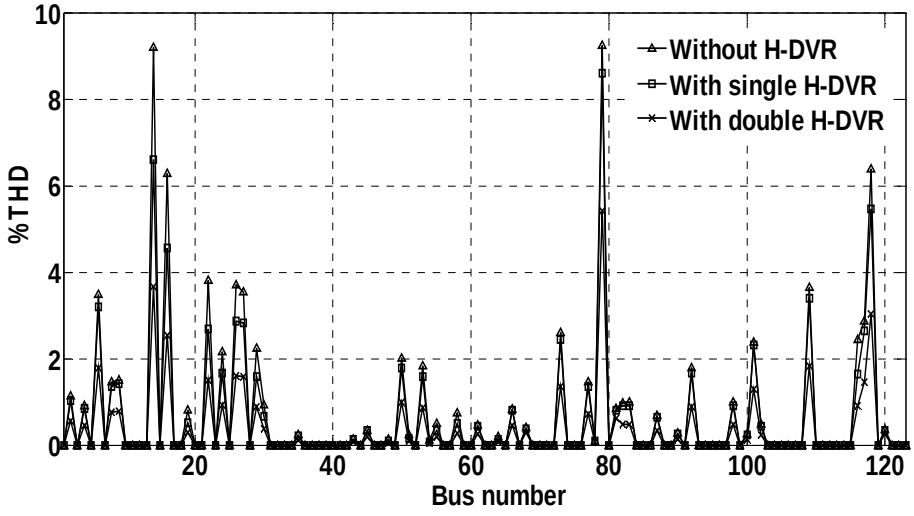

(c)

Fig.4.14. Impact of H-DVRs on %THD variation of IEEE 123 bus test system at (a)a-phase, (b)b-phase, (c)c-phase

- **Impact of H-DVR on individual harmonics**

From Fig.4.15, it is shown that without H-DVR, in the test system, the maximum 5^{th}, 7^{th}, 11^{th}, 13^{th}, 17^{th} and 19^{th} voltage harmonic magnitudes are found to be 5.013%, 5.011%, 5.01%, 4.995%, 4.987% and 4.981% respectively. Fig.4.15 also shows that with the installation of two H-DVR on their optimal locations, the maximum 5^{th} harmonic in IEEE123 node test system is found to be 2.98%, which is within limit and accordingly, the higher order voltage harmonic magnitudes fall below 3% also.

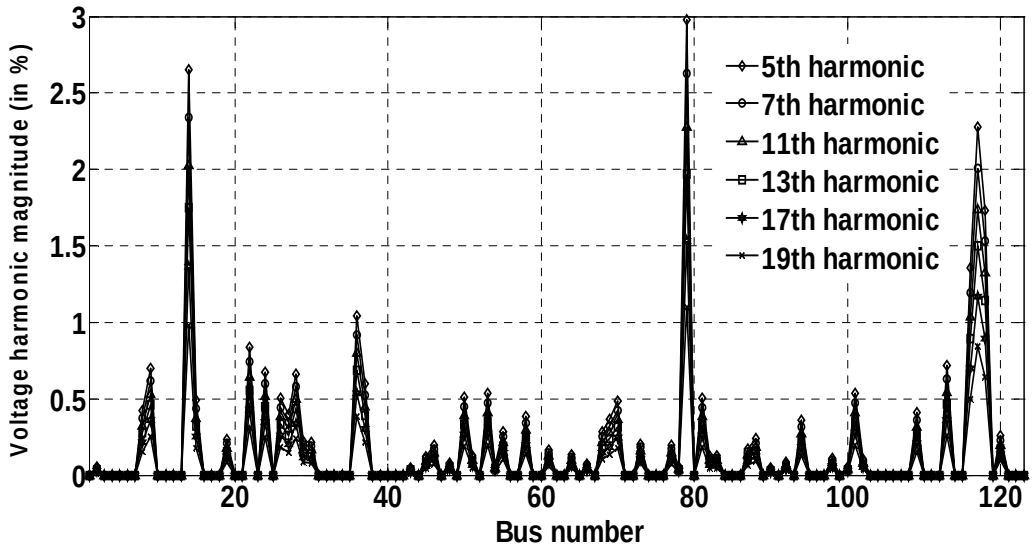

(a)

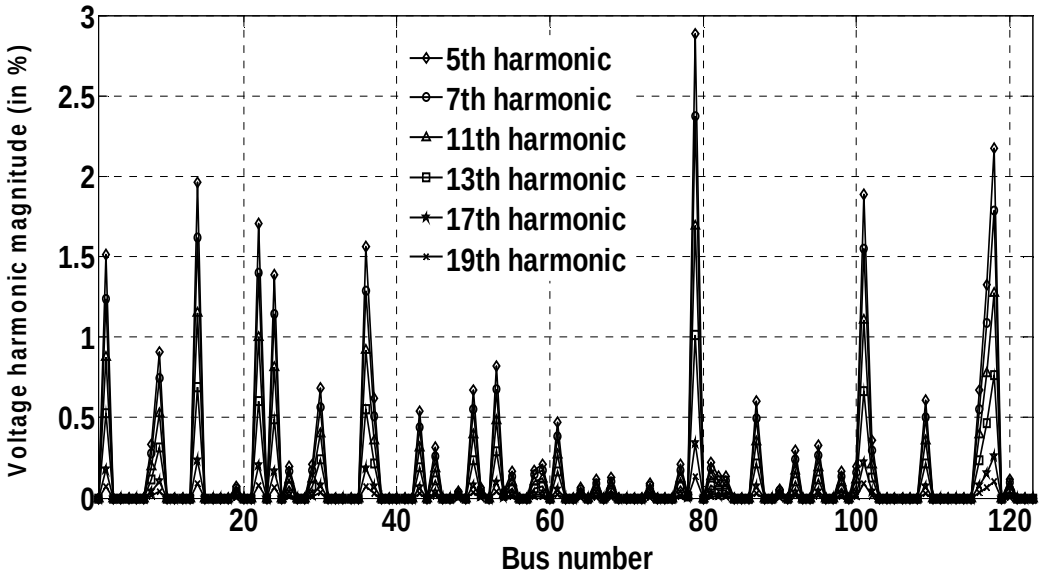

(b)

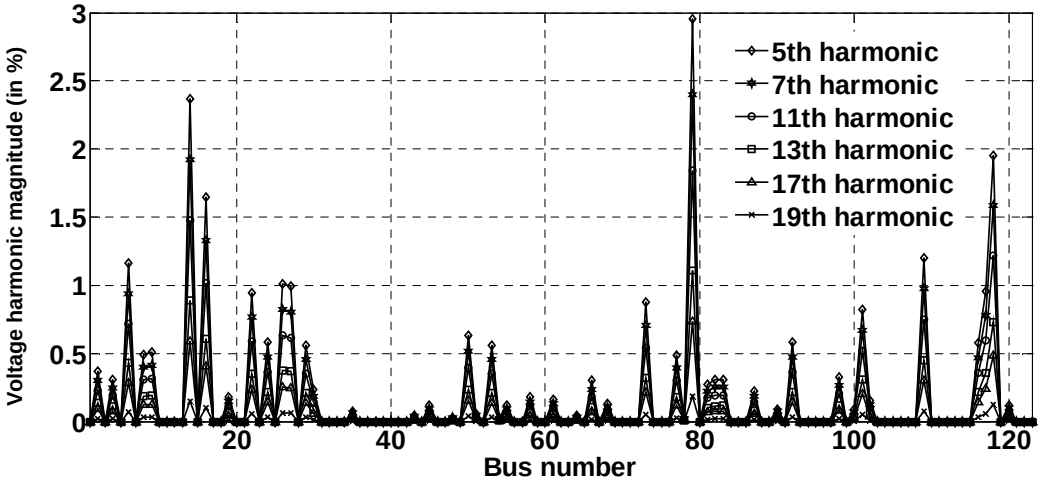

(c)

Fig.4.15. Change in individual harmonics at different buses with optimal installation of 2 H-DVRs in IEEE 123 bus test system, (a) a-phase, (b) b-phase, (c) c-phase

- **Effect of H-DVR on voltage unbalance**

The variation of bus voltage unbalances with respect to the number of H-DVR is shown in Fig.4.16. From Fig.4.16, it is obvious that without any H-DVR in the test system the maximum voltage unbalance is 4.34% and with the addition of single H-DVR at its optimal location it falls to 3.03%. With the installation of second H-DVR in the test system, the maximum voltage unbalance reaches to 1.95% and it is within limit.

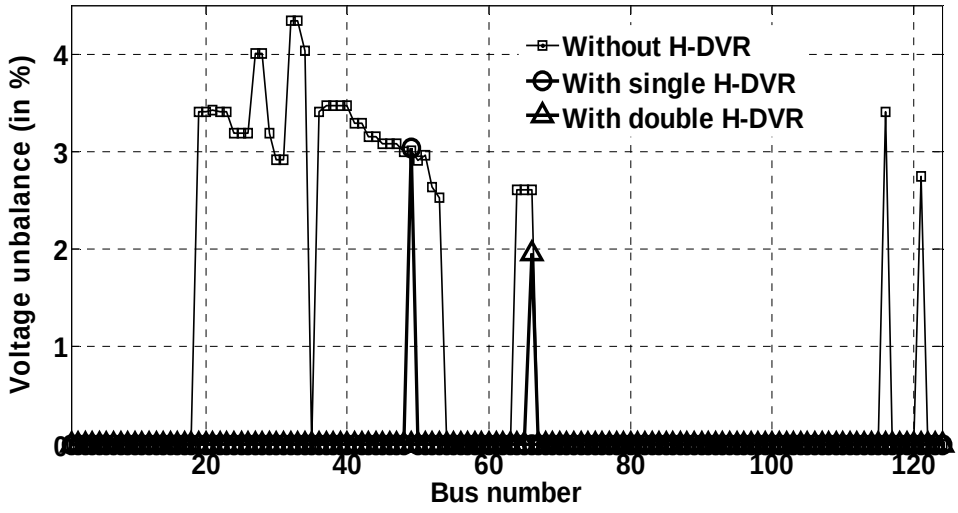

Fig.4.16. Effect of H-DVRs on variation of three phase bus voltage unbalance of IEEE123 bus test system

- **Influence of H-DVR on real power loss, load disturbance and cost savings for 30% non-linear load**

From Table 4.5, it is shown that the addition of single H-DVR in the faulty system reduces the real power loss from 2,822 kW to 1130 kW and load disturbed from 282.215 MVA to 83.241 MVA. Besides, with the installation of second H-DVR at its optimal location, the real power loss is changed from 1130 kW to 966 kW and the load disturbed is changed from 83.241MVA to 0 MVA. The addition of these real power loss and load disturbance reductions ultimately result in cost savings of 50.25% and 95.035% in the former and latter cases of H-DVR installation respectively.

Table4.5. Optimal location of H-DVR, loss, cost, savings, sag and size with load disturbance of 0.85 p.u.

Control Variables	Without compensating device	With single H-DVR	With double H-DVR
Optimal location of compensating device (line number)	-	72-76	72-76, 44-47
Total Cost (in billion $)	10187	5067.6	505.8
Savings (in %)	-	50.25	95.035
Loss(in kW)	2,822	1130	966
Load disturbance, MVA	282.215	83.241	0
Compensating device size (in kVAr)	-	500	200

The optimal number of H-DVR is found to be two and their optimal locations are the distribution line connected between buses 72-76 and 44-47 respectively. The installation of single and double H-DVR results in operating costs of 5067.6 and 505.8 billion $ respectively. The variation of load disturbance and cost savings with the increase in H-DVR number are shown graphically in Fig.4.17 and Fig.4.18 respectively for IEEE123 node test system.

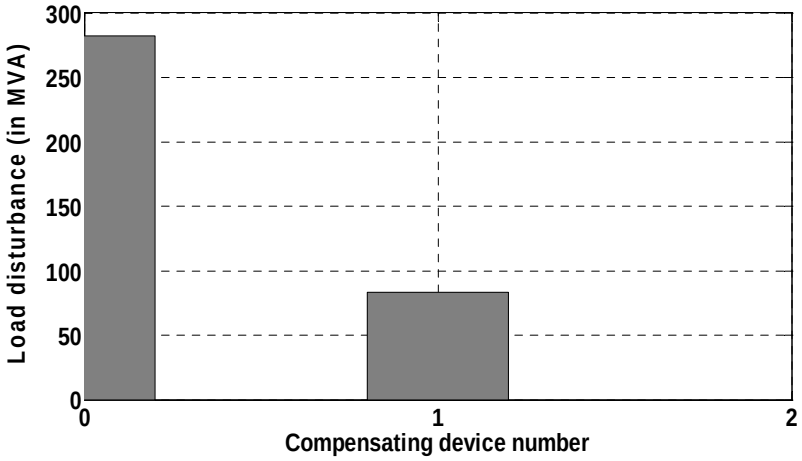

Fig.4.17. Effect of H-DVRs on Change in load disturbance

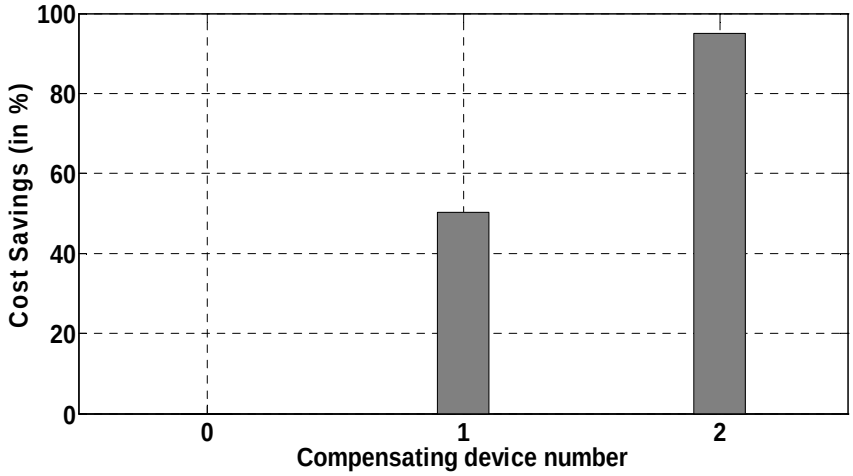

Fig.4.18. Change in cost savings with the change in H-DVR number in IEEE 123 bus test system

- **Effect of H-DVR on voltage sag**

The result corresponding to voltage variation of IEEE123 node test system is shown in Fig.4.19, while considering the worst case of voltage sag. From Fig.4.19, it is found that a-phase voltage magnitude at bus 67 falls from 0.9991 p.u. to 0.6999 p.u at t=1.71 sec and it increases again to 0.999 p.u at t=1.8 sec while a-phase fault occurs on line (1-7). But during this sag condition, the single H-DVR installation at its optimal location of IEEE123 bus test system helps to improve the bus voltage magnitude to 0.9811 p.u., which is above the threshold voltage. In addition, there is a small improvement from 0.9811 p.u. to 0.985 p.u, when another one H-DVR is installed on its optimal location in the test system.

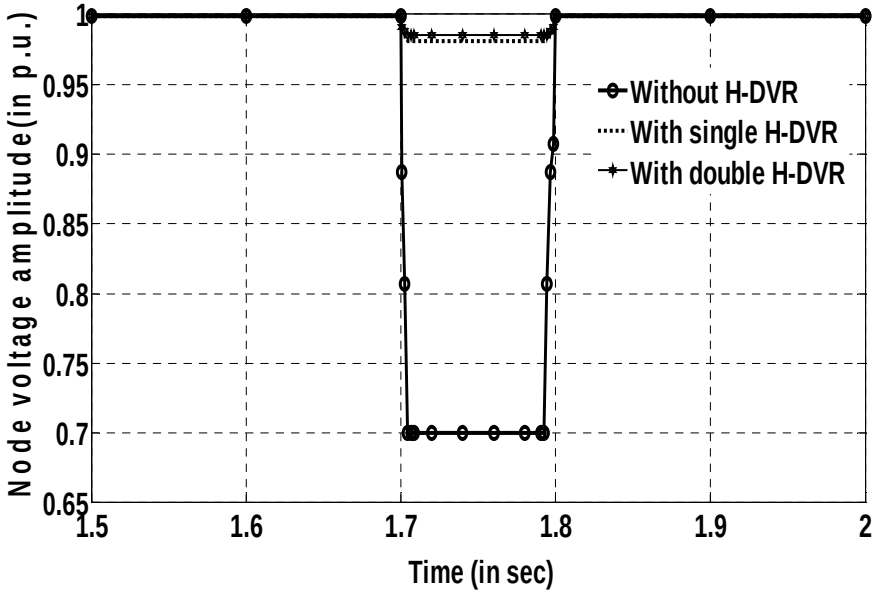

Fig.4.19. Change in sag voltage amplitude at bus 67 with the change in H-DVR number for IEEE123 bus test system

- **Comparative analysis on the performance of different optimization techniques in H-DVR placement problem**

The parameters used for different soft computing techniques are same as reported in Table 4.3. However, the application of different soft computing techniques mentioned in this chapter give almost similar results for 30% non-linear load also, as furnished in Table:4.6. But Fig.4.20 proves the better convergence characteristic of COA among the four different soft computing techniques mentioned in this chapter.

Table 4.6. Comparative results of different methods for optimal installation of H-DVR problem in IEEE123 bus test system

Number of H-DVR	Control Variables	COA	GSA	ABC	DE
1	Optimal location of H-DVR (line number)	72-76	72-76	72-76	72-76
	Total cost (in million $)	5067.6	5067.6	5067.6	5067.6
	Savings (in %)	50.25	50.25	50.25	50.25
	Loss(in kW)	1130	1130	1130	1130
	Load disturbance, MVA	83.241	83.241	83.241	83.241
2	Optimal location of H-DVR (line number)	72-76, 44-47	72-76, 44-47	72-76, 44-47	72-76, 44-47
	Total cost (in million $)	505.8	505.8	505.8	505.8
	Savings (in %)	95.035	95.035	95.035	95.035
	Loss(in kW)	966	966	966	966
	Load disturbance, MVA	0	0	0	0

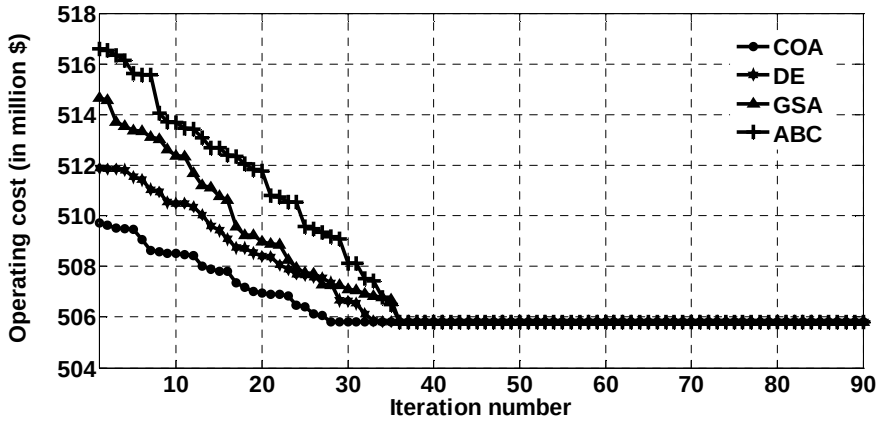

Fig.4.20. Cost optimization with installation of two H-DVR in IEEE 123 bus test system

Fig.4.21 illustrates that optimal placement of H-DVR in IEEE123 node radial test system removes the fault within 6 cycles. This phenomena ultimately results in better voltage profile and satisfies the CBEMA curve [78].

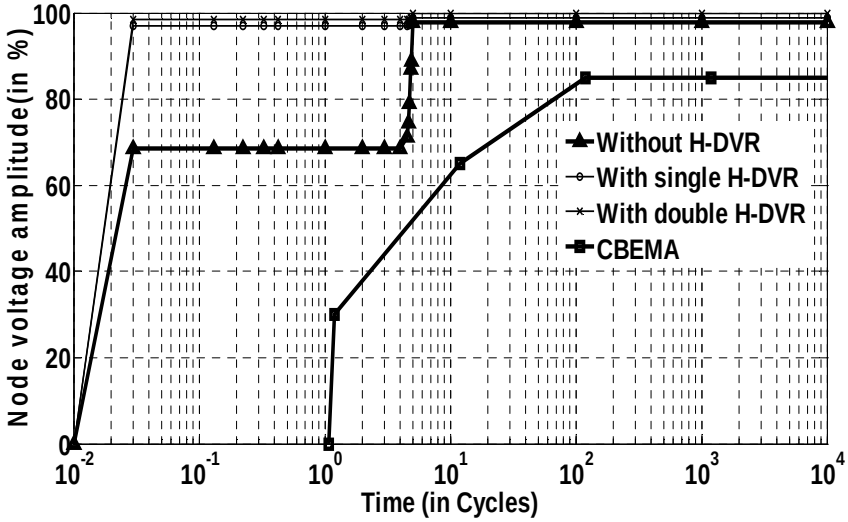

Fig.4.21. Sensitivity range of equipment with voltage sag in IEEE123 bus test system at bus 67

Both the optimization and circuit simulation have been executed in MATLAB 7.8 and performed on an Intel I Core i5 CPU with 2.67 GHz and 4.00 GB memory

4.6. Conclusion

In this chapter the H-DVR placement problem in distribution system has been solved. H-DVR placement is a very complex problem requiring transient simulation along with an optimization technique. To analyze the performance of H-DVR, different cases of H-DVR placement have been studied on a IEEE123 node test feeder system. It is found that the installation of H-DVRs in their optimal locations in the test systems result in

- Improvement in bus voltage during fault resulting in a reduction of load disturbance.
- Individual and total harmonic distortions are reduced.
- Reduction in voltage unbalance.
- Reduction in real power loss resulting in increased cost savings.
- Faster removal of fault satisfies the CBEMA requirements.

The use of H-DVR in the test systems are compared with the use of DVR and investigated by COA, DE, GSA and ABC techniques. Same results found by different techniques prove COA's suitability in this application. The comparative analysis of H-DVR and DVR shows the acceptability of H-DVR in the power system.

Chapter-5:

Improved Power System Observability through Optimal Placement of PMU and PFM

Summary: *This chapter proposes a new technique for optimal placement of phasor measurement unit (PMU) and power flow measurement (PFM) device so that the power system network remains observable. The proposed method integrates the effect of contingency due to single PMU outage into the optimal PMU and PFM allocation strategy to obtain the fully observable power system under contingency also. In addition, zero injection bus has also taken into account for further reduction in number of required PMU and PFM devices in the proposed technique. Finally, a heuristic technique, cuckoo optimization algorithm (COA) is applied for optimal installation of monitoring devices. At last, 7-bus test system, IEEE-14, 57 and 118 bus test systems and a real power system are employed to prove the acceptability of the proposed method. The results got by the proposed technique are compared with those found in literature to prove the efficiency and effectiveness of present method.*

5.1. Introduction

Phasor measurement unit (PMU) makes the power system observable through synchronized measurements of voltage and current phasors through a global positioning system (GPS) [90]. PMU installed at a bus records the reading of voltage phasor at that bus and current phasors at all buses incident at that bus. A bus becomes observable when its voltage is known and for an observable power system all the buses must have to be observable. In fact, PMU may serve several purposes such as state estimation, protection and control in power systems [91]. But it is very essential to place PMUs optimally so as to ensure observability and economy of operation.

The PMU placement problem has been reported in open literature. A dual search algorithm based on simulated annealing technique to find minimal PMU placement is studied in [91]. Tree search placement technique depending upon concept of graph theory for PMU allocation problem is presented in [92]. An integer linear programming method for optimal PMU placement problem solution by multistage scheduling is furnished in [93]. Generalized integer linear programming technique based on incidence matrix concept is studied in [94, 95] to get optimal position of PMU. Immunity genetic algorithm to solve optimal PMU placement problem is studied in [96]. A multi criteria decision making approach based on Jaccobian matrix concept is established in [97] by integer linear programming technique. Recursive tabu search method to find optimal allocation along with optimal number of PMUs are found in [98]. The consideration of zero injection model, reported in [92] reduces the optimal number of PMU in observable power system. Besides, the implementation of power flow measurement (PFM) in [99], gives further reduction in optimal number of PMU to get fully observable power system network. In addition to the normal operating condition, few researchers have studied the observability of the network during contingency also. These contingencies may occur in the transmission network due to branch outage [100-101], PMU loss [101-102] etc, which affect the monitoring system in the power system network. So, to improve the observability of the affected network, contingency constraint has also been incorporated in OPP problem [103]. [92] has established the observability of power system during PMU outage by ILP method. The unobservability in the fully observable network arising due to measurements loss or branch outages during fault condition is of great concern and state estimation method based binary integer programming technique is furnished in [100] to solve OPP having this problem. In [101] the contingency due to PMU loss has been considered and to solve OPP associated with this problem Local Redundancy (LR) method is implemented. The contingency due to single PMU failure or due to single branch outage have been modelled with the OPP problem and solved by mixed-integer linear programming technique in [102].

This chapter proposes an optimization technique of PMU allocation by considering following issues:-

- Modeling of zero injection busses
- Single PMU loss

The author proposes sequential reduction of unobservable buses connected with more than one unobservable bus by PMU and rest of the unobservable buses to be observed by PFM during normal working condition. Further, the double observability procedure of the healthy power system network has been proposed in this chapter to incorporate the contingency arising from single PMU outage. This chapter proposes an optimization technique for both PMU and PFM placement to get a fully observable system. A heuristic method based on Cuckoo Optimization Algorithm (COA) [56] is proposed to find optimal number and position of PMU and flow measurement devices. The proposed algorithm has been tested on several test power systems and some of the results are produced.

The present chapter is arranged as follows. Section 5.2 covers problem formulation by considering both normal condition and contingency. Section 5.3 deals with COA based proposed solution technique. In section 5.4 the authors present different case studies involving 7-bus system, IEEE 14, 57 and 118 bus test system. Section 5.5 compares the proposed technique with other techniques found in open literature to establish the robustness of the proposed solution and section 5.6 concludes the chapter.

5.2. Problem formulation

Phasors are fundamental tools by which the power system van be analyzed under both steady state as well as different transient conditions. In this case PMU with synchronized signals from GPS are matured tools Application of PMU include frequency measurement, instability prediction, adaptive relaying and improved control. But it is not economical to install a PMU at each bus of the network for having full observability. So, in the present chapter, the author has adopted proper utilization of Power Flow Meter (PFM) also for further reduction of PMU number.

Besides it, a zero-injection bus has neither generation nor load. So, presence of zero injection bus can further reduce number of PMUs required for observability.

This section describes problem formulation under normal condition and under single contingency in sections 5.2.1 and 5.2.2 respectively without zero injection and with zero injection considerations.

5.2.1. Under Normal Condition

1) Individual Objective Function:

In this chapter, the authors have optimized the number of PMU and PFM placed optimally. Thus objective functions included in this problem are given as follows

- Minimization of PMU Number:

It is important to optimize the number and locations of PMU for a power system operating reliably. Without zero injection, the objective function is given by,

$$F_1 = \sum_{i=1}^{b} PMU\left(Ob_i\right) \tag{5.1}$$

Subject to equality constraint given as,

$$\sum_{i=1}^{b} Ob_i = 0 \tag{5.2}$$

- Minimization of PFM Number

In advanced power system PFM plays an important role to substitute PMU and thereby it is important to optimize PFM number. In case of power flow meter (PFM) number the objective function is given by,

$$F_2 = \sum_{m=1}^{l} PFM\left(Ob_m\right) \tag{5.3}$$

Subject to equality constraint expressed as,

$$\sum_{m=1}^{l} Ob_m = 0 \tag{5.4}$$

$$\sum_{m=1}^{l} I_m\left(i\right) = 0 \tag{5.5}$$

Ob_i = Observability of bus i

Where, =1, if i is not observable (5.6)

=0, if i is observable

Ob_m = Observability of line m

=1, if m is not observable (5.7)

=0, if m is observable

b and l are the total number of buses and total number of lines in the network. $I_m(i)$ is the current flowing through m^{th} line connected with i^{th} bus.

The driving equations of PFM required for observability are as,

$$P_{ij} + jQ_{ij} = V_i \times I_{ij}^* \tag{5.8}$$

and $V_j = V_i - I_{ij} Z_{ij}$ (5.9)

where, P_{ij}, Q_{ij}, I_{ij} and Z_{ij} are active power, reactive power, current and line impedances of the line connected between buses i and j respectively. V_i is the voltage read by PMU and V_j is the calculated voltage from equation (5.9).

2) Overall Objective Function:

To simplify the problem raised here, both the objective functions mentioned in sections (5.2.1) are converted into single multi-objective function and this objective function may be written as summation of equations (5.1) and (5.3), i.e.,

$$\begin{aligned} F &= F_1 + F_2 \\ &= \sum_{i=1}^{b} PMU(Ob_i) + \sum_{m=1}^{l} PFM(Ob_m) \end{aligned} \tag{5.10}$$

For zero-injection, if n number of buses among b number of total buses have no load or generator connected with them, then the objective function written in equation (5.10), can be modified as,

$$F = \sum_{i=1}^{b-n} \left(PMU(Ob_i) + \sum_{m=1}^{l} PFM(Ob_m(i)) \right) \tag{5.11}$$

Subject to equality constraints given as,

$$\sum_{i=1}^{b-m} Ob_i = 0 \tag{5.12}$$

$$\sum_{m=1}^{l} Ob_m(i) = 0 \tag{5.13}$$

5.2.2. Under Contingencies Considering Single PMU Loss

In a network, if single PMU outage occurs, then to obtain observable network, each bus should be monitored by two different set of PMU and PFM. The objective function will be same as equations (5.10) and (5.11) under zero-injectionless and zero-injection conditions respectively. But the values of the observabilities given in equations (5.6) and (5.7) will be modified as,

Ob_i = Observability of bus i
=2, if i is not observable
=1, if i is observable by one set of PMU and PFM
=0, if i is observable by two different set of PMU and PFM (5.14)

Ob_m = Observability of line m
=2, if m is not observable
=1, if m is observable by one set of PMU and PFM
=0, if m is observable by two different set of PMU and PFM (5.15)

In case of loss of a PMU each bus will be observable by at least one PMU and PFM.

5.3. Proposed solution techniques

The simultaneous PMU and PFM placement problem solution under both normal and contingency situations results in full observability of the respective network. The solution of this multi-dimentional single objective function is not very easy by using conventional optimization techniques and that's why soft computing techniques are required. Cuckoo Search technique [56] has been adopted to get the solutions of the problems. To achieve the optimal solution, optimization technique is examined in MATLAB.

For example, a 5-bus transmission system with 7 branches is given in Fig.5.1.

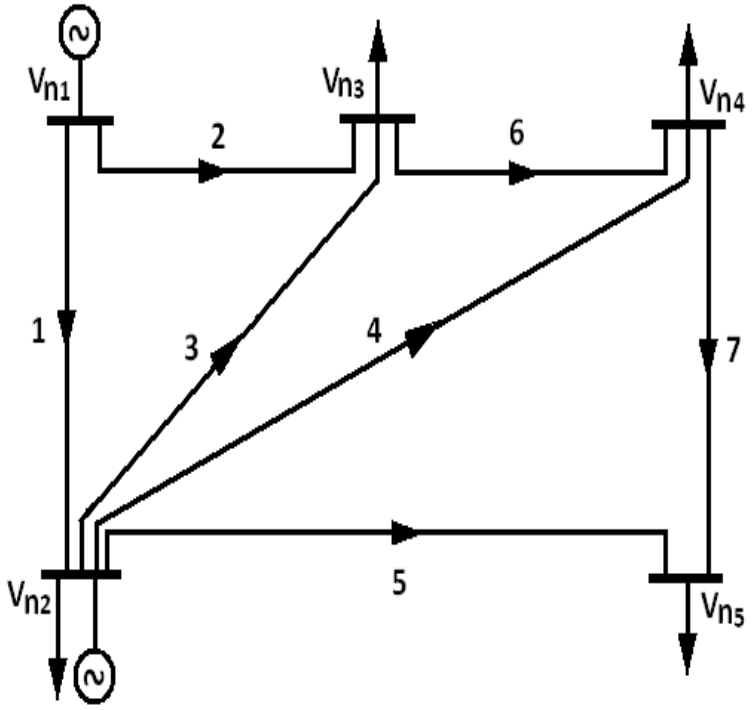

Fig. 5.1. Five-bus power system example

From Fig.5.1, the branch voltages may be expressed by node voltages as follows:

For branch 1: $V_1 = V_{n_1} - V_{n_2}$

For branch 2: $V_2 = V_{n_1} - V_{n_3}$

For branch 3: $V_3 = V_{n_2} - V_{n_3}$

For branch 4: $V_4 = V_{n_2} - V_{n_4}$

For branch 5: $V_5 = V_{n_2} - V_{n_5}$

For branch 6: $V_6 = V_{n_3} - V_{n_4}$

For branch 7: $V_7 = V_{n_4} - V_{n_5}$

Summarizing, the branch voltages may be represented in matrix form by equations (5.16) and (5.17).

$$\begin{bmatrix} 1 & -1 & 0 & 0 & 0 \\ 1 & 0 & -1 & 0 & 0 \\ 0 & 1 & -1 & 0 & 0 \\ 0 & 1 & 0 & -1 & 0 \\ 0 & 1 & 0 & 0 & -1 \\ 0 & 0 & 1 & -1 & 0 \\ 0 & 0 & 0 & 1 & -1 \end{bmatrix} \begin{bmatrix} V_{n_1} \\ V_{n_2} \\ V_{n_3} \\ V_{n_4} \\ V_{n_5} \end{bmatrix} = \begin{bmatrix} V_1 \\ V_2 \\ V_3 \\ V_4 \\ V_5 \\ V_6 \\ V_7 \end{bmatrix} \quad (5.16)$$

Or, $[A]^T [V_n] = [V_b]$ (5.17)

where, $[A]$ =Incidence matrix

$[V_n]$ = Node voltage vector

$[V_b]$ = Branch voltage vector

From incidence matrix, the connectivity of each bus with other buses is shown in Table 5.1.

Table5.1. Connectivity of 5 bus test system

Bus	Connected bus	Number of connectivity
1	1, 2, 3	3
2	1,2,3,4, 5	5
3	1, 2,3,4	4
4	2, 3,4,5	4
5	2,4,5	3

Brief description of COA is given in Appendix A.2 and procedural steps for the solution of the problem is given in following section.

5.3.1. Implementation of COA

Based on the purpose of this work, this section presents a simple PMU and PFM placement strategy such that full observability can be achieved. Optimal PMU and PFM placement proceeds with four different conditions:

- Under healthy condition and without zero injection
- Under healthy condition and with zero injection
- Under single contingency and without zero injection
- Under single contingency and with zero injection

The flow-chart shown in Fig.5.2 gives the optimal positions and numbers of primary set of PMU and PFM by considering healthy conditions with zero injection and without zero injection. To satisfy single contingency with zero injection and without zero injection conditions by equations (2.14) and (2.15), the entire procedure shown in Fig.5.2 is repeated to obtain backup set of monitoring devices. If any similarity is found between the position of primary PMU and backup PMU, then the procedure is repeated to get distinct locations of primary and backup PMUs. If primary and backup locations of PFM match with each other, then only one PFM is required instead of two. Thus double observable system is found in normal condition, which in turn, becomes a single observable system during contingency arising from single PMU outage.

From Table 5.1, it is obvious that bus 2 has highest connectivity. So 1st PMU is installed at bus 2. It makes buses 1, 2, 3, 4 and 5 observable. The voltage phasor of bus 2 is directly monitored and the current phasors of the branches incident at PMU bus are monitored, which in turn gives voltages of other buses by equation (5.10). Thus single observability of the system is found. This test system has no zero-injection bus. Table 5.1 also shows that among the remaining, buses 3 and 4 have next maximum connectivity. So, to get double observable system the backup PMU has to be installed either at bus 3 or at bus 4. It is found that if PMU

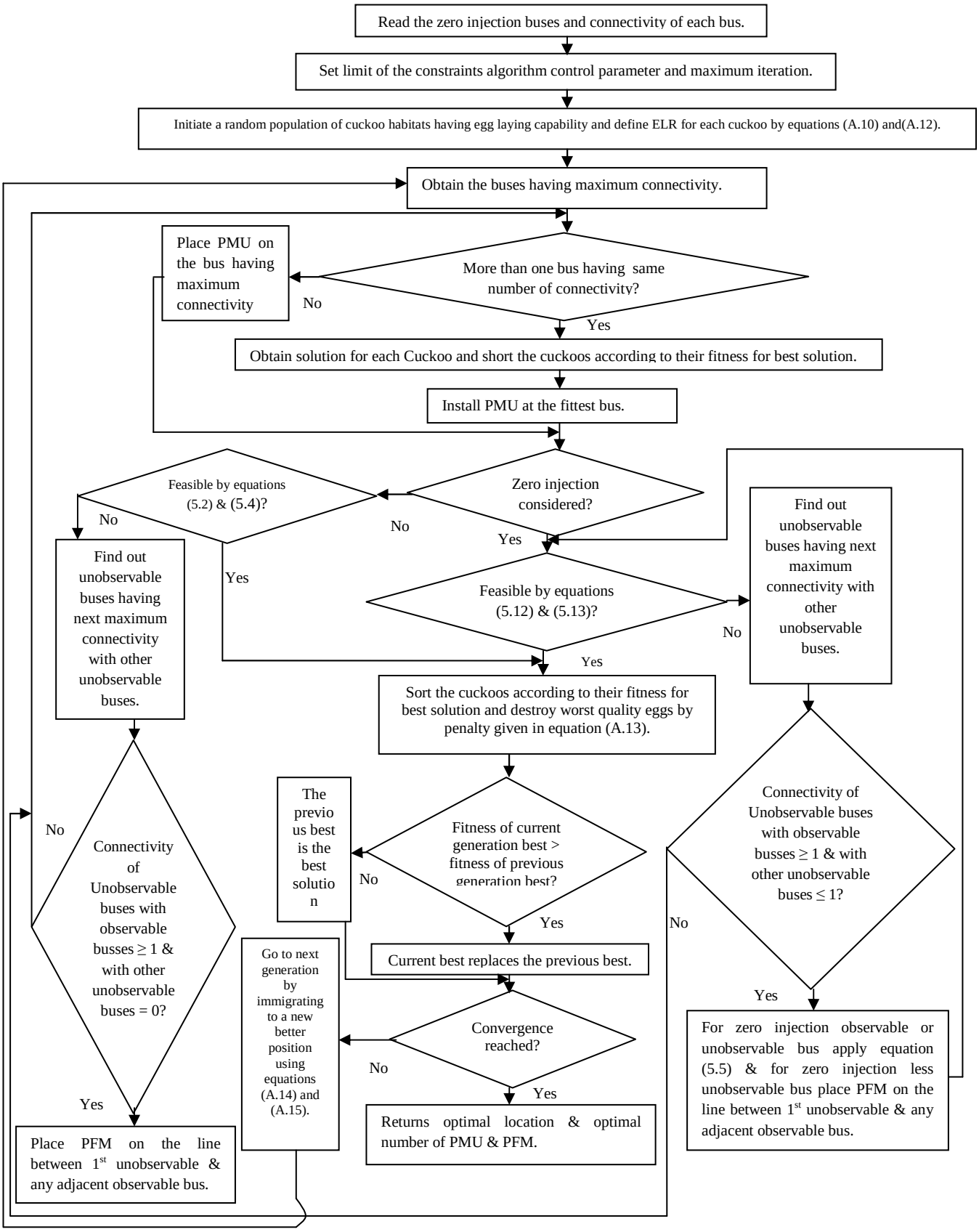

Fig.5.2. Flow chart of PMU and PFM installation by COA during healthy condition

is installed at bus 3, it makes buses 1, 2, 3 and 4 observable. Then bus 5 will be observable by installing a PFM on the line joining buses 2 and 5 or on the line between buses 4 and 5. Thus the system will be double observable under normal condition and single observable under contingency due to single PMU loss.

5.4. Applications and results

The proposed method is examined on four test systems, namely 7-bus, IEEE-14, 57 and 118 bus systems. For each system, results are reported under three conditions:

- Without zero-injection bus consideration and under healthy condition.
- With zero-injection bus consideration and under healthy condition.
- With zero-injection bus consideration and under contingency due to single PMU outage.

The zero-injection buses for test systems (from [99]) are given in the following:

7-bus system: {no zero injection bus}

IEEE 14 bus :{ 7}

IEEE 57 bus: {4, 7, 11, 21, 22, 24, 26, 34, 36, 37, 39, 40, 45, 46, 48}

IEEE 118 bus: {5, 9, 30, 37, 38, 63, 64, 68, 71, 81}

Case: 1 Without zero-injection and under healthy condition

Under this condition, the optimal allocations of PMU and PFM along with their respective number on different test systems are given in table 5.2.

From Table 5.2, the optimal PMU number required for 7-bus test system, IEEE-14, IEEE-57 and IEEE-118 bus test system are 1, 2, 14 and 24 respectively, while the optimal number of PFM required for those test systems are 2, 4, 6 and 12 respectively to get complete observable test system.

Table5.2. Joint placement of PMU and PFM under healthy condition and without zero injection

System	PMU number	PMU location (bus)	PFM number	PFM location (line)
7 bus	1	2	2	4-7, 4-5
IEEE-14	2	4,13	4	1-2,7-8,10-11,13-14
IEEE-57	14	1, 4, 9, 20, 28, 30, 32, 36, 41, 44, 46, 50, 53, 56	6	6-7,21-22,23-24,26-27,37-39,47-48
IEEE-118	24	5, 9, 12, 17, 20, 23, 28, 34, 37, 45, 49, 51, 59, 61, 68, 71, 75, 77, 80, 85, 92, 100, 105, 110	12	1-2, 13-15, 26-30, 41-42, 53-54, 56-57, 66-67, 86-87, 90-91, 95-96, 114-32, 115-27

Case: 2 With zero-injection and under healthy condition

Under this condition, optimal number of PMU and PFM are placed at their respective optimal locations of different test systems, as shown in table 5.3.

Table5.3. Joint placement of PMU and PFM under healthy condition and with zero injection

System	PMU number	PMU location (bus)	PFM number	PFM location (line)
7 bus	1	2	2	4-7, 4-5
IEEE-14	2	4,13	3	1-2,10-11,13-14
IEEE-57	8	1, 4, 9, 28, 31, 41, 50, 53	12	13-14,18-19,20-21,22-23,25-30,32-33,34-35,38-49,38-44,46-47,54-55,56-57
IEEE-118	13	5, 12, 19, 32, 37, 49, 59, 70, 80, 85, 100, 105, 110	32	1-3, 8-9, 17-30, 20-21, 22-23, 25-26, 27-28, 29-31, 34-43, 44-45, 51-52, 53-54, 61-62, 66-67, 77-78, 82-83, 85-88, 89-90, 91-92, 94-95, 96-97, 27-115, 75-118, 11-13, 35-36, 40-41, 46-47, 56-57, 51-58, 71-72, 92-93, 101-102

From Table 5.2 and 5.3, it is seen that with the consideration of zero-injection busses, the number of PMU required for observability is reduced from 14 to 8 in IEEE 57-bus system and from 24 to 13 in IEEE 118-bus system. But there is no change in the number of PMU for IEEE 14-bus system. In this situation, there are few lines consisting of only one unobservable node in the test network. That's why the number of PFM is increased from 6 to 12 in IEEE 57-bus system and from 12 to 32 in IEEE 118-bus system respectively. But PFM number is reduced from 4 to 3 in case of IEEE 14-bus system. So, by comparing results obtained in Tables 5.2 and 5.3, it is obvious that as PMU number is decreased, PFM number is increased to get full observability.

From the results, it is also seen that as there is no zero-injection bus in case of 7-bus test system, Table 5.2 and 5.3 show the same results.

Case: 3 With zero-injection and under contingency due to single PMU outage

Under this condition, optimal placement of PMU and PFM are shown in table 5.4 on different test systems.

Table5.4. Joint placement of PMU and PFM under contingency and with zero injection

System	PMU number	PMU location (bus)	PFM number	PFM location (line)
7 bus	2	2, 3	4	1-2, 2-7, 4-5, 4-7
IEEE-14	5	2, 4, 6,9, 13	3	1-2,10-11,13-14
IEEE-57	15	1, 4, 6, 9, 12, 13, 24, 28, 31, 41, 50, 51, 53, 54, 56	24	13-14,18-19,20-21,22-23,25-30,32-33,34-35,38-49,38-44,46-47,54-55,56-57, 3-4, 1-15, 46-14, 11-41, 48-49, 39-57, 2-15, 12-16, 12-17, 28-29, 31-32, 52-29
IEEE-118	29	5, 11, 12, 17, 19, 23, 28, 32, 34, 37, 42, 46, 49, 52, 56, 59, 62, 70, 71, 77, 80, 84, 85, 92, 96, 100, 103, 105, 110	60	1-3, 8-9, 17-30, 20-21, 22-23, 25-26, 27-28, 29-31, 34-43, 44-45, 51-52, 53-54, 61-62, 66-67, 77-78, 82-83, 85-88, 89-90, 91-92, 94-95, 96-97, 27-115, 75-118, 11-13, 35-36, 40-41, 46-47, 56-57, 51-58, 71-72, 92-93, 101-102, 2-12, 19-20, 21-22, 85-86, 86-87, 105-106, 105-107, 105-108, 109-110, 32-114, 7-12, 14-15, 33-37, 39-40, 50-57, 74-75, 78-79, 98-100, 80-99, 110-11, 110-112, 12-117, 3-5, 8-30, 37-38, 63-59, 80-81, 68-116

Comparing the results furnished in Table 5.3 and 5.4, it is seen that the PMU number required for double observability during healthy condition and to meet single PMU loss, is increased from 1 to 2 in 7-bus test system, from 2 to 5 in IEEE 14-bus system, from 8 to 15 in IEEE 57-bus system and from 13 to 29 in IEEE 118-bus system respectively. It can be noted that the number of PMUs required for double observability is roughly doubled of that in single observability.

Besides, the required PFM number is increased from 2 to 4 in 7-bus system, from 12 to 24 in IEEE 57-bus system and from 32 to 60 in IEEE 118-bus system respectively, i. e., PFM numbers is also almost doubled in these systems. But there is no change in the PFM number in case of IEEE 14-bus system.

5.5. Comparative analysis of different technique

Table 5.5 and 5.6 show the comparative results on different test systems under normal and contingency conditions respectively.

From Table 5.5, the PMU placement results are same as those found by ILP method reported in [99]. On the other hand, there is a small reduction in PFM number from 14 [99] to 12 (in proposed method) and from 3 [99] to 2 (in proposed method) for IEEE 57-bus system and 7-bus test system respectively. But there is no change in PFM number for IEEE 14 and 118-bus systems.

These comparative results found in Table 5.5 agree with earlier results reported in [99], thus validating the proposed method.

Table 5.6 shows the comparative results obtained by LR method reported in [101] and the results found by the proposed method. In case of LR method zero-injection bus consideration is not done while it is incorporated in the present work.

Table5.5. With zero injection and normal condition

System	PMU number		PFM number	
	ILP method	Proposed method	ILP method	Proposed method
7 bus	1	1	3	2
IEEE-14	2	2	3	3
IEEE-57	8	8	14	12
IEEE-118	13	13	32	32

Table 5.6 shows that the required number of PMUs for observable system during contingency is reduced from 9 to 5 in IEEE 14, from 25 to 15 in IEEE 57, from 61 to 29 in IEEE 118 and from 5 to 2 in 7-bus system respectively. These results conclude that the optimal presence of PFM reduces the required PMU number to

almost half in case of proposed technique compare to LR method. So, it is obvious that present optimization strategy has a better suitability in handling contingency problem arising from single PMU loss.

Table5.6. Under contingency due to single PMU loss

System	PMU number		PFM number	
	LR method (without zero-injection)	Proposed method (with zero-injection)	LR method (without zero-injection)	Proposed method (with zero-injection)
7 bus	5	2	-	4
IEEE-14	9	5	-	3
IEEE-57	25	15	-	24
IEEE-118	61	29	-	60

5.6. Conclusion

In this chapter the joint optimal placement of PMU and PFM problem has been solved during healthy condition and contingency due to single PMU outage. To analyze the performance of the proposed technique, different cases of PMU and PFM placement have been studied on 7-bus, IEEE 14, IEEE57 and IEEE 118-bus systems respectively. To apply the formulation on large system, heuristic method COA is used to solve the optimization problem. The following observations may be made:

- With the consideration of zero-injection busses the optimal PMU number is decreased and PFM number is increased to get full observable system during normal working condition.
- With the consideration of contingency and zero-injection buses, required PMU and PFM number are doubled compared to that of healthy condition. These results assure the double observability of each bus in a test system during normal condition.

The influence of the proposed technique for the test systems is investigated by COA. By comparing these results with those found by LR method, COA gives a better results and hence COA proves its suitability in this application.

Chapter 6:
Conclusions

Summary: *This chapter draws the conclusion of the work presented in the thesis. The contribution of the present work along with its outcomes are briefed in this chapter. In addition, this chapter also discusses about the scope of the future work.*

6.1. Brief summary of the work

In the present thesis work, the installation of UPFCs on optimal positions of tested transmission systems improves bus voltage profiles as well as reduces line losses and operational cost of the system. The performance of UPFC devices are tested on IEEE-14 bus test system, IEEE-30 bus test system, IEEE-57 bus test system and NER system. In addition, the optimal sizes of UPFC by considering voltage magnitudes and angles fed by both series and shunt converters of UPFC to the system are also analyzed. For this purpose, GSA method has been chosen as solver of this multi-constrained cost function.

Besides, the voltage sag calculation technique has also been discussed in this thesis work. The sag is mitigated by applying UPQC in the distribution system. Apart from it, the performance of UPQC in terms of reduction of load disturbed area due to fault, harmonic distortions, voltage unbalance, real power loss are also analyzed, which ultimately results in cost savings. In this context, the UPQC sizes as well as UPQC parameters are also taken into consideration for optimal number of UPQC. All the corresponding results are furnished by testing on IEEE123 bus distribution system and 25 bus distribution system. From the results it is also found that the fault is cleared more quickly compared to the system having no FACTS devices.

The authors have added a proposed model of H-DVR in the present thesis work. The performance of this H-DVR is tested on IEEE123 bus radial distribution system and is compared with DVR also. The uniqueness of this H-DVR is also discussed in this research work and the performance of H-DVR is evaluated in terms of reduction of load disturbed area due to fault, voltage sag, harmonic distortions, voltage unbalance, real power loss and cost savings. In addition, H-DVR installation at optimal location in optimal number clears the fault very fast which satisfies the CBEMA curve. Besides, the optimal size of H-DVR is also taken as constraint in this thesis work. Apart from it the performance of H-DVR with variation of percentage of non-linearity in the loads is also produced in the present thesis work.

Apart from it, to get fully observable power system, the addition of PMU in the different test system is also analysed. In this context, the contingency arising in the system due to single PMU outage is also added to objective function. For further reduction of PMU in the test system, PFM is also added in the test network on optimal position. So the cost function is formulated by taking both PMU and PFM constraints. The performance of PMU and PFM together is experimented on 7-bus test system, IEEE-14, 57 and 118 bus test systems and a real power system. The results found in this thesis work is compared with those found by LR method. Though

many heuristic methods can be adopted to solve this multi-dimensional objective function, COA has been adopted here for optimal allocation of UPQC, H-DVR and PMU-PFM in the respective test systems. The results found by GSA/COA in this work have compared with those found by other soft-computing techniques also.

From the results produced in the present thesis work it is obvious that by adopting the technique mentioned here, the customers will also be benefited as well as suppliers. Specially, the modern power industries where stricter electrical power quality is required will be more benefited in the said approach. Besides, integration of power electronics devices connected with the load end in distribution system does not affect very much the voltages at load terminals due to presence of these FACTS devices. In addition, the total operational cost associated with test system is formulated after calculating different parts involved in the operational cost. This simplified single objective cost function will be very easy to understand to both electrical power suppliers and customers.

6.2. Contributions of the present work

The following may be identified as the contributions of the present work:

- Development of the simplified algorithm by using UPFC for transmission line loss reduction and power system cost reduction.
- Development of the method for optimal allocation of different FACTS devices in transmission and distribution system.
- Development of the proposed model of H-DVR and implementation in distribution system.
- Development of economic and cost savings method by using UPQC/H-DVR for reduction in bus voltage harmonics, voltage unbalance, real power loss in distribution system.
- Development of simplified algorithm to identify the fault in distribution system and clearing them within permissible limit cycles.
- Development of method to improve bus voltage profile and thereby reduction in load disturbing area during fault.
- Development of the algorithm to get fully observable power system by using PMU and PFM.

6.3. Shortcomings and scope for further work

While the above contributions have been made, the work reported has certain shortcomings as well as listed below:

- Renewable power generation sources are increasingly being installed at the low voltage network of power system. These sources are mostly intermittent in nature. It is expected that in near future renewable sources will have a considerable share of the total generation capacity. Thus, the uncertainty associated with the renewable sources should be considered while determining the location of the control devices in power system. The present author, however, has not considered this issue while determining the optimum location of the control devices.
- In the present thesis work only the contingency due to single PMU outage has been considered and the results are furnished accordingly. The outcome of multiple contingencies on system observability and reliability should be studied further.
- The proposed method may be implemented on the system having other % of non-linear loads connected in distribution system and the obtained results may be compared with the results furnished in the present work.
- Performance of power system in a Simulation environment having UPFC, UPQC, H-DVR and PMU-PFM installed at optimum locations may be studied further to assess the operation of Power grid as Smart grid.

Appendix

A.1 Overview of Gravitational Search Algorithm

Gravitational Algorithm is a soft computing technique based on Newton's law. This algorithm is based on the Newtonian gravity: In universe, each and every particle attracts every other particle with a force. The motion of the heaviest mass is very small compare to that of lighter mass. Each mass represent the optimization problem solution. The heaviest mass is the optimal solution where as the lighter mass represent the worst solution of the problem In this context, the behavior of Newtonian mass and GSA algorithm are given in sections A.1.1 and A.1.2 respectively.

A.1.1 Behaviour of Newtonian mass

The attractive/repulsive force between any two particles is directly proportional to their masses and inversely proportional to the square of the distance between them". This force equation can be represented as

$$F = G\frac{M_1 M_2}{R^2} \tag{A.1}$$

Where, M_1 and M_2 represent the masses of two agents or objects taken in this thesis work. R is the distance between these two objects. The heavy mass corresponds to good solutions and lighter mass indicates the worst solution. G is the gravitational constant.

According to Newton's second law, the acceleration of a particle when a force is applied to it is dependent only on applied force and particle mass and it can be written as

$$a = \frac{F}{M} \tag{A.2}$$

According to theoretical physics, there are three kind of masses, namely: Active gravitational mass, passive gravitational mass and inertial mass. The active gravitational mass is a measure of the strength of gravitational field due to a particular object. On the other hand, passive gravitational mass is a measure of the strength of object's interaction with the gravitational field. In addition, inertial mass is a measure of an object resistance to changing its state of motion when a force is applied.

By considering the above aspects, in GSA, each mass (agent) has four specifications: position, inertial mass, active gravitational mass, and passive gravitational mass. The position of the mass corresponds to a solution of the problem, and its gravitational and inertial masses are determined using a fitness function. By lapse of time, all the masses will be attracted by the heaviest mass, which is optimal solution in this thesis work. Based on this

law of algorithm along with different mass concept, the procedural steps of GSA algorithm is given in section A.1.2.

A.1.2 Gravitational Search Algorithm (GSA)

In this algorithm, $\boldsymbol{R}$ is used instead of $\boldsymbol{R^2}$, as the authors reported that this case provided better results [18]. Gravitational constant value is proportional to the ratio of the initial time with respect to the actual time, represented as

$$G(t) = G(t_0) \times \left(\frac{t_0}{t} \right)^{\beta} \tag{A.3}$$

Where $G(t_0)$ is the value of the gravitational constant at the initial time, t_0 . $\beta \leq 1$

The procedural steps of the GSA for solving the optimal power system problem can be summarized as follows:

(i) Set gravitational constant $G = G_0 \geq 0$ and the number of agents N .

(ii) Read the dimension n.

(iii) The positions X of agents N are randomly selected from their initialized dimensions by applying equation (A.4) as

$$X_i = \left(x_i^1, \cdots, x_i^d, \cdots x_i^n \right) \text{ for } i = 1, 2, \cdots N \tag{A.4}$$

This in effect means providing the upper limits and the lower limits of the optimization variables.

(iv) Determine the solution vectors.

(v) Check the feasibility of the constraints.

(vi) If the constraint violates it limit, then discard the initial set of agents and go to step (iii) in the next iteration. This process continues until all the constraints are satisfied using equations.

(vii) Decrease the Gravitational constant G by using equation (A.3).

(viii) Evaluate fitness of each object by calculating the gravitational masses (M_{ai}, M_{pi}) and inertial masses (M_{ii}) by using following equations,

$$M_{ai} = M_{pi} = M_{ii} = M_i \text{ for } i = 1, 2, \cdots, N; m_i(t) = \frac{fitness_i(t) - worst(t)}{best(t) - worst(t)}; \; M_i(t) = \frac{m_i(t)}{\sum_{j=1}^{N} m_j(t)} \tag{A.5}$$

(ix) Compute the total force (F) acting on object i in d dimension by using

$$F_i^d(t) = \sum_{j \in kbest, j \neq 1}^{N} rand_j F_{ij}^d(t) \tag{A.6}$$

where, $rand_j$ =random number between 0 and 1. $Kbest$ =set of first K objects with the best fitness value and biggest mass

(x) Evaluate the acceleration a, velocity v and position x of mass i by using equations (A.7-A.9) respectively as

$$a_i^d(t) = \frac{F_i^d}{M_{ii}(t)} \quad \text{(A.7)}$$

$$v_i^d(t+1) = rand_i \times v_i^d(t) + a_I^d \quad \text{(A.8)}$$

$$x_i^d(t+1) = x_i^d(t) + v_i^d(t+1) \quad \text{(A.9)}$$

where, $rand_i$ =random number between 0 and 1

(xi) Check the feasibility of each agent set as a problem solution.

(xii) If the difference between two fittest values of two consecutive iterations is less than a specified tolerance value, or the feasible value does not change for a specified number of iterations, then the optimal solution will be obtained, otherwise the process will be repeated from step (iii).

(xiii) If the current iteration is greater than or equal to the specified maximum iteration, then the iterative process is terminated.

A.2 Overview of Cuckoo Optimization Algorithm

Cuckoo Optimization algorithm is a soft computing technique based on cuckoo's character to lay egg. The mother cuckoo lays her own egg in host bird's nest and flies off with the host egg. Cuckoos carefully mimic the colour and pattern of their own eggs to match with that of their hosts. Each female cuckoo specializes on one particular host species. But many bird species learn to recognize a cuckoo egg dumped in their own nest and either throw out the strange egg or leave the old nest to start a fresh one. So the cuckoo constantly tries to improve its mimicry of its hosts' eggs, while the hosts try to find ways of detecting the cuckoo's egg. In COA each cuckoo's egg determines the optimization problem solution. The behaviour of cuckoos and COA optimization algorithm are described in sections A.2.1 and A.2.2 respectively.

A.2.1 Behaviour of Cuckoos

The principle of COA reported in [56], is based on the breed behavior of cuckoos. In this algorithm, the problem variables formed in an array, is called "habitat" and expressed as

$$habitat = \left[x_1, x_2, \ldots, x_{N_{\text{var}}} \right] \tag{A.10}$$

where, x represents variable values and N_{var} is the total number of variables.

As some of the eggs hatched by all the cuckoos set in habitats are killed by the host birds due to their worst quality, so the cost function is expressed as

$$Cost\left(habitat\right) = f_c\left(x_1, x_2, \ldots, x_{N_{\text{var}}}\right) \tag{A.11}$$

The maximum distance from the habitat at which the cuckoos lay eggs is called "Egg Laying Radius (ELR)" and is expressed as

$$ELR = \alpha \times \frac{\text{Number of current cuckoo's eggs}}{\text{Total number of eggs}} \times \left(Var_{hi} - Var_{low}\right) \tag{A.12}$$

Where, α is an integer, to handle the maximum value of ELR. Var_{hi} and Var_{low} are upper and lower limits of variables respectively.

The $P_a\%$ of all eggs with less profit will be destroyed and it is expressed as,

$$P_a = 0.25 \tag{A.13}$$

After survival, the matured cuckoos immigrate in a new better destination. $\lambda\%$ of total distance toward destination habitat as reported in [56] is expressed as,

$$\lambda \sim \cup(0,1) \tag{A.14}$$

Where, $\cup(0,1)$ means random number uniformly distributed between 0 and 1.

The angular deviation from the distance connecting old and new habitats is represented by,

$$\varnothing \sim \cup(-\omega, \omega) \tag{A.15}$$

Where, $\omega = \pi / 6$ rad.

A.2.2 Cuckoo Optimization Algorithm (COA)

The procedural steps of the COA for solving the optimal power system problem can be summarized as follows:

(i) Set generation, population size, penalty multiplier.

(ii) Set randomly the position of each hatched egg.

(iii) Compute the solution vector corresponding to each egg.

(iv) Check the feasibility of each egg and destroy the poor quality egg by penalty multiplier.

(v) If the cuckoos coming from survived eggs retain in environment then they immigrate to better destination by using equations (A.14-A.15).

(vi) This process continues until the current generation quality is greater than or equal to the previous generation quality.

A.3 Voltage sag calculation

Voltage sag may occur in the system due to occurrence of fault, switching, overload, short circuit and so on. To decide the characteristics of voltage sag, the parameters such as voltage magnitude, duration, unbalance and phase angle jump are to be estimated. Again, these parameters depend upon the location and type of fault in the system. As location and type of fault can not be predicted, a rational approach has to be adopted to take care of the problem. The number and type of faults occurring in any system depends upon many factors of which system design, quality of the devices/apparatus used and their maintenance are some of the important issues. Occurrence of faults also depends upon some external natural events which are neither controllable nor predictable. Thus, predicting the quality of load disturbed due to voltage sag is very difficult. There are several methods in open literature to predict about the type and location of fault. Among them, statistical approach [104-105] has been taken in this section and the remaining voltage at PCC (point of common coupling) has been considered for this purpose. In this section, fault locations are randomly selected to match the statistical figures reported in [104-105]. The estimated values of the load disturbed are dependent upon the selected locations of the faults. In order to overcome the impact of this random selection on the value of the load disturbed, the fault simulation of each sag estimation event is repeated and the average of the estimated load disturbed values are taken. The number of such repetitions of sag estimation is decided by performing experimentation on the test system with repeated trials. The voltage sag at the nodes are calculated by using equations (A.16)-(A.19), as reported in [62].

For three-phase faults (3PF),

$$V_m^{fault} = V_m^{pref} - \frac{Z_{mK}^1}{Z_{KK}^1} V_K^{pref} \tag{A.16}$$

For single line-to-ground faults (SLGF),

$$V_{A,m}^{fault} = V_{A,m}^{pref} - \frac{Z_{mK}^0 + Z_{mK}^1 + Z_{mK}^2}{Z_{KK}^0 + Z_{KK}^1 + Z_{KK}^2} V_K^{pref}$$
$$V_{B,m}^{fault} = \alpha^2 V_{B,m}^{pref} - \frac{Z_{mK}^0 + \alpha^2 Z_{mK}^1 + \alpha Z_{mK}^2}{Z_{KK}^0 + Z_{KK}^1 + Z_{KK}^2} V_K^{pref} \quad \text{(A.17)}$$
$$V_{C,m}^{fault} = \alpha V_{C,m}^{pref} - \frac{Z_{mK}^0 + \alpha Z_{mK}^1 + \alpha^2 Z_{mK}^2}{Z_{KK}^0 + Z_{KK}^1 + Z_{KK}^2} V_K^{pref}$$

For line-to-line faults (LLF),

$$V_{A,m}^{fault} = V_{A,m}^{pref} - \frac{Z_{mK}^1 - Z_{mK}^2}{Z_{KK}^1 + Z_{KK}^2} V_K^{pref}$$
$$V_{B,m}^{fault} = \alpha^2 V_{B,m}^{pref} - \frac{Z_{mK}^1 - \alpha Z_{mK}^2}{Z_{KK}^1 + Z_{KK}^2} V_K^{pref} \quad \text{(A.18)}$$
$$V_{C,m}^{fault} = \alpha V_{C,m}^{pref} - \frac{Z_{mK}^1 - \alpha^2 Z_{mK}^2}{Z_{KK}^1 + Z_{KK}^2} V_K^{pref}$$

For double line-to-ground faults (LLGF)

$$V_{A,m}^{fault} = V_{A,m}^{pref} - \frac{\left[\left(Z_{mK}^1 - Z_{mK}^0\right) Z_{KK}^2 + \left(Z_{mK}^1 - Z_{mK}^2\right) Z_{KK}^0\right]}{Z_{KK}^0 Z_{KK}^1 + Z_{KK}^1 Z_{KK}^2 + Z_{KK}^2 Z_{KK}^0} V_K^{pref}$$
$$V_{B,m}^{fault} = V_{B,m}^{pref} - \frac{\left[\left(\alpha^2 Z_{mK}^1 - Z_{mK}^0\right) Z_{KK}^2 + \left(\alpha^2 Z_{mK}^1 - \alpha Z_{mK}^2\right) Z_{KK}^0\right]}{Z_{KK}^0 Z_{KK}^1 + Z_{KK}^1 Z_{KK}^2 + Z_{KK}^2 Z_{KK}^0} V_K^{pref} \quad \text{(A.19)}$$
$$V_{C,m}^{fault} = V_{C,m}^{pref} - \frac{\left[\left(\alpha Z_{mK}^1 - Z_{mK}^0\right) Z_{KK}^2 + \left(\alpha Z_{mK}^1 - \alpha^2 Z_{mK}^2\right) Z_{KK}^0\right]}{Z_{KK}^0 Z_{KK}^1 + Z_{KK}^1 Z_{KK}^2 + Z_{KK}^2 Z_{KK}^0} V_K^{pref}$$

Where, m and k are the random bus and the fault location on the line. $V_{A,m}^{pref}, V_{B,m}^{pref}$ and $V_{C,m}^{pref}$ are the pre-fault voltages at phase-A, B and C respectively of bus m. $V_{A,m}^{fault}, V_{B,m}^{fault}$ and $V_{C,m}^{fault}$ are the fault voltages at phase-A, B and C respectively of bus m. Z_{mK}^{012}, Z_{KK}^{012} and α represent the sequence transfer impedances corresponding to buses m and k, the sequence driving point impedances at bus k and the complex number operator, e^{j120°.

Thus the sag voltage can be obtained by following procedural steps:

(i) The lengths of all the distribution lines are calculated.

(ii) The time period during which fault occurs is set to a value.

(iii) From Table-A.1 the fault type is determined by satisfying statistical data, as reported in [104-105].

(iv) By using equations (A.16)-(A.19), all the node voltages are determined during fault conditions.

(v) If any node voltage falls below the threshold voltage, then that bus is considered as affected bus and all the disturbed loads connected with that bus is calculated. Otherwise, the bus number is increased by 1 and step (v) is repeated.

(vi) Steps (iv-v) are repeated to accumulate all the individual loads disturbed by respective fault and steps (i-vi) are repeated until the total load disturbance during fault converges.

(vii) At last, total cost of the disturbed loads associated with the faults are obtained.

As load disturbed values can not be predicted previously, so a trial process is done to get load disturbed values, matched with statistical data. It has been found from Fig.A.1that for IEEE-123 node test system the average of the estimated load disturbed values converges at 8^{th} and 7^{th} trial number for IEEE123 node test system [105] and for 25 node test system respectively. After 8^{th} /7^{th} iteration there is no such change in average load curtailment in IEEE123 node test system/25 node test system.

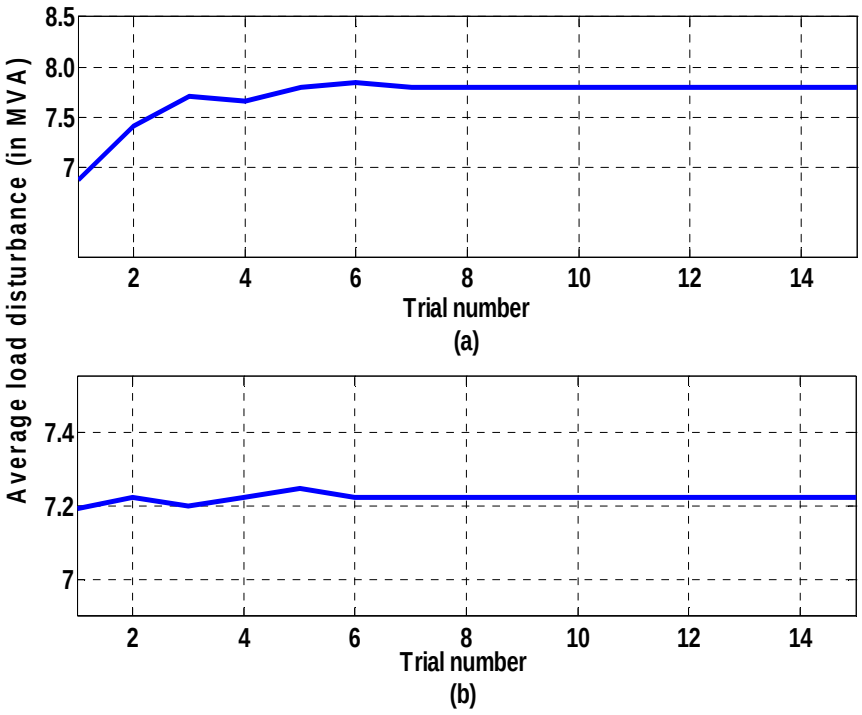

Fig.A.1. Average load disturbance vs. trial number for (a) IEEE123 node test system, (b) 25 node test system

TableA.1. System fault rates

Type of fault	Fault type distribution, %	Bus fault rate, events/year	Average fault rate, events/year	Line fault rate, events/100km/year	Average fault rate, events/100km/year	Exact number of faults
LG	70	3	2.1	25	17.5	39
LLG	17		0.51		4.25	10
LL	7		0.21		1.75	4
LLLG	6		0.18		1.5	3
Total						56

In this thesis work, the fault rate is taken as 25/100 km/year [62]. The total number of faults within these periods is calculated to be 56, as furnished in Table A.1.There are four types of faults, i.e., line-ground (LG), line-line-ground (LLG), line-line (LL), line-line-line-ground (LLLG) and are as 70%:17%:7%:6% times, reported in Table A.1.

A.4 Test System Data

A.4.1 IEEE-14 bus transmission system

Table A.2. Bus data for IEEE 14-bus transmission system

Bus No.	Bus Type	Voltage (P.U)	PL (MW)	QL (MVAR)	PG (MW)	Pgmax (MW)	Pgmin (MW)	QG(MVAR)	Qgmax (MVAR)	Qgmin(MVAR)
1	Swing	1.06	30.38	17.78	40	160	10	-40	0	0
2	PV	1.045	0	0	232	80	20	0	50	-40
3	PV	1.01	131.88	26.6	0	50	20	0	40	0
4	PQ	1	66.92	10	0	0	0	0	0	0
5	PQ	1	10.64	2.24	0	0	0	0	0	0
6	PV	1.07	15.68	10.5	0	0	0	0	24	-6
7	PQ	1	0	0	0	0	0	0	0	0
8	PV	1.009	0	0	0	0	0	0	24	-6
9	PQ	1	41.3	23.24	0	0	0	0	0	0
10	PQ	1	12.6	8.12	0	0	0	0	0	0
11	PQ	1	4.9	2.52	0	0	0	0	0	0
12	PQ	1	8.54	2.24	0	0	0	0	0	0
13	PQ	1	18.9	8.12	0	0	0	0	0	0
14	PQ	1	20.86	7	0	0	0	0	0	0

Table A.3. Line data for IEEE 14-bus transmission system

Line no.	From Bus	To Bus	R (p.u)	X (p.u)	B (p.u)
1	1	2	0.0194	0.0592	0.0264
2	2	3	0.047	0.198	0.0219
3	2	4	0.0581	0.1763	0.0187
4	1	5	0.054	0.223	0.0246
5	2	5	0.057	0.1739	0.017
6	3	4	0.067	0.171	0.0173
7	4	5	0.0134	0.0421	0.0064
8	5	6	0	0.252	0
9	4	7	0	0.2091	0
10	7	8	0	0.1762	0
11	4	9	0	0.5562	0
12	7	9	0	0.11	0
13	9	10	0.0318	0.0845	0
14	6	11	0.095	0.1989	0
15	6	12	0.1229	0.2558	0
16	6	13	0.0662	0.1303	0
17	9	14	0.1271	0.2704	0
18	10	11	0.082	0.1921	0
19	12	13	0.2209	0.1999	0
20	13	14	0.1709	0.348	0

Table A.4. Generator cost data for IEEE 14-bus transmission system

Bus No.	a	b	c
1	0.0252	16	0
2	0.14	14	0
3	0.5	8	0
6	0.0667	26	0
8	0.2	24	0

A.4.2 IEEE-30 bus transmission system

Table A.5. Bus data for IEEE 30-bus transmission system

Bus No.	Bus Type	Voltage (P.U)	PL (MW)	QL (MVAR)	PG (MW)	Pgmax (MW)	Pgmin (MW)	QG (MVAR)	Qgmax (MVAR)	Qgmin (MVAR)
1	Swing	1.1	0	0	0	200	50	0	0	0
2	PV	1.085	21.7	12.7	40	80	20	0	50	-40
3	PQ	1	2.4	1.2	0	0	0	0	0	0
4	PQ	1	7.6	1.6	0	0	0	0	0	0
5	PV	1.052	94.2	19	0	50	15	0	40	-40

Bus No.	Bus Type	Voltage (P.U)	PL (MW)	QL (MVAR)	PG (MW)	Pgmax (MW)	Pgmin (MW)	QG (MVAR)	Qgmax (MVAR)	Qgmin (MVAR)
6	PQ	1	0	0	0	0	0	0	0	0
7	PQ	1	22.8	10.9	0	0	0	0	0	0
8	PV	1.054	30	30	0	35	10	0	40	-10
9	PQ	1	0	0	0	0	0	0	0	0
10	PQ	1	5.8	2	0	0	0	0	0	0
11	PV	1.1	0	0	0	30	10	0	24	-10
12	PQ	1.05	11.2	7.5	0	0	0	0	0	0
13	PV	1.063	0	0	0	40	12	0	24	-6
14	PQ	1	6.2	1.6	0	0	0	0	0	0
15	PQ	1	8.2	2.5	0	0	0	0	0	0
16	PQ	1	3.5	1.8	0	0	0	0	0	0
17	PQ	1	9	5.8	0	0	0	0	0	0
18	PQ	1	3.2	0.9	0	0	0	0	0	0
19	PQ	1	9.5	3.4	0	0	0	0	0	0
20	PQ	1	2.2	0.7	0	0	0	0	0	0
21	PQ	1	17.5	11.2	0	0	0	0	0	0
22	PQ	1	0	0	0	0	0	0	0	0
23	PQ	1	3.2	1.6	0	0	0	0	0	0
24	PQ	1	8.7	6.7	0	0	0	0	0	0
25	PQ	1	0	0	0	0	0	0	0	0
26	PQ	1	3.5	2.3	0	0	0	0	0	0
27	PQ	1	0	0	0	0	0	0	0	0
28	PQ	1	0	0	0	0	0	0	0	0
29	PQ	1	2.4	0.9	0	0	0	0	0	0
30	PQ	1	10.6	1.9	0	0	0	0	0	0

Table A.6. Line data for IEEE 30-bus transmission system

Line no.	From Bus	To Bus	R (p.u)	X (p.u)	B (p.u)
1	1	2	0.0192	0.0575	0.0264
2	1	3	0.0452	0.1852	0.0204
3	2	4	0.057	0.1737	0.0184
4	3	4	0.0132	0.0379	0.0042
5	2	5	0.0472	0.1983	0.0209
6	2	6	0.0581	0.1763	0.0187
7	4	6	0.0119	0.0414	0.0045
8	5	7	0.046	0.116	0.0102
9	6	7	0.0267	0.082	0.0085
10	6	8	0.012	0.042	0.0045

Line no.	From Bus	To Bus	R (p.u)	X (p.u)	B (p.u)
11	6	9	0	0.208	0
12	6	10	0	0.556	0
13	9	11	0	0.208	0
14	9	10	0	0.11	0
15	4	12	0	0.256	0
16	12	13	0	0.14	0
17	12	14	0.1231	0.2559	0
18	12	15	0.0662	0.1304	0
19	12	16	0.0945	0.1987	0
20	14	15	0.221	0.1997	0
21	16	17	0.0824	0.1923	0
22	15	18	0.1073	0.2185	0
23	18	19	0.0639	0.1292	0
24	19	20	0.034	0.068	0
25	10	20	0.0936	0.209	0
26	10	17	0.0324	0.0845	0
27	10	21	0.0348	0.0749	0
28	10	22	0.0727	0.1499	0
29	21	22	0.0116	0.0236	0
30	15	23	0.1	0.202	0
31	22	24	0.115	0.179	0
32	23	24	0.132	0.27	0
33	24	25	0.1885	0.3292	0
34	25	26	0.2544	0.38	0
35	25	27	0.1093	0.2087	0
36	28	27	0	0.396	0
37	27	29	0.2198	0.4153	0
38	27	30	0.3202	0.6027	0
39	29	30	0.2399	0.4533	0
40	8	28	0.0636	0.2	0.0214
41	6	28	0.0169	0.0599	0.065

Table A.7. Generator cost data for IEEE 30-bus transmission system

Bus No.	a	b	c
1	0.0037	2	0
2	0.0175	1.75	0
5	0.0625	1	0
8	0.0083	3.25	0
11	0.025	3	0
13	0.025	3	0

A.4.3 IEEE-57 bus transmission system

Table A.8. Bus data for IEEE 57-bus transmission system

Bus No.	Bus Type	Voltage (P.U)	PL (MW)	QL (MVAR)	PG (MW)	Pgmax (MW)	Pgmin (MW)	QG (MVAR)	Qgmax (MVAR)	Qgmin (MVAR)
1	Swing	1.04	0	17	478	575.88	0	128.9	0	0
2	PV	1.01	21.7	88	0	100	0	-0.8	50	-17
3	PV	0.985	2.4	21	40	140	0	-1	60	-10
4	PQ	1	7.6	0	0	0	0	0	0	0
5	PQ	1	94.2	4	0	0	0	0	0	0
6	PV	0.98	0	2	0	100	0	0.8	25	-8
7	PQ	1	22.8	0	0	0	0	0	0	0
8	PV	1.005	30	22	450	550	0	62.1	200	-140
9	PV	0.98	0	26	0	100	0	2.2	9	-3
10	PQ	1	5.8	2	0	0	0	0	0	0
11	PQ	1	0	0	0	0	0	0	0	0
12	PV	1.015	11.2	24	310	410	0	128.5	155	-50
13	PQ	1	0	2.3	0	0	0	0	0	0
14	PQ	1	6.2	5.3	0	0	0	0	0	0
15	PQ	1	8.2	5	0	0	0	0	0	0
16	PQ	1	3.5	3	0	0	0	0	0	0
17	PQ	1	9	8	0	0	0	0	0	0
18	PQ	1	3.2	9.8	0	0	0	0	0	0
19	PQ	1	9.5	6	0	0	0	0	0	0
20	PQ	1	2.2	1	0	0	0	0	0	0
21	PQ	1	17.5	0	0	0	0	0	0	0
22	PQ	1	0	0	0	0	0	0	0	0
23	PQ	1	3.2	2.1	0	0	0	0	0	0
24	PQ	1	8.7	0	0	0	0	0	0	0
25	PQ	1	0	3.2	0	0	0	0	0	0
26	PQ	1	3.5	0	0	0	0	0	0	0
27	PQ	1	0	0.5	0	0	0	0	0	0
28	PQ	1	0	2.3	0	0	0	0	0	0
29	PQ	1	2.4	2.6	0	0	0	0	0	0
30	PQ	1	10.6	1.8	0	0	0	0	0	0
31	PQ	1	0.058	2.9	0	0	0	0	0	0
32	PQ	1	0.016	0.8	0	0	0	0	0	0
33	PQ	1	0.038	1.9	0	0	0	0	0	0
34	PQ	1	0	0	0	0	0	0	0	0
35	PQ	1	0.06	3	0	0	0	0	0	0

Bus No.	Bus Type	Voltage (P.U)	PL (MW)	QL (MVAR)	PG (MW)	Pgmax (MW)	Pgmin (MW)	QG (MVAR)	Qgmax (MVAR)	Qgmin (MVAR)
36	PQ	1	0	0	0	0	0	0	0	0
37	PQ	1	0	0	0	0	0	0	0	0
38	PQ	1	0.14	7	0	0	0	0	0	0
39	PQ	1	0	0	0	0	0	0	0	0
40	PQ	1	0	0	0	0	0	0	0	0
41	PQ	1	0.063	3	0	0	0	0	0	0
42	PQ	1	0.071	4.4	0	0	0	0	0	0
43	PQ	1	0.02	1	0	0	0	0	0	0
44	PQ	1	0.12	1.8	0	0	0	0	0	0
45	PQ	1	0	0	0	0	0	0	0	0
46	PQ	1	0	0	0	0	0	0	0	0
47	PQ	1	0.297	11.6	0	0	0	0	0	0
48	PQ	1	0	0	0	0	0	0	0	0
49	PQ	1	0.18	8.5	0	0	0	0	0	0
50	PQ	1	0.21	10.5	0	0	0	0	0	0
51	PQ	1	0.18	5.3	0	0	0	0	0	0
52	PQ	1	0.049	2.2	0	0	0	0	0	0
53	PQ	1	0.2	10	0	0	0	0	0	0
54	PQ	1	0.041	1.4	0	0	0	0	0	0
55	PQ	1	0.068	3.4	0	0	0	0	0	0
56	PQ	1	0.076	2.2	0	0	0	0	0	0
57	PQ	1	0.067	2	0	0	0	0	0	0

Table A.9. Line data for IEEE 57-bus transmission system

Line no.	From Bus	To Bus	R (p.u)	X (p.u)	B (p.u)
1	1	2	0.0083	0.028	0.0645
2	2	3	0.0298	0.085	0.0409
3	3	4	0.0112	0.0366	0.019
4	4	5	0.0625	0.132	0.0129
5	4	6	0.043	0.148	0.0174
6	6	7	0.02	0.102	0.0138
7	6	8	0.0339	0.173	0.0235
8	8	9	0.0099	0.0505	0.0274
9	9	10	0.0369	0.1679	0.022
10	9	11	0.0258	0.0848	0.0109
11	9	12	0.0648	0.295	0.0386
12	9	13	0.0481	0.158	0.0203
13	13	14	0.0132	0.0434	0.0055
14	13	15	0.0269	0.0869	0.0115

Line no.	From Bus	To Bus	R (p.u)	X (p.u)	B (p.u)
15	1	15	0.0178	0.091	0.0494
16	1	16	0.0454	0.206	0.0273
17	1	17	0.0238	0.108	0.0143
18	3	15	0.0162	0.053	0.0272
19	4	18	0	0.242	0
20	5	6	0.0302	0.0641	0.0062
21	7	8	0.0139	0.0712	0.0097
22	10	12	0.0277	0.1262	0.0164
23	11	13	0.0223	0.0732	0.0094
24	12	13	0.0178	0.058	0.0302
25	12	16	0.018	0.0813	0.0108
26	12	17	0.0397	0.179	0.0238
27	14	15	0.0171	0.0547	0.0074
28	18	19	0.461	0.685	0
29	19	20	0.283	0.434	0
30	21	20	0	0.7767	0
31	21	22	0.0736	0.117	0
32	22	23	0.0099	0.0152	0
33	23	24	0.166	0.256	0.0042
34	24	25	0	0.603	0
35	24	26	0	0.0473	0
36	26	27	0.165	0.254	0
37	27	28	0.0618	0.0954	0
38	28	29	0.0418	0.0587	0
39	7	29	0	0.0648	0
40	25	30	0.135	0.202	0
41	30	31	0.326	0.497	0
42	31	32	0.507	0.755	0
43	32	33	0.0392	0.036	0
44	34	32	0	0.953	0
45	34	35	0.052	0.078	0.0016
46	35	36	0.043	0.0537	0.0008
47	36	37	0.029	0.0366	0
48	37	38	0.0651	0.1009	0.001
49	37	39	0.0239	0.0379	0
50	36	40	0.03	0.0466	0
51	22	38	0.0192	0.0295	0
52	11	41	0	0.749	0
53	41	42	0.207	0.352	0
54	41	43	0	0.412	0
55	38	44	0.0289	0.0585	0.001
56	15	45	0	0.1042	0

Line no.	From Bus	To Bus	R (p.u)	X (p.u)	B (p.u)
57	14	46	0	0.0735	0
58	46	47	0.023	0.068	0.0016
59	47	48	0.0182	0.0233	0
60	48	49	0.0834	0.129	0.0024
61	49	50	0.0801	0.128	0
62	50	51	0.1386	0.22	0
63	10	51	0	0.0712	0
64	13	49	0	0.191	0
65	29	52	0.1442	0.187	0
66	52	53	0.0762	0.0984	0
67	53	54	0.1878	0.232	0
68	54	55	0.1732	0.2265	0
69	11	43	0	0.153	0
70	44	45	0.0624	0.1242	0.002
71	40	56	0	1.195	0
72	56	41	0.553	0.549	0
73	56	42	0.2125	0.354	0
74	39	57	0	1.355	0
75	57	56	0.174	0.26	0
76	38	49	0.115	0.177	0.003
77	38	48	0.0312	0.0482	0
78	9	55	0	0.1205	0

Table A.10. Generator cost data for IEEE 57-bus transmission system

Bus No.	a	b	c
1	0.01	0.3	0.2
2	0.01	0.3	0.2
3	0.01	0.3	0.2
6	0.01	0.3	0.2
8	0.01	0.3	0.2
9	0.01	0.3	0.2
12	0.01	0.3	0.2

A.4.4 NER transmission system

Table A.11. Bus data for NER transmission system

Bus No.	Bus Type	Voltage (P.U)	PL (MW)	QL (MVAR)	PG (MW)	Pgmax (MW)	Pgmin (MW)	QG (MVAR)	Qgmax (MVAR)	Qgmin (MVAR)	Bus Name
1	PV	0.955	51	27	0	100	0	0	15	-5	%BTPS1
2	PQ	0.971	20	9	0	0	0	0	0	0	%SARSUJAI
3	PQ	0.968	39	10	0	0	0	0	0	0	%KAHELIPARA
4	PV	0.998	39	12	0	100	0	0	300	-300	%CHANDRAPUR
5	PQ	1.002	0	0	0	0	0	0	0	0	%JAGRID
6	PV	0.99	52	22	0	100	0	0	50	-13	%GOURIPUR
7	PQ	0.989	19	2	0	0	0	0	0	0	%GOSSAIGAON
8	PV	1.015	28	0	0	100	0	0	300	-300	%DHALIGAON
9	PQ	1.043	0	0	0	0	0	0	0	0	%JGIGHOPA
10	PV	1.05	0	0	450	550	0	0	200	-147	%RANGIA
11	PQ	0.985	70	23	0	0	0	0	0	0	%ROWTA
12	PV	0.99	47	10	85	185	0	0	120	-35	%AMINGAON
13	PQ	0.968	34	16	0	0	0	0	0	0	%BARANAGAR
14	PQ	0.984	14	1	0	0	0	0	0	0	%TEZPUR
15	PV	0.97	90	30	0	100	0	0	30	-10	%GOHPUR
16	PQ	0.984	25	10	0	0	0	0	0	0	%NORTH LAKHIMPUR
17	PQ	0.995	11	3	0	0	0	0	0	0	%DHEMAJI
18	PV	0.973	60	34	0	100	0	0	50	-16	%SAMAGURI 1
19	PV	0.963	45	25	0	100	0	0	24	-8	%MARIANI1
20	PQ	0.958	18	3	0	0	0	0	0	0	%JORHAT
21	PQ	0.959	14	8	0	0	0	0	0	0	%BADARPUR
22	PQ	0.97	10	5	0	0	0	0	0	0	%PAILAPOL
23	PQ	1	7	3	0	0	0	0	0	0	%DULLAVCHERRA
24	PV	0.992	13	0	0	100	0	0	300	-300	%LANKA
25	PV	1.05	0	0	220	320	0	0	140	-47	%UMTRU

Bus No.	Bus Type	Voltage (P.U)	PL (MW)	QL (MVAR)	PG (MW)	Pgmax (MW)	Pgmin (MW)	QG (MVAR)	Qgmax (MVAR)	Qgmin (MVAR)	Bus Name
26	PV	1.015	0	0	314	414	0	0	1000	-1000	%UMIUM-I
27	PV	0.968	71	13	0	100	0	0	300	-300	%UMIUM-II
28	PQ	0.962	17	7	0	0	0	0	0	0	%UMIUM-III
29	PQ	0.963	24	4	0	0	0	0	0	0	%UMIUM-IV
30	PQ	0.968	0	0	0	0	0	0	0	0	%SHILLONG(MAWLI)
31	PV	0.967	43	27	7	107	0	0	300	-300	%NEHU
32	PV	0.964	59	23	0	100	0	0	42	-14	%KHLIERIAT
33	PQ	0.972	23	9	0	0	0	0	0	0	%CHERAPUNJEE
34	PV	0.986	59	26	0	100	0	0	24	-8	%NANGALBIBRA
35	PQ	0.981	33	9	0	0	0	0	0	0	%TURA
36	PV	0.98	31	17	0	100	0	0	24	-8	%CCL
37	PQ	0.992	0	0	0	0	0	0	0	0	%KARONG
38	PQ	0.962	0	0	0	0	0	0	0	0	%IMPHAL
39	PQ	0.97	27	11	0	0	0	0	0	0	%NINGTHOUKHONG
40	PV	0.97	66	23	0	100	0	0	300	-300	%MELURI
41	PQ	0.967	37	10	0	0	0	0	0	0	%KOHIMA
42	PV	0.985	96	23	0	100	0	0	300	-300	%DIMAPUR
43	PQ	0.978	18	7	0	0	0	0	0	0	%MOKOKCHUNG
44	PQ	0.985	16	8	0	0	0	0	0	0	%ZEMABAWK1
45	PQ	0.987	53	22	0	0	0	0	0	0	%SERCHIP
46	PV	1.005	28	10	19	119	0	0	100	-100	%KOLASIB1
47	PQ	1.017	34	0	0	0	0	0	0	0	%LUNGLEI
48	PV	1.021	20	11	0	0	0	0	0	0	%DHARMANAGAR
49	PV	1.025	87	30	204	304	0	0	210	-85	%AMBASSA
50	PQ	1.001	17	4	0	0	0	0	0	0	%KUMARGHAT

Bus No.	Bus Type	Voltage (P.U)	PL (MW)	QL (MVAR)	PG (MW)	Pgmax (MW)	Pgmin (MW)	QG (MVAR)	Qgmax (MVAR)	Qgmin (MVAR)	Bus Name
51	PQ	0.967	17	8	0	0	0	0	0	0	%AGARTALA
52	PQ	0.957	18	5	0	0	0	0	0	0	%ROKHIA
53	PQ	0.946	23	11	0	0	0	0	0	0	%LTPS(LAKWA)
54	PV	0.955	113	32	48	148	0	0	300	-300	%NTPS1(NAMRUP)
55	PV	0.952	63	22	0	100	0	0	23	-8	%DIBRUGARH
56	PV	0.954	84	18	0	100	0	0	15	-8	%ITANAGAR
57	PQ	0.971	12	3	0	0	0	0	0	0	%DIMAPUR(PG)
58	PQ	0.959	12	3	0	0	0	0	0	0	%IMPHAL(PG)
59	PV	0.985	277	113	155	255	0	0	180	-60	%LOKTAK
60	PQ	0.993	78	3	0	0	0	0	0	0	%JIRIBUM(PG)
61	PV	0.995	0	0	160	260	0	0	300	-100	%AIZWAL(PG)
62	PV	0.998	77	14	0	100	0	0	20	-20	%AGTPP
63	PQ	0.969	0	0	0	0	0	0	0	0	%HAFLONG
64	PQ	0.984	0	0	0	0	0	0	0	0	%KHANDONG
65	PV	1.005	0	0	391	491	0	0	200	-67	%KOPILI1
66	PV	1.05	39	18	392	492	0	0	200	-67	%SALKATI1
67	PQ	1.02	28	7	0	0	0	0	0	0	%KHLIERIAT(PG)
68	PQ	1.003	0	0	0	0	0	0	0	0	%BADARPUR(PG)
69	Slack	1.035	0	0	516.4	805.2	0	0	300	-300	%GEYLPHU
70	PV	0.984	66	20	0	100	0	0	32	-10	%RANGANADI1
71	PQ	0.987	0	0	0	0	0	0	0	0	%NIRJULI
72	PV	0.98	12	0	0	100	0	0	100	-100	%DOYANG1
73	PV	0.991	6	0	0	100	0	0	100	-100	%ZIRO
74	PV	0.958	68	27	0	100	0	0	9	-6	%TINSUKIA1
75	PQ	0.967	47	11	0	0	0	0	0	0	%MARGAREETA

Bus No.	Bus Type	Voltage (P.U)	PL (MW)	QL (MVAR)	PG (MW)	Pgmax (MW)	Pgmin (MW)	QG (MVAR)	Qgmax (MVAR)	Qgmin (MVAR)	Bus Name
76	PV	0.953	68	36	0	100	0	0	23	-8	%EKBARI
77	PV	1.006	61	28	0	100	0	0	70	-20	%UDAYPUR
78	PQ	1.003	71	26	0	0	0	0	0	0	%NLAGUN
79	PQ	1.009	39	32	0	0	0	0	0	0	%DAPORIZO
80	PV	1.04	130	26	477	577	0	0	280	-165	%ALONG

Table A.12. Line data for NER transmission system

Line no.	From Bus	To Bus	R (p.u)	X (p.u)	B (p.u)
1	1	2	0.0303	0.0999	0.0254
2	1	3	0.0129	0.0424	0.0108
3	2	12	0.0187	0.0616	0.0157
4	3	5	0.0241	0.108	0.0284
5	3	12	0.0484	0.16	0.0406
6	4	5	0.0018	0.008	0.0021
7	4	11	0.0209	0.0688	0.0175
8	5	6	0.0119	0.054	0.0143
9	5	11	0.0203	0.0682	0.0174
10	6	7	0.0046	0.0208	0.0055
11	7	12	0.0086	0.034	0.0087
12	8	5	0	0.0267	0
13	8	9	0.0024	0.0305	1.162
14	8	30	0.0043	0.0504	0.514
15	9	10	0.0026	0.0322	1.23
16	11	12	0.006	0.0196	0.005
17	11	13	0.0222	0.0731	0.0188
18	12	14	0.0215	0.0707	0.0182
19	12	16	0.0212	0.0834	0.0214
20	13	15	0.0744	0.2444	0.0627
21	14	15	0.0595	0.195	0.0502
22	15	17	0.0132	0.0437	0.0444
23	15	19	0.012	0.0394	0.0101
24	15	33	0.038	0.1244	0.0319
25	16	17	0.0454	0.1801	0.0466
26	17	18	0.0123	0.0505	0.013
27	17	31	0.0474	0.1563	0.0399
28	18	19	0.0112	0.0493	0.0114
29	19	20	0.0252	0.117	0.0298
30	19	34	0.0752	0.247	0.0632
31	20	21	0.0183	0.0849	0.0216
32	21	22	0.0209	0.097	0.0246
33	22	23	0.0342	0.159	0.0404
34	23	24	0.0135	0.0492	0.0498
35	23	25	0.0156	0.08	0.0864

Line no.	From Bus	To Bus	R (p.u)	X (p.u)	B (p.u)
36	23	32	0.0317	0.1153	0.1173
37	24	70	0.0022	0.4115	0.102
38	24	72	0.0488	0.196	0.0488
39	25	27	0.0318	0.163	0.1764
40	26	25	0	0.0382	0
41	26	30	0.008	0.086	0.908
42	27	28	0.0191	0.0855	0.0216
43	27	32	0.0229	0.0755	0.0193
44	28	29	0.0237	0.0943	0.0238
45	29	31	0.0108	0.0331	0.0083
46	30	17	0	0.0388	0
47	30	38	0.0046	0.054	0.422
48	31	32	0.0298	0.0985	0.0251
49	33	37	0.0415	0.142	0.0366
50	34	37	0.0026	0.0094	0.0098
51	34	36	0.0087	0.0268	0.0057
52	34	43	0.0413	0.1681	0.0423
53	35	36	0.0022	0.0102	0.0027
54	35	37	0.011	0.0497	0.0132
55	37	39	0.0321	0.106	0.027
56	37	40	0.0593	0.168	0.042
57	38	37	0	0.0375	0
58	38	65	0.009	0.0986	1.046
59	39	40	0.0184	0.0605	0.0155
60	40	41	0.0145	0.0487	0.0122
61	40	42	0.0555	0.183	0.0466
62	41	42	0.041	0.135	0.0344
63	42	49	0.0357	0.161	0.043
64	43	44	0.0608	0.2454	0.0607
65	44	45	0.0224	0.0901	0.0224
66	45	46	0.04	0.1356	0.0332
67	45	49	0.0684	0.186	0.0444
68	46	47	0.038	0.127	0.0316
69	46	48	0.0601	0.189	0.0472
70	47	49	0.0191	0.0625	0.016
71	47	69	0.0844	0.2778	0.0709
72	48	49	0.0179	0.0505	0.0126
73	49	50	0.0267	0.0752	0.0187
74	49	51	0.0486	0.137	0.0342
75	49	54	0.073	0.289	0.0738

Line no.	From Bus	To Bus	R (p.u)	X (p.u)	B (p.u)
76	49	66	0.018	0.0919	0.0248
77	49	69	0.0985	0.324	0.0828
78	50	57	0.0474	0.134	0.0332
79	51	52	0.0203	0.0588	0.014
80	51	58	0.0255	0.0719	0.0179
81	52	53	0.0405	0.1635	0.0406
82	53	54	0.0263	0.122	0.031
83	54	55	0.0169	0.0707	0.0202
84	54	56	0.0027	0.0095	0.0073
85	54	59	0.0503	0.2293	0.0598
86	55	56	0.0049	0.0151	0.0037
87	56	57	0.0343	0.0966	0.0242
88	56	58	0.0343	0.0966	0.0242
89	56	59	0.0825	0.251	0.0569
90	59	60	0.0317	0.145	0.0376
91	59	61	0.0328	0.15	0.0388
92	60	61	0.0026	0.0135	0.0146
93	60	62	0.0123	0.0561	0.0147
94	61	62	0.0082	0.0376	0.0098
95	62	66	0.0482	0.218	0.0578
96	62	67	0.0258	0.117	0.031
97	63	59	0	0.0386	0
98	63	64	0.0017	0.02	0.216
99	64	61	0	0.0268	0
100	64	65	0.0027	0.0302	0.38
101	65	66	0	0.037	0
102	66	67	0.0224	0.1015	0.0268
103	65	68	0.0014	0.016	0.638
104	68	69	0	0.037	0
105	69	70	0.03	0.127	0.122
106	69	75	0.0405	0.122	0.124
107	69	77	0.0309	0.101	0.1038
108	70	71	0.0088	0.0355	0.0088
109	70	74	0.0401	0.1323	0.0337
110	70	75	0.0428	0.141	0.036
111	71	72	0.0446	0.18	0.0444
112	71	73	0.0087	0.0454	0.0118
113	74	75	0.0123	0.0406	0.0103

Line no.	From Bus	To Bus	R (p.u)	X (p.u)	B (p.u)
114	75	77	0.0601	0.1999	0.0498
115	76	77	0.0444	0.148	0.0368
116	77	78	0.0038	0.0124	0.0126
117	77	80	0.017	0.0485	0.0472
118	78	79	0.0055	0.0244	0.0065
119	79	80	0.0156	0.0704	0.0187

Table A.13. Generator cost data for NER transmission system

Bus No.	a	b	c
1	0.01	40	0
4	0.01	40	0
6	0.01	40	0
8	0.01	40	0
10	0.0222	20	0
12	0.1176	20	0
15	0.01	40	0
18	0.01	40	0
19	0.01	40	0
24	0.01	40	0
25	0.0455	20	0
26	0.0318	20	0
27	0.01	40	0
31	1.4286	20	0
32	0.01	40	0
34	0.01	40	0
36	0.01	40	0
40	0.01	40	0
42	0.01	40	0
46	0.5263	20	0
49	0.049	20	0
54	0.2083	20	0
55	0.01	40	0
56	0.01	40	0
59	0.0645	20	0
61	0.0625	20	0
62	0.01	40	0
65	0.0256	20	0
66	0.0255	20	0
69	0.0194	20	0
70	0.01	40	0
72	0.01	40	0
73	0.01	40	0
74	0.01	40	0
76	0.01	40	0
77	0.01	40	0

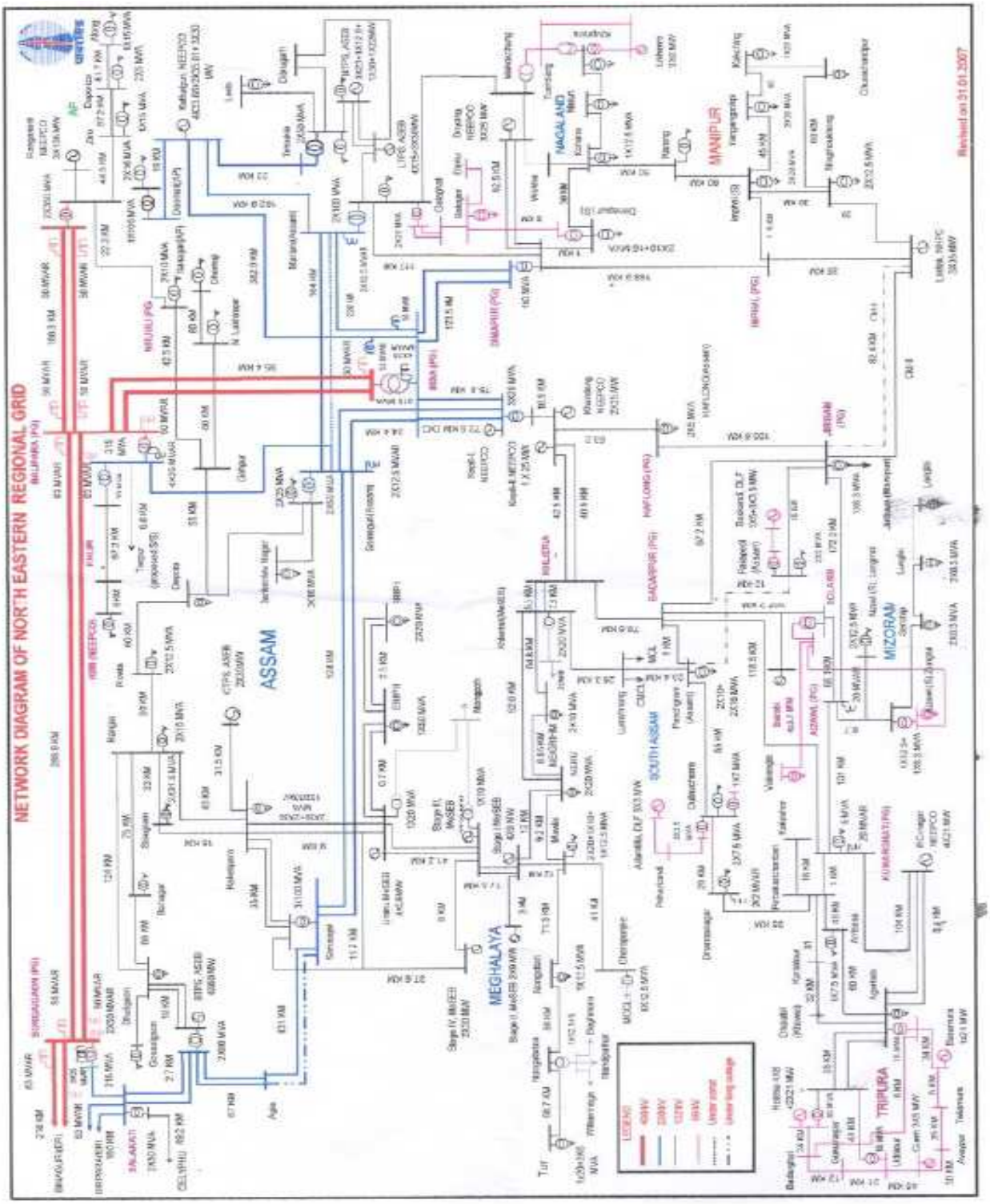

Fig.A.2. Single-line diagram of the NER-Grid, India

Fig.A.2 illustrates the complete single-line diagram of North-Eastern Regional (NER) Transmission Grid.

A.4.5 IEEE-123 bus distribution system

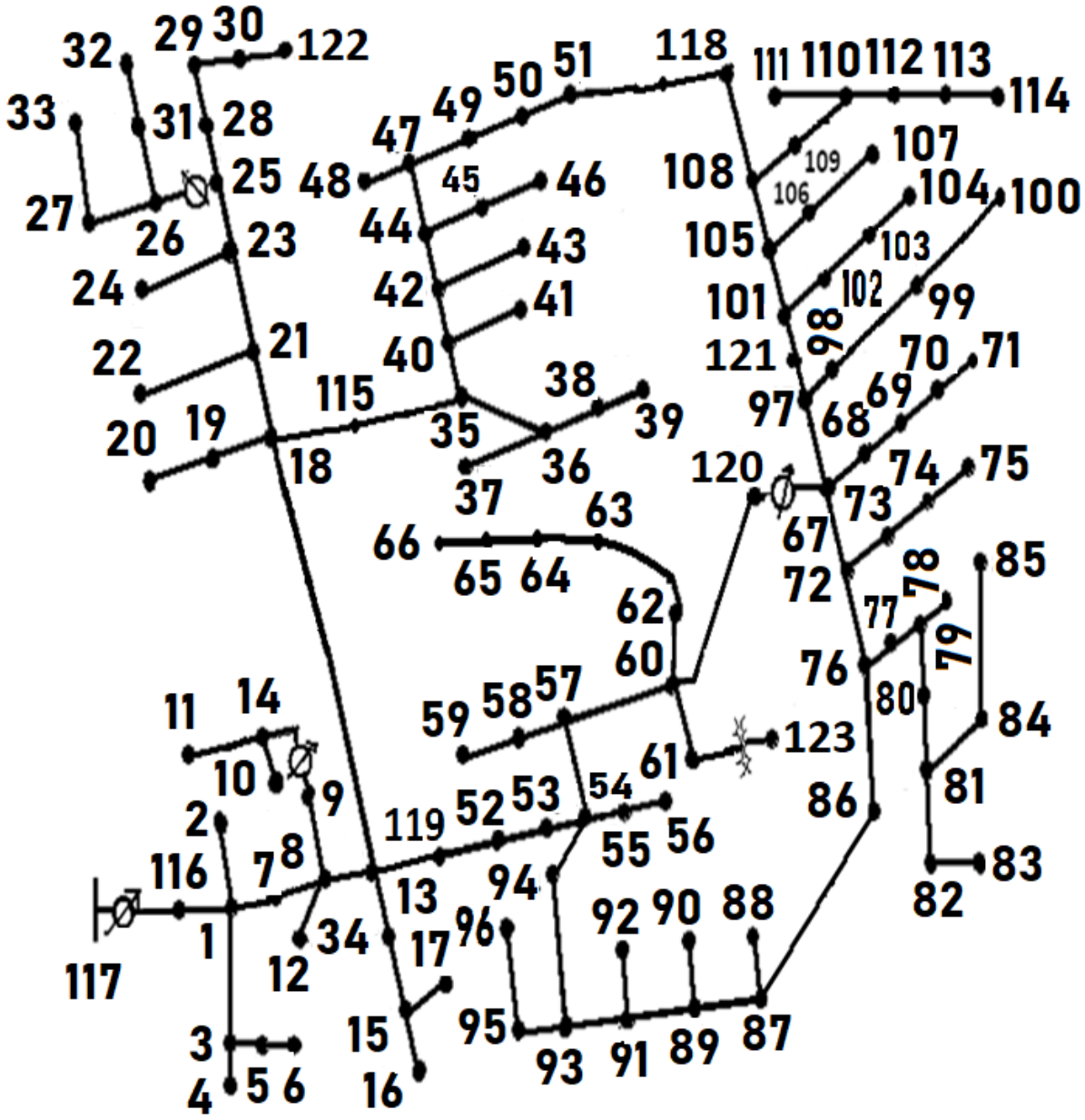

Fig.A.3. IEEE 123 Node Test Feeder System

Fig.A.3 depicts the complete single-line diagram of IEEE 123 node test feeder system.

A.4.6 25-bus test distribution system

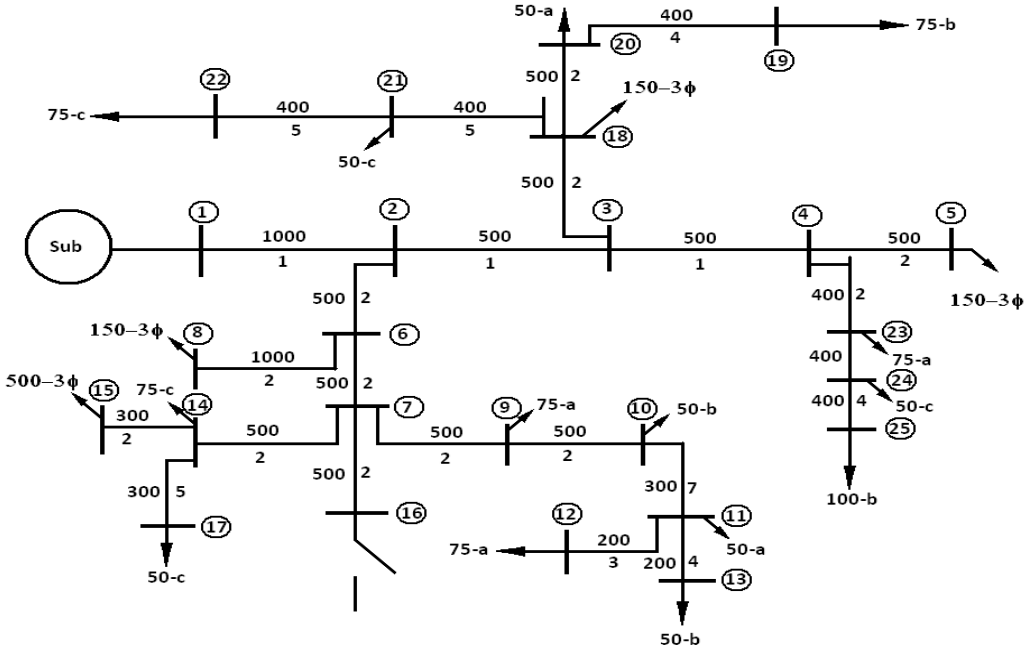

Fig.A.4. 25- Node Test Feeder System

Fig.A.4 shows the complete single-line diagram of 25-node test feeder system.

Bibliography

[1] European Commission (2006) European Smart Grids Technology Platform: Vision and Strategy for Europe's Electricity, http://ec.europa.eu/research/energy/pdf/smartgrids_en.pdf (accessed on 4 August, 2011).

[2] U.S. Department of Energy, Smart Grid System Report, July 2009, http://www.oe.energy.gov/sites/prod/files/oeprod/DocumentsandMedia/SGSRMain_090707_lowers.pdf (accessed on 4 August, 2011)

[3] A Compendium of Modern Grid Technologies, July 2009, http://www.netl.doe.gov/smartgrid/referenceshelf/whitepapers/Compendium_of_Technologies_APPROVED_2009_08_18.pdf (accessed on 4 August, 2011).

[4] European Commission, ICT for a Low Carbon Economy: Smart Electricity Distribution Networks, July 2009,http://ec.europa.eu/information_society/activities/sustainable_growth/docs/sb_publications/pub_smart/edn_web.pdf (accessed on 4 August, 2011).

[5] World Economic Forum (2009) Accelerating Smart Grid Investment, http://www.weforum.org/pdf/SlimCity/SmartGrid2009.pdf (accessed on 4 August, 2011).

[6] www.indiasmartgrid.org/document/ISGF%20FLYER.pdf .

[7] www.indiasmartgrid.org/reports/Smart%20Grid%20Vision%20and%20Roadmao%20for%20India.pdf .

[8] https://www.thehindubusinessline.com/news/...smart-meters...in.../article25952042.ece .

[9] Mohd Rihan; Mukhtar Ahmad and M. Salim Beg, "Phasor Measurement Units in the Indian Smart Grid".

[10] N. Hingorani, "FACTS, Flexible Transmission Systems", In Proceedings of Fifth International Conference on AC and DC Power Transmission, London, September 1991, pp. 1-7.

[11] Jose´ A. Dominguez-Navarro, Jose´ L. Bernal-Agustin, Alexis Diaz, Durlym Requena, Emilio P. Vargas, "Optimal parameters of FACTS devices in electric power systems applying evolutionary strategies", Int J Electrical Power and Energy Systems 29 (2007) 83–90.

[12] Narayana Prasad Padhy, M.A. Abdel Moamen, "Power flow control and solutions with multiple and multi-type FACTS devices". Electric Power Syst. Res. 74 (2005) 341-351.

[13] L.Gyugyi, et.al, "The unified Power Flow Controller: A New Approach To Power Transmission Control", Presented at 1994 IEEE Summer Meeting, Paper No. 94-SM 474-7 PWRD.

[14] GYUGYI, L.: "Unified power-flow control concept for flexible AC transmission system", IEE Proc. C, 1992, 139, (4), pp. 323-331

[15] Gyugyi, L., Schauder, C.D., Williams, S.L., Rietman,T.R., Torgerson, D.R., and Edris, A.: "The unified power flow controller: A new approach to power transmission control", IEEE Trans. Power Deliv., 1995, 10, (2), pp. 1085-1097

[16] Mohamed Elsaid Elgamal, Ahmed Lotfy, G.E.M. Ali, "Voltage profile enhancement by fuzzy controlled MLI UPFC", Int J Electrical Power and Energy Systems 34 (2012) 10–18.

[17] Fuerte-Esquivel, C.R., and Acha, E.: "A Newton-type Algorithm for the Control of Power Flow in Electrical Power Networks", IEEE Trans. on Power Systems, 1997, vol:12, Issue:4, 1474-1480.

[18] Rashedi, E., H. Nezamabadi-pour, and S. Saryazdi, "GSA: A gravitational search algorithm," Information Sciences, Vol. 179, No. 13, 2232{2248, 2009.

[19] S. Rebennack, P.M.Pardalos, M.V.F.Pereira and N.A.Iliadis, "Handbook of Power Systems II" , Springer.

[20] A. Lashkar Ara , A. Kazemi , S.A. Nabavi Niaki , "Modelling of Optimal Unified Power Flow Controller (OUPFC) for optimal steady-state performance of power systems", Energy Conversion and Management 52 (2011) 1325–1333.

[21] G. W. Stagg and A. Abiad, "Computer Methods in Power System Analysis", McGraw-Hill, New York, First Edition.

[22] Chico Hermanu; Muhammad Nizam; Fasda Ilhaq Robbani, "Optimal Placement of Unified Power Flow Controllers (UPFC) for Losses Reduction and Improve Voltage Stability Based on Sensitivity Analysis in 500 kV Java-Bali Electrical Power System", 2018, 5th International Conference on Electric Vehicular Technology (ICEVT), 83-87

[23] Sanjeev Kumar, D.K. Chaturvedi, "Optimal power flow solution using fuzzy evolutionary and swarm optimization". Int J Electrical Power and Energy Systems 47 (2013) 416–423.

[24] R. A. Jabr , "Optimal Power Flow Using an Extended Conic Quadratic Formulation", IEEE Trans. Power Syst., vol. 23, no. 3, August 2008.

[25] S. Affijulla and S. Chauhan, "A New Intelligence Solution for Power System Economic Load Dispatch", 978-1-4244-8782-0/11/2011 IEEE.

[26] Shaul Salomon; Gideon Avigad; Peter J. Fleming; Robin C. Purshouse, "Active Robust Optimazation: Enhancing Robustness to Uncertain Environments", IEEE Trans. on Cybernetics, 2014, vol:44, Issue:11, 2221-2231.

[27] Babak Asadzadeh; Vahid Asadzadeh; Seyed Hossein Hossein; Gevorg B. Gharehpetian, "Allocation of UPFC in North West grid of Iran to increase power system security", IEEE Pes T&D, 2010, 1-8.

[28] D. Simon, "Biogeography-based optimization," IEEE Trans. Evol. Comput., vol.12, no. 6, pp.702-713, Dec.2008

[29] O. Ceylan, A. Ozdemir and H. Dag, "Gravitational Search Algorithm for Post-Outage Bus Voltage Magnitude Calculations", UPEC2010, 31st Aug - 3rd Sept 2010.

[30] Binod Shaw, V. Mukherjee, S.P. Ghoshal, "A novel opposition-based gravitational search algorithm for combined economic and emission dispatch problems of power systems", Int J Electrical Power and Energy Systems 35 (2012) 21–33.

[31] Serhat Duman, Ugur Guvenc, Yusuf Sonmez, Nuran Yorukeren, "Optimal power flow using gravitational search algorithm", Energy Conversion and Management 59 (2012) 86–95.

[32] Chaoshun Li, Jianzhong Zhou, "Parameters identification of hydraulic turbine governing system using improved gravitational search algorithm", Energy Conversion and Management 52 (2011) 374–381.

[33] Sourav Mallick , S.P. Ghoshal, P. Acharjee, S.S. Thakur, "Optimal static state estimation using improved particle swarm optimization and gravitational search algorithm". Int J Electrical Power and Energy Systems 52 (2013) 254–265.

[34] Soumitra Mondal, Aniruddha Bhattacharya, Sunita Halder nee Dey, "Multi-objective economic emission load dispatch solution using gravitational search algorithm and considering wind power penetration". Int J Electrical Power and Energy Systems 44 (2013) 282–292.

[35] Provas Kumar Roy, "Solution of unit commitment problem using gravitational search algorithm". Int J Electrical Power and Energy Systems 53 (2013) 85–94.

[36] Fuerte-Esquivel, C.R., and Acha, E.: "Unified power flow controller: A critical comparison of Newton-Raphson UPFC algorithms in power flow studies", IEE Proc. Gener. Transrn. Distrib., 1997.

[37] S.A. Taher and S. A. Afsari, "Optimal Location and Sizing of UPQC in Distribution Networks Using Differential Evolution Algorithm", Mathematical Problems in Engineering, vol. 2012, Article ID 838629.

[38] Y. Liu; M. Steurer; P. Ribeiro, "A Novel Approach to Power Quality Assessment: Real Time Hardware-in-the-loop test bed", IEEE Trans. on Power Delivery, 2005, vol:20, Issue:2, 1200-1201.

[39]Timothy J. Browne; Gerald T. Heydt, "Power Quality as an Educational Opportunity", IEEE Trans. on Power Systems, 2008, vol:23, Issue: 2, 814-815.

[40] Kerry D. McBee; Marcelo G. Simoes, "Evaluating the Long-Term Impact of a Continuously Increasing Harmonic Demand on Feeder-Level Volatge Distortion", IEEE Trans. on Industry Applications, 2014, vol:50, Issue:3, 2142-2149.

[41] M.J. Newman; D.G. Holmes; J.G. Nielsen; F. Blaabjerg, "A Dynamic Voltage Restorer (DVR) with Selective Harmonic Compensation at Medium Voltage Level", IEEE Trans. on Industry Applications, 2005, vol:41, Issue:6, 1744-1753.

[42] Fu-Sheng Pai; Shyh-Jier Huang, "A Novel Design of Line-interactive Uninterruptible Power Supplies without Load Current Sensors", IEEE Trans. On Power Electronics, 2006, vol:21, Issue:1, 202-210.

[43] A. Medina-Rios; H.A. Ramos-Carranza, "An Active Power Filter in Phase Coordinates for Harmonic Mitigation", IEEE Trans. On Power Delivery, 2007, vol:22, Issue:3, 1991-1993.

[44] R. Arnold, "Solutions to the Power Quality Problem", Power Engg. Journal, 2001, vol:15, Issue:2, 65-73.

[45] V. Khadhikar and A. Chandra, "A New Control Philosophy for a Unified Power Quality Conditioner (UPQC)" to Coordinate Load-Reactive Power Demand between Shunt and Series Inverters", IEEE Trans. Power Deliv., vol. 23, no. 4, October 2008.

[46] A. E. Leon, S. J. Amodeo, J. A. Solsona and M. I. Valla, "Non-Linear Optimal Controller for Unified Power Quality Conditioners", IET Power Electron., 2010.

[47] I. Axente, J. Navilgone Ganesh, M. Basu, Michael F. Conlon and Kevin Gaughan, "A 12-kva DSP-Controlled Laboratory Prototype UPQC Capable of Mitigating Unbalance in Source Voltage and Load Current", IEEE Trans. Power Electron., vol. 25, no. 6, June 2010.

[48] M.E.C. Brito, L.R. Limongi, M.C. Cavalcanti, F.A.S. Neves, G.M.S. Azevedo, "A Step-Dynamic Voltage Regulator Based on Cascaded Reduced-Power Series Transformers" , Electric Power Systems Research 108 (2014) 245– 253.

[49] H. Akagi, "Trends in Active Power Line Conditioners", IEEE Trans. Power Electron., vol.9, no.3, pp. 263-268, May 1994.

[50] B. Singh, K. Al-Hadad, and A. Chandra, "A Review of Active Filters for Power Quality Improvement", IEEE Trans. Ind. Electron., vol. 46, no. 5, pp.960-971, October 1999.

[51] Arindam Ghosh and Gerard Ledwich, "A Unified Power Quality Conditioner (UPQC) for Simultaneous Voltage and Current Compensation", Electric Power Systems Research 59 (2001) 55-63.

[52] V. Khadhikar and A. Chandra, "UPQC-S: A Novel Concept of Simultaneous Voltage Sag/Swell and Load Reactive Power Compensation Utilizing Series Inverter of UPQC", IEEE Trans. Power Electron., vol.26, no.9, Sept 2011.

[53] K. Palanisamy, D.P.Kothari, Mahesh K. Mishra, S. Meikandashivam and I.Jacob Raglend, "Effective Utilization of Unified Power Quality Conditioner for Interconnecting PV Modules with Grid Using Power Angle Control Method", Int. J. Electical Power and Energy Systems, 48 (2013) 131-138.

[54] N. Patnaik and A.K.Panda, "Performance Analysis of a 3 Phase 4 Wire UPQC System Based on PAC Based SRF Controller with Real Time Digital Simulation", Int. J. Electical Power and Energy Systems, 74 (2016) 212-221.

[55] Yash Pal, A. Swarup and Bhim Singh, "A Comparative Analysis of Different Magnetics Supported Three-Phase Four-Wire Unified Power Quality Conditioners- A Simulation Study", Int. J. Electical Power and Energy Systems, 47 (2013) 436-447.

[56] R. Rajabioun, "Cuckoo Optimization Algorithm", Applied Soft Computing 11 (2011) 5508-5518.

[57] M. Ucar and S. Ozdemir, "3-Phase 4-Leg Unified Series-Parallel Active Filter System with Ultracapacitor Energy Storage for Unbalanced Voltage Sag Mitigation", Int. J. Electical Power and Energy Systems, 49 (2013) 149-159.

[58] Ahmet Teke, Lütfü Saribulut, and Mehmet Tümay, "A Novel Reference Signal Generation Method for Power-Quality Improvement of Unified Power-Quality Conditioner", IEEE Trans. Power Deliv., vol. 26, no. 4, October 2011.

[59] S. Ganguly, "Impact of Unified Power-Quality Conditioner Allocation on Line Loading, Losses and Voltage Stability of Radial Distribution Systems", IEEE Trans. Power Deliv., vol. 29, no. 4, August 2014.

[60] V. Khadkikar, A. Chandra, A.O. Barry and T.D. Nguyen, "Power Quality Enhancement Utilising Single-Phase Unified Power Quality Conditioner: Digital Signal Processor-Based Experimental Validation", IET Power Electron., 2011, vol. 4, Iss. 3, pp. 323–331.

[61] Srinivas Bhaskar Karanki, Mahesh K. Mishra and B. Kalyan Kumar, "Particle Swarm Optimization- Based Feedback Controller for Unified Power-Quality Conditioner", IEEE Trans. Power Deliv., vol. 25, no.4, October 2010.

[62] S. Biswas, S. K. Goswami and A. Chatterjee, "Optimal Distributed Generation Placement in Shunt Capacitor Compensated Distribution Systems Considering Voltage Sag and Harmonics Distortions", IET Gener. Transm. Distrib.,2014, vol. 8, Iss. 5, pp. 783–797.

[63] S.A. Taher and S. A. Afsari, "Optimal Location and Sizing of UPQC in Distribution Networks Using Differential Evolution Algorithm", Mathematical Problems in Engineering, vol. 2012, Article ID 838629.

[64] F. Shahnia, P.J. Wolfs and A. Ghosh, "Voltage Unbalance Reduction in Low Voltage Feeders by Dynamic Switching of Residential Customers among Three Phases", IEEE Trans. Smart Grid, vol. 5, no. 3, May 2014.

[65] Metin Kesler and Engin Ozdemir, "Synchronous-Reference-Frame-Based Control Method for UPQC under Unbalanced and Distorted Load Conditions", IEEE Trans. Ind. Electron., vol. 58, no. 9, September 2011.

[66] R. Azizipanah-Abarghooee, T. Niknam, M. Zare and M. Gharibzadeh, "Multi-Objective Short-Term Scheduling of Thermoelectric Power Systems Using a Novel Multi-Objective θ-Improved Cuckoo Optimization Algorithm", IET Gener. Transm. Distrib.,2014, vol. 8, Iss. 5, pp. 873–894.

[67] Dieu N. Vo, P. Schegner and W. Ongsakul, "Cuckoo Search Algorithm for Non-Convex Economic Dispatch", IET Gener. Transm. Distrib.,2013, vol. 7, Iss. 6, pp. 645–654.

[68] Attia A. EI-Fergany and Almoataz Y. Abdelaziz, "Capacitor Allocation in Radial Distribution Networks Using Cuckoo Search Algorithm", IET Gener. Transm. Distrib.,2014, vol. 8, Iss. 2, pp. 223-232.

[69] P.Dash, L.C. Saikia and N. Sinha, "Comparison of Performances of Several FACTS Devices Using Cuckoo Search Algorithm Optimized 2DOF Controllers in Multi-area AGC", Int. J. Electical Power and Energy Systems, 65 (2015) 316-324.

[70] T. T. Nguyen and A. V. Truong, "Distribution Network Reconfiguration for Power Loss Minimization and Voltage Profile Improvement Using Cuckoo Search Algorithm", Int. J. Electical Power and Energy Systems, 68 (2015) 233-242.

[71] A. Y. Abdelaziz and E. S. Ali, "Cuckoo Search Algorithm Based Load Frequency Controller Design for Nonlinear Interconnected Power System", Int. J. Electical Power and Energy Systems, 73 (2015) 632-643.

[72] S. M. Abd Elazim and E.S Ali, "Optimal Power System Stabilizers Design via Cuckoo Search Algorithm", Int. J. Electical Power and Energy Systems, 75 (2016) 99-107.

[73] V. Khadhikar and A. Chandra, "A Novel Structure for Three-Phase Four-Wire Distribution System Utilizing Unified Power Quality Conditioner (UPQC)", IEEE Trans. Ind. Application, vol.45, no. 5, September/October 2009.

[74] http://ewh.ieee.org/soc/pes/dsacom/testfeeders/ .

[75] Srinivas Bhaskar Karanki, Nagesh Geddada, Mahesh K. Mishra and B. Kalyan Kumar, "A Modified Three-Phase Four-Wire UPQC Topology with Reduced DC-Link Voltage Rating", IEEE Trans. Ind. Electron,, vol. 60, no. 9, September 2013.

[76] Attia A. EI-Fergany, "Optimal Capacitor Allocations Using Evolutionary Algorithms", IET Gener. Transm. Distrib.,2013, 6, (7), pp. 593-601.

[77] D. Karaboga and B. Basturk, “On the Performance of Artificial Bee Colony (ABC) Algorithm”, Appl. Soft Comput., 2008, 8, pp. 687-697.

[78] J. Carlos Gomez and M. M. Morcos, “Coordination of Voltage Sag and Over Current Protection in DG Systems”, IEEE Trans. Power Deliv., vol. 20, no. 1, January 2005.

[79] S. K. Goswami and S. K. Basu, “Direct Solution of Distribution Systems”, IEE Proc. C, vol. 138, no. 1, January 1991.

[80] M. Bollen, “Understanding Power Quality Problems, Voltage Sags and Interruptions”, New York: IEEE press, 1999.

[81] Mostafa I. Marei, Ehab F. El-Saadany and Magdy M. A. Salama, “A New Approach to Control DVR Based on Symmetrical Components Estimation”, IEEE Trans. Power Deliv. Vol. 22, No. 4, October 2007.

[82] Jovica. V. Milanovic and Yan Zhang, “Global Minimization of Financial Losses Due to Voltage Sags with FACTS Based Devices”, IEEE Trans. Power Deliv. Vol. 25, No. 1, October 2010.

[83] K. Bhumkittipich and N. Mithulananthan, “Performance Enhancement of DVR for Mitigating Voltage Sag/Swell using Vector Control Strategy”, Energy Procedia 9 (2011) 366 – 379.

[84] E. Babaei, M.F. Kangarlu and M. Sabahi, “Mitigation of Voltage Disturbances Using Dynamic Voltage Restorer Based on Direct Converters”, in IEEE Transactions on Power Delivery, vol. 25, no.4, pp. 2676-2683, Oct.2010.

[85] B. Wang and G. Venkataramanan “Dynamic Voltage Restorer Utilizing a Matrix Converter and Flywheel Energy Storage”, IEEE Trans. Ind. Appl., Vol. 45, No. 1, January/February 2009.

[86] Kimbark, E.W., “How to Improve System Stability without Risking Subsynchronous Resonance”, IEEE Trans. PAS-96, no.5, September/October 1977.

[87] Hailian Xie; Lennart Angquist; Hans-Peter Nee, “Design and Analysis of a Controller for a Converter Interface Interconnecting an Energy Storage with the DC Link of a VSC”, IEEE Trans. on Power Systems, 2010, vol:25, Issue:2, 1007-1015.

[88] F.A.L. Jowder, “Design and Analysis of Dynamic Voltage Restorer for Deep Voltage Sag and Harmonic Compensation”, IET Generation, Transmission & Distribution, 2009, vol:3, Issue:6, 547-560.

[89] Ebrahim Babaei, Mohammad Farhadi Kangarlu, “Sensitive Load Voltage Compensation against Voltage Sagds/Swells and Harmonics in The Grid Voltage and Limit Downstream Fault Currents using DVR”, Electric Power Systems Research, Volume 83, Issue 1, 2012, Pages 80-90.

[90] Phadke, A. G, "Synchronized Phasor Measurements in Power Systems", IEEE Comput. Appl. Power, vol. 6, no. 2, pp. 10-15, 1993.

[91] T. L. Baldwin, L. Mili, M. B. Boisen and Adapa, "Power System Observability With Minimal Phasor Measurement Placement", IEEE Trans. Power Syst., vol. 8, no. 2, pp. 707-715, May 1993.

[92] Reynaldo F. Nuqui, and Arun G. Phadke, " Phasor Measurement Unit Placement Techniques for Complete and incomplete Observability", IEEE Trans. Power Del., vol. 20, no. 4, pp. 2381-2388, October 2005.

[93] Bei Gou, "Optimal Placement of PMUs by Integer Linear Programming", IEEE Trans. Power Syst., vol. 23, no. 3, pp. 1525-1526, August 2008.

[94] Bei Gou, "Generalized Integer Linear Programming Formulation for Optimal PMU Placement", IEEE Trans. Power Syst., vol. 23, no. 3, pp. 1099-1103, August 2008.

[95] L.Jiao and L. Wang, "A Novel Genetic Algorithm based on Immunity", IEEE Trans Syst., Man, Cybern., vol.30, no.5, pp.552-561, Sep.2000.

[96] F. Aminifar, C. Lucas, A. Khodaei and M. Fotuhi-Firuzabad, "Optimal Placement of Phasor Measurement Units Using Immunity Genetic Algorithm", IEEE Trans. Power Del., vol. 24, no. 3, pp. 1014-1020, July 2009.

[97] R. Sodhi, S.C. Srivastava and S. N. Sing, "Multi-criteria Decision-making Approach for Multi-stage Optimal Placement of Phasor Measurement Units", IET Gener. Transm. Distrib., vol. 5, iss. 2, pp. 181-190, 2011.

[98] N. C. Koutsoukis, N. M. Manousakis. P. S. Georgilakis and G. N. Korres, "Numerical Observability Method for Optimal Phasor Measurement Units Placement Using Recursive Tabu search Method", IET Gener. Transm. Distrib., vol. 7, iss. 4, pp. 347-356, 2013.

[99] R. Kavasseri and S. K. Srinivasan, "Joint Placement of Phasor and Power Flow Measurement for Observability of Power Systems", IEEE Trans. Power Syst., vol. 26, no. 4, pp. 1929-1935, November 2011.

[100] C. Rakpenthai, S. Premrudeepreechacharn, S. Uatrongjit and Neville R. Watson, "An Optimal PMU Placement Method Against Measurement Loss and Branch Outage", IEEE Trans. Power Del., vol. 22, no. 1, pp. 101-107, January 2007.

[101] Nabil H. Abbasy and H. M. Ismail, "A Unified Approach for the Optimal PMU Location for Power System State Estimation", IEEE Trans. Power Syst., vol. 24, no. 2, pp. 806-812, May 2009.

[102] M. Esmaili, K. Gharani and H. A. Shayanfar, "Redundant Observability PMU Placement in the Presence of Flow Measurements Considering Contingencies", IEEE Trans. Power Syst., vol. 28, no. 4, pp. 3765-3773, November 2013.

[103] S. M. Mazhari, H. Monsef, and A. Fereidunian, "A Multi-Objective PMU Placement Method Considering Measurement Redundency and Observability Value Under Contingencies", IEEE Trans. Power Syst., vol. 28, no. 3, pp. 2136-2146, August 2013.

[104] E. E. Juarez and A. Hernandez, "An Analytical Approach for Stochastic Assessment of Balanced and Unbalanced Voltage Sags in Large System". IEEE Trans. Power Deliv., 2006, 21, (3), pp.1493-1500.

[105] M. N. Moschakis and N. C. Hatziargyriou, "Analytical Calculation and Stochastic Assessment of Voltage Sags", IEEE Trans. Power Deliv., 2006, 21, (7), pp. 1727-1734.

(Jayanti Sarker (Bhattacharjee))

Candidate